ENGINEERING MULTIPRONGED GLYCOSAMINOGLYCAN-BASED ANTICANCER THERAPEUTIC APPROACHES

by

Karthik Raman

A dissertation submitted to the faculty of
The University of Utah
in partial fulfillment of the requirements for the degree of

Doctor of Philosophy

Department of Bioengineering

The University of Utah

December 2015

The University of Utah Graduate School

STATEMENT OF DISSERTATION APPROVAL

The following faculty members served as the supervisory committee chair and members for the dissertation of___Karthik Raman_____.
Dates at right indicate the members' approval of the dissertation.

____Kuberan Balagurunathan_____, Chair	9/28/14_____ Date Approved
____Vladimir Hlady_____, Member	10/8/14_____ Date Approved
____Jindrich Kopecek_____, Member	10/02/14_____ Date Approved
____Hamidreza Ghandehari_____, Member	9/30/14_____ Date Approved
____Randy Jensen_____, Member	9/29/14_____ Date Approved

The dissertation has also been approved by___Patrick A. Tresco_____, Chair of the Department of__Bioengineering_____
and by David B. Kieda, Dean of The Graduate School.

ABSTRACT

Glioblastoma is the most common primary malignant brain tumor in adults. It is characterized by extensive invasion, an aberrant local blood brain barrier, and increased intercerebral pressure due to edema. Although there have been several advances in therapeutic strategies to treat gliomas, the current median survival for glioblastoma remains less than 2 years. A major impediment to the treatment of glioblastoma is the lack of drugs that can overcome the blood brain barrier, treat cancer cells, and not affect nearby glia and neurons. Additionally, most therapeutic strategies against cancers merely target cancer growth without affecting invasion, angiogenesis and metastasis.

Glycosaminoglycans, particularly heparan sulfate and chondroitin sulfate, are responsible for regulating several pathological processes associated with the progression of glioblastoma. They interact with growth factors, chemokines, and other molecules in the extracellular matrix and within cells, to modulate aberrant cell signaling pathways that influence cancer invasion, metastasis, angiogenesis, and growth.

In this dissertation, a therapeutic strategy based on glycosaminoglycan biology is designed and developed to treat gliomas and other cancers *in vivo*. The strategy is composed of two parts: glycosaminoglycan-based drugs (xylosides and glycosaminoglycan mimetics) and a glycosaminoglycan-based drug delivery vehicle conjugated to doxorubicin. Xylosides are small sugar monomers attached to aglycone moieties that cause cells to produce and release glycosaminoglycan chains without a core

protein attached. It is shown that upon treatment of gliomas by xylosides, the released glycosaminoglycans dramatically reduce tumor-associated invasion and angiogenesis *in vitro*. As xylosides are nontoxic even at high dosages, they are an incredibly powerful means to curb tumor invasion and angiogenesis. In addition to xylosides, an optimized heparin-based drug delivery vehicle, composed of heparosan conjugated to aprotinin and doxorubicin, is developed to deliver toxic doses of doxorubicin across the blood brain barrier to gliomas. This conjugate is an exciting therapeutic not only because it can curb glioma growth, but also because it is biodegradable and easy to produce in large quantities. Based on exciting *in vivo* results in mice, it is expected that this strategy will show promise in future clinical studies in humans.

.

This work is dedicated to my family. Thank you for mentoring me, supporting me, and inspiring me.

TABLE OF CONTENTS

LIST OF ABBREVIATIONS

GAG:	Glycosaminoglycan
HS:	Heparan Sulfate
CS:	Chondoroitin Sulfate
NA:	Heparosan
NS:	*N*-sulfo Heparosan
Hep:	Heparin
FGF:	Fibroblast growth factor
VEGF:	Vascular endothelial growth factor
BLMVEC:	Bovine lung microvascular endothelial cells
HLP:	Heparin-like polysaccharide
HDA:	Heparin-Doxorubicin-Aprotinin conjugate
ECM:	Extracellular matrix
3-OST:	3-*O* Sulfotransferase enzyme
6-OST:	6-*O* Sulfotransferase enzyme
2-OST:	2-*O* Sulfotransferase enzyme
NDST:	*N*-Deacetylase *N-sulfo*transferase enzyme
EPI:	C5-Epimerase enzyme
GlcNAc:	*N*-Acetyl Glucosamine
UA:	Uronic acid
GlcA:	Glucuronic acid

IdoA:	Iduronic acid
Sdc-1:	Syndecan-1 proteoglycan
Gpc-1:	Glypican-1 proteoglycan
Hpa:	Heparanase
Hep I, II, III:	Heparitinase I, II, and III
TMZ:	Temozolomide
MGMT:	Methylguanine methyltransferase
DOX:	Doxorubicin
BBB:	Blood brain barrier
DDV:	Drug delivery vehicle
CNS:	Central nervous system
GBM:	Glioblastoma Multiforme
ABC:	ATP-binding cassette
BCRP:	Breast cancer resistance protein
MDR1:	Multiple drug resistance protein 1
P-GP:	Permeability Glycoprotein
LRP:	LDL receptor protein
EPR:	Enhanced permeability and retention
PG:	Proteoglycan
EDC:	N-Ethyl-N′-(3-dimethylaminopropyl)carbodiimide hydrochloride
NHS:	N-Hydroxysuccinimide (may also be referred to as Sulfo-NHS)
DLS:	Dynamic light scattering
SEC:	Size exclusion chromatography

HPLC:	High performance liquid chromatography
SAX:	Strong Anion Exchange Chromatography
DEAE:	Weak Anion Exchange Chromatography
TEM:	Transmission Electron Microscopy
IVIS:	*In vivo* imaging system
MWCO:	Molecular weight cut-off
Fluoro xyloside:	4-Deoxy 4-Fluoroxyloside
RGD:	Arginylglycylaspartic acid

ACKNOWLEDGEMENTS

I would like to thank my mentor Dr. Kuberan Balagurunathan for guiding me and supporting me in all my ventures. His passion for science motivated me to approach all my problems with enthusiasm and confidence. I would also like to thank my lab mates, both past and present, for their camaraderie and support during these past years. I will miss the time we spent together in "the lab." To my co-mentors Dr. Randy Jensen and Dr. David Gillespie, I thank you for your advice and instruction in performing animal experiments. And, to my other committee members, Dr. Kopecek, Dr. Ghandehari, and Dr. Hlady, thank you for your guidance throughout my dissertation work.

CHAPTER 1

INTRODUCTION TO GLYCOSAMINOGLYCANS AND THEIR ROLES IN CANCER

1.1 Chemical Tumor Biology of Heparan Sulfate Proteoglycans

Manuscript reproduced with permission from: Raman, K. and Kuberan, B. (2010) Chemical Tumor Biology of Heparan Sulfate Proteoglycans, *Curr Chem Bio 4*, 20-31.

Published in final edited form as:
Curr Chem Biol. 2010 January 1; 4(1): 20–31. doi:10.2174/187231310790226206.

Chemical Tumor Biology of Heparan Sulfate Proteoglycans

Karthik Raman[1] and **Balagurunathan Kuberan**[2,3,*]

[1]Department of Bioengineering, University of Utah, Salt Lake City, UT 84112, USA

[2]Department of Medicinal Chemistry, University of Utah, Salt Lake City, UT 84112, USA

[3]Graduate Program in Neuroscience, University of Utah, Salt Lake City, UT 84112, USA

Abstract

Heparan sulfate proteoglycans (HSPGs) play vital roles in every step of tumor progression allowing cancer cells to proliferate, escape from immune response, invade neighboring tissues, and metastasize to distal sites away from the primary site. Several cancers including breast, lung, brain, pancreatic, skin, and colorectal cancers show aberrant modulation of several key HS biosynthetic enzymes such as 3-*O* Sulfotransferase and 6-*O* Sulfotransferase, and also catabolic enzymes such as HSulf-1, HSulf-2 and heparanase. The resulting tumor specific HS fine structures assist cancer cells to breakdown ECM to spread, misregulate signaling pathways to facilitate their proliferation, promote angiogenesis to receive nutrients, and protect themselves against natural killer cells. This review focuses on the changes in the expression of HS biosynthetic and catabolic enzymes in several cancers, the resulting changes in HS fine structures, and the effects of these tumor specific HS signatures on promoting invasion, proliferation, and metastasis. It is possible to retard tumor progression by modulating the deregulated biosynthetic and catabolic pathways of HS chains through novel chemical biology approaches.

Keywords

Proteoglycan; Cancer; Heparanase; Sulfotransferase; Sulfatase; Heparan Sulfate

Introduction

It has been known for decades that heparan sulfate proteoglycans (HSPGs) and chondroitin sulfate proteoglycans (CSPGs) are involved in the progression of cancer at various stages [1–3]. Many excellent reviews have described cancer growth, development, and metastasis [4–6]. However, knowledge on the detailed molecular interactions between tumor cells and ECM components including HS chains has only recently been devolved. In lieu of this new knowledge, this review article focuses on the role of HSPGs in several types of cancer and provides insights into how future cancer therapies can be developed based on changes in HS biosynthesis and catabolism.

Tumor Transformation, Growth, Invasion and Metastasis

The development of cancer typically involves four distinct stages: transformation into a cancerous phenotype, sequestration of nutrition through angiogenesis, invasion into nearby tissue, and metastasis to distal sites away from the primary location. While the transformation of normal cells into a cancerous phenotype hasn't yet been linked to HSPGs, there is an

*Address correspondence: Kuberan Balagurunathan, University of Utah, 30 S 2000 E, Skaggs Hall Room 307, Salt Lake City, UT 84112, USA, Phone: (+1) 801-587-9474; Fax: (+1) 801-585-9119; KUBY@pharm.utah.edu.

abundance of evidence relating HSPG fine structures to cancer growth, invasion, and metastasis.

Tumor cells upregulate the production of several angiogenic factors such as fibroblast growth factor (FGF) and vascular endothelial cell growth factor (VEGF) [7]. In order to support altered growth patterns and metabolism, these molecules trigger angiogenesis, the growth of blood vessels, which provides nearby cells with increased nutrition and oxygen-supply [8].

Malignant cancers are characterized by their invasiveness into nearby tissues and metastasis to distal locations away from the primary tumor site. In order for these processes to take place, tumor cells breakdown the surrounding ECM by activating or releasing various proteases such as matrix metalloproteases (MMPs) and serine proteases [9–12]. These proteases make the ECM more permeable for invading cells to pass through established ECM boundaries [13]. Malignant cancers can even invade into the blood stream and metastasize to distal locations in the body by cleaving off their adhesions to the ECM, entering the bloodstream, and then binding to ECM at a distal location. Since HSPGs are implicated in the above-mentioned critical processes, controlling their fine structures can significantly impact the growth, invasion and metastatic properties of tumor cells.

Common HSPG- Growth factor and Cytokine interactions

One of the primary methods by which HSPGs control cancer progression is by regulating the interactions between cells and signaling molecules such as growth factors and cytokines. Several insightful reviews discuss the roles that HSPGs play in binding to signaling molecules and localizing them to their cognate receptors on cell surfaces, storing them in tissues for later use, and/or helping to form molecular gradients for directional cellular activities during the development [14–16].

FGF2-HS interactions are well-studied example of GAG-growth factor interactions. The binding of FGF2 to its receptor causes autophosphorylation of the receptor's tyrosine kinase domains and leads to increased growth, migration and differentiation in several cancers [17, 18]. HSPGs play an integral role in the FGF2-FGFR interactions by localizing FGF2 near the receptor and forming a bridge that stabalizes the ligand-receptor complex and allows for signal transduction [19,20].

However, only specific HS fine structures allow FGF2-FGFR-mediated signaling. To bind FGF2, HS chains require N-Sulfated glucosamine units and 2-*O*-Sulfonated iduronic acid units [21–23]. Concurrently, for HS chains to bind FGFR, they require 6-*O*-Sulfonated glucosamine residues in addition to 2-*O*-Sulfonated iduronic acid and N-Sulfonated glucosamine residues [21,23,24].

Similar to HS-FGF2 interactions, HSPGs are essential to the signaling pathways triggered by other growth factors and cytokines as well. The following are some particularly important signaling molecules affected by HSPG interactions: VEGF, Heparin binding epidermal growth factor (HB-EGF), Transforming growth factor (TGF), Bone morphogenic protein (BMP), and FGF. Manipulating HS biosynthesis and catabolism can drastically affect several of these signaling pathways.

Proteoglycans: Biosynthesis and Catabolism

Cancer cells have inherently altered proteoglycan fine structures that allow them to invade, metastasize and grow uncontrollably [25,26]. These fine structural changes are due to errors in the regulation of biosynthetic and catabolic enzymes that control proteoglycan fine

structures. The following section details several of the enzymes that are responsible for PG synthesis and catabolism.

Proteoglycans are composed of a core protein substituted with one or more glycosaminoglycan (GAG) polysaccharide side chains [27,28]. PG assembly involves the following steps: (1) assembly of the linkage tetrasaccharide (2) concurrent elongation and modification of the GAG backbone such as epimerization, deacetylation and N-/O- sulfonation (Fig. 1).

Synthesis begins with the transfer of xylose residues to certain serine amino acids in the core protein. Next, transfer of galactose and glucuronic acid residues by glycosyl transferases such as GalT-I, GalT-II, and GlcAT-I results in the formation of a tetrasaccharide linkage region [29,30]. Subsequently, the GAG chain is elongated via the alternate addition of D-glucuronic acid (GlcA) and *N*-acetyl-*D*-hexosamine (*N*-acetyl-D-glucosamine, GlcNAc or *N*-acetyl-D-galactosamine, GalNAc) to the tetrasaccharide linker [31–34]. HS contains GlcNAc and GlcA/Iduronic acid (IdoA), CS contains GalNAc and GlcA, and dermatan sulfate (DS) contains GalNAc and GlcA/IdoA disaccharide units.

Subsequently EXT enzymes and CS synthases elongate HS and CS chains, respectively, by adding the appropriate sugar building blocks [35–40]. While the elongation is in progress, parts of the GAG chain are modified via sulfonation and epimerization to yield the final complex PG structure [41–43]. A host of HS biosynthetic and catabolic enzymes that have been implicated in cancer progression are listed below:

HSulf-1 and HSulf-2

A set of HS 6-*O*-endosulfatases that are secreted from the Golgi and localized in the ECM. HSulfs selectively remove 6-*O* sulfate groups on GlcN residues of HS; preferentially catalyzing the desulfonation on trisulfated disaccharides (Fig. 2) [44–48].

3-*O Sulfotransferase (3-OST)*

A group of 7 related enzyme isoforms that catalyze the 3-*O* sulfonation of GlcN residues, a rare HS modification [49–52].

6-*O Sulfotransferase (6-OST)*

A group of three enzyme isoforms that catalyze the 6-*O* sulfonation of GlcNAc as well as GlcNS residues [53–56].

Heparanase (Hpa)

The Heparanase (Hpa) family consists of endo-β-D-glucuronidases that cleave HS into several smaller chains ~5–7 kDa in size (Fig. 3) [57–59].

In several cancer cells, these enzymes and their isoforms are either up- or down- regulated. Bret *et al*. found that RT-PCR analysis of several melanoma cells revealed a significant difference in the expression of genes encoding for *EXT2, HS3ST2* (3-OST-2), *HS2ST1*(2-OST-1), *HPSE* (Heparanase), and *SULF2* (HSulf-2) between normal and malignant plasma cells [60]. Determining enzymes and their isoforms that are misregulated, decoding their respective PG fine structural modifications, and understanding how these changes affect cancer progression, are essential for directing future research endeavors that could lead to the development of anti-cancer drugs.

Roles of HS and Important HS-Protein Interactions in Cancer

Growth

Cell-surface HSPGs, especially glypican-1 (Gpc1) and syndecan-1 (Sdc1), are greatly upregulated in late-stage (malignant) breast cancer tissue [61]. It is possible that these changes allow increased growth factor signaling since certain sulfated residues of HS are required for FGF receptor (FGFR) activation [62,63]. These HSPGs could also be responsible for protecting the cancer cells from natural killer cell (NK) recognition [64]. Since NK cells recognize particular HS fine structural patterns, cancer cells modify their HS patterns to evade NK cells and the immune system. Emerging evidence suggests that interactions between HS and HSulf-1, HSulf-2, and 3-OST, may also play an important role in breast tumor growth. The gene encoding HSulf-1 is down regulated in breast cancer cells [46]. Lower HSulf-1 expression increases autocrine activation of the EGFR-ERK (epidermal growth factor receptor-extracellular signal regulated kinase) pathway and stimulates cell growth [46]. Breast carcinoma cells also express 8-fold more HSulf-2 mRNA than normal tissues [65] Increased HSulf-2 mRNA correlates with increased angiogenesis and FGF binding capacity [65]. Several cancers also demonstrate 3-OST-2-gene silencing via methylation [66]. While it is unknown how 3-OST-2 specifically modulates growth factor binding to HS, it is possible that 3-OST-2 has anti-tumor properties that are stifled in cancer cells.

Invasion and Metastasis

Over expression of Hpa, which cleaves HS chains and facilitates migration of tumor cells through the ECM, is a key indicator of malignant breast cancers. In a clinical study, Hpa-1 expression was significantly upregulated in microinvasive lesions in ductal carcinoma *in situ* (DCIS) [67]. Hpa over-expressing breast tumors are 7 times larger and significantly more vascularized [68]. Increased Hpa also induces shedding of cell surface Sdc-1, which forms a paracrine signaling complex and in-turn signals distal breast cancer cells to proliferate [69, 70]. Surprisingly, breast cancer can increase Hpa expression throughout the body. Lymphocytes in peripheral blood mononuclear cell fractions (PBMCs) from breast cancer patients express Hpa [71]. When serum containing these leukocytes is introduced to fresh lymphocytes, Hpa expression is stimulated in the normal lymphocytes [71]. Such tumor-system interactions lead to increased systemic heparanase expression in breast cancer [71]. Given the multitude of functions of Hpa, systemic Hpa amplification can perpetuate the tumor-promoting autocrine, paracrine, and growth factor signaling. Heparanase inhibitors can be effective against invasive cancers. However, it is also possible to control Hpa activity by controlling HS sulfonation since Hpa substrate recognition requires certain sulfonation and acetylation patterns [72].

Pancreatic Cancer

Growth—HSPGs such as Gpc-1 and Sdc-1 play key roles in the interactions between stromal elements and pancreatic cancer cells. Pancreatic ductal adenocarcinoma (PDAC) cells and adjacent fibroblasts over express Gpc-1, which is involved in FGF2, HB-EGF, VEGF, BMP, activin, and TGF-β signaling [73–76]. Down-regulation of Gpc-1 in PANC-1 cells attenuates tumor growth, angiogenesis, and metastasis *in vivo* in athymic mice [75]. Both HSulf-1 and HSulf-2 are also significantly upregulated in PDAC cell lines and stimulate autocrine Wnt signaling, which augments cancer growth [77]. HSulf-2 silencing blocks Wnt signaling and significantly reduces PDAC cell growth in an immuno-compromised mouse model. As with breast cancer, pancreatic cancer cells also protect themselves from NK activity. Since NK cells can only recognize cancer cells exhibiting certain 6-*O*-Sulfonation and *N*-Acetylation patterns, pancreatic cancer cells that express increased extracellular Hpa and aberrant HSulf activity exhibit much lower NK cell recognition [78].

Invasion and Metastasis—Sdc-1 is overexpressed in the majority of the pancreatic cancer tissue, surrounding metastatic lesions, and a significant amount is shed into serum [79]. Sdc-1 shedding correlates with increased mitogenic activity and cell invasive potential [79]. Hpa plays an important role in pancreatic cancer invasion and metastasis as well. Hpa1 mRNA is upregulated 7.9- and 30.2-fold in chronic pancreatitis and pancreatic cancer cells, respectively [80,81]. Hpa mRNA over expression is preferentially higher in primary tumor sites and correlates with decreased postoperative survival of patients [80]. Overexpression of Hpa leads to Sdc-1 and Gpc-1 cleavage, which in-turn leads to cellular growth via FGF-2 signaling and invasion of surrounding tissue [3].

Skin Cancer

Growth—Smetsers *et al*. found that melanoma cells only displayed certain GAG epitopes with particular sulfonation patterns on their cell-surface [82]. While the identity of these GAGs wasn't devolved in their findings, it is possible that the GAGs represented a combination of fragments from Glypican, Syndecan, and Perlecan (Plc) HSPGs. Gpc, Sdc, and Plc are involved in growth factor binding. Plc, overexpressed (upto 150 fold) in human melanoma samples, also acts as a co-receptor for growth factors such as FGF-2 and FGF-7 [83,84]. Plc knockdown greatly inhibits murine melanoma tumor growth and neovascularization [85].

Invasion and Metastasis—Exogenous Hpa and cell-surface Gpc expression moderate the ability of skin cancer to metastasize. Lung metastatic melanoma cells overexpress Hpa1 mRNA (upto 29-fold) compared to normal lung tissue [86]. In melanoma patients with lung metastases, Hpa1 is found around vascularized regions and in blood vessels near the invasion front, whereas tumor nodules contain very little Hpa [86,87]. Hpa1-expressing melanoma cells demonstrate increased invasion *in vitro* and metastasis to lung and liver *in vivo* [88,89]. Gpc expression also affects melanoma invasion and metastasis characteristics since antisense-mediated-Gpc1-knockdown reduces B16-F10 melanoma cell pulmonary metastasis by attenuating Gpc1-HBGF (Heparin binding growth factor) signaling [75]. In combination with Hpa overexpression, melanoma cells exhibit 3-OST gene hypermethylation and subsequent gene silencing [90]. While the implications of this modification are not yet known, it is possible that certain patterns of 3-*O* sulfonation impart cancerous phenotypic changes. Ma *et al*. have found that P-Selectin, a cell adhesion molecule, bound to HS-like molecules on melanoma cells even in the absence of its recognition motif [91]. Interplay between 3-OST, 6-OST, and HSulf-1/2 might play a role in modifying HS to confer P-Selectin binding ability and hence promote metastasis by allowing cells to migrate to secondary sites.

Colorectal Cancer

Growth—In human colorectal cancers, Sdc-1 and Sdc-4 are downregulated while Sdc-2 is upregulated [92,93]. In conjunction with these HSPGs, 6-OST-2 is also upregulated. Sdc-2 knockdown leads to G0/G1 cell cycle arrest, increased expression of tumor suppressor proteins, and consequentially reduced tumorigenic activity [93]. In contrast, Sdc-2 expression in colorectal cancer cells contributes to cell evolution into a migratory mesenchymal-like phenotype (flatter shape, more membranal projections, and loss of intercellular contacts) [94]. 6-OST-2 mRNA is also significantly upregulated in colonic mucinous adenocarcinoma whereas 6-OST-3 is the predominant isoform present in normal mucosa [95]. Evidence from ovarian cancer suggests that 6-OST overexpression correlates with FGF-2 signaling and cell proliferation [96].

Invasion and Metastasis—Hpa over- expression correlates with increased colon cancer proliferation, invasion, and metastatic potential. Friedmann *et al*. have found high levels of Hpa in lung, liver, and lymph tumor metastases, while the highest amounts were found in deeply invading colon carcinoma cells [97]. Hpa activity is critical in colon cancer progression

because stored FGFs attached to cell-surface HS are released by Hpa and MMP-7 [98]. Thus, in addition to making the ECM more permeable and susceptible to invasion, Hpa expression promotes cell proliferation and other growth factor related signals.

Lung and Brain Cancer

Growth—The roles of HS in lung and brain cancer are largely unknown, perhaps due to the delicacy of lung and brain tissue. Furthermore, since both these tissues are highly vascularized, cancers here are usually secondary metastases [99]. For lung cancer patients, serum Sdc-1 (S-Sdc-1) levels decline following tumor resection; whereas recurrent lung cancers demonstrate elevated S-Sdc-1 levels [100]. High S-Sdc-1 levels probably indicate high Hpa activity and extensive paracrine growth and proliferation signals.

Similarly, malignant glioma cells express high levels of Sdc-1 whereas nonneoplastic tissues do not [101]. Cell-surface Sdc-1 expression may correspond with FGF based growth factor signaling. It is also possible that overexpression of Sdc-1 and similar HSPGs is a distinguishing mark of cancer. Steck et al. generated antibodies that bound favorably to HSPGs from higher-grade gliomas [102]. From this they hypothesized that alternate HSPG expression patterns, and possibly sulfonation patterns, pertained to malignant transformation and growth potential of glial-cells. However, it is uncertain whether these alterations in HSPG expression are a cause or an effect of the transformation process.

Invasion and Metastasis—Hpa activity and mRNA are upregulated in lung and brain cancers as well. In a clinical study involving 114 lung cancer patients, cancer cells from 75% of the patients overexpressed Hpa [103]. Hpa over expression indicates increased invasive potential since Hpa knockdown in A549 lung cancer cells decreases their invasive potential *in vivo* [104]. Similarly in brain tumors, melanoma cells that are highly metastatic to the brain overexpress Hpa1 [105]. Hpa1 pretreated cells invade brain tissue in greater numbers and to greater tissue depths [105].

Other Cancers

While the focus of this review is on cancers of the brain, breast, lung, skin, pancreas, and colon, aberrant HS biosynthesis and catabolism play a role in several other cancers as well. EXT-1 and EXT-2, involved in heparan sulfate biosynthesis, are known tumor suppressor genes involved in preventing progression of osteochondromas to chondrosarcomas [106]. Several cancers, including ovarian cancer and head and neck squamous carcinoma, demonstrate extensive HSulf-1 silencing [107,108]. Re-expression of HSulf-1 in these cancers suppresses proliferation, enhances apoptosis *in vitro* and reduces angiogenesis [109]. Chen *et al*. found that the HSulf-1 promoter was more frequently methylated in DNA samples from cell-free serum samples of gastric cancer patients (55%) compared to healthy patients (19%) [109]. They proposed that this methylation-induced silencing of HSulf-1 could be used as an early diagnostic tool for cancer. Hpa is overexpressed in the invading front of endometrial cancers in humans where Hpa expression correlates with tumor-associated angiogenesis and invasion into lymph vascular space and myometrium [110,111]. It is also over expressed in renal cell carcinomas and head and neck carcinomas [112,113].

Underlying patterns of HSPG involvement in all cancers

Based on the previously stated roles of HS biosynthetic and catabolic enzymes in cancer, it is now possible to see several overarching patterns (Table 1, Fig. 4). Hpa, the sole mammalian enzyme to degrade HS, is overexpressed in most cancers. Hpa activity breaks down proteoglycans, increases endothelium permeability, releases stored cell-surface FGFs, and permits serum-HS to interact with FGFs. 3-OST, an enzyme that moderates rare HS fine

structural changes, is silenced by hypermethylation in several cancers [66]. Although demethylation of 3-OST in breast cancer cells didn't produce any visible changes, there must be a reason behind 3-OST silencing in such an array of cancers [66]. HSulf-1 also seems to be downregulated (via methylation) in several cancers. Since re-expressing HSulf-1 decreases cancer mitogenesis, cancer cells probably utilize hyper-sulfated residues that are normally controlled by HSulf-1 for growth signaling via FGF-2 signaling [114]. Interplay between Hpa and Sdc-1 in several cancers is also noteworthy. Both entities seem to act together to induce proliferation and autocrine growth signaling. Changes in HS biosynthetic and catabolic enzymes are essential to cancer growth. HS is a profound target for developing novel cancer therapeutics because modifying HS chains would affect Hpa, HSulf-1, HSulf-2, and 3-OST activity in tumor cells, which in turn would affect angiogenesis, growth-factor signal over-amplification, and tumor growth, invasion, and metastasis.

Current HS-based treatments

It has been known for decades that HS and other GAGs modulate tumor biology and are essential to cell survival. However, HS-specific treatments have only recently begun preliminary clinical trials. Several different treatment strategies have been the focus of recent research efforts. These strategies include: inhibition of Hpa with HS analogs such as PI-88, inhibition of tumor invasion and metastasis using non-anti-coagulant LMWH analogs, and inhibition of tumor growth using carbodiimide modified GAGs or 'neoglycans'.

Difficulties associated with cancer treatment

Treating cancer poses a challenge because cancer cells have several inherent defense mechanisms. Not only do cancer cells originate from the host system, but they also use natural cellular metabolic pathways to grow. Additionally, due to the genetic errors that manifest cancer, tumors are composed of heterogeneous populations of cells that respond differently to treatments and impart multi-drug resistance to tumors [115]. Moreover, cancer patients exhibit a hyper-coagulable state because cancer cells employ platelets and modified HS to evade immune cells. Several insightful studies implicate platelets in forming barriers that prevent NK cells from recognizing and destroying tumors by coagulating around cancer cells [116–118]. Depletion of platelet P-Selectins, which allow platelets to adhere to tumor cells, leads to reduced tumor dissemination, and increased tumor cell death [119]. To further complicate cancer diagnosis, there is an epigenetic aspect to the development of cancer. The probability of being diagnosed with cancer increases with age, as published by the American Cancer Society [120]. Since the disease manifests at varying ages, it is not yet possible to predict the onset of cancer. To combat such a variety of defense mechanisms employed by cancer cells, effective cancer therapies should be based on multiple anti-tumor mechanisms while utilizing pathways that are essential to survival of all cells.

Heparanase, a potent anti-cancer target

Hpa is a potent anti-cancer target because it is upregulated in a majority of cancers and plays a major role in tumor-induced angiogenesis, invasion and metastasis (Fig. 5). Based on available information, it is possible to propose one comprehensive pathway by which Hpa aids cancer by providing tumor cells with a self-induced proliferation loop. During hypoxia, cancer cells overexpress Hpa well above their normal Hpa levels [121]. Overexpressed Hpa is secreted in a pro-enzyme form. After reuptake, the proenzyme is cleaved, activated, and secreted once again [57,122]. The active enzyme then cleaves cell surface HS (i.e. Sdc-1 shedding) to form paracrine and autocrine signaling complexes [69].

Autocrine signaling complexes enhance FGF-HS-FGFR interactions and upregulate cellular signaling pathways. On one hand shed Sdc-1 are taken up by cancer cells and localized to the

nucleus where they affect expression of MMP-9, VEGF, and tissue factors [123,124]. On the other hand, shed Sdc-1 form trimeric complexes to stabilize FGFR-1 and FGF-1 interactions [114] Paracrine signaling complexes induce other tumor cells to proliferate as in breast cancer. The MMP activity then potentiates tumor invasion whereas VEGF and FGF activity increase tumor lymph node metastasis, angiogenesis and growth. Moreover, tissue factors promote clotting, angiogenesis, and platelet barrier formation around the tumor [125–129]. Newly formed cancer cells and improved nutrient supply then perpetuate tumor growth and heparanase production so that the self-proliferation loop continues (Fig. 5).

PI-88 and related Heparan Sulfate analogs

The structures, advantages, and disadvantages of several Hpa inhibitors have been discussed in detail by Ferro et al.[130] One particularly interesting Hpa inhibitor is PI-88 (Fig. 6), a highly sulfated oligosaccharide mixture, which is currently undergoing phase II clinical trials for treating patients with metastatic melanoma [131,132]. It prevents angiogenesis and tumor growth by blocking FGF-1, FGF-2, and VEGF interactions with their receptors and HS [131] PI-88 reduces the growth of invasive rat mammary adenocarcinoma cells by 50%. It also reduces lymph node and blood metastases [133]. Among 400 patients already tested, PI-88 has shown minimal side-effects and excellent efficacy whereby one patient with melanoma had a partial response for >50 months [131]. Based on improvements to PI-88 chemistry, several new analogs of PI-88, known as the PG500 series, have been developed [134]. Some advantages of these new molecules include improved inhibition of FGF- and VEGF- induced endothelial cell tube formation and lower plasma clearance levels compared to PI-88 [131]

Low molecular weight non-anticoagulant heparins

Another current HS-based treatment strategy is based on heparin's natural anti-cancer properties. While the molecular details of heparin's effects on cancer have not been completely resolved, it is believed that heparin inhibits tumor metastasis by inhibiting Hpa activity, preventing P-Selectin mediated cell-platelet interactions, and releasing tissue factor pathway inhibitor, a potent endogenous anti-angiogenic agent [135,136]. However, heparin is also a potent anti-coagulant and cannot be used to treat cancer patients for a prolonged period of time because it may lead to bleeding complications. Several groups have prepared low molecular weight anti-coagulant heparin (LMWH) derivates to mimic heparin's anti-mitogenic activity without its anti-coagulant properties. Non-anticoagulant LMWH are produced by separating the anti-thrombin binding sequence from unfractionated heparin, chemically desulfating heparin at the 2-O and 3-O sulfonation sites or by using periodate oxidation (also known as the 'glycol split') to decrease the number of glucuronic acid residues which are critical for binding to antithrombin III [136] Dalteparin, a 5kD non-anticoagulant LMWH, has been shown to improve 1- year survival of cancer patients with small cell lung cancer by 11% and 2-year survival by 17% in clinical studies without presenting bleeding complications [137]. Anti-coagulant LMWHs have shown promise in mouse models but have not yet entered clinical trials [136].

Neoglycan and carbodiimide modified GAGs

Pumphrey *et al*. have developed a new class of anti-cancer agents, termed 'neoglycans', based on carbodiimide-modified CS and heparin chains. While the actual structure of these chains is unclear, carbodiimide modification of GAG chains could produce crosslinked chains that form GAG complexes via reaction of the free amine groups. These crosslinked meshes may resemble multimeric arrays of GAGs found on syndecans/glypicans. However, it is essential to note that GAG chains have abundant carboxyl groups and limited amine functionality. Therefore, the carbodiimide reaction may not go to completion and thus may produce highly sulfated neoglycans functionalized with several *O*-acylisourea groups along the chains.

These molecules significantly reduce myeloma and breast cancer cell viability *in vitro* in a dose dependent manner [138]. NeoCS treatment at 32 μg/ml reduced ARP-1 cell viability by 96%. As reported in this study, the IC_{50} values for neoHeparin and neoCS on ARP-1 myeloma cells are 21.94 μg/ml and 14.79 μg/ml, respectively. These molecules trigger apoptosis in ARP-1 and MDA-MB-231 (breast cancer) cells, however the mechanism of their action and uptake are still not known. neoCS was a more potent inhibitor for a majority of cell lines tested *in vitro* and a single dose of neoCS completely eliminated MDA-MB-231 tumors implanted into BALB/c nu/nu mice. After treatment with the neoCS, only 1 tumor reemerged out of 15 separate *in vivo* tests. These modified GAGs show promise for future anti-cancer drug development. However, one should exercise caution because these modified GAG chains are unlikely to be metabolized in vivo and therefore may possess toxicity.

There are also several other therapeutic strategies based on HS-like molecules. Other areas of research include: developing FGF-2 inhibitors that prevent FGF-HS-induced cellular growth, developing drug delivery vehicles that utilize HS-mediated internalization into cells, and modulating HS-GAG production in cancer cells using novel drugs [139–142]. Suramin, a non-heparin Hpa inhibitors, has also shown promise *in vitro* and has undergone several phase I clinical trials [143]. Preliminary results from these studies are promising and reinforce our hypothesis that modulating HS fine structures, their biosynthesis and interactions with the tumor microenvironment will lead to potential drug therapies for cancer in the near future.

Future Directions

HS-based treatments can be more effective against cancer

Cancer cells have been suggested to mimic misbehaving stem cells where erroneous cellular machinery causes cells to trigger abnormal signals, misinterpret incoming signals, and differentiate into several families of cancerous cells [144]. HS chains, ubiquitously expressed on cell-surfaces and in ECM throughout the body, act as molecular antennae that send and receive signals through binding to a wide variety of molecules such as FGF-2, VEGF, HB-EGF, P-Selectin, MMP-7 and MMP-9 [15,123,135,145,146] or releasing these sequestered molecules from the cell surface/ECM. Thus, therapeutics that modify HS will be able to attack cancer cells on multiple fronts because they can target P-Selectin interactions, growth factor binding, the coagulation cascade, protease activation and inhibition, Heparanase activation and activity, and possibly tumor evolution/differentiation [147].

Novel chemical biology approaches to treating cancer

Future research should utilize knowledge of the downstream effects of fine structural changes in HS to invent novel therapeutics that affect a wide range of tumor-specific pathological processes. Unraveling the mysteries of ‘GAGOSOMES’, which are responsible for forming and controlling the HS biosynthesis enzyme complex, may also yield a valuable target [148, 149]. Modulating HS fine structures will affect HS-ECM, HS-FGF, and HS-protein interactions and prevent cancer growth without causing any adverse downstream effects.

It is possible to inhibit HS/CS biosynthesis by utilizing 4-deoxy-4-fluoro-xylosides [150]. Decreasing overall levels of HS may reduce FGF and VEGF signaling and affect tumor proliferation, invasion and metastasis. Inhibiting HS production may also prevent Hpa activation and hence restrain Hpa activity [122]. It is also possible to stimulate HS and CS GAG production by utilizing xylosides to prime GAG chains *in vitro* or *in vivo* [151]. Increasing HS can render cancer cells more adherent and less metastatic due to enhanced integrin binding [152]. However, these methods produce a wide array of GAGs with no specific properties. Further research into the chemistry and biology of these xylosides is necessary to make treatments from xyloside-induced GAGs with fine structural elements that can compete

with endogenous GAGs made by cancer cells and disrupt cancer growth factor signaling and Hpa activity.

In summary, this article proposes that controlling GAG biosynthesis and catabolism in general, and HS biosynthesis and catabolism in particular, may be a powerful tool to design effective treatments against cancer and perhaps even other diseases. Key enzymes involved in `HS biosynthesis and catabolism include HSulf-1, HSulf-2, Hpa, 3-OST, and 6-OST; each of these enzymes is differentially expressed in various cancers. By changing HS structure, these enzymes affect several downstream cellular processes that are integral to cancer progression. However, there are still several unanswered questions relating to the use of HS in treating cancer. Which Xylosides prime GAGs with fine structural elements that prevent FGF binding and inhibit cancerous phenotype changes? What is the role of 3-O sulfation, a rare HS modification, in cancer progression? In a novel experiment, Liu et al. injected Heparinase I and III into mice with B16BL6 melanoma and found that the specificity of the enzymes dictated whether tumors regressed (Heparinase III) or advanced (Heparinase I) due to enzymatic cleavage of cellular HS [153]. They found that the tumor cell GAG fragments produced by Heparinase III digestion caused upto 75% tumor growth inhibition whereas fragments produced by Heparinase I digestion significantly enhanced growth. This experiment reinforces the concept that there is an incredible specificity to the structural/biological relationships between HS fine structures and the biological effects of these molecules on cancers. However, the metaphorical HS elephant has many facets that need to be extensively studied before we can develop any effective anti-cancer drugs [154]. Thus, chemical biologists, who are at the interface of understanding both the biological as well as the chemical roles of HS, have ample opportunity to research and collaborate in order to find an effective HS-based scaffold for treating cancer without any side effects.

Acknowledgments

B. K. is supported by grants from the National Institutes of Health (GM075168), Mizutani Foundation for Glycoscience, American Heart Association National Scientist development award, and the Human Frontier Science Program

References

1. Sasisekharan R, Shriver Z, Venkataraman G, Narayanasami U. Roles of heparan-sulphate glycosaminoglycans in cancer. Nat Rev Cancer 2002;2:521–528. [PubMed: 12094238]
2. Sanderson RD. Heparan sulfate proteoglycans in invasion and metastasis. Semin Cell Dev Biol 2001;12:89–98. [PubMed: 11292374]
3. Sanderson RD, Yang Y, Kelly T, MacLeod V, Dai Y, Theus A. Enzymatic remodeling of heparan sulfate proteoglycans within the tumor microenvironment: growth regulation and the prospect of new cancer therapies. J Cell Biochem 2005;96:897–905. [PubMed: 16149080]
4. Liotta LA, Kohn EC. The microenvironment of the tumour-host interface. Nature 2001;411:375–379. [PubMed: 11357145]
5. Carmeliet P. Angiogenesis in life, disease and medicine. Nature 2005;438:932–936. [PubMed: 16355210]
6. Liu D, Shriver Z, Qi Y, Venkataraman G, Sasisekharan R. Dynamic regulation of tumor growth and metastasis by heparan sulfate glycosaminoglycans. Semin Thromb Hemost 2002;28:67–78. [PubMed: 11885027]
7. Ribatti D, Marimpietri D, Pastorino F, Brignole C, Nico B, Vacca A, Ponzoni M. Angiogenesis in neuroblastoma. Ann N Y Acad Sci 2004;1028:133–142. [PubMed: 15650239]
8. Folkman J. Tumor angiogensis: role in regulation of tumor growth. Symp Soc Dev Biol 1974;30:43–52. [PubMed: 4600889]
9. Turk V, Kos J, Turk B. Cysteine cathepsins (proteases)--on the main stage of cancer? Cancer Cell 2004;5:409–410. [PubMed: 15144947]

10. Giannelli G, Falk-Marzillier J, Schiraldi O, Stetler-Stevenson WG, Quaranta V. Induction of cell migration by matrix metalloprotease-2 cleavage of laminin-5. Science 1997;277:225–228. [PubMed: 9211848]
11. Ravanko K, Jarvinen K, Helin J, Kalkkinen N, Holtta E. Cysteine cathepsins are central contributors of invasion by cultured adenosylmethionine decarboxylase-transformed rodent fibroblasts. Cancer Res 2004;64:8831–8838. [PubMed: 15604241]
12. Matrisian LM, Wright J, Newell K, Witty JP. Matrix-degrading metalloproteinases in tumor progression. Princess Takamatsu Symp 1994;24:152–161. [PubMed: 8983072]
13. Liabakk NB, Talbot I, Smith RA, Wilkinson K, Balkwill F. Matrix metalloprotease 2 (MMP-2) and matrix metalloprotease 9 (MMP-9) type IV collagenases in colorectal cancer. Cancer Res 1996;56:190–196. [PubMed: 8548762]
14. Whitelock JM, Melrose J, Iozzo RV. Diverse cell signaling events modulated by perlecan. Biochemistry 2008;47:11174–11183. [PubMed: 18826258]
15. Coombe DR. Biological implications of glycosaminoglycan interactions with haemopoietic cytokines. Immunol Cell Biol 2008;86:598–607. [PubMed: 18626488]
16. Laguri C, Arenzana-Seisdedos F, Lortat-Jacob H. Relationships between glycosaminoglycan and receptor binding sites in chemokines-the CXCL12 example. Carbohydr Res 2008;343:2018–2023. [PubMed: 18334249]
17. Adatia R, Albini A, Carlone S, Giunciuglio D, Benelli R, Santi L, Noonan DM. Suppression of invasive behavior of melanoma cells by stable expression of anti-sense perlecan cDNA. Ann Oncol 1997;8:1257–1261. [PubMed: 9496392]
18. Su G, Meyer K, Nandini CD, Qiao D, Salamat S, Friedl A. Glypican-1 is frequently overexpressed in human gliomas and enhances FGF-2 signaling in glioma cells. Am J Pathol 2006;168:2014–2026. [PubMed: 16723715]
19. Plotnikov AN, Schlessinger J, Hubbard SR, Mohammadi M. Structural basis for FGF receptor dimerization and activation. Cell 1999;98:641–650. [PubMed: 10490103]
20. Stauber DJ, DiGabriele AD, Hendrickson WA. Structural interactions of fibroblast growth factor receptor with its ligands. Proc Natl Acad Sci U S A 2000;97:49–54. [PubMed: 10618369]
21. Guimond S, Maccarana M, Olwin BB, Lindahl U, Rapraeger AC. Activating and inhibitory heparin sequences for FGF-2 (basic FGF). Distinct requirements for FGF-1, FGF-2, and FGF-4. J Biol Chem 1993;268:23906–23914. [PubMed: 7693696]
22. Jia J, Maccarana M, Zhang X, Bespalov M, Lindahl U, Li JP. Lack of L-iduronic acid in heparan sulfate affects interaction with growth factors and cell signaling. J Biol Chem 2009;284:15942–15950. [PubMed: 19336402]
23. Lundin L, Larsson H, Kreuger J, Kanda S, Lindahl U, Salmivirta M, Claesson-Welsh L. Selectively desulfated heparin inhibits fibroblast growth factor-induced mitogenicity and angiogenesis. J Biol Chem 2000;275:24653–24660. [PubMed: 10816596]
24. Sugaya N, Habuchi H, Nagai N, Ashikari-Hada S, Kimata K. 6-O-sulfation of heparan sulfate differentially regulates various fibroblast growth factor-dependent signalings in culture. J Biol Chem 2008;283:10366–10376. [PubMed: 18281280]
25. Pauli BU, Schwartz DE, Thonar EJ, Kuettner KE. Tumor invasion and host extracellular matrix. Cancer Metastasis Rev 1983;2:129–152. [PubMed: 6352011]
26. Nakato H, Kimata K. Heparan sulfate fine structure and specificity of proteoglycan functions. Biochim Biophys Acta 2002;1573:312–318. [PubMed: 12417413]
27. Jansson L, Lindahl U. Evidence for the existence of a multichain proteoglycan of heparan sulphate. Biochem J 1970;117:699–702. [PubMed: 4247363]
28. Iozzo RV. Matrix proteoglycans: from molecular design to cellular function. Annu Rev Biochem 1998;67:609–652. [PubMed: 9759499]
29. Lindahl U, Roden L. The chondroitin 4-sulfate-protein linkage. J Biol Chem 1966;241:2113–2119. [PubMed: 4287762]
30. Fransson LA, Silverberg I. Carlstedt I. Structure of the heparan sulfateprotein linkage region. Demonstration of the sequence galactosyl-galactosyl-xylose-2-phosphate. J Biol Chem 1985;260:14722–14726. [PubMed: 2932448]

31. Salmivirta M, Lidholt K, Lindahl U. Heparan sulfate: a piece of information. FASEB J 1996;10:1270–1279. [PubMed: 8836040]
32. Rabenstein DL. Heparin and heparan sulfate: structure and function. Nat Prod Rep 2002;19:312–331. [PubMed: 12137280]
33. Esko JD, Selleck SB. Order out of chaos: assembly of ligand binding sites in heparan sulfate. Annu Rev Biochem 2002;71:435–471. [PubMed: 12045103]
34. Lindahl U, Kusche M, Lidholt K, Oscarsson LG. Biosynthesis of heparin and heparan sulfate. Ann N Y Acad Sci 1989;556:36–50. [PubMed: 2525361]
35. Ahn J, Ludecke HJ, Lindow S, Horton WA, Lee B, Wagner MJ, Horsthemke B, Wells DE. Cloning of the putative tumour suppressor gene for hereditary multiple exostoses (EXT1). Nat Genet 1995;11:137–143. [PubMed: 7550340]
36. Sugahara K, Kitagawa H. Heparin and heparan sulfate biosynthesis. IUBMB Life 2002;54:163–175. [PubMed: 12512855]
37. Kitagawa H, Shimakawa H, Sugahara K. The tumor suppressor EXT-like gene EXTL2 encodes an alpha1, 4-Nacetylhexosaminyltransferase that transfers N-acetylgalactosamine and N-acetylglucosamine to the common glycosaminoglycan-protein linkage region. The key enzyme for the chain initiation of heparan sulfate. J Biol Chem 1999;274:13933–13937. [PubMed: 10318803]
38. Izumikawa T, Koike T, Shiozawa S, Sugahara K, Tamura J, Kitagawa H. Identification of chondroitin sulfate glucuronyltransferase as chondroitin synthase-3 involved in chondroitin polymerization: chondroitin polymerization is achieved by multiple enzyme complexes consisting of chondroitin synthase family members. J Biol Chem 2008;283:11396–11406. [PubMed: 18316376]
39. Kitagawa H, Uyama T, Sugahara K. Molecular cloning and expression of a human chondroitin synthase. J Biol Chem 2001;276:38721–38726. [PubMed: 11514575]
40. Lind T, Tufaro F, McCormick C, Lindahl U, Lidholt K. The putative tumor suppressors EXT1 and EXT2 are glycosyltransferases required for the biosynthesis of heparan sulfate. J Biol Chem 1998;273:26265–26268. [PubMed: 9756849]
41. Prydz K, Dalen KT. Synthesis and sorting of proteoglycans. J Cell Sci 2000;113(Pt 2):193–205. [PubMed: 10633071]
42. Rosenberg RD, Shworak NW, Liu J, Schwartz JJ, Zhang L. Heparan sulfate proteoglycans of the cardiovascular system. Specific structures emerge but how is synthesis regulated? J Clin Invest 1997;100:S67–S75. [PubMed: 9413405]
43. Esko JD, Lindahl U. Molecular diversity of heparan sulfate. J Clin Invest 2001;108:169–173. [PubMed: 11457867]
44. Morimoto-Tomita M, Uchimura K, Werb Z, Hemmerich S, Rosen SD. Cloning and characterization of two extracellular heparin-degrading endosulfatases in mice and humans. J Biol Chem 2002;277:49175–49185. [PubMed: 12368295]
45. Dai Y, Yang Y, MacLeod V, Yue X, Rapraeger AC, Shriver Z, Venkataraman G, Sasisekharan R, Sanderson RD. HSulf-1 and HSulf-2 are potent inhibitors of myeloma tumor growth in vivo. J Biol Chem 2005;280:40066–40073. [PubMed: 16192265]
46. Narita K, Chien J, Mullany SA, Staub J, Qian X, Lingle WL, Shridhar V. Loss of HSulf-1 expression enhances autocrine signaling mediated by amphiregulin in breast cancer. J Biol Chem 2007;282:14413–14420. [PubMed: 17363371]
47. Ohto T, Uchida H, Yamazaki H, Keino-Masu K, Matsui A, Masu M. Identification of a novel nonlysosomal sulphatase expressed in the floor plate, choroid plexus and cartilage. Genes Cells 2002;7:173–185. [PubMed: 11895481]
48. Ai X, Do AT, Lozynska O, Kusche-Gullberg M, Lindahl U, Emerson CP Jr. QSulf1 remodels the 6-O sulfation states of cell surface heparan sulfate proteoglycans to promote Wnt signaling. J Cell Biol 2003;162:341–351. [PubMed: 12860968]
49. Shworak NW, Liu J, Fritze LM, Schwartz JJ, Zhang L, Logeart D, Rosenberg RD. Molecular cloning and expression of mouse and human cDNAs encoding heparan sulfate D-glucosaminyl 3-O-sulfotransferase. J Biol Chem 1997;272:28008–28019. [PubMed: 9346953]
50. Tiwari V, Clement C, Duncan MB, Chen J, Liu J, Shukla D. A role for 3-O-sulfated heparan sulfate in cell fusion induced by herpes simplex virus type 1. J Gen Virol 2004;85:805–809. [PubMed: 15039523]

51. Liu J, Shworak NW, Sinay P, Schwartz JJ, Zhang L, Fritze LM, Rosenberg RD. Expression of heparan sulfate D-glucosaminyl 3-O-sulfotransferase isoforms reveals novel substrate specificities. J Biol Chem 1999;274:5185–5192. [PubMed: 9988768]

52. Mochizuki H, Yoshida K, Gotoh M, Sugioka S, Kikuchi N, Kwon YD, Tawada A, Maeyama K, Inaba N, Hiruma T, Kimata K, Narimatsu H. Characterization of a heparan sulfate 3-O-sulfotransferase-5, an enzyme synthesizing a tetrasulfated disaccharide. J Biol Chem 2003;278:26780–26787. [PubMed: 12740361]

53. Smeds E, Habuchi H, Do AT, Hjertson E, Grundberg H, Kimata K, Lindahl U, Kusche-Gullberg M. Substrate specificities of mouse heparan sulphate glucosaminyl 6-O-sulphotransferases. Biochem J 2003;372:371–380. [PubMed: 12611590]

54. Zhang L, Beeler DL, Lawrence R, Lech M, Liu J, Davis JC, Shriver Z, Sasisekharan R, Rosenberg RD. 6-O-sulfotransferase-1 represents a critical enzyme in the anticoagulant heparan sulfate biosynthetic pathway. J Biol Chem 2001;276:42311–42321. [PubMed: 11551899]

55. Kusche M, Backstrom G, Riesenfeld J, Petitou M, Choay J, Lindahl U. Biosynthesis of heparin. O-sulfation of the antithrombin-binding region. J Biol Chem 1988;263:15474–15484. [PubMed: 3139669]

56. Habuchi H, Nagai N, Sugaya N, Atsumi F, Stevens RL, Kimata K. Mice deficient in heparan sulfate 6-O-sulfotransferase-1 exhibit defective heparan sulfate biosynthesis, abnormal placentation, and late embryonic lethality. J Biol Chem 2007;282:15578–15588. [PubMed: 17405882]

57. Vlodavsky I, Abboud-Jarrous G, Elkin M, Naggi A, Casu B, Sasisekharan R, Ilan N. The impact of heparanese and heparin on cancer metastasis and angiogenesis. Pathophysiol Haemost Thromb 2006;35:116–127. [PubMed: 16855356]

58. Naparstek Y, Cohen IR, Fuks Z, Vlodavsky I. Activated T lymphocytes produce a matrix-degrading heparan sulphate endoglycosidase. Nature 1984;310:241–244. [PubMed: 6205275]

59. Oosta GM, Favreau LV, Beeler DL, Rosenberg RD. Purification and properties of human platelet heparitinase. J Biol Chem 1982;257:11249–11255. [PubMed: 7118882]

60. Bret C, Hose D, Reme T, Sprynski AC, Mahtouk K, Schved JF, Quittet P, Rossi JF, Goldschmidt H, Klein B. Expression of genes encoding for proteins involved in heparan sulphate and chondroitin sulphate chain synthesis and modification in normal and malignant plasma cells. Br J Haematol 2009;145:350–368. [PubMed: 19298595]

61. Matsuda K, Maruyama H, Guo F, Kleeff J, Itakura J, Matsumoto Y, Lander AD, Korc M. Glypican-1 is overexpressed in human breast cancer and modulates the mitogenic effects of multiple heparin-binding growth factors in breast cancer cells. Cancer Res 2001;61:5562–5569. [PubMed: 11454708]

62. Nurcombe V, Smart CE, Chipperfield H, Cool SM, Boilly B, Hondermarck H. The proliferative and migratory activities of breast cancer cells can be differentially regulated by heparan sulfates. J Biol Chem 2000;275:30009–30018. [PubMed: 10862617]

63. Delehedde M, Deudon E, Boilly B, Hondermarck H. [Involvement of sulfated proteoglycans in the control of proliferation of MCF-7 breast cancer cells]. Bull Cancer 1996;83:129–134. [PubMed: 8652906]

64. Damiens E, El Yazidi I, Mazurier J, Elass-Rochard E, Duthille I, Spik G, Boilly-Marer Y. Role of heparan sulphate proteoglycans in the regulation of human lactoferrin binding and activity in the MDA-MB-231 breast cancer cell line. Eur J Cell Biol 1998;77:344–351. [PubMed: 9930659]

65. Morimoto-Tomita M, Uchimura K, Bistrup A, Lum DH, Egeblad M, Boudreau N, Werb Z, Rosen SD. Sulf-2, a proangiogenic heparan sulfate endosulfatase, is upregulated in breast cancer. Neoplasia 2005;7:1001–1010. [PubMed: 16331886]

66. Miyamoto K, Asada K, Fukutomi T, Okochi E, Yagi Y, Hasegawa T, Asahara T, Sugimura T, Ushijima T. Methylation-associated silencing of heparan sulfate D-glucosaminyl 3-O-sulfotransferase-2 (3-OST-2) in human breast, colon, lung and pancreatic cancers. Oncogene 2003;22:274–280. [PubMed: 12527896]

67. Maxhimer JB, Pesce CE, Stewart RA, Gattuso P, Prinz RA, Xu X. Ductal carcinoma in situ of the breast and heparanase-1 expression: a molecular explanation for more aggressive subtypes. J Am Coll Surg 2005;200:328–335. [PubMed: 15737842]

68. Cohen I, Pappo O, Elkin M, San T, Bar-Shavit R, Hazan R, Peretz T, Vlodavsky I, Abramovitch R. Heparanase promotes growth, angiogenesis and survival of primary breast tumors. Int J Cancer 2006;118:1609–1617. [PubMed: 16217746]
69. Yang Y, Macleod V, Miao HQ, Theus A, Zhan F, Shaughnessy JD Jr, Sawyer J, Li JP, Zcharia E, Vlodavsky I, Sanderson RD. Heparanase enhances syndecan-1 shedding: a novel mechanism for stimulation of tumor growth and metastasis. J Biol Chem 2007;282:13326–13333. [PubMed: 17347152]
70. Su G, Blaine SA, Qiao D, Friedl A. Shedding of syndecan-1 by stromal fibroblasts stimulates human breast cancer cell proliferation via FGF2 activation. J Biol Chem 2007;282:14906–14915. [PubMed: 17344212]
71. Theodoro TR, de Matos LL, Sant Anna AV, Fonseca FL, Semedo P, Martins LC, Nader HB, Del Giglio A, da Silva Pinhal MA. Heparanase expression in circulating lymphocytes of breast cancer patients depends on the presence of the primary tumor and/or systemic metastasis. Neoplasia 2007;9:504–510. [PubMed: 17603633]
72. Pikas DS, Li JP, Vlodavsky I, Lindahl U. Substrate specificity of heparanases from human hepatoma and platelets. J Biol Chem 1998;273:18770–18777. [PubMed: 9668050]
73. Kleeff J, Ishiwata T, Kumbasar A, Friess H, Buchler MW, Lander AD, Korc M. The cell-surface heparan sulfate proteoglycan glypican-1 regulates growth factor action in pancreatic carcinoma cells and is overexpressed in human pancreatic cancer. J Clin Invest 1998;102:1662–1673. [PubMed: 9802880]
74. Kayed H, Kleeff J, Keleg S, Jiang X, Penzel R, Giese T, Zentgraf H, Buchler MW, Korc M, Friess H. Correlation of glypican-1 expression with TGF-beta, BMP, and activin receptors in pancreatic ductal adenocarcinoma. Int J Oncol 2006;29:1139–1148. [PubMed: 17016645]
75. Aikawa T, Whipple CA, Lopez ME, Gunn J, Young A, Lander AD, Korc M. Glypican-1 modulates the angiogenic and metastatic potential of human and mouse cancer cells. J Clin Invest 2008;118:89–99. [PubMed: 18064304]
76. Li J, Kleeff J, Kayed H, Felix K, Penzel R, Buchler MW, Korc M, Friess H. Glypican-1 antisense transfection modulates TGF-beta-dependent signaling in Colo-357 pancreatic cancer cells. Biochem Biophys Res Commun 2004;320:1148–1155. [PubMed: 15249209]
77. Nawroth R, van Zante A, Cervantes S, McManus M, Hebrok M, Rosen SD. Extracellular sulfatases, elements of the Wnt signaling pathway, positively regulate growth and tumorigenicity of human pancreatic cancer cells. PLoS ONE 2007;2:e392. [PubMed: 17460759]
78. Bloushtain N, Qimron U, Bar-Ilan A, Hershkovitz O, Gazit R, Fima E, Korc M, Vlodavsky I, Bovin NV, Porgador A. Membrane-associated heparan sulfate proteoglycans are involved in the recognition of cellular targets by NKp30 and NKp46. J Immunol 2004;173:2392–2401. [PubMed: 15294952]
79. Conejo JR, Kleeff J, Koliopanos A, Matsuda K, Zhu ZW, Goecke H, Bicheng N, Zimmermann A, Korc M, Friess H, Buchler MW. Syndecan-1 expression is up-regulated in pancreatic but not in other gastrointestinal cancers. Int J Cancer 2000;88:12–20. [PubMed: 10962434]
80. Koliopanos A, Friess H, Kleeff J, Shi X, Liao Q, Pecker I, Vlodavsky I, Zimmermann A, Buchler MW. Heparanase expression in primary and metastatic pancreatic cancer. Cancer Res 2001;61:4655–4659. [PubMed: 11406531]
81. Kim AW, Xu X, Hollinger EF, Gattuso P, Godellas CV, Prinz RA. Human heparanase-1 gene expression in pancreatic adenocarcinoma. J Gastrointest Surg 2002;6:167–172. [PubMed: 11992801]
82. Smetsers TF, van de Westerlo EM, ten Dam GB, Clarijs R, Versteeg EM, van Geloof WL, Veerkamp JH, van Muijen GN, van Kuppevelt TH. Localization and characterization of melanoma-associated glycosaminoglycans: differential expression of chondroitin and heparan sulfate epitopes in melanoma. Cancer Res 2003;63:2965–2970. [PubMed: 12782604]
83. Iozzo RV, Cohen IR, Grassel S, Murdoch AD. The biology of perlecan: the multifaceted heparan sulphate proteoglycan of basement membranes and pericellular matrices. Biochem J 1994;302(Pt 3):625–639. [PubMed: 7945186]
84. Cohen IR, Murdoch AD, Naso MF, Marchetti D, Berd D, Iozzo RV. Abnormal expression of perlecan proteoglycan in metastatic melanomas. Cancer Res 1994;54:5771–5774. [PubMed: 7954396]

85. Sharma B, Handler M, Eichstetter I, Whitelock JM, Nugent MA, Iozzo RV. Antisense targeting of perlecan blocks tumor growth and angiogenesis in vivo. J Clin Invest 1998;102:1599–1608. [PubMed: 9788974]
86. Murry BP, Greiter-Wilke A, Paulsen DP, Hiatt KM, Beltrami CA, Marchetti D. Selective heparanase localization in malignant melanoma. Int J Oncol 2005;26:345–352. [PubMed: 15645118]
87. Komatsu N, Waki M, Sue M, Tokuda C, Kasaoka T, Nakajima M, Higashi N, Irimura T. Heparanase expression in B16 melanoma cells and peripheral blood neutrophils before and after extravasation detected by novel anti-mouse heparanase monoclonal antibodies. J Immunol Methods 2008;331:82–93. [PubMed: 18162185]
88. Roy M, Reiland J, Murry BP, Chouljenko V, Kousoulas KG, Marchetti D. Antisense-mediated suppression of Heparanase gene inhibits melanoma cell invasion. Neoplasia 2005;7:253–262. [PubMed: 15799825]
89. Vlodavsky I, Friedmann Y, Elkin M, Aingorn H, Atzmon R, Ishai-Michaeli R, Bitan M, Pappo O, Peretz T, Michal I, Spector L, Pecker I. Mammalian heparanase: gene cloning, expression and function in tumor progression and metastasis. Nat Med 1999;5:793–802. [PubMed: 10395325]
90. Furuta J, Umebayashi Y, Miyamoto K, Kikuchi K, Otsuka F, Sugimura T, Ushijima T. Promoter methylation profiling of 30 genes in human malignant melanoma. Cancer Sci 2004;95:962–968. [PubMed: 15596045]
91. Ma YQ, Geng JG. Heparan sulfate-like proteoglycans mediate adhesion of human malignant melanoma A375 cells to P-selectin under flow. J Immunol 2000;165:558–565. [PubMed: 10861096]
92. Giordano RJ. Heparanase-2 and syndecan-1 in colon cancer: the ugly ducklings or the beautiful swans? Eur J Gastroenterol Hepatol 2008;20:716–718. [PubMed: 18528290]
93. Park H, Kim Y, Lim Y, Han I, Oh ES. Syndecan-2 mediates adhesion and proliferation of colon carcinoma cells. J Biol Chem 2002;277:29730–29736. [PubMed: 12055189]
94. Contreras HR, Fabre M, Granes F, Casaroli-Marano R, Rocamora N, Herreros AG, Reina M, Vilaro S. Syndecan-2 expression in colorectal cancer-derived HT-29 M6 epithelial cells induces a migratory phenotype. Biochem Biophys Res Commun 2001;286:742–751. [PubMed: 11520060]
95. Seko A, Nagata K, Yonezawa S, Yamashita K. Ectopic expression of a GlcNAc 6-O-sulfotransferase, GlcNAc6ST-2, in colonic mucinous adenocarcinoma. Glycobiology 2002;12:379–388. [PubMed: 12107080]
96. Backen AC, Cole CL, Lau SC, Clamp AR, McVey R, Gallagher JT, Jayson GC. Heparan sulphate synthetic and editing enzymes in ovarian cancer. Br J Cancer 2007;96:1544–1548. [PubMed: 17437011]
97. Friedmann Y, Vlodavsky I, Aingorn H, Aviv A, Peretz T, Pecker I, Pappo O. Expression of heparanase in normal, dysplastic, and neoplastic human colonic mucosa and stroma. Evidence for its role in colonic tumorigenesis. Am J Pathol 2000;157:1167–1175. [PubMed: 11021821]
98. Vlodavsky I, Elkin M, Pappo O, Aingorn H, Atzmon R, Ishai-Michaeli R, Aviv A, Pecker I, Friedmann Y. Mammalian heparanase as mediator of tumor metastasis and angiogenesis. Isr Med Assoc J 2000; (2 Suppl):37–45. [PubMed: 10909416]
99. Chambers AF, Groom AC, MacDonald IC. Dissemination and growth of cancer cells in metastatic sites. Nat Rev Cancer 2002;2:563–572. [PubMed: 12154349]
100. Anttonen A, Leppa S, Heikkila P, Grenman R, Joensuu H. Effect of treatment of larynx and hypopharynx carcinomas on serum syndecan-1 concentrations. J Cancer Res Clin Oncol 2006;132:451–457. [PubMed: 16557382]
101. Watanabe A, Mabuchi T, Satoh E, Furuya K, Zhang L, Maeda S, Naganuma H. Expression of syndecans, a heparan sulfate proteoglycan, in malignant gliomas: participation of nuclear factor-kappaB in upregulation of syndecan-1 expression. J Neurooncol 2006;77:25–32. [PubMed: 16132527]
102. Steck PA, Moser RP, Bruner JM, Liang L, Freidman AN, Hwang TL, Yung WK. Altered expression and distribution of heparan sulfate proteoglycans in human gliomas. Cancer Res 1989;49:2096–2103. [PubMed: 2522816]
103. Cohen E, Doweck I, Naroditsky I, Ben-Izhak O, Kremer R, Best LA, Vlodavsky I, Ilan N. Heparanase is overexpressed in lung cancer and correlates inversely with patient survival. Cancer 2008;113:1004–1011. [PubMed: 18618498]

104. Uno F, Fujiwara T, Takata Y, Ohtani S, Katsuda K, Takaoka M, Ohkawa T, Naomoto Y, Nakajima M, Tanaka N. Antisense-mediated suppression of human heparanase gene expression inhibits pleural dissemination of human cancer cells. Cancer Res 2001;61:7855–7860. [PubMed: 11691803]
105. Murry BP, Blust BE, Singh A, Foster TP, Marchetti D. Heparanase mechanisms of melanoma metastasis to the brain: Development and use of a brain slice model. J Cell Biochem 2006;97:217–225. [PubMed: 16288472]
106. Schrage YM, Hameetman L, Szuhai K, Cleton-Jansen AM, Taminiau AH, Hogendoorn PC, Bovee JV. Aberrant heparan sulfate proteoglycan localization, despite normal exostosin, in central chondrosarcoma. Am J Pathol 2009;174:979–988. [PubMed: 19179614]
107. Lai J, Chien J, Staub J, Avula R, Greene EL, Matthews TA, Smith DI, Kaufmann SH, Roberts LR, Shridhar V. Loss of HSulf-1 up-regulates heparin-binding growth factor signaling in cancer. J Biol Chem 2003;278:23107–23117. [PubMed: 12686563]
108. Lai JP, Chien J, Strome SE, Staub J, Montoya DP, Greene EL, Smith DI, Roberts LR, Shridhar V. HSulf-1 modulates HGF-mediated tumor cell invasion and signaling in head and neck squamous carcinoma. Oncogene 2004;23:1439–1447. [PubMed: 14973553]
109. Chen Z, Fan JQ, Li J, Li QS, Yan Z, Jia XK, Liu WD, Wei LJ, Zhang FZ, Gao H, Xu JP, Dong XM, Dai J, Zhou HM. Promoter hypermethylation correlates with the Hsulf-1 silencing in human breast and gastric cancer. Int J Cancer 2009;124:739–744. [PubMed: 19006069]
110. Inamine M, Nagai Y, Hirakawa M, Mekaru K, Yagi C, Masamoto H, Aoki Y. Heparanase expression in endometrial cancer: analysis of immunohistochemistry. J Obstet Gynaecol 2008;28:634–637. [PubMed: 19003663]
111. Watanabe M, Aoki Y, Kase H, Tanaka K. Heparanase expression and angiogenesis in endometrial cancer. Gynecol Obstet Invest 2003;56:77–82. [PubMed: 12904690]
112. Mikami S, Oya M, Shimoda M, Mizuno R, Ishida M, Kosaka T, Mukai M, Nakajima M, Okada Y. Expression of heparanase in renal cell carcinomas: implications for tumor invasion and prognosis. Clin Cancer Res 2008;14:6055–6061. [PubMed: 18809970]
113. Cohen-Kaplan V, Doweck I, Naroditsky I, Vlodavsky I, Ilan N. Heparanase augments epidermal growth factor receptor phosphorylation: correlation with head and neck tumor progression. Cancer Res 2008;68:10077–10085. [PubMed: 19074873]
114. Escobar Galvis ML, Jia J, Zhang X, Jastrebova N, Spillmann D, Gottfridsson E, van Kuppevelt TH, Zcharia E, Vlodavsky I, Lindahl U, Li JP. Transgenic or tumor-induced expression of heparanase upregulates sulfation of heparan sulfate. Nat Chem Biol 2007;3:773–778. [PubMed: 17952066]
115. Ravna AW, Sager G. Molecular modeling studies of ABC transporters involved in multidrug resistance. Mini Rev Med Chem 2009;9:186–193. [PubMed: 19200023]
116. Palumbo JS, Talmage KE, Massari JV, La Jeunesse CM, Flick MJ, Kombrinck KW, Jirouskova M, Degen JL. Platelets and fibrin(ogen) increase metastatic potential by impeding natural killer cell-mediated elimination of tumor cells. Blood 2005;105:178–185. [PubMed: 15367435]
117. dos Santos VM, Rodrigues DB, Castro EC, Saldanha JC, Soares S, Teixeira VP, dos Reis MA. Widespread hematogenous metastases and Trousseau's syndrome in gastric adenocarcinoma. Rev Hosp Clin Fac Med Sao Paulo 2001;56:91–96. [PubMed: 11514909]
118. Kamocka M, Rozalski M, Krajewska U, Wierzbicki R, Mielicki WP. Effect of cancer procoagulant (CP) on the growth and adhesion of MCF-7 cells to vitronectin in vitro. Cancer Lett 2005;222:89–94. [PubMed: 15837545]
119. Ho-Tin-Noe B, Goerge T, Cifuni SM, Duerschmied D, Wagner DD. Platelet granule secretion continuously prevents intratumor hemorrhage. Cancer Res 2008;68:6851–6858. [PubMed: 18701510]
120. Probability of Developing Invasive Cancers Over Selected Age Intervals by Sex, US, 2001 to 2003. National Cancer Institute. 2007.
121. He X, Brenchley PE, Jayson GC, Hampson L, Davies J, Hampson IN. Hypoxia increases heparanase-dependent tumor cell invasion, which can be inhibited by antiheparanase antibodies. Cancer Res 2004;64:3928–3933. [PubMed: 15173004]
122. Gingis-Velitski S, Zetser A, Kaplan V, Ben-Zaken O, Cohen E, Levy-Adam F, Bashenko Y, Flugelman MY, Vlodavsky I, Ilan N. Heparanase uptake is mediated by cell membrane heparan sulfate proteoglycans. J Biol Chem 2004;279:44084–44092. [PubMed: 15292202]

123. Purushothaman A, Chen L, Yang Y, Sanderson RD. Heparanase stimulation of protease expression implicates it as a master regulator of the aggressive tumor phenotype in myeloma. J Biol Chem 2008;283:32628–32636. [PubMed: 18812315]

124. Chen L, Sanderson RD. Heparanase regulates levels of syndecan-1 in the nucleus. PLoS ONE 2009;4:e4947. [PubMed: 19305494]

125. Baek SK, Jung KY, Lee SH, Woo JS, Kwon SY, Chung EJ, Kim TH, Chae YS. Prognostic significance of vascular endothelial growth factor-C expression and lymphatic vessel density in supraglottic squamous cell carcinoma. Laryngoscope. 2009

126. Saito K, Khan K, Sosnowski B, Li D, O'Malley BW Jr. Cytotoxicity and antiangiogenesis by fibroblast growth factor 2-targeted Ad-TK cancer gene therapy. Laryngoscope 2009;119:665–674. [PubMed: 19213040]

127. Beenken A, Mohammadi M. The FGF family: biology, pathophysiology and therapy. Nat Rev Drug Discov 2009;8:235–253. [PubMed: 19247306]

128. Kim S, Choi JH, Lim HI, Lee SK, Kim WW, Cho S, Kim JS, Kim JH, Choe JH, Nam SJ, Lee JE, Yang JH. EGF-induced MMP-9 expression is mediated by the JAK3/ERK pathway, but not by the JAK3/STAT-3 pathway in a SKBR3 breast cancer cell line. Cell Signal 2009;21:892–898. [PubMed: 19385051]

129. Chen L, Luo G, Tan Y, Wei J, Wu C, Zheng L, Zhang X, Xu N. Immunolocalisation of tissue factor in esophageal cancer is correlated with intratumoral angiogenesis and prognosis of the patient. Acta Histochem. 2009

130. Ferro V, Hammond E, Fairweather JK. The development of inhibitors of heparanase, a key enzyme involved in tumour metastasis, angiogenesis and inflammation. Mini Rev Med Chem 2004;4:693–702. [PubMed: 15279603]

131. Ferro V, Dredge K, Liu L, Hammond E, Bytheway I, Li C, Johnstone K, Karoli T, Davis K, Copeman E, Gautam A. PI-88 and novel heparan sulfate mimetics inhibit angiogenesis. Semin Thromb Hemost 2007;33:557–568. [PubMed: 17629854]

132. Trial of PI-88 With Dacarbazine in Patients With Metastatic Melanom. Progen Pharmaceuticals. 2005.

133. Parish CR, Freeman C, Brown KJ, Francis DJ, Cowden WB. Identification of sulfated oligosaccharide-based inhibitors of tumor growth and metastasis using novel in vitro assays for angiogenesis and heparanase activity. Cancer Res 1999;59:3433–3441. [PubMed: 10416607]

134. Dredge K, Hammond E, Davis K, Li CP, Liu L, Johnstone K, Handley P, Wimmer N, Gonda TJ, Gautam A, Ferro V, Bytheway I. The PG500 series: novel heparan sulfate mimetics as potent angiogenesis and heparanase inhibitors for cancer therapy. Invest New Drugs. 2009

135. Hostettler N, Naggi A, Torri G, Ishai-Michaeli R, Casu B, Vlodavsky I, Borsig L. P-selectin- and heparanase-dependent antimetastatic activity of non-anticoagulant heparins. FASEB J 2007;21:3562–3572. [PubMed: 17557930]

136. Casu B, Vlodavsky I, Sanderson RD. Non-anticoagulant heparins and inhibition of cancer. Pathophysiol Haemost Thromb 2008;36:195–203. [PubMed: 19176992]

137. Gerotziafas GT, Papageorgiou C, Hatmi M, Samama MM, Elalamy I. Clinical studies with anticoagulants to improve survival in cancer patients. Pathophysiol Haemost Thromb 2008;36:204–211. [PubMed: 19176993]

138. Pumphrey CY, Theus AM, Li S, Parrish RS, Sanderson RD. Neoglycans, carbodiimide-modified glycosaminoglycans: a new class of anticancer agents that inhibit cancer cell proliferation and induce apoptosis. Cancer Res 2002;62:3722–3728. [PubMed: 12097281]

139. Hibino S, Shibuya M, Hoffman MP, Engbring JA, Hossain R, Mochizuki M, Kudoh S, Nomizu M, Kleinman HK. Laminin alpha5 chain metastasis- and angiogenesis-inhibiting peptide blocks fibroblast growth factor 2 activity by binding to the heparan sulfate chains of CD44. Cancer Res 2005;65:10494–10501. [PubMed: 16288042]

140. Berry D, Lynn DM, Sasisekharan R, Langer R. Poly(beta-amino ester)s promote cellular uptake of heparin and cancer cell death. Chem Biol 2004;11:487–498. [PubMed: 15123243]

141. Galcheva-Gargova Z, Zhidkova N, Geisler S, Ozug J, Wudyka S, Gunay NS, Qi YW, Shriver Z, Venkataraman G. Overexpression of Merlin in B16F10 mouse melanoma cells reduces their

metastatic activity: role of the cell surface heparan sulfate glycosaminoglycans. Int J Oncol 2008;32:1237–1243. [PubMed: 18497985]

142. Fuster MM, Esko JD. The sweet and sour of cancer: glycans as novel therapeutic targets. Nat Rev Cancer 2005;5:526–542. [PubMed: 16069816]
143. Marchetti D, Reiland J, Erwin B, Roy M. Inhibition of heparanase activity and heparanase-induced angiogenesis by suramin analogues. Int J Cancer 2003;104:167–174. [PubMed: 12569571]
144. Trosko JE. Review paper: cancer stem cells and cancer nonstem cells: from adult stem cells or from reprogramming of differentiated somatic cells. Vet Pathol 2009;46:176–193. [PubMed: 19261629]
145. Dai J, Rabie AB. VEGF: an essential mediator of both angiogenesis and endochondral ossification. J Dent Res 2007;86:937–950. [PubMed: 17890669]
146. Tsunezumi J, Higashi S, Miyazaki K. Matrilysin (MMP-7) cleaves C-type lectin domain family 3 member A (CLEC3A) on tumor cell surface and modulates its cell adhesion activity. J Cell Biochem 2009;106:693–702. [PubMed: 19173304]
147. Manduteanu I, Calb M, Lupu C, Simionescu N, Simionescu M. Increased adhesion of human diabetic platelets to cultured valvular endothelial cells. J Submicrosc Cytol Pathol 1992;24:539–547. [PubMed: 1458440]
148. Gorsi B, Stringer SE. Tinkering with heparan sulfate sulfation to steer development. Trends Cell Biol 2007;17:173–177. [PubMed: 17320398]
149. Victor XV, Nguyen TK, Ethirajan M, Tran VM, Nguyen KV, Kuberan B. Investigating the elusive mechanism of glycosaminoglycan biosynthesis. J Biol Chem. 2009 (in press).
150. Garud DR, Tran VM, Victor XV, Koketsu M, Kuberan B. Inhibition of heparan sulfate and chondroitin sulfate proteoglycan biosynthesis. J Biol Chem 2008;283:28881–28887. [PubMed: 18708345]
151. Kuberan B, Ethirajan M, Victor XV, Tran V, Nguyen K, Do A. "Click" xylosides initiate glycosaminoglycan biosynthesis in a mammalian cell line. Chembiochem 2008;9:198–200. [PubMed: 18085541]
152. Choi S, Kim Y, Park H, Han IO, Chung E, Lee SY, Kim YB, Lee JW, Oh ES, Yi JY. Syndecan-2 overexpression regulates adhesion and migration through cooperation with integrin alpha2. Biochem Biophys Res Commun. 2009
153. Liu D, Shriver Z, Venkataraman G, El Shabrawi Y, Sasisekharan R. Tumor cell surface heparan sulfate as cryptic promoters or inhibitors of tumor growth and metastasis. Proc Natl Acad Sci U S A 2002;99:568–573. [PubMed: 11805315]
154. Varki A. Six blind men and the elephant--the many faces of heparan sulfate. Proc Natl Acad Sci U S A 2002;99:543–545. [PubMed: 11805308]

Abbreviations

HS	Heparan Sulfate
CS	Chondroitin Sulfate
DS	Dermatan Sulfate
HSPG	Heparan Sulfate Proteoglycan
CSPG	Chondroitin Sulfate Proteoglycan
Sdc	Syndecan
S-Sdc	Shed Syndecan
Gpc	Glypican
Hpa	Heparanase
HSulf	HS 6-O Endosulfatase
3-OST	3-O Sulfotransferase

6-OST	6-O Sulfotransferase
FGF	Fibroblast Growth Factor
VEGF	Vascular Endothelial Cell Growth Factor
HBGF	Heparin Binding Growth Factor
HB-EGF	Heparin Binding Epidermal Growth Factor
FGFR	Fibroblast Growth Factor receptor
VEGFR	Vascular Endothelial Cell Growth Factor Receptor
BMP	Bone Morphogenic Protein
TGF-β	Transforming Growth Factor Beta
MMP	Matrix Metalloprotease
GAG	Glycosaminoglycan
ECM	Extraceullar Matrix
PG	Proteoglycan
DCIS	Ductal Carcinoma *in situ*
PBMC	Peripheral blood mononuclear cell fraction
NK	Natural Killer Cell
LMWH	low molecular weight heparin

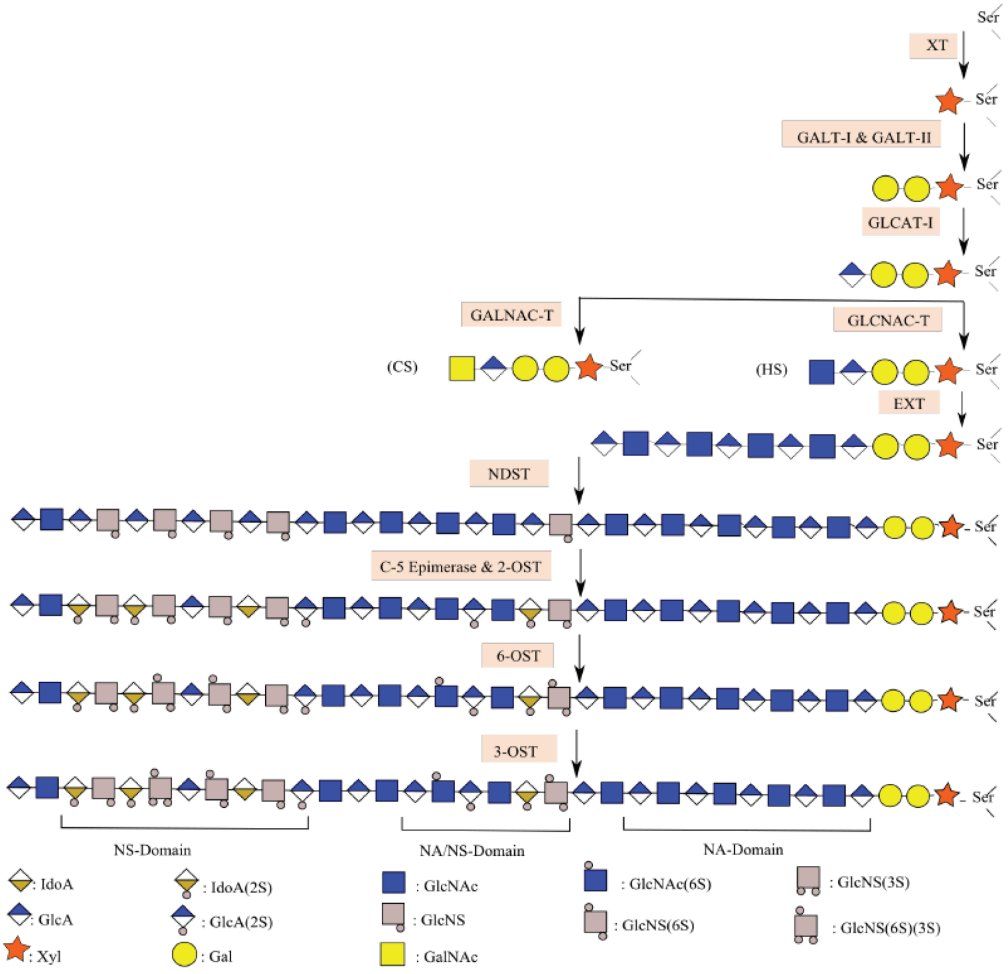

Fig. 1. Proteoglycan Biosynthesis

Biosynthesis begins with the addition of xylose to serine residues of the core protein. Subsequently, glycosyl transferases add two Gal residues and one GlcA residue. EXT-1 and EXT-2 then extend the GAG chain by alternatively adding GlcNAc and GlcA. While elongation takes place, NDST-1 and NDST-2 convert certain GlcNAc to GlcNS residues. Epimerization and 2-O Sulfonation also occur in parallel; certain GlcA are converted to IdoA while 2-OST acts on certain GlcA and IdoA residues. Subsequent action of 6-OST and 3-OST yields the final PG chain that contains regions that have several *N*-Sulfated residues (NS Domain), others that have several *N*-Acetylated residues (NA Domain), and short regions that have a mixture of both (NA/NS Domain).

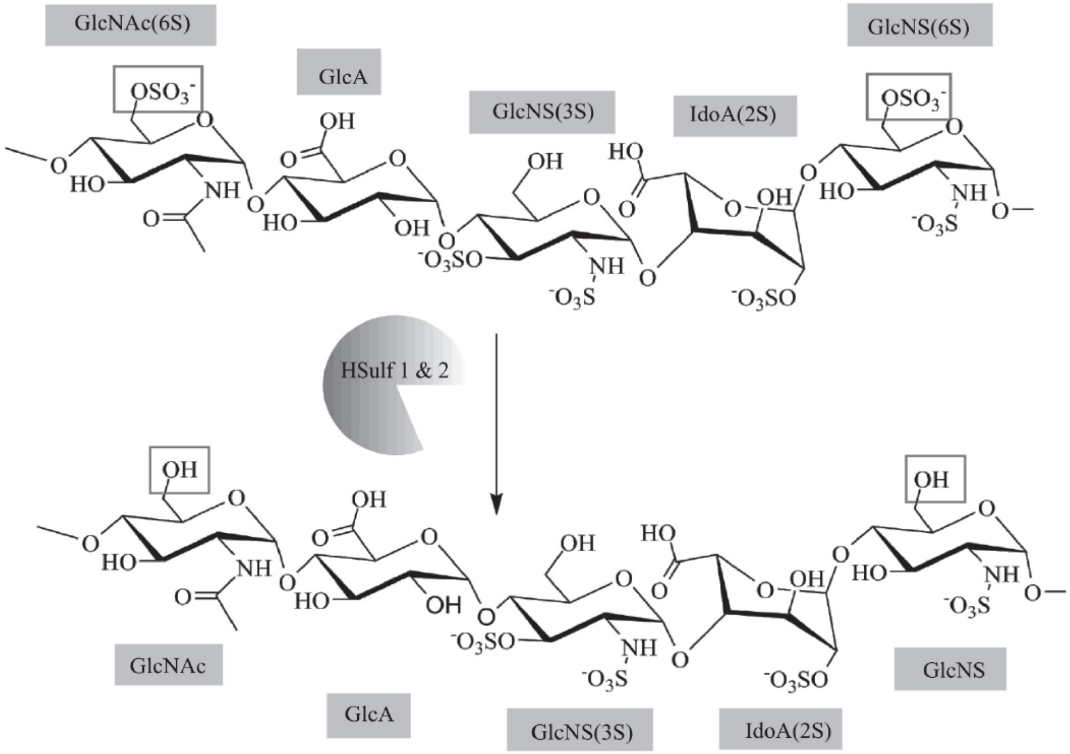

Fig. 2. HSulf 1 & 2 Enzymatic Activity

HSulfs provide arylsulfatase activity selectively removing 6-*O*-Sulfate groups from GlcNAc and GlcNS residues. Deviant H-Sulf mRNA expression is present in several cancers.

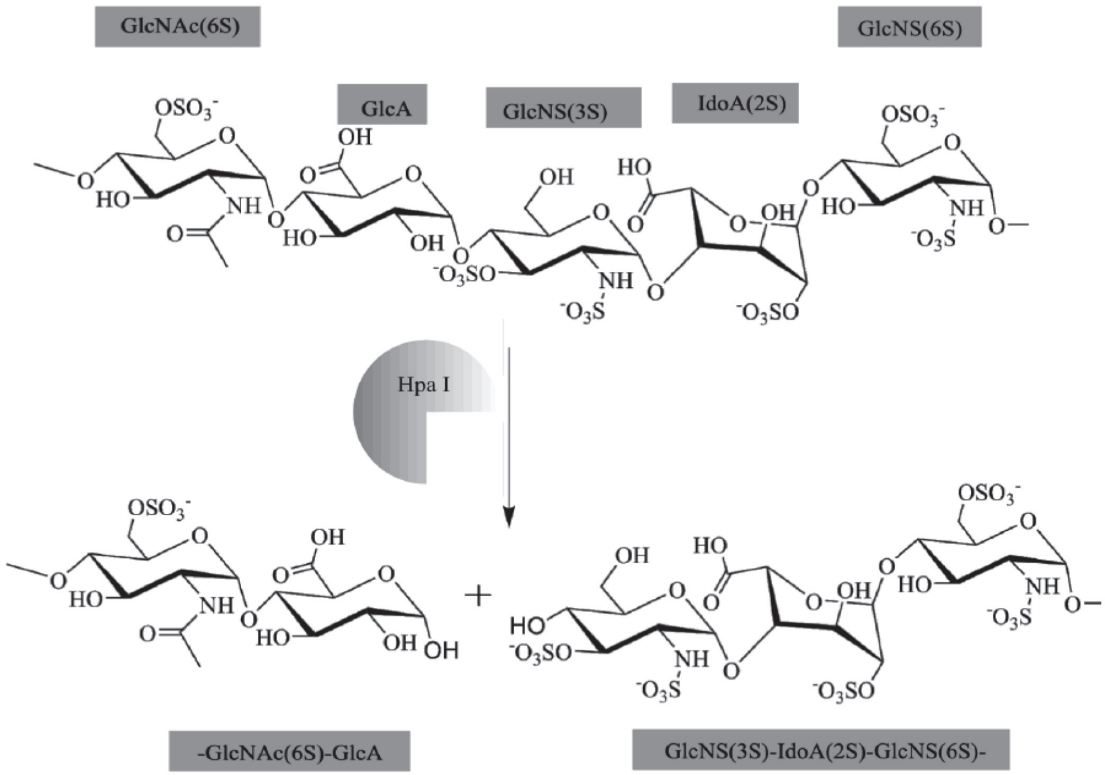

Fig. 3. Hpa I Enzymatic Activity

The Heparanase family is the only mammalian enzyme family that can cleave HS to form oligosaccharide units. Due to its unique activity, Hpa modulates growth factor signaling, ECM permeability and remodeling, cell clustering and adhesion, and several other cancer-related functions. Increased extracellular Hpa is an early indicator of malignant carcinomas.

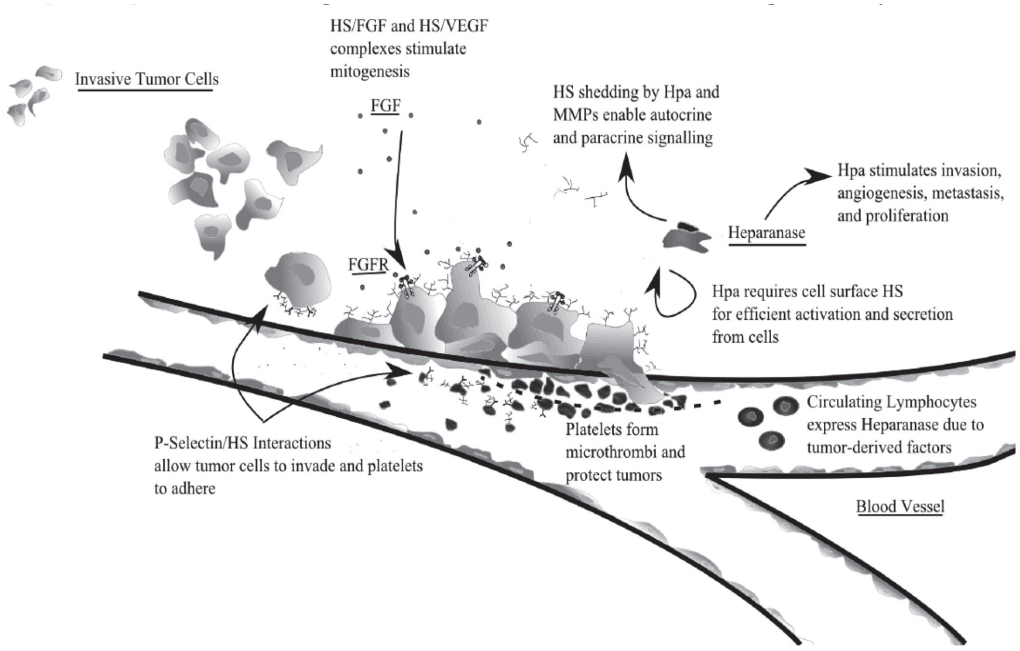

Fig. 4. The roles of HS in cancer

From gathered evidence presented in this article, HS is involved in several key functions regarding cancer progression. Cell metastasis depends on HS to provide P-Selectin binding so cells can adhere. As an antenna molecule, HS also plays a role in transducing signals from external growth factors by forming complexes with growth factor receptors. Additionally it is necessary for efficient activation of Heparanase, which is necessary for invasion, angiogenesis, and inflammation. By binding P-Selectins on platelets, HS also protects cancer cells from natural killer (NK) cell activity. Systemically, shed cell-surface HS can form paracrine signaling complexes FGFRs. Additionally, though not completely understood, cancer cells instigate circulating lymphocytes to upregulate heparanase activity; as an antenna molecule, HS is probably involved in this pathway as well.

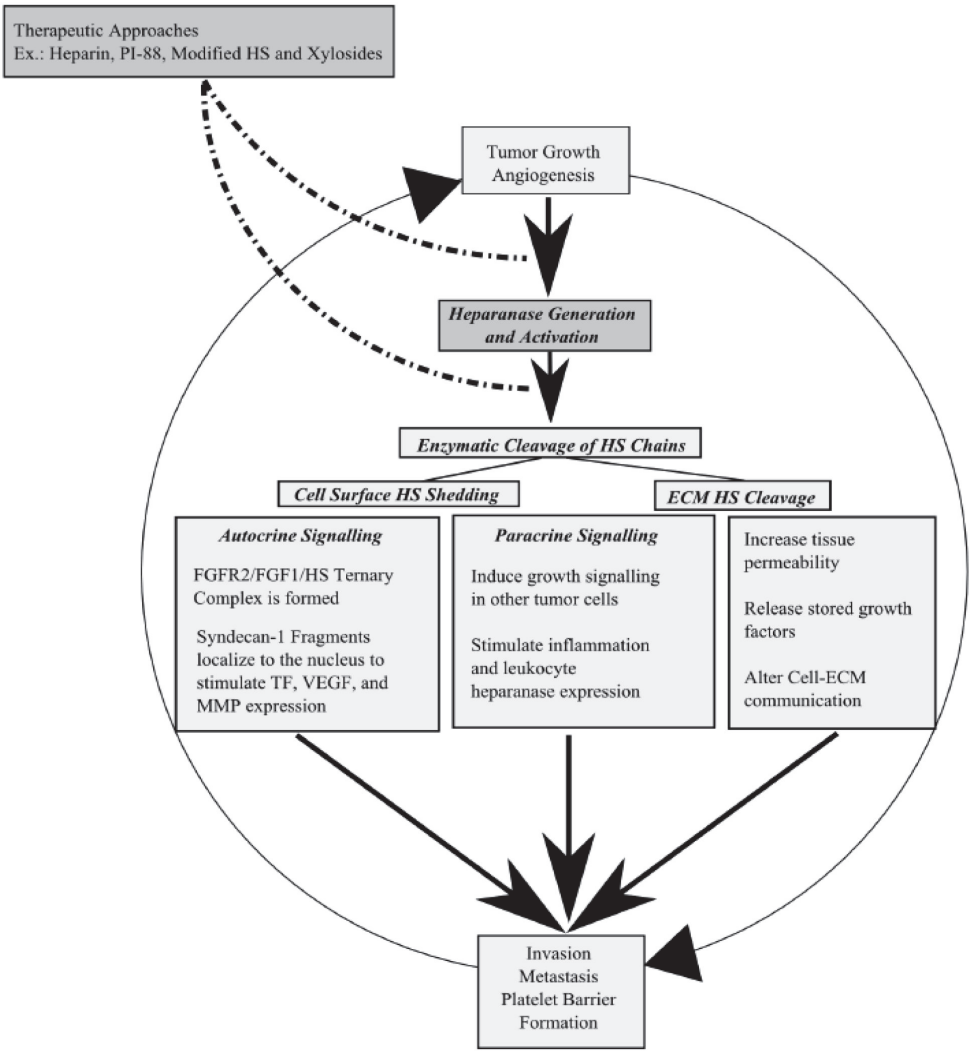

Fig. 5. Current HS-Based drug development strategies and their target signaling pathways in the Heparanase-induced self-proliferation loop

PI-88 and related oligosaccharides are potent anti-cancer agents because they interrupt Heparanase activity and also affect several growth signaling pathways such as the FGF2 pathway. Heparin and its low molecular weight anti-coagulant derivatives are natural Hep inhibitors that competitively inhibit Heparnase enzymatic activity by acting as the enzyme substrate. However, it is possible to affect both Heparanase as well as HS binding growth factors by utilizing modified HS and xylosides to tailor endogenous HS on cells to resist Hpa enzymatic activity and growth factor binding.

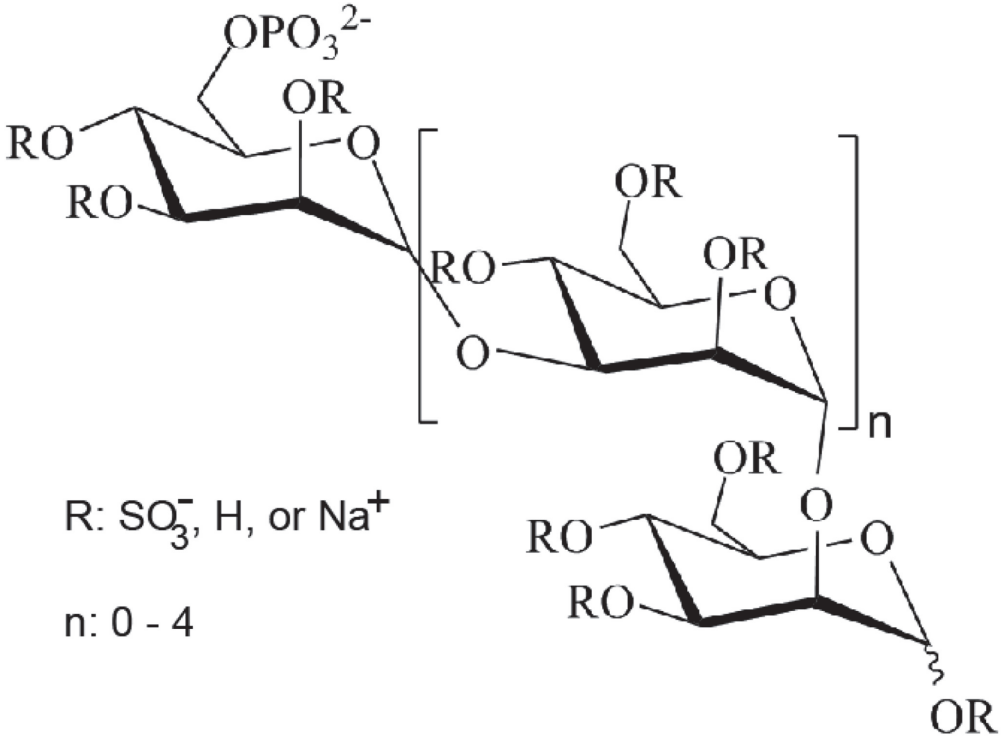

Fig. 6. Chemical Structure of PI-88

A potent Heparanase inhibitor, PI-88 is a hyper-sulfated oligosaccharide that blocks Hpa and several HS/Growth factor interactions.

Table 1

Summary of HS and HS-related-enzyme expression aberrations.

	HSPGs	
	Sdc-1	*Gpc-1*
Breast Cancer	↑	↑
Pancreatic Cancer	↑	↑
Skin Cancer	-	-
Colorectal Cancer	↓	-
Lung Cancer	↑	-
Brain Cancer	↑	-

	HS Catabolic Enzymes		
	Hpa-1	*HSulf-1*	*HSulf-2*
Breast Cancer	↑	↓	↑
Pancreatic Cancer	↑	↑	↑
Skin Cancer	↑	-	-
Colorectal Cancer	↑	-	-
Lung Cancer	↑	-	-
Brain Cancer	↑	-	-

	HS Biosynthetic Enzymes	
	3-OST-2	*6-OST-2*
Breast Cancer	**X**, ↑	-
Pancreatic Cancer	**X**	-
Skin Cancer	**X**	-
Colorectal Cancer	**X**, ↑	↑
Lung Cancer	**X**	-
Brain Cancer	-	-

*↑: Upregulated ↓: Downregulated **x:** Gene silenced --: Not known

1.2 Glioma Biology and Drug Delivery to the Brain

1.2.1 Glioma Introduction

Gliomas are a group of heterogeneous and highly invasive brain tumors. They are known for their diffused growth patterns, hypoxia, and disintegrated local blood brain barrier (BBB).[1] Glioblastoma Multiforme, classified by the WHO as a grade IV glioma, is one of the most common primary gliomas and is a particularly aggressive cancer.[2] Fewer than 5 percent of patients survive more than 5 years despite a variety of aggressive treatment strategies.

1.2.2 The Current Standard of Care for Gliomas

The current standard of care for newly diagnosed GBM patients is to maximally resect the tumor and follow up with a 6-week course of radiotherapy along with concomitant systemic dosing of temozolomide (TMZ).[2] Following this 6-week course, an additional 6-month treatment with TMZ is prescribed as an adjuvant therapy. Some patients are prescribed TMZ therapy for 12 months due to its excellent tolerability.

1.2.3 Challenges Faced in the Clinic

Unfortunately, the current standard of care has several disadvantages. Patients with gliomas in difficult- to-operate regions of the brain have poorer prognosis.[2, 3] Areas such as the eloquent cortex, basal ganglia, and brain stem are typically difficult to treat due to the sensitive nature of nearby healthy brain tissue. Additionally, the sensitivity of tumors to TMZ therapy is linked to the methylation of the methylguanine methyltrasferase (MGMT) promoter.[4] Tumors with methylated MGMT are more sensitive to TMZ therapy. If a tumor is resistant to TMZ, there are very few other options

available as most chemotherapeutics are unable to cross the BBB in therapeutic concentrations. The size of the molecule, its lypophilicity, the presence of drug efflux pumps, and the integrity of the BBB all affect the antiglioma activity of chemotherapeutics.[5] Furthermore, most patients with gliomas also receive treatments for other CNS-related illnesses such as epileptic seizures and inflammation. These other therapies may reduce the effect of chemotherapeutics that are being utilized.

Recurrent gliomas represent another barrier to cancer-free survival of patients. Currently there is no standard of care for patients with recurrent GBM.[6] A second dose of radiation or surgery may be employed when safe. However, radiation necrosis and the dangers of a second surgery preclude many patients from receiving any additional treatments. Drug resistance also poses a major hurdle to the treatment of recurrent gliomas. Bevacizumab, an antiVEGF antibody, was recently approved for the treatment of recurrent GBM. In combination or as a single treatment, it significantly reduces glioma-associated edema and "normalizes vasculature."[6, 7]

1.2.4 The Blood Brain Barrier

The blood brain barrier (BBB) is crucial in regulating the passage of molecules from the plasma into the brain parenchyma and for maintaining a biochemical balance in the brain.[8] It is formed by endothelial cells that line capillaries in the spinal cord and the brain. Additionally, several perivascular cells such as smooth muscle cells, pericytes, microglial cells, and astrocytes help to enforce that only certain molecules are able to permeate into the brain. These cells form not only a physical barrier, but also metabolic, transport, and immunological barriers.

The physical barrier is composed of tight junctions and adherens junctions

between adjacent endothelial cells. Small molecules that are less than 4Å may cross tight junctions if they have an appropriate ionic charge density while larger molecules require specific transporter proteins or disrupted tight junctions.[9] The metabolic barrier is formed by a variety of ecto-enzymes like peptidases and intracellular enzymes such as monoamine oxidase which can change drug structures to inactivate them or restrict their permeability. Transport barriers in the BBB are composed primarily of ATP-binding cassette (ABC)-transporters. Examples of transporters that are part of this family include: Multiple drug resistance protein 1(MDR1), Permeability glycoprotein (P-gp), and Breast cancer resistance protein (BCRP). Several medicinal drugs such as doxorubicin, tenofovir, methotrexate, and topotecan are actively effluxed out of the brain by these efflux pumps. Molecules that overcome all of these barriers finally have to evade the brain's immunological barrier which is composed of microglia, perivascular macrophages, and mast cells that phagocytose molecules and provide both innate and adaptive immunity.[10]

1.2.5 Local Delivery Strategies for Treating Brain Tumors

Due to the blood brain barrier, chemotherapeutics are unable to effectively treat gliomas. While tumors receive low doses of drugs, they quickly develop resistances against known brain-partitioning chemotherapeutics. Therefore, there is a need for more effective drug delivery strategies across the BBB and into the brain to improve the probability of giving a therapeutic dose to tumors. Several local and systemic delivery strategies have been developed to tackle the difficulties of treating gliomas.[11, 12] Local delivery strategies include injections, infusions, and local implants. Systemic delivery strategies include the use of temporary disruption of the BBB, chemical modification of

the drug, and modification with certain polymers or other brain partitioning molecules.

Local delivery strategies offer enormous advantages to the therapeutic dosing of tumors with drugs. By utilizing injections it is possible to directly attack a tumor with cytotoxic drugs. Previously it has been shown that interneoplastic injections of BCNU can significantly reduce the tumor load and increase rat survival.[13] Conjugation to a controlled-release polymer combined with interneoplastic injection further improves rat survival due to the prolonged duration that the drug maintains therapeutic concentration in the tumor. Injections may also be administered after resection to prolong the time to tumor resurgence.[14] Similar to injections, chemotherapeutic drugs may be infused directly into brain tissue using pumps and a catheter system. An infusion system minimizes the probability of an edema while still maintaining similar efficacy. More recently, several research groups have utilized implanted biomaterials as a means to control tumor growth. Gliadel wafers consisting of polifeprosan 20 and carmustine have been utilized in several clinical trials.[15] Currently, gliadel is indicated as an adjunct to surgery and radiation for newly diagnosed and recurrent glioblastoma multiforme patients. Other releaseable drugs tested as part of implanted systems in clinical studies for treatment of gliomas include AP12009 and IL13-PE38QQR.[16, 17] However, the use of local delivery strategies for treatment in the clinical setting is limited by their inherent disadvantages. Local injections and infusions are prone to infection, edemas, and backflow of the solution into the catheter (in the case of infusions). Additionally, if treatments need to be administered multiple times, the side effects and risks of local injections/infusions are exponentially increased. Furthermore, access to deep tissue tumors or tumors in sensitive areas of the brain is limited and this inhibits use of local delivery strategies. Implants overcome the

challenge of repeat injections being necessary for treatment. However, while implants are able to effectively release drugs for prolonged periods of time, there is a need for repeat implantation procedures once the drug reservoir is completely exhausted.[11, 12] Additionally, drug penetration into nearby tissue is restricted to very short distances from the implant region. These complications are common to implanted polymers, gels, wafers, and particulate systems. However, systemic delivery solutions overcome several of the drawbacks of local delivery solutions and effectively treat tumors.

1.2.6 Systemic Delivery Strategies for Treating Brain Tumors

Systemic delivery of chemotherapeutics presents clinicians with a strategy to target gliomas that are deep within tissue or too invasive to resect. Systemic delivery approaches include chemical modification to increase lipophilicity, increasing BBB permeability transiently, and modification of drugs with polymers/other macromolecules which enable brain targeting. As a general rule, highly hydrophobic small molecules 400-600 Da in weight are able to diffuse across the blood brain barrier.[12] One strategy to increase brain partitioning of drugs is to increase their lipophilicity via chemical modification. Researchers have previously functionalized small molecule drugs with fatty acyl groups, methyl groups, chloro groups, and other hydrophobic groups. Maintaining a strict balance between hydrophobicity and hydrophilicity while also keeping the molecular weight low, it is possible to greatly enhance the antiglioma efficacy of chemotherapeutics. However, these molecules are also able to diffuse into other tissues easily and therefore exhibit significant toxicity. Recently, several research groups have attempted to overcome the BBB using transient and partial opening of the BBB which create therapeutic windows of opportunity. Hyperosmotic mannitol infusions have long

been known to increase BBB permeability.[18] Additionally, bradykinin analogs, surfactants, and several different chemokines, are able to effectively improve BBB traversal of therapies.[12] Through temporary openings, small molecules as well as larger macromolecules such as antibodies and viruses may access the brain parenchyma. Furthermore, researchers have found that such vasoactive compounds are especially effective at tumor vasculature due to its aberrant structure. However, clinical use of this strategy is difficult because of the need for interarterial infusions. A third method to deliver chemotherapeutics across the BBB using systemic therapy is to use brain targeting peptides (TAT, LDL receptor peptides, aprotinin/angiopep etc.) and macromolecular drug delivery systems (liposomes, PBCA nanoparticles, polysorbate 80 nanoparticles, etc.). Brain targeting peptides such as TAT and Angiopep utilize receptor mediated endocytosis to transport drugs across the BBB.[19, 20] Angiopep is a 19 amino-acid sequence, derived from Aprotinin, which is designed to utilize LRP-1 to transcytose across the BBB. Ang1005, a conjugate of Angiopep and Paclitaxel, has shown significant promise in clinical trials involving the treatment of glioblastoma multiforme and other brain cancers.[21] Whereas Paclitaxel does not cross the BBB in therapeutic quantities, Ang1005 has shown to increase BBB penetration of the drug by 100 fold. Together with targeting peptides, macromolecular drug carriers increase accumulation of drugs in the brain and within tumors due to the enhanced permeability and retention (EPR) effect. Without targeting peptides, macromolecules are only acutely effective against brain tumors when given via intrathecal injection, intranasal injection, or direct spinal cord injection. With targeting peptides, macromolecular carriers can be given intravenously or via an intraperitoneal injection and demonstrate higher clinical efficacy. Several clinical

trials have evaluated the effectiveness of liposomes in the treatment of gliomas and other cancers. Currently ongoing trials include NCT00992602 (high dose methotrexate together with liposomal cytrabine) and NCT01386580 (glutathione enriched pegylated doxorubicin in combination with transtuzumab or as a single agent).

1.3 Research Objectives

It is clear that a "one glove fits all" strategy is not effective against gliomas. Since tumor resection is technically challenging, systemic therapy with free drugs is inhibited by the BBB, tumor recurrence is common, and drug resistance effectively decreases the efficacy of singular therapies, a more effective strategy to treat gliomas requires a multitarget approach which requires minimal surgical intervention. Proteoglycan-based therapeutics offer the advantage of affecting several cellular pathways concurrently.

In this dissertation, we design a novel treatment regime for attacking cancers, including brain cancer, by reengineering the tumor microenvironment in addition to attacking tumor growth. This goal is achieved by utilizing xylosides to modify GAG biosynthesis and by employing a heparin-like drug delivery vehicle (DDV) to deliver doxorubicin to tumor cells. To optimize this treatment strategy for brain tumors, aprotinin is attached to the polymer to ensure that it can overcome the blood brain barrier and attack F98 glioma growth in mouse flanks as well as brains. The following specific aims outline the development of this novel treatment strategy:

1.3.1 Specific Aim I

Evaluate the *in vitro* efficacy of xylosides and glycosaminoglycan mimetics in treating glioma growth, invasion, and angiogenesis. The working hypothesis is that

modification of GAG production or GAG-growth factor binding ability in the glioma microenvironment can prevent tumor progression *in vitro*. In order to test this hypothesis, several types of xylosides are tested for their ability to modify GAG chain production in U87 Mg glioma cells and endothelial cells and to affect cellular invasion and angiogenesis. Additionally, GAG mimetics such as sulfonated aromatic scaffolds and chemically modified heparin are examined for their ability to inhibit tumor associated angiogenesis.

1.3.2 Specific Aim II

Develop a Heparin-based polymer-DOX conjugate and test its *in vitro* efficacy. The working hypothesis is that heparin's sulfation pattern can be modified to generate a heparin-like DDV that will enter tumor cells to a greater extent than heparin alone. This conjugate will be able to deliver its cytotoxic cargo directly into cellular nuclei similar to natural proteoglycans such as Syndecan-1. To test this hypothesis, a library of chemically modified heparins and heparosans are generated and tested for their ability to enter multiple cancer cells. The internalization properties of each polymer are also analyzed to determine the localization, rate, mechanism, and maximum accumulation in cells. Next, doxorubicin is conjugated with the most promising polysaccharide and these conjugates are analyzed for their cellular localization, effect on cell viability, and mechanism of action.

1.3.3 Specific Aim III

Probe the *in vivo* and *in vitro* efficacy of a combination therapy consisting of xyloside and aprotinin-HLP-DOX. The working hypothesis is that a combination

therapy with xylosides and a HLP-dox conjugate will effectively diminish tumor progression *in vivo* in CD-1 nu/nu athymic mice. To confirm this hypothesis, the most promising vehicle from aim 2 is first modified with aprotinin to enable LRP-mediated transcytosis across the BBB. After *in vitro* testing, mice are then inoculated with F98 in the flank. Various treatment regimens that combine the use of promising xylosides from aim 1 and an aprotinin conjugate of the most effective DDV from aim 2 are then used to treat mice. At the end of the study, animals are sacrificed and treatment regimens that show efficacy in the flank model are then retested in mice with intracranial gliomas. Analysis of tumor volume and animal weight are performed to determine if the treatment is efficacious.

The results of the dissertation research provide a new clinical strategy to treat vascularized cancers without significant systemic toxicity. A combinatorial treatment utilizing nontoxic xyloside-based drugs and a biocompatible HLP-Doxorubicin conjugate modifies the tumor environment and eradicates tumors. It is expected that the proposed treatment regimen will be significantly more effective than current clinical anticancer practices.

1.4 Dissertation Overview

The central goal of this dissertation is to develop a novel treatment regime for attacking cancers that include brain cancers. To achieve this goal, experiments are performed to achieve a series of specific aims and organized as chapters in this dissertation. GAGs are utilized as key backbones for developing new therapeutics because of their inherent biocompatibility and biological activity.

In Chapter 2, a variety of different GAG-based drugs are developed to treat tumor

invasion and tumor-associated angiogenesis including click-xylosides, fluoro-xylosides, sulfonated GAG mimetics, and chemoenzymatically synthesized GAGs. It is found that click-xylosides, which cause cells to produce and release GAGs outside the cell, are effective antiinvasive small molecules. Additionally, fluoro-xylosides, which prevent cells from producing GAGs altogether, are shown to reduce tumor-associated angiogenesis *in vitro*. Such xyloside-based therapies are clinically-advantageous because xylosides do not affect cell viability even at high doses. Sulfonated GAG mimetics are also developed and found to reduce tumor-associated angiogenesis. The advantages of these molecules include their size, hydrophilicity, and ease of synthesis. Finally, the chapter also describes the design and production of an Acharan Sulfate-like GAG which hinders tumor-associated angiogenesis. This polymeric antiangiogenic agent is expected to be more biocompatible and have a longer circulation time than other state of the art antiangiogenic small molecules.

In Chapter 3, a GAG-based drug delivery vehicle is synthesized and tested *in vitro* for its ability to deliver doxorubicin *in vitro*. Whereas xylosides, developed in Chapter 2, are antiinvasive and antiangiogenic molecules, the administration of a cytotoxic drug is expected to work synergistically with xylosides *in vivo* to attack tumors using multiple approaches. GAGs make excellent drug delivery vehicles because of their biocompatibility, biological activity, ease of functionalization, and hydrophilicity. Therefore, initially a series of GAGs are tested for their ability to internalize into a variety of normal and tumor cells. It is determined that NA and NS polymers internalize into cells to the greatest extent and NA polymers are even able to target cellular nuclei. Internalization proceeds using a variety of endocytosis pathways including receptor-

mediated endocytosis, dynamin-mediated endocytosis, and micropinocytosis. GAG sulfation patterns determine their internalization efficacy in a variety of cell types. In the next part of the chapter, doxorubicin is conjugated to NA and NS polymers and tested for its ability to affect cell growth. In comparison to free doxorubicin, NA and NS polymers are equally effective, but since they are polymeric in nature, their circulation time and tumor-targeting capability *in vivo* is expected to be significantly better. Heparin-DOX conjugates are also compared to the NA and NS polymers to show that sulfation patterns affect the drug-delivery efficacy of GAGs. Heparin-DOX conjugates are not as effective at reducing cell viability relative to NA-DOX, NS-DOX, or free DOX. Surprisingly, all the GAG-DOX conjugates are able to shuttle DOX to cellular nuclei and affect cell viability without utilizing cleavable linkers to link the polymer to the drug. Against DOX-resistant cells, NA-DOX and free DOX are not effective even at high dosages. However NS-DOX and HEP-DOX are able to reduce cell viability whereby NS-DOX is significantly more potent as a DDV. Therefore, sulfation patterns are found to affect the ability of GAGs to overcome DOX resistance as well.

In Chapter 4, NA-DOX conjugates are modified with Aprotinin to enable drug delivery across the blood brain barrier and tested *in vivo* for their anticancer efficacy. A combination of these NA-DOX-APRO conjugates (HDA) and click-xylosides is also evaluated for its anticancer activity *in vivo* in nude mice. In the initial portion of the chapter, the synthesis and *in vitro* evaluation of HDA conjugates is described. These conjugates are shown to reduce glioma viability and to enter cellular nuclei to deliver doxorubicin. In combination with xylosides, HDA conjugates are effective at reducing cell viability and xylosides are effective at reducing glioma invasion; therefore, there are

no antagonistic interactions between the two therapies. In the next section, *in vivo* experiments are utilized to show the effectiveness of various combinations of HDA and xyloside against F98 gliomas in the flank and in the brain. It is found that HDA conjugates localize to flank tumors and the brain more than free DOX. They also localize to the heart less than DOX and are therefore expected to be less cardiotoxic. Furthermore, HDA conjugates are equally effective against flank tumors as DOX and XYL alone. However, a combination of HDA and XYL seems to have antagonistic effects *in vivo* against flank gliomas since tumor growth is not hindered when a combination therapy is utilized for treatment. Against orthotopic gliomas, it is found that neither DOX, XYL, nor HDA is effective. The use of bradykinin and elacridar to chemically open the blood brain barrier and prevent drug efflux also has no effect on the efficacy of HDA conjugates against orthotopic gliomas. Nonetheless, HDA conjugates and xylosides are novel antitumor therapeutics that warrant further investigation due to their efficacy against flank tumors and their lower toxicity compared to state of the art drugs like DOX.

In Chapter 5, the dissertation is concluded and future directions are discussed. The appendix includes additional information related to heparan sulfate biosynthesis that was a byproduct of the dissertation research. Overall, this dissertation describes the design and development of several novel GAG-based antitumor therapeutics that show promise *in vivo* and *in vitro*. Utilizing the inherent advantages of GAGs it is possible to target and treat cancers with a multipronged treatment approach that includes xylosides and GAG-based drug delivery vehicles to control tumor invasion, angiogenesis, and growth.

1.5 Author Contributions

Permission from the publisher has been acquired for each research article contained in this dissertation. Author (Karthik Raman) contributions for individual articles are denoted here.

Chemical Tumor Biology of Heparan Sulfate Proteoglycans

Author Contribution: Literature Review and Writing
Co-author Contribution: Editing, Revisions

Differential effects of Heparitinase I and Heparitinase III on endothelial tube formation in vitro

Author Contributions: Conducted and analyzed all experiments, Wrote article
Co-author Contribution: Editing, Revisions

Click-xylosides mitigate glioma cell invasion in vitro

Author Contributions: Synthesized chemicals, Conducted and analyzed all experiments, Wrote article
Co-author Contribution: Editing, Revisions

Novel glycosaminoglycan biosynthetic inhibitors affect tumor-associated angiogenesis

Author Contributions: Utilized chemicals in biological assays, Wrote article
Co-author Contributions: Synthesized chemicals, Editing, Revisions

Discovery of novel sulfonated small molecules that inhibit vascular tube formation

Author Contributions: Utilized chemicals in biological assays, Wrote article
Co-author Contributions: Synthesized chemicals, Corroborated with duplicate experiments, Wrote article, Editing, Revisions

Chemogenesis of an Antiangiogenic Glycosaminoglycan

Author Contributions: Synthesized polymer, Utilized polymer in biological assays, Wrote article
Co-author Contributions: Analyzed polymer NMR, Wrote sections on NMR, Editing, Revisions

Sulfation Patterns Determine Cellular Internalization of Heparin-Like Polysaccharides

Author Contributions: Synthesized polymers, Utilized polymers in biological assays, Wrote article
Co-author Contributions: Corroborated experiments, Editing, Revisions

Is N-sulfation just a gateway modification during heparan sulfate biosynthesis?

Author Contributions: Synthesized polymers, Utilized polymers in biological assays, Wrote article
Co-author Contributions: Prepared materials and enzymes for experiments, Editing, Revisions

1.6 References

1. Jovcevska, I.; Kocevar, N.; Komel, R., Glioma and glioblastoma - how much do we (not) know? *Mol Clin Oncol* **2013**, 1, (6), 935-941.

2. Rogers, L. R., Chemotherapy and immunotherapy of brain tumors: what the epileptologist must know. *Epilepsia* **2013**, 54 Suppl 9, 105-8.

3. Mrugala, M. M., Advances and challenges in the treatment of glioblastoma: a clinician's perspective. *Discov Med* **2013**, 15, (83), 221-30.

4. Fiano, V.; Trevisan, M.; Trevisan, E.; Senetta, R.; Castiglione, A.; Sacerdote, C.; Gillio-Tos, A.; De Marco, L.; Grasso, C.; Magistrello, M.; Tondat, F.; Ruda, R.; Cassoni, P.; Soffietti, R.; Merletti, F., MGMT promoter methylation in plasma of glioma patients receiving temozolomide. *J Neurooncol* **2014**, 117, (2), 347-57.

5. Agarwal, S.; Sane, R.; Oberoi, R.; Ohlfest, J. R.; Elmquist, W. F., Delivery of molecularly targeted therapy to malignant glioma, a disease of the whole brain. *Expert Rev Mol Med* 13, e17.

6. Chowdhary, S.; Chamberlain, M., Bevacizumab for the treatment of glioblastoma. *Expert Rev Neurother* **2013***,* 13, (8), 937-49.

7. Juratli, T. A.; Schackert, G.; Krex, D., Current status of local therapy in malignant gliomas--a clinical review of three selected approaches. *Pharmacol Ther* **2013***,* 139, (3), 341-58.

8. Abbott, N. J.; Ronnback, L.; Hansson, E., Astrocyte-endothelial interactions at the blood-brain barrier. *Nat Rev Neurosci* **2006,** 7, (1), 41-53.

9. Alyautdin, R.; Khalin, I.; Nafeeza, M. I.; Haron, M. H.; Kuznetsov, D., Nanoscale drug delivery systems and the blood-brain barrier. *Int J Nanomedicine* **2014**, 9, 795-811.

10. Anderson, J. M.; Van Itallie, C. M., Physiology and function of the tight junction. *Cold Spring Harb Perspect Biol* **2009,** 1, (2), a002584.

11. Allhenn, D.; Boushehri, M. A.; Lamprecht, A., Drug delivery strategies for the treatment of malignant gliomas. *Int J Pharm* **2012**, 436, (1-2), 299-310.

12. Serwer, L. P.; James, C. D., Challenges in drug delivery to tumors of the central nervous system: an overview of pharmacological and surgical considerations. *Adv Drug Deliv Rev* **2012**, 64, (7), 590-7.

13. Buahin, K. G.; Brem, H., Interstitial chemotherapy of experimental brain tumors: comparison of intratumoral injection versus polymeric controlled release. *J*

Neurooncol **1995,** 26, (2), 103-10.

14. Garfield, J. S., Neurosurgical aspects of supratentorial malignant gliomas. *Proc R Soc Med* **1976,** 69, (1), 53-5.

15. Duntze, J.; Litre, C. F.; Eap, C.; Theret, E.; Debreuve, A.; Jovenin, N.; Lechapt-Zalcman, E.; Metellus, P.; Colin, P.; Guillamo, J. S.; Emery, E.; Menei, P.; Rousseaux, P.; Peruzzi, P., Implanted carmustine wafers followed by concomitant radiochemotherapy to treat newly diagnosed malignant gliomas: prospective, observational, multicenter study on 92 cases. *Ann Surg Oncol* **2013***,* 20, (6), 2065-72.

16. Kunwar, S.; Chang, S.; Westphal, M.; Vogelbaum, M.; Sampson, J.; Barnett, G.; Shaffrey, M.; Ram, Z.; Piepmeier, J.; Prados, M.; Croteau, D.; Pedain, C.; Leland, P.; Husain, S. R.; Joshi, B. H.; Puri, R. K., Phase III randomized trial of CED of IL13-PE38QQR vs Gliadel wafers for recurrent glioblastoma. *Neuro Oncol* **2010***,* 12, (8), 871-81.

17. Schlingensiepen, K. H.; Jaschinski, F.; Lang, S. A.; Moser, C.; Geissler, E. K.; Schlitt, H. J.; Kielmanowicz, M.; Schneider, A., Transforming growth factor-beta 2 gene silencing with trabedersen (AP 12009) in pancreatic cancer. *Cancer Sci* **2011***,*102, (6), 1193-200.

18. Boockvar, J. A.; Tsiouris, A. J.; Hofstetter, C. P.; Kovanlikaya, I.; Fralin, S.; Kesavabhotla, K.; Seedial, S. M.; Pannullo, S. C.; Schwartz, T. H.; Stieg, P.; Zimmerman, R. D.; Knopman, J.; Scheff, R. J.; Christos, P.; Vallabhajosula, S.; Riina, H. A., Safety and maximum tolerated dose of superselective intraarterial cerebral infusion of bevacizumab after osmotic blood-brain barrier disruption for recurrent malignant glioma. Clinical article. *J Neurosurg* **2011***,* 114, (3), 624-32.

19. Qin, Y.; Chen, H.; Zhang, Q.; Wang, X.; Yuan, W.; Kuai, R.; Tang, J.; Zhang, L.; Zhang, Z.; Zhang, Q.; Liu, J.; He, Q., Liposome formulated with TAT-modified cholesterol for improving brain delivery and therapeutic efficacy on brain glioma in animals. *Int J Pharm* **2011***,* 420, (2), 304-12.

20. Xin, H.; Sha, X.; Jiang, X.; Zhang, W.; Chen, L.; Fang, X., Anti-glioblastoma efficacy and safety of paclitaxel-loading Angiopep-conjugated dual targeting PEG-PCL nanoparticles. *Biomaterials* **2012**, 33, (32), 8167-76.

21. Drappatz, J.; Brenner, A.; Wong, E. T.; Eichler, A.; Schiff, D.; Groves, M. D.; Mikkelsen, T.; Rosenfeld, S.; Sarantopoulos, J.; Meyers, C. A.; Fielding, R. M.; Elian, K.; Wang, X.; Lawrence, B.; Shing, M.; Kelsey, S.; Castaigne, J. P.; Wen, P. Y., Phase I study of GRN1005 in recurrent malignant glioma. *Clin Cancer Res* **2013***,* 19, (6), 1567-76.

CHAPTER 2

EVALUATION OF THE *IN VITRO* EFFICACY OF XYLOSIDES AND GLYCOSAMINOGLYCAN MIMETICS IN TREATING GLIOMA-ASSOCIATED INVASION AND ANGIOGENESIS

2.1 Introduction

In order to develop an efficient anticancer therapy based on proteoglycan biology, it is necessary to first determine if proteoglycan-based therapeutics are effective *in vitro*. Proteoglycans serve critical roles in angiogenesis, invasion, and growth due to their ability to bind to growth factors and chemokines, among other molecules. Therefore, if one were able to develop molecules that competed with or modified proteoglycan synthesis, it would be possible to alter proteoglycan biology in the local environment. Xylosides, sulfonated GAG mimetics, and chemically/chemoenzymatically synthesized GAGs represent a diverse set of therapeutic molecules that show promising anticancer activity *in vitro*.

Xylosides provide the ability to reengineer the tumor microenvironment. Click-xylosides are small scaffolds consisting of xylose residues attached to aglycone moieties. Click-xylosides compete with endogenous proteoglycan production and cause cells to release GAGs instead of attaching them to proteoglycans. In Figure 1 of "Chemical Tumor Biology of Heparan Sulfate Proteoglycans," it is explained that under

physiological conditions, a xylose attaches to the serine residue of the core protein to initiate GAG synthesis. When treated with click-xylosides, the xylose moiety of the click-xyloside serves as the initiator for GAG synthesis and does not bind to the serine of a core protein. These xyloside-primed GAGs are then released outside the cell where they can bind to growth factors and chemokines without being attached to cell surfaces. While the correlation between xyloside structure and their biological activity is still unclear, it is known the aglycone structure and linkage affect the stability and priming ability of xylosides. For example, a triazole linkage between the aglycone and the xylose is expected to improve blood stability whereas ester linkages are labile and cleaved by hydrolysis.[1] Additionally, it has been found that "cluster" xylosides, with multiple xylose residues per scaffold, are able to prime multiple chains per scaffold and affect FGF-8 signaling in zebrafish even though similar xylosides with one chain per scaffold do not have the same effect.[2]

In normal physiology, GAG synthesis begins on the 4-O position of xylose after it attaches to a serine residue on a core protein; 4-fluoro-xylosides have fluorine residues instead of hydroxyl residues at the 4-O position and thus inhibit the attachment of GAG chains onto the xyloside scaffold. By competing with endogenous xylose in cells, 4-fluoro-xylosides can perturb normal GAG biosynthesis. Previously it has been found that 4-fluoro-xylosides inhibit PG biosynthesis by outcompeting endogenous xylose and preventing chain attachment to the core protein. In this chapter we also show that treatment with various 4-fluoro-xylosides inhibits angiogenesis *in vitro* in a dose dependent manner.

In addition to xyloside based therapeutics, this chapter also describes the design

and development of novel GAG mimetics that can effectively alter proteoglycan biology in the cellular environment *in vitro*. Acharan sulfate is a newly discovered GAG from the giant African snail *Achatina Fulica*. It has a unique structure that is unlike heparin or heparan sulfate. Heparin is primarily composed of trisulfated disaccharides of 2*N*-sulfamido-6-O-sulfo-α-D-glucopyranoside (1→4)- 2-O-sulfo-α-L-idopyranosyluronate, whereas the primary structure of acharan sulfate is composed of 2*N*-acetamido- α-D-glucopyrnoside (1→4)- 2-*O*-sulfo- α-L-idopyranosyl uronate. However, natural acharan sulfate is difficult to isolate in large quantities and can be contaminated with other GAGs during the purification process. We synthesize an acharan sulfate mimetic chemically by modifying heparin's sulfation pattern. This mimetic is able to alter tumor associated angiogenesis *in vitro* and can easily be produced in large quantities.

Furthermore, several sulfonated small molecule scaffolds that can mimic disaccharide units of GAGs are developed as promising antiangiogenic compounds. Typical GAGs such as heparin are composed of repeating disaccharide units that carry one carboxyl group and up to four sulfate groups. Utilizing microwave sulfation, a series of organic scaffolds are persulfonated to confer a similar charge density with varying distances between adjacent sulfate groups. Additionally, since the size is maintained under 500 Da, these molecules are similar to GAG disaccharide units which are typically in the range of 378 Da to 596 Da. Evaluation of these molecules *in vitro* in an angiogenesis tube formation assay demonstrates their value as glycosaminoglycan mimics that can perturb GAG biology.

By modifying endogenous proteoglycan biology using small molecules, it is possible to target a diverse set of tumor-related functions using individual small

molecules. In addition, xylosides and other GAG mimics are nontoxic; thus, as part of an adjuvant therapy, it is likely that these molecules will dramatically improve the prognosis of patients with gliomas and other cancers.

2.2 Differential Effects of Heparitinase I and Heparitinase III on Endothelial Tube Formation *In vitro*

Manuscript reproduced with permission from: Raman, K. and Kuberan, B. (2010) Differential effects of Heparitinase I and Heparitinase III on endothelial tube formation *in vitro*, *Biochem. Biophys. Res. Commun. 398*, 191-193.

Biochemical and Biophysical Research Communications 398 (2010) 191–193

Contents lists available at ScienceDirect

Biochemical and Biophysical Research Communications

journal homepage: www.elsevier.com/locate/ybbrc

Differential effects of Heparitinase I and Heparitinase III on endothelial tube formation *in vitro*

Karthik Raman [a], Balagurunathan Kuberan [a,b,c,*]

[a] Department of Bioengineering, University of Utah, Salt Lake City, UT 84112, USA
[b] Department of Medicinal Chemistry, University of Utah, Salt Lake City, UT 84112, USA
[c] Graduate Program in Neuroscience, University of Utah, Salt Lake City, UT 84112, USA

ARTICLE INFO

Article history:
Received 5 June 2010
Available online 17 June 2010

Keywords:
Heparan sulfate
Angiogenesis
Heps
Heparin lyases
Heparitinases
Endothelial cell
Tube formation assay

ABSTRACT

Heparan sulfate proteoglycans (HSPGs) play vital roles in many steps of angiogenesis under physiological and pathological conditions. HSPGs on endothelial cell surfaces act as co-receptors for a variety of pro-angiogenic growth factors such as FGF and VEGF and anti-angiogenic factors such as endostatin. However, the fine structural requirements of these binding interactions are dependent on the sulfation patterns of HSPGs. Previous studies have shown that Heparitinases, heparin lyases isolated from *Flavobacterium heparinum*, can cleave heparan sulfate chains. These enzymes have been shown to reduce tumor–derived neovascularization *in vivo* in mice. However, the results from these experiments could not conclusively pinpoint the origin of the HS fragments. Thus, in this study we utilized an *in vitro* assay to assess the differential effects of Heparitinase I (Hep I) and Heparitinase III (Hep III) on endothelial tube formation. Hep III was found to be a more potent inhibitor of tube formation than Hep I. In conclusion, differential cleavage of endothelial cell surface bound HS can affect the extent of inhibition of tube formation.

1. Introduction

It is well known that solid tumors require extensive angiogenesis in order to facilitate their aberrant growth [1]. Targeting angiogenesis has been proven to be an effective strategy to starve tumors and increase patient survival. Heparan sulfate proteoglycans, present on cell surfaces and within the extracellular matrix, are intimately involved with endothelial cell function and are important in angiogenesis and tumor progression [2,3]. By binding to growth factors such as FGF, HBEGF, and VEGF, heparan sulfates act as co-receptors that are integral to signal transduction [4]. However, in order to bind growth factors, HS chains need certain sulfation patterns. A well-studied example, FGF2-binding-HS chains contain *N*-sulfated glucosamine units and 2-*O* sulfated iduronic acid [5]. Additionally, only HS chains containing 6-*O* sulfated glucosamine residues and 2-*O* sulfated iduronic acid along with *N*-sulfated glucosamine can bind to FGF receptor [6,7]. Thus, a combination of unique sulfation codes is necessary to potentiate FGF/FGFR mediated signaling. Tumors tailor their sulfation patterns using aberrant expression of HS biosynthetic and catabolic enzymes to improve their survivability [3,8].

Heparitinases, isolated from *Flavobacterium heparinum*, have been found to cleave heparan sulfate chains at defined locations (Fig. 1). Heparitinase I (Hep I, EC 4.2.2.8) cleaves HS chains containing glucuronic acid residues adjacent to glucosamine residues containing either *N*-acetyl or *N*-sulfate groups [9,10]. Heparitinase III (Hep III, EC 4.2.2.7) cleaves near sulfated iduronic acid residues [9–11].

It has been known for a long time that low molecular weight heparins, formed by treatment of unfractionated heparin with heparin lyases, have anti-angiogenic properties [12]. Previously, it has also been found that cell surface HS, digested with Hep I and III, reduces $VEGF_{165}$ binding and activity in endothelial cells [13,14]. Hep I and III also reduced neovascularization in an ex vivo CAM assay by reducing bFGF binding and subsequent signaling [15]. Additionally, both direct Hep I injections and Hep I-generated fragments have been found to inhibit myeloma growth *in vivo* in SCID mice [16]. Hep I and III have also shown differential effects in reducing tumor growth and angiogenesis *in vivo* [17].

Past results have shown the anti-angiogenic activity of Hep I and III. However, several of these results are muddled due to digestion of tumor derived GAGs or due to digestion of heparan sulfate chains from surrounding tissue as well as from endothelial cell surfaces. The effects of direct Heparitinase digestion of endothelial GAGs on angiogenesis have not yet been examined. Thus, in this study we examined the differential effects of Hep I and III on tube formation of BLMVEC on RGF-BME *in vitro*.

* Corresponding author. Address: Department of Medicinal Chemistry, University of Utah, 30 S 2000 E, Skaggs Hall Room 307, Salt Lake City, UT 84112, USA. Fax: +1 801 585 9119.
E-mail address: kuby@pharm.utah.edu (B. Kuberan).

0006-291X/$ - see front matter © 2010 Elsevier Inc. All rights reserved.
doi:10.1016/j.bbrc.2010.06.055

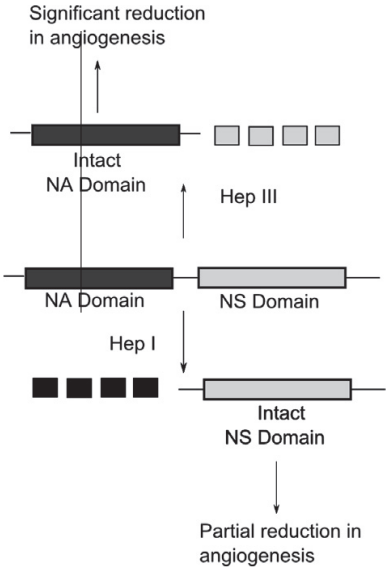

Fig. 1. Site of action of (A) Hep I and (B) Hep III. Hep I fragments NA domains so that only NS domains are left intact. Hep III fragments NS domains and leaves NA domains intact. Hep I: Heparitinase I, Hep III: Heparitinase III, NA: N-Acetylated domain, NS: N-Sulfated domain.

2. Materials and methods

2.1. Cell culture

Bovine lung microvascular endothelial cells of passage 4–8 (a kind gift from Dr. Randal Dull) were cultured in MCDB-131 Complete media (Vec Technologies). Hep I and Hep III from *F. heparinum* were expressed and purified as previously described [18].

2.2. Tube formation assay

Reduced growth factor basement membrane matrix (RGF-BME, Trevigen) was thawed overnight for 16 h at 4 °C. Fifty microliters of RGF-BME was then plated out in each well of a 96 well plate. Plates were then incubated in a humidified incubator at 37 °C for 1 h. BLMVEC were then suspended by incubation with Tryp LE Express (Invitrogen). 1×10^5 cells were then added to each well along with MCDB-131 Complete media and different amounts of Hep I and Hep III. Plates were then incubated in the incubator for 16 h prior to Calcein staining and imaging.

2.3. Calcein staining

Media was removed from wells in the 96 well plate by gentle dabbing with a paper towel. Cells were then washed twice with PBS and incubated in 100 μl of 2 μM Calcein AM for 30 min in the humidified incubator at 37 °C. After incubation in the Calcein AM working solution, the cells were washed once again with PBS and imaged in a Olympus IX81 microscope with an attached color CCD Filter and a GFP emission filter using 485 nm excitation/520 nm emission.

3. Results and discussion

Amounts of Hep I and Hep III needed to have comparable enzymatic activity were added to BLMVEC as described in the methods section. Since BLMVEC form tubes spontaneously on the basement membrane extract in the culture media, wells without any additives were used as positive controls. Sulforaphane (included with the tube formation assay) at 20 μM final concentration was used as a negative control. Thirty and 100 mU of either enzyme were added to 200 μl of total volume including cells and media. Hep III was found to be a much stronger inhibitor of angiogenesis compared to Hep I as shown in Fig. 2. Tube formation in the well containing 100 mU Hep I is comparable to that in the well containing 30 mU Hep III in terms of the qualitative extent of tube formation and the number of tubes. The 100 mU Hep III well is comparable to the inhibition shown in the negative control. Additional tests performed at 60 mU of activity also led to the same conclusion (data not provided).

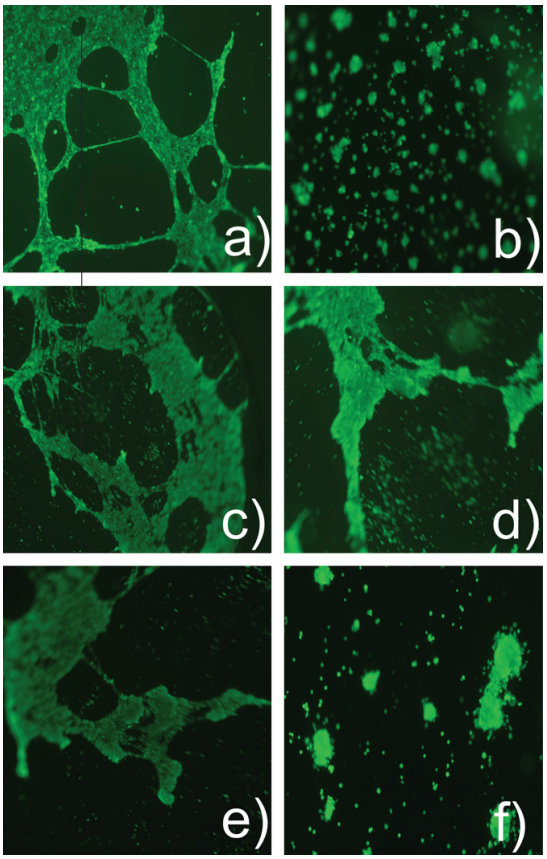

Fig. 2. Hep III and Hep I were added at equal activities onto BLMVEC on GFR matrigel. (a) Control without enzymes. (b) Control with 20 μM sulforaphane. (c) Hep I 30 mU. (d) Hep I 100 mU. (e) Hep III 30 mU. (f) Hep III 100 mU. Results are from three independent experiments performed in triplicate.

Angiogenesis is critical to tumor growth and heparan sulfates play key roles in this process by acting as co-receptors for growth factors among other functions. Thus, altering heparan sulfate interactions using drugs or enzymes can be a potent method of mitigating tumor growth and survival. Several studies have already shown the efficacy of this treatment strategy. Heparin, an antagonist of P-Selectin mediated interactions with platelets, has been known to reduce tumor metastasis and increase tumor–monocyte interactions by inhibiting the formation of a platelet 'cloak' [19].

Additionally, PI-88, a highly charged heparin analog, has entered human clinical trials because it prevents angiogenesis mediated by FGF and VEGF among other effects [20]. By targeting heparan sulfates, it is possible to reduce cancer growth and increase patient survival.

Heparan sulfates represent a potent target for angiogenesis treatments because of their numerous interactions with growth factors on cell surfaces and within the extracellular matrix. In this study we found that Hep treatment of endothelial cell heparan sulfates reduces their capability to form capillary tubes *in vitro*. Hep III was a more potent inhibitor of tube formation when compared with Hep I at equal activity. We attribute this difference to the substrate specificities of the two enzymes. Hep I cleaves at undersulfated, NA, regions of HS chains whereas Hep III cleaves at highly sulfated, NS, regions. Hep III therefore may disrupt the growth factor binding domains that are important for angiogenesis. Hep I, on the other hand, still generates fragments that retain their growth factor binding capability and therefore still potentiate tube formation.

This conclusion is also supported by previous studies that show that heparan sulfate proteoglycans on endothelial cells are essential to VEGF and FGF binding (potent pro-angiogenesis factors). Future studies will probe the relative importance of the different sulfate groups in the highly sulfated HS regions with the aid of specific and reversible biosynthetic inhibitors that are currently under development in our lab. Utilizing such knowledge will allow researchers to further understand the structure–function relationships of heparan sulfate proteoglycans in angiogenesis. In conclusion, we have discovered that the NS domains of heparan sulfates are more important to endothelial tube formation than the non-sulfated domains.

Acknowledgments

This work was supported by National Institutes of Health grant (GM075168), Human Frontier Science Program grant and American Heart Association National Scientist Development Award to B.K.

References

[1] J. Folkman, Tumor angiogenesis: role in regulation of tumor growth, Symp. Soc. Dev. Biol. 30 (1974) 43–52.
[2] I. Vlodavsky, A. Eldor, M. Bar-Ner, R. Fridman, I.R. Cohen, M. Klagsbrun, Heparan sulfate degradation in tumor cell invasion and angiogenesis, Adv. Exp. Med. Biol. 233 (1988) 201–210.
[3] K. Raman, B. Kuberan, Chemical tumor biology of heparan sulfate proteoglycans, Curr. Chem. Biol. 4 (2010) 20–31.
[4] J.T. Gallagher, I.N. Hampson, Proteoglycans in cellular differentiation and neoplasia, Biochem. Soc. Trans. 12 (1984) 541–543.
[5] S. Guimond, M. Maccarana, B.B. Olwin, U. Lindahl, A.C. Rapraeger, Activating and inhibitory heparin sequences for FGF-2 (basic FGF). Distinct requirements for FGF-1, FGF-2, and FGF-4, J. Biol. Chem. 268 (1993) 23906–23914.
[6] N. Sugaya, H. Habuchi, N. Nagai, S. Ashikari-Hada, K. Kimata, 6-*O*-sulfation of heparan sulfate differentially regulates various fibroblast growth factor-dependent signalings in culture, J. Biol. Chem. 283 (2008) 10366–10376.
[7] L. Lundin, H. Larsson, J. Kreuger, S. Kanda, U. Lindahl, M. Salmivirta, L. Claesson-Welsh, Selectively desulfated heparin inhibits fibroblast growth factor-induced mitogenicity and angiogenesis, J. Biol. Chem. 275 (2000) 24653–24660.
[8] M. Morimoto-Tomita, K. Uchimura, A. Bistrup, D.H. Lum, M. Egeblad, N. Boudreau, Z. Werb, S.D. Rosen, Sulf-2, a proangiogenic heparan sulfate endosulfatase, is upregulated in breast cancer, Neoplasia 7 (2005) 1001–1010.
[9] V.C. Yang, R.J. Linhardt, H. Bernstein, C.L. Cooney, R. Langer, Purification and characterization of heparinase from *Flavobacterium heparinum*, J. Biol. Chem. 260 (1985) 1849–1857.
[10] D.L. Lohse, R.J. Linhardt, Purification and characterization of heparin lyases from *Flavobacterium heparinum*, J. Biol. Chem. 267 (1992) 24347–24355.
[11] P. Hovingh, A. Linker, The enzymatic degradation of heparin and heparitin sulfate. 3. Purification of a heparitinase and a heparinase from flavobacteria, J. Biol. Chem. 245 (1970) 6170–6175.
[12] K. Norrby, Low-molecular-weight heparins and angiogenesis, APMIS 114 (2006) 79–102.
[13] H. Gitay-Goren, S. Soker, I. Vlodavsky, G. Neufeld, The binding of vascular endothelial growth factor to its receptors is dependent on cell surface-associated heparin-like molecules, J. Biol. Chem. 267 (1992) 6093–6098.
[14] S. Gengrinovitch, B. Berman, G. David, L. Witte, G. Neufeld, D. Ron, Glypican-1 is a VEGF165 binding proteoglycan that acts as an extracellular chaperone for VEGF165, J. Biol. Chem. 274 (1999) 10816–10822.
[15] R. Sasisekharan, M.A. Moses, M.A. Nugent, C.L. Cooney, R. Langer, Heparinase inhibits neovascularization, Proc. Natl. Acad. Sci. USA 91 (1994) 1524–1528.
[16] Y. Yang, V. MacLeod, Y. Dai, Y. Khotskaya-Sample, Z. Shriver, G. Venkataraman, R. Sasisekharan, A. Naggi, G. Torri, B. Casu, I. Vlodavsky, L.J. Suva, J. Epstein, S. Yaccoby, J.D. Shaughnessy Jr., B. Barlogie, R.D. Sanderson, The syndecan-1 heparan sulfate proteoglycan is a viable target for myeloma therapy, Blood 110 (2007) 2041–2048.
[17] D. Liu, Z. Shriver, G. Venkataraman, Y. El Shabrawi, R. Sasisekharan, Tumor cell surface heparan sulfate as cryptic promoters or inhibitors of tumor growth and metastasis, Proc. Natl. Acad. Sci. USA 99 (2002) 568–573.
[18] P. Babu, B. Kuberan, Fluorescent-tagged heparan sulfate precursor oligosaccharides to probe the enzymatic action of heparitinase I, Anal. Biochem. 396 (2010) 124–132.
[19] L. Borsig, R. Wong, J. Feramisco, D.R. Nadeau, N.M. Varki, A. Varki, Heparin and cancer revisited: mechanistic connections involving platelets, P-selectin, carcinoma mucins, and tumor metastasis, Proc. Natl. Acad. Sci. USA 98 (2001) 3352–3357.
[20] V. Ferro, K. Dredge, L. Liu, E. Hammond, I. Bytheway, C. Li, K. Johnstone, T. Karoli, K. Davis, E. Copeman, A. Gautam, PI-88 and novel heparan sulfate mimetics inhibit angiogenesis, Semin. Thromb. Hemost. 33 (2007) 557–568.

2.2.1 Additional Analysis of Data

In order to quantify the effects of treatment with heparitinase I and III, images of tubes formed by BLMVEC were processed in ImageJ software and analyzed using an Angioanalyzer script developed by Giles Carpentier.[1] Additional experiments to discern the antiangiogenic potential of heparitinase I and III may include a variety of vessel outgrowth assays performed in matrigel, *ex vivo* chick chorioallantoic membrane (CAM) assay, and corneal angiogenesis assays, among others.

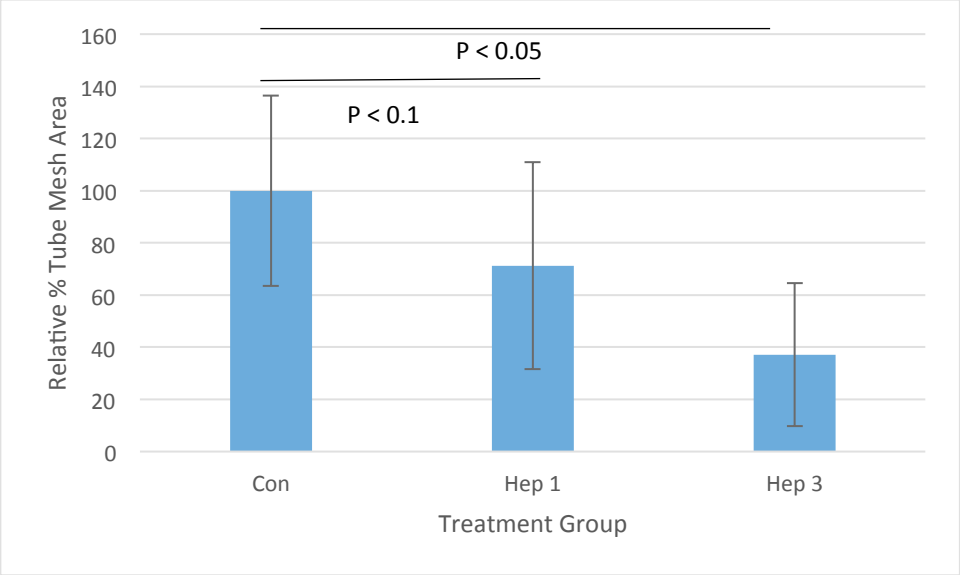

Figure 2.1. Relative mesh area covered by tubes. Tube formation was quantified using ImageJ software using an Angioanalyzer script. Statistical analysis was performed using a paired 1-tailed t-test. Error bars indicate standard deviations.

2.2.2 References

1. Carpentier G, Martinelli M, Courty J and Cascone I. Angiogenesis Analyzer for ImageJ. 4th ImageJ User and Developer Conference proceedings. Mondorf-les-Bains, Luxembourg. ISBN: 2-919941-18-6 : 198-201, 2012.

2.3 Click-Xylosides Mitigate Glioma Cell Invasion *In vitro*

Raman, K. and Kuberan, B. (2010) Click-Xylosides mitigate glioma cell invasion *in vitro*, *Mol Biosyst., 6*, 1800-1802 - Reproduced by permission of The Royal Society of Chemistry.

COMMUNICATION www.rsc.org/molecularbiosystems | Molecular BioSystems

Click-xylosides mitigate glioma cell invasion *in vitro*†

Karthik Raman[a] and Balagurunathan Kuberan*[abc]

Received 26th May 2010, Accepted 29th June 2010
DOI: 10.1039/c0mb00020e

Tumor related invasion allows cancers to spread beyond tissue boundaries and significantly affects patient prognosis. In this study we show that several click-xylosides markedly inhibit the invasive capability of a highly invasive glioma cell line *in vitro*. These novel xylosides are promising chemical biology tools to probe the role of the proteoglycan glycome in regulating tumor biology.

Neuroblastomas, especially glioblastoma multiforme (GBM), are extremely aggressive cancers characterized by hypoxia-mediated necrotic centers, extensive tumor-associated angiogenesis, and significant invasion into nearby neural tissues.[1] Invasion provides such cancers with improved nutrition and greatly increases their capacity to metastasize and eventually cause cancer-related death. Proteoglycans, composed of a core protein substituted with several glycosaminoglycan (GAG) side chains, act as co-receptors for growth factors such as FGF, VEGF, HBGF, *etc*. and play several central roles in modulating the cell-extra cellular matrix interactions involved in tumor associated invasion and angiogenesis.[2–4] Several GAG based drugs such as PI-88 and Suramin have shown great promise in clinical trials in combating invasive cancers.[5] Additionally, animal derived heparin, a highly sulfated GAG family member commonly used as an anticoagulant, has been shown to significantly inhibit cancer metastasis.[6] Tumor cell associated chondroitin sulfate and dermatan sulfate chains have also been shown to regulate proliferation and angiogenesis.[7]

Xylosides carrying certain hydrophobic aglycones, which can act as acceptors for GAG chain elongation in the Golgi, have been shown to prime free GAGs that are secreted into ECM.[8,9] Xylosides have been used to determine the importance of GAGs *in vitro* and *in vivo* because free GAGs are known to disrupt the molecular interactions of endogenous GAGs with their ligands.[8,10] Previously, it was found that 2(6-hydroxynaphthyl)-beta-D-xylopyranoside significantly reduced tumor growth *in vivo*.[11] Recently, it was reported that β-D-xyloside inhibited the invasive capability of HeLa cells in culture medium containing SDF-1/CXCL12.[12] However, most xylosides studied until now are unstable *O*-xylosides. It is difficult to synthesize *O*-xylosides in a stereoselective manner to produce exclusively a β-glycosidic linkage, which is required for GAG priming activity, due to the lack of a stereodirecting *C*-6 hydroxyl group. Additionally, a majority of *O*-xylosides prime chondroitin sulfate chains of low molecular weight. Our lab has developed a method to address the limitations of *O*-xylosides by utilizing click chemistry to synthesize a library of click-xylosides containing various aglycone groups. These xylosides have been shown to produce GAGs of differing lengths, compositions, and sulfation densities in CHO pgsA-745 cells (Table 1).[13]

Based on these findings and the fact that GAGs play an important role in tumor invasion, we hypothesized that different GAGs produced by click-xylosides would have variable effects on the invasive nature of U87MG glioma cells. The results reported here provide the first direct evidence for the anti-invasive capability of click-xylosides and provide an opportunity to test the effects of aglycone groups of click-xylosides to design more potent anti-invasive GAG primers.

The click-xylosides utilized in this study were found to inhibit U87MG invasion to differing degrees without affecting cell viability (ESI†) *in vitro* at 100 μM concentration (Fig. 1). The most significant inhibition was seen in xylosides **2** and **5** where upto ~70% fewer cells invaded through the matrigel matrix compared to untreated controls. While it is uncertain what structural features of xylosides are necessary for inhibiting invasion, it was found that click-xylosides primed a significant amount of GAGs in U87MG cells seeded on matrigel (Fig. 2). In fact, xyloside **4** increased GAG production by ~800% relative to control cells. It is interesting to note that the priming activity did not seem to have any correlation with the anti-invasive activity of click-xylosides. However, some conclusions can be drawn regarding the correlation between click-xyloside aglycone structure and the ability to inhibit invasion. Comparing napthalene containing click-xylosides (**2** and **5**) *vs*. phenyl containing click-xylolsides (**1**, **3**, **4** and **6**), it can be seen that the inclusion of a naphthalene ring potentiates the inhibition of invasion. Mani *et al*. have earlier observed that *O*-xyosides carrying napthyl derivatives inhibited tumor cell proliferation.[11] Additionally, comparing xylosides **3** and **6** which differ by the lengths of their aglycone linkages, it can be seen that xyloside **3** (a shorter linker) is a better inhibitor of invasion than xyloside **6**. More extensive studies are required to better define the molecular basis for these observations.

The effects of click-xylosides on the invasive capability of U87MG cells were also examined at 10 μM and 500 μM concentrations by adding them to both the top and bottom wells of the invasion chamber (Fig. 3). While both xylosides **1** and **3** showed a general increase in inhibition at higher

[a] *Department of Bioengineering, University of Utah, 30 S 2000 E, Skaggs Hall Room 307, Salt Lake City, Utah 84112, USA*
[b] *Department of Medicinal Chemistry, University of Utah, 30 S 2000 E, Skaggs Hall Room 307, Salt Lake City, Utah 84112, USA*
[c] *Interdepartmental Program in Neuroscience, University of Utah, 30 S 2000 E, Skaggs Hall Room 307, Salt Lake City, Utah 84112, USA. E-mail: KUBY@pharm.utah.edu; Fax: (+1) 801-585-9119; Tel: (+1) 801-587-9474*

† Electronic supplementary information (ESI) available: Priming activity and cell viability of U87MG incubated with xylosides. See DOI: 10.1039/c0mb00020e

Table 1 Click-xylosides used to probe glioma cell invasion

1	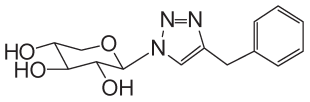
2	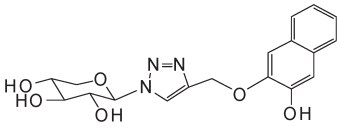
3	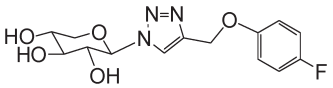
4	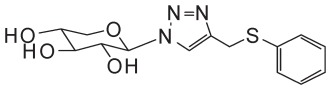
5	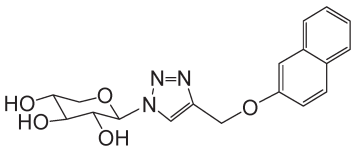
6	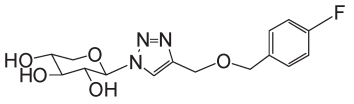

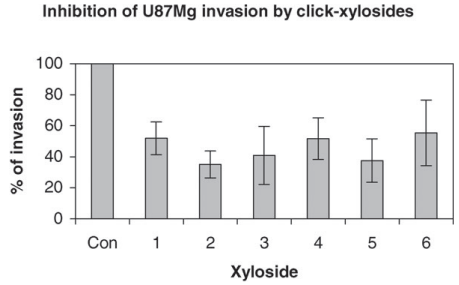

Fig. 1 Click-xylosides inhibit U87MG invasion: Inhibition of invasion is plotted as a percentage of control (untreated) cells and treated cells with various click-xylosides (100 μM) that passed through the matrigel invasion chamber at the end of 72 h. Results are from three independent experiments performed in duplicate.

concentrations, it is noteworthy that the maximal rate of change of inhibition occurred at lower concentrations.

Invasion into nearby tissues is a characteristic feature of malignant cancers. By containing cancers to specific regions, it may be easier to provide localized treatment and improve patient survivability. Additionally, if used in combination with anti-angiogenic treatment, anti-invasive compounds may effectively destroy cancers without selecting for drug resistant cells.[14,15] Anti-invasive therapy may also control cancer spread in cases where it is not possible to resect tumors.

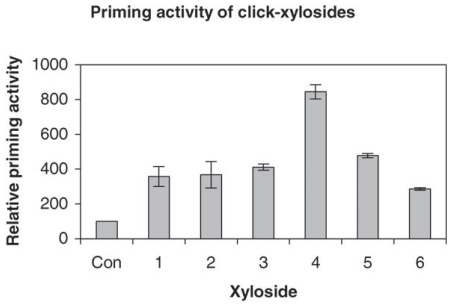

Fig. 2 Relative priming activity of various click-xylosides in U87MG cells: Xyloside priming is plotted as a percent of GAGs secreted into the supernatant from treated cells relative to control cells. Results are from two independent experiments performed in duplicate.

Several reviews have detailed the effects of proteoglycans such as heparan and chondroitin sulfate on promoting as well as inhibiting cancer growth, invasion, and metastasis.[4,7] We have found a series of xylosides that are potent inhibitors of invasion without affecting cell viability. These xylosides have shown to inhibit invasion *in vitro* in matrigel invasion chambers at micromolar concentrations (Fig. 1). Additionally, similar to traditional anticancer drugs, these xylosides show dose-dependency (Fig. 3). However, as stated in the results, the slope of the inhibition curve is much steeper at lower concentrations. This observation can be expected if the GAG products of the xylosides bind to specific chemokines present in serum (such as SDF-1) and saturate this interaction at higher concentrations. Efforts are currently underway to deduce the exact mechanism of action that will be disseminated in future studies.

Click-xylosides offer several advantages if used as drugs. They possess high diffusion coefficients and therefore they can easily penetrate cells because they are small and contain hydrophobic groups. Additionally, since they do not affect cell viability, they cannot select for drug resistant tumor cells. However, a major disadvantage of xyosides is that the size and composition of primed GAGs depends on cell type.[13] Thus, the anticancer activity of xylosides may be variable depending

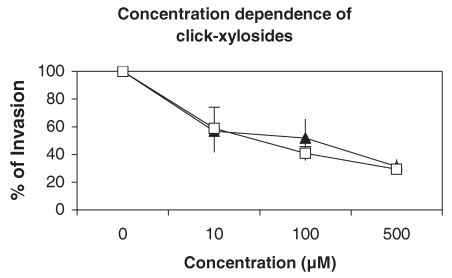

Fig. 3 Dose dependence of click-xyloside mediated inhibition of glioma cell invasion. Open squares (□) represent click-xyloside 3 and closed triangles (▲) represent click-xyloside **1**. Results are representative of three independent experiments performed at 10 μM, 100 μM, and 500 μM concentrations of click-xylosides.

on the cells they penetrate. In summary, we have found novel click-xylosides that selectively inhibit invasion of U87MG glioma cells *in vitro*. Future studies will detail the *in vivo* effects of these click-xylosides as well as their effects in different cell types.

Acknowledgements

This work is supported by National Institutes of Health grant (GM075168), Human Frontier Science Program grant, and American Heart Association National Scientist Development Award to BK.

Notes and references

1 R. L. Jensen, *J. Neuro-Oncol.*, 2009, **92**, 317–335.
2 R. Sasisekharan, Z. Shriver, G. Venkataraman and U. Narayanasami, *Nat. Rev. Cancer*, 2002, **2**, 521–528.
3 R. D. Sanderson, Y. Yang, T. Kelly, V. MacLeod, Y. Dai and A. Theus, *J. Cell. Biochem.*, 2005, **96**, 897–905.
4 K. Raman and B. Kuberan, *Curr. Chem. Biol.*, 2010, **4**, 20–31.
5 V. Ferro, K. Dredge, L. Liu, E. Hammond, I. Bytheway, C. Li, K. Johnstone, T. Karoli, K. Davis, E. Copeman and A. Gautam, *Semin. Thromb. Hemostasis*, 2007, **33**, 557–568.
6 H. C. Hoover, Jr and A. S. Ketcham, *Cancer*, 1975, **35**, 5–14.
7 G. W. Yip, M. Smollich and M. Gotte, *Mol. Cancer Ther.*, 2006, **5**, 2139–2148.
8 M. Okayama, K. Kimata and S. Suzuki, *J. Biochem.*, 1973, **74**, 1069–1073.
9 B. Kuberan, M. Ethirajan, X. V. Victor, V. Tran, K. Nguyen and A. Do, *ChemBioChem*, 2008, **9**, 198–200.
10 N. B. Schwartz, L. Galligani, P. L. Ho and A. Dorfman, *Proc. Natl. Acad. Sci. U. S. A.*, 1974, **71**, 4047–4051.
11 K. Mani, M. Belting, U. Ellervik, N. Falk, G. Svensson, S. Sandgren, F. Cheng and L. A. Fransson, *Glycobiology*, 2004, **14**, 387–397.
12 S. Brule, V. Friand, A. Sutton, F. Baleux, L. Gattegno and N. Charnaux, *Biochim. Biophys. Acta, Gen. Subj.*, 2009, **1790**, 1643–1650.
13 X. V. Victor, T. K. Nguyen, M. Ethirajan, V. M. Tran, K. V. Nguyen and B. Kuberan, *J. Biol. Chem.*, 2009, **284**, 25842–25853.
14 G. Minniti, R. Muni, G. Lanzetta, P. Marchetti and R. M. Enrici, *Anticancer Res.*, 2009, **29**, 5171–5184.
15 I. Appelmann, R. Liersch, T. Kessler, R. M. Mesters and W. E. Berdel, *Recent Results Cancer Res.*, 2010, **180**, 51–81.

Supplemental data

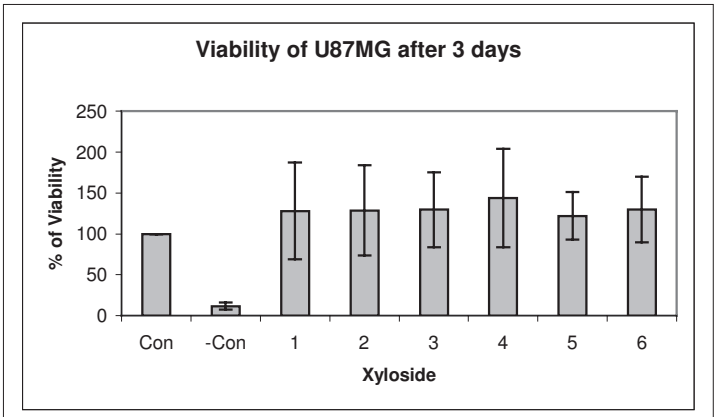

Fig. 1. Viability of U87MG cells 3 days after treatment with xylosides. Data from xylosides is plotted as a percentage relative to positive control (untreated cells) and negative control (cells treated with 5% SDS). Results are from two independent experiments performed in triplicate.

Methods

Cell Culture: U87MG human glioma cells (generously provided by Dr. Randy Jensen, University of Utah) were cultured in DMEM (Invitrogen) with 10% FBS, penicillin/streptomycin in a humidified incubator at 37 °C and 5 % O_2.

Matrigel Invasion: U87MG human glioma cells were plated at $1x10^5$ cells/well in the top well of a 6 well matrigel invasion chamber (BD Biosciences, San Jose, CA, USA). HAM S/ F-12 media with penicillin/streptomycin was added to the top well and HAMS/F-12 (Invitrogen) media with 10% FBS and penicillin/streptomycin (P/S) was added to the bottom well. Upon trypsinization (Tryp LE Express, Invitrogen Inc.), xyloside solutions (Table 1) were added to indicated final concentrations to both the top and bottom invasion wells. Invasion chambers were maintained in a humidified incubator at 37 ^oC for 3 days. After this time period, supernatant from the top well was aspirated and cells with matrigel were removed using a cotton swab and the well was washed twice with PBS. Subsequently the PET membrades were cut from the well using a razor and placed in trypsin to remove cells that had invaded through and deposited on the bottom side of the PET membrane. Invaded cells were then counted using a hemocytometer.

Priming activity: 500 µl of LDEV-free Matrigel (BD Biosciences) was thawed overnight, added to 6 well plates, and then incubated at 37 °C for 1 hr. U87MG cells were then plated at $1x10^5$ cells per well in HamS/F-12 media supplemented with 10% dialyzed FBS and pennicilin/streptomycin. Xylosides and Sulfur-35 (Perkin Elmer) were added to wells to final concentration s of 100 µM and 10 µCi/ml, respectively. After 3 days, supernatants from the wells were collected. Subsequently, cell recovery solution was added at 2 ml/well and plates were stored at 4 °C for 1 hr. The solubilized matrigel was then centrifuged at 1000 x g for 10 min to remove cell debris. Both the supernatants (before and after cell recovery) were then combined and diluted 1:2 with 0.016% Triton X-100. The diluted supernatant mix was then loaded onto a DEAE Sepharose column (0.5 ml) pre-equilibriated with 10 column volumes of wash buffer (20 mM NaOAc buffer (pH 6.0), 0.1 M NaCl, 0.01% Triton X-100). The column was then washed with 30 column volumes of wash buffer. Bound HS/CS chains were then eluted with 6 column volumes of elution buffer (20 mM NaOAc,1 M NaCl, pH 6.0). Priming activity was determined as the counts per minute detectable in 50 µl of eluant.

Cell Viability: U87MG cells were tested for viability in the presence of xylosides using Cell Titer Blue reagent (Promega). Cells were seeded into triplicate wells of a 96 well plate at 2.5 x 10^4 cells/well in 125 µl of Ham's F-12 media +10% FBS +P/S. Xylosides were added to final concentrations of 100 µM per well and cells were incubated in a humidified incubator for 3 days. After the incubation period, negative controls were treated with 50 µl of 3% SDS solution for 10 minutes. Subsequently 25 µl of Cell Titer-Blue reagent was added as per manufacturer's protocol. Cells were incubated in incubator for 2 hrs and fluorescence substrate generation was then stopped by addition of 50 µl of 3% SDS to all wells. The fluorescence was measured using a Spectra-Max M5 microplate reader (Molecular Devices, Sunnyvale, CA) at an excitation wavelength of 560 nm and an emission wavelength of 590 nm

2.3.1 Additional Analysis of Data

Additional analysis of data from the click-xyloside experiments are shown in Figure 2.2.

2.4 Novel Glycosaminoglycan Biosynthetic Inhibitors Affect Tumor-Associated Angiogenesis

Manuscript reproduced with permission from: Raman, K., Ninomiya, M., Nguyen, T K., Tsuzuki, Y., Koketsu, M., and Kuberan, B. (2011) Novel glycosaminoglycan biosynthetic inhibitors affect tumor-associated angiogenesis, *Biochem. Biophys. Res. Commun. 404*, 86-89.

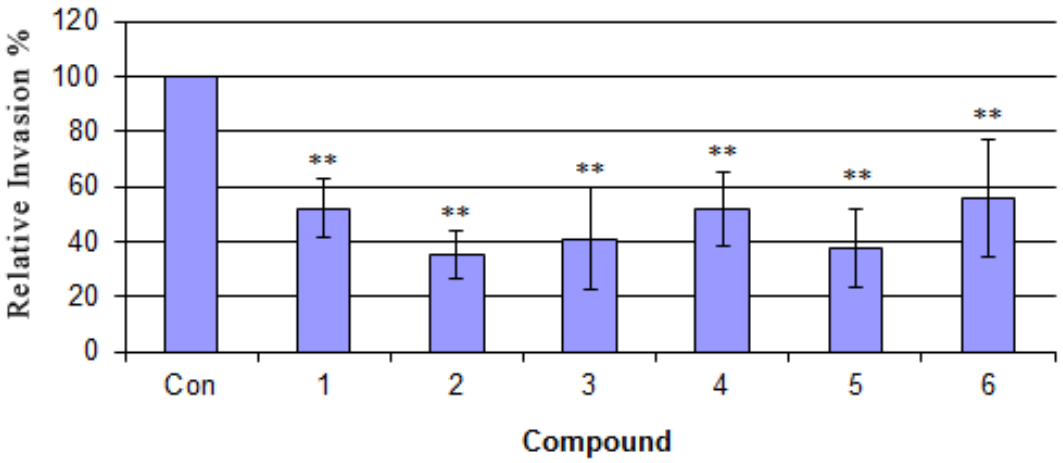

Figure 2.2. Invasion inhibition by click xylosides with statistical significance denoted. Inhibition of invasion is plotted as a relative percentage compared to control untreated cells. ** indicates that a $P<0.05$ as determined by a 1-tailed paired t-test compared to control untreated cells. Error bars indicate standard deviations.

Biochemical and Biophysical Research Communications 404 (2011) 86–89

Contents lists available at ScienceDirect

Biochemical and Biophysical Research Communications

journal homepage: www.elsevier.com/locate/ybbrc

Novel glycosaminoglycan biosynthetic inhibitors affect tumor-associated angiogenesis

Karthik Raman [a], Masayuki Ninomiya [b], Thao Kim Nu Nguyen [a], Yasuhiro Tsuzuki [c], Mamoru Koketsu [b], Balagurunathan Kuberan [a,d,e,*]

[a] Department of Bioengineering, University of Utah, Salt Lake City, UT 84112, USA
[b] Department of Materials Science and Technology, Faculty of Engineering, Gifu University, Gifu 501-1193, Japan
[c] Department of Chemistry, Faculty of Engineering, Gifu University, Gifu 501-1193, Japan
[d] Interdepartmental Program in Neuroscience, University of Utah, Salt Lake City, UT 84112, USA
[e] Department of Medicinal Chemistry, University of Utah, Salt Lake City, UT 84112, USA

ARTICLE INFO

Article history:
Received 29 October 2010
Available online 19 November 2010

Keywords:
Heparan sulfate
Angiogenesis
Xyloside
Proteoglycan
Inhibitor
Matrigel

ABSTRACT

Heparan sulfate proteoglycans (HSPGs) are essential players in several steps of tumor-associated angiogenesis. As co-receptors for several pro-angiogenic factors such as VEGF and FGF, HSPGs regulate receptor–ligand interactions and play a vital role in signal transduction. Previously, we have employed an enzymatic strategy to show the importance of cell surface HSPGs in endothelial tube formation *in vitro*. We have recently found several fluoro-xylosides that can selectively inhibit proteoglycan synthesis in endothelial cells. The current study demonstrates that these fluoro-xylosides are effective inhibitors of endothelial tube formation *in vitro* using a matrigel based assay to simulate tumor-associated angiogenesis. These first generation scaffolds offer a promising stepping-stone to the discovery of more potent fluoro-xylosides that can effectively neutralize tumor growth.

1. Introduction

Inhibiting tumor angiogenesis is a powerful approach to mitigate cancer growth [1]. Heparan sulfate proteoglycans (HSPGs), cell-surface and ECM proteins containing highly sulfated glycosaminoglycan (GAG) chains, play vital roles throughout the various stages of angiogenesis and tumor growth [2–4]. They act as co-receptors for a variety of pro-angiogenic factors including VEGF and FGF [5–7]. As co-receptors, HSPGs facilitate receptor–ligand interactions and signal transduction. HS chains require certain sulfation patterns in order to bind to growth factors [8]. In particular, the binding of HS and FGF2 requires *N*-sulfated glucosamine units and 2-*O* sulfated iduronic acid units [9]. Furthermore, to bind to FGF receptor, HS chains require 6-*O* sulfated glucosamine residues and 2-*O* sulfated iduronic acid along with *N*-sulfated glucosamine [10,11]. Thus, only HS chains containing such a sulfation pattern can potentiate FGF/FGFR mediated signaling.

Xylosides containing certain hydrophobic aglycone groups can act as acceptors for GAG biosynthesis in the Golgi [12–14]. The primed GAGs are then secreted outside the cell and can have a variety of biological consequences by competing with endogenous proteoglycan chains [15]. Previously, it was found that β-D-xylopyranoside virtually eliminated the invasion of wound microvascular endothelial cells into fibrin gels [16]. Xylosides have also shown efficacy in preventing tumor progression [17–19]. It is also possible to inhibit proteoglycan synthesis by utilizing fluorine-containing xylosides [20].

Previously, we have shown that cell surface HS is essential for tube formation *in vitro* using heparitinase I and III [21]. Recently, we found that several novel fluoro-xylosides selectively inhibited GAG synthesis *in vitro* in endothelial cells (Table 1) [22]. Based on these results, we hypothesized that these fluoro-xylosides would be effective inhibitors of endothelial tube formation as well. In this article, we utilize the matrigel tube formation assay to show the anti-angiogenic efficacy of these novel fluoro-xylosides.

2. Methods

2.1. Cell culture

Bovine lung microvascular endothelial cells of passage 4–8 (a generous gift from Dr. Randall Dull) were cultured in MCDB-131 Complete media (Vec Technologies) in a humidified 37 °C incubator. Cells were split 24 h prior to conducting tube formation assays in order to keep them in the log phase of growth.

* Corresponding author. Address: University of Utah, 30 S 2000 E, Skaggs Hall Room 307, Salt Lake City, UT 84112, USA. Fax: +1 801 585 9119.
E-mail address: kuby@pharm.utah.edu (B. Kuberan).

0006-291X/$ - see front matter © 2010 Elsevier Inc. All rights reserved.
doi:10.1016/j.bbrc.2010.11.069

Table 1
Fluoro-xylosides tested for their ability to inhibit tube formation of BLMVEC *in vitro*.

I
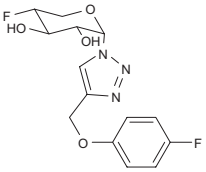

II
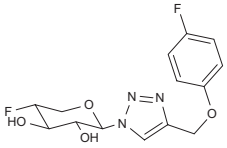

III
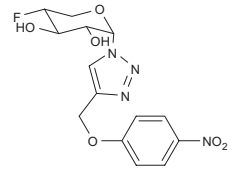

IV
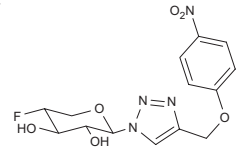

V
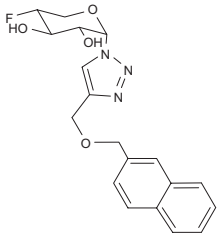

VI
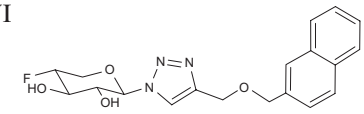

VII
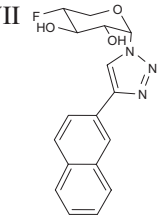

2.2. Tube formation assay

Reduced growth factor basement membrane matrix (RGF-BME, Trevigen) was thawed overnight at 4 °C in a frost free refrigerator. Fifty microliters of RGF-BME were then added to wells of a chilled 96 well plate using chilled pipette tips. The 96 well plates were then incubated in a humidified incubator for 1 h. Concurrently, BLMVEC were suspended by incubation with Tryp LE Express (Invitrogen). 1×10^5 cells were then added to each well along with MCDB-131 complete media and various fluoro-xylosides. The plates were then incubated at 37 °C for 16 h prior to Calcein staining and imaging.

2.3. Calcein staining

Media was removed from each well containing cells by gentle dabbing with a paper towel. The wells were then washed twice with PBS and then 100 μl of 2 μM Calcein AM was added to each well. Cells were then stored for 30 min in the incubator. After incubation in the calcein AM working solution, the cells were washed once again with PBS and imaged with an Olympus IX81 microscope attached to a color CCD Filter and a GFP emission filter using 485 nm excitation/520 nm emission.

3. Results and discussion

Tube formation experiments were performed on reduced growth factor basement membrane extract (matrigel) which simulates angiogenesis near the tumor microenvironment (Fig. 1). Since BLMVEC spontaneously form tubes on RGF-BME, wells without any compounds were used as positive controls. Sulforaphane (provided by the manufacturer) was used at 20 μM as a negative control.

Initially tube formation experiments were performed at a 300 μM concentration of each fluoro-xyloside as this concentration has previously been shown to inhibit GAG biosynthesis [22]. As shown in Fig. 1, only xylosides III and IV were able to inhibit tube formation at 300 μM concentration. No other fluoro-xylosides tested had any effect on tube formation at this concentration.

Based on these initial results, two other concentrations of xylosides III and IV were tested for their ability to inhibit tube formation in order to understand the dose-dependent nature of these small molecule drug candidates (Fig. 2). Xylosides III and IV did not inhibit tube formation at 150 μM concentration whereas they strongly inhibited tube formation at 600 μM concentration. At this concentration, the extent of inhibition of tube formation is comparable to the Sulforaphane negative control.

Angiogenesis is a complex multistep process whereby blood vessels sprout from existing vessels. It requires a multitude of molecular players including integrins, ECM components, proteases, and growth factors.

Several potent anti-cancer agents such as Bevacizumab (Avastin) have utilized this knowledge to attack tumors in the past [23]. However, drugs such as Avastin, which act only on singular molecular targets, may not be as efficacious as drugs that can affect multiple targets. The fluoro-xylosides presented in this paper represent a novel and powerful tool to inhibit angiogenesis because of their ability to target GAG biosynthesis and hence affect the multitude of interactions that are affiliated with cell-surface GAGs and proteoglycans.

In this paper, we have shown two fluoro-xylosides (III and IV) that are potent inhibitors of endothelial tube formation *in vitro*. There is a direct correlation between the most potent inhibitors of tube formation and the most potent inhibitors of GAG synthesis [22]. Since we have previously shown that cell surface heparan sulfates are essential players in the process of tube formation, it is likely that these fluoro-xylosides prevent tube formation by inhibiting GAG production [21]. Not only are these fluoro-xylosides ideal drug candidates due to their small size and their ability to penetrate cells, they are also excellent chemical biology tools to probe proteoglycan biology.

It can be argued that these first generation fluoro-xylosides are ineffective because of their high dosage requirements (300 μM). However, there are several methods of improving their potency.

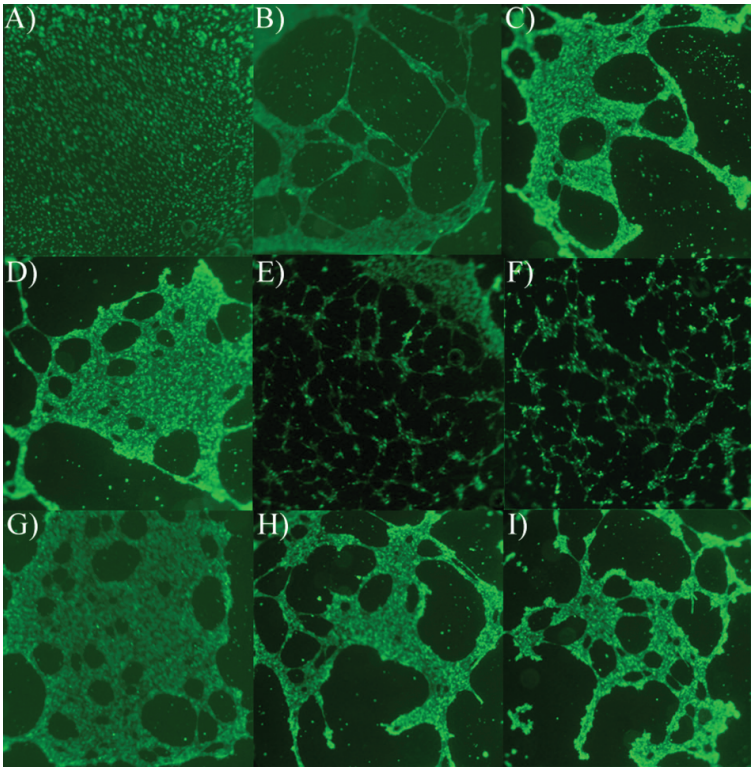

Fig. 1. Several fluoro-xylosides were added to BLMVEC on RGF matrigel at 300 μM concentrations. Representative images are: (A) 20 μM sulforaphane control. (B) Positive control. (C) Xyloside I. (D) Xyloside II. (E) Xyloside III. (F) Xyloside IV. (G) Xyloside V. (H) Xyloside VI. (I) Xyloside VII. These experiments were performed three times in duplicate wells.

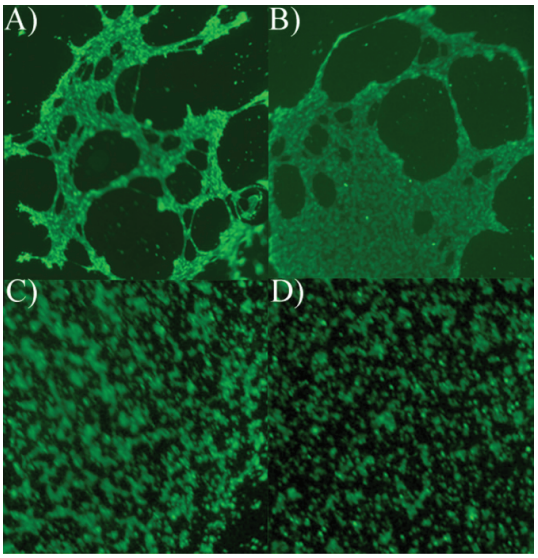

Fig. 2. Dose-dependent inhibition of tube formation by xylosides III and IV. Representative images are: (A) Xyloside III 150 μM. (B) Xyloside IV 150 μM. (C) Xyloside III 600 μM. (D) Xyloside IV 600 μM. These experiments were performed three times in duplicate wells.

Our lab has previously shown that varying the aglycone moiety attached to the xyloside can greatly affect its ability to prime distinct GAGs [12]. Additionally, several methods exist for targeting activated endothelial cells in the tumor microenvironment [24,25]. Future studies will utilize this information to design more potent fluoro-xylosides and test them *in vivo*. In conclusion, we have found novel fluoro-xylosides that inhibit GAG production in endothelial cells and also inhibit tumor-associated angiogenesis.

Acknowledgments

This work was supported by the National Institutes of Health Grant (GM075168), Human Frontier Science Program grant and American Heart Association National Scientist development Award to B.K. T.N. acknowledges a graduate fellowship support from Vietnam Education Foundation.

References

[1] J. Folkman, Tumor angiogenesis: therapeutic implications, N. Engl. J. Med. 285 (1971) 1182–1186.
[2] K. Raman, B. Kuberan, Chemical tumor biology of heparan sulfate proteoglycans, Curr. Chem. Biol. 4 (2010) 20–31.
[3] R.D. Sanderson, Y. Yang, T. Kelly, V. MacLeod, Y. Dai, A. Theus, Enzymatic remodeling of heparan sulfate proteoglycans within the tumor microenvironment: growth regulation and the prospect of new cancer therapies, J. Cell. Biochem. 96 (2005) 897–905.
[4] R. Sasisekharan, S. Ernst, G. Venkataraman, On the regulation of fibroblast growth factor activity by heparin-like glycosaminoglycans, Angiogenesis 1 (1997) 45–54.

[5] J. Folkman, M. Klagsbrun, J. Sasse, M. Wadzinski, D. Ingber, I. Vlodavsky, A heparin-binding angiogenic protein–basic fibroblast growth factor–is stored within basement membrane, Am. J. Pathol. 130 (1988) 393–400.
[6] M. Klagsbrun, Mediators of angiogenesis: the biological significance of basic fibroblast growth factor (bFGF)-heparin and heparan sulfate interactions, Semin. Cancer Biol. 3 (1992) 81–87.
[7] H. Nakato, K. Kimata, Heparan sulfate fine structure and specificity of proteoglycan functions, Biochim. Biophys. Acta 1573 (2002) 312–318.
[8] C.I. Gama, L.C. Hsieh-Wilson, Chemical approaches to deciphering the glycosaminoglycan code, Curr. Opin. Chem. Biol. 9 (2005) 609–619.
[9] S. Guimond, M. Maccarana, B.B. Olwin, U. Lindahl, A.C. Rapraeger, Activating and inhibitory heparin sequences for FGF-2 (basic FGF). Distinct requirements for FGF-1, FGF-2, and FGF-4, J. Biol. Chem. 268 (1993) 23906–23914.
[10] N. Sugaya, H. Habuchi, N. Nagai, S. Ashikari-Hada, K. Kimata, 6-*O*-sulfation of heparan sulfate differentially regulates various fibroblast growth factor-dependent signallings in culture, J. Biol. Chem. 283 (2008) 10366–10376.
[11] L. Lundin, H. Larsson, J. Kreuger, S. Kanda, U. Lindahl, M. Salmivirta, L. Claesson-Welsh, Selectively desulfated heparin inhibits fibroblast growth factor-induced mitogenicity and angiogenesis, J. Biol. Chem. 275 (2000) 24653–24660.
[12] X.V. Victor, T.K. Nguyen, M. Ethirajan, V.M. Tran, K.V. Nguyen, B. Kuberan, Investigating the elusive mechanism of glycosaminoglycan biosynthesis, J. Biol. Chem. 284 (2009) 25842–25853.
[13] F.N. Lugemwa, J.D. Esko, Estradiol beta-D-xyloside, an efficient primer for heparan sulfate biosynthesis, J. Biol. Chem. 266 (1991) 6674–6677.
[14] M.A. Bourdon, T. Krusius, S. Campbell, N.B. Schwartz, E. Ruoslahti, Identification and synthesis of a recognition signal for the attachment of glycosaminoglycans to proteins, Proc. Natl. Acad. Sci. USA 84 (1987) 3194–3198.
[15] N.B. Schwartz, L. Galligani, P.L. Ho, A. Dorfman, Stimulation of synthesis of free chondroitin sulfate chains by beta-D-xylosides in cultured cells, Proc. Natl. Acad. Sci. USA 71 (1974) 4047–4051.
[16] C.A. Henke, U. Roongta, D.J. Mickelson, J.R. Knutson, J.B. McCarthy, CD44-related chondroitin sulfate proteoglycan, a cell surface receptor implicated with tumor cell invasion, mediates endothelial cell migration on fibrinogen and invasion into a fibrin matrix, J. Clin. Invest. 97 (1996) 2541–2552.
[17] S. Brule, V. Friand, A. Sutton, F. Baleux, L. Gattegno, N. Charnaux, Glycosaminoglycans and syndecan-4 are involved in SDF-1/CXCL12-mediated invasion of human epithelioid carcinoma HeLa cells, Biochim. Biophys. Acta 1790 (2009) 1643–1650.
[18] K. Raman, B. Kuberan, Click-xylosides mitigate glioma cell invasion in vitro, Mol. BioSyst. 6 (2010) 1800–1802.
[19] K. Mani, M. Belting, U. Ellervik, N. Falk, G. Svensson, S. Sandgren, F. Cheng, L.A. Fransson, Tumor attenuation by 2(6-hydroxynaphthyl)-beta-D-xylopyranoside requires priming of heparan sulfate and nuclear targeting of the products, Glycobiology 14 (2004) 387–397.
[20] D.R. Garud, V.M. Tran, X.V. Victor, M. Koketsu, B. Kuberan, Inhibition of heparan sulfate and chondroitin sulfate proteoglycan biosynthesis, J. Biol. Chem. 283 (2008) 28881–28887.
[21] K. Raman, B. Kuberan, Differential effects of Heparitinase I and Heparitinase III on endothelial tube formation in vitro, Biochem. Biophys. Res. Commun. 398 (2010) 191–193.
[22] Y. Tsuzuki, T.K.N. Nguyen, D.R. Garud, B. Kuberan, M. Koketsu, 4-Deoxy-4-fluoro-xyloside derivatives as inhibitors of glycosaminoglycan biosynthesis, Bioorg. Med. Chem. Lett. 20 (2010) 7269–7273.
[23] L.S. Rosen, Clinical experience with angiogenesis signaling inhibitors: focus on vascular endothelial growth factor (VEGF) blockers, Cancer Control 9 (2002) 36–44.
[24] V.M. Tran, X.V. Victor, J.W. Yockman, B. Kuberan, RGD-xyloside conjugates prime glycosaminoglycans, Glycoconj. J. 27 (2010) 625–633.
[25] S.D. Rosen, Ligands for L-selectin: homing, inflammation, and beyond, Annu. Rev. Immunol. 22 (2004) 129–156.

2.4.1 Additional Analysis of Data

It is noteworthy that Xyloside I is not as effective at reducing tube formation compared to xylosides III or IV (Figure 2.3). For further analysis of the mechanism of inhibition, a combination of cell inhibition studies and gene upregulation/knockdown experiments may be utilized to probe the effects of F-xylosides on cell invasion, migration, and proliferation. For example, it may be possible to upregulate AKT to enhance cell migration. The rescue of tube formation in the presence of such perturbations would indicate that F-xylosides likely deplete the ability of cells to utilize these processes for tube-formation. Similarly alteration of NO production, or upregulation of MMP/Heparanase may be utilized to probe other physiological processes and determine the mechanism of F-xyloside activity

2.5 Discovery of Novel Sulfonated Small Molecules that Inhibit Vascular Tube Formation

Manuscript reproduced with permission from: Raman, K., Karuturi, R., Swarup, V. P., Desai, U. R., and Kuberan, B. (2012) Discovery of novel sulfonated small molecules that inhibit vascular tube formation, *Bioorg. Med. Chem. Lett., 22*, 4467-4470.

.

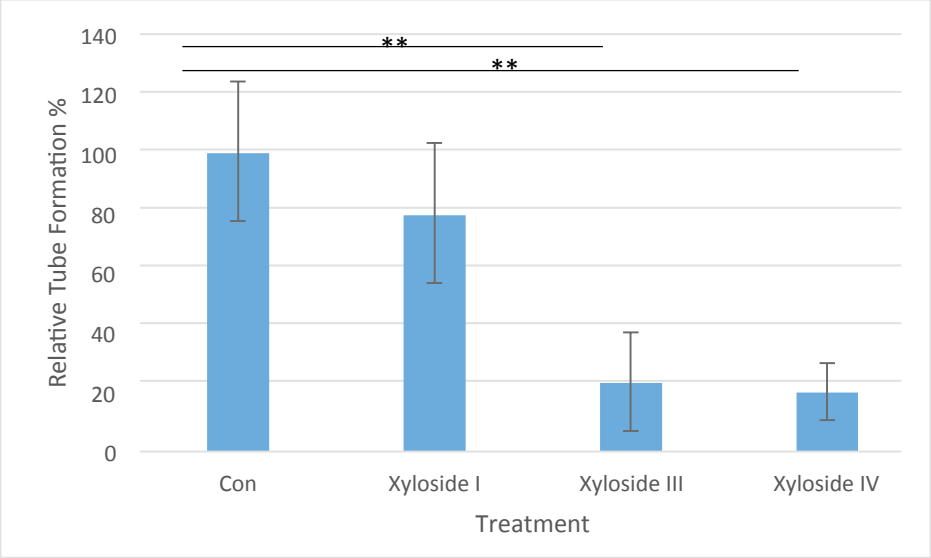

Figure 2.3. Relative tube formation of BLMVEC with and without treatment with 4-fluoro-xylosides. Tube formation is quantified as a relative mesh area covered by tube formation of control BLMVEC. Tubes are quantified using ImageJ software and analyzed using Angioanalyzer. ** indicates $P<0.05$ as determined by a one-tailed paired t-test. Error bars indicate standard deviations.

Bioorganic & Medicinal Chemistry Letters 22 (2012) 4467–4470

Contents lists available at SciVerse ScienceDirect

Bioorganic & Medicinal Chemistry Letters

journal homepage: www.elsevier.com/locate/bmcl

Discovery of novel sulfonated small molecules that inhibit vascular tube formation

Karthik Raman [a,†], Rajesh Karuturi [b,†], Vimal P. Swarup [a], Umesh R. Desai [b], Balagurunathan Kuberan [a,c,d,*]

[a] Department of Bioengineering, University of Utah, Salt Lake City, UT 84112, USA
[b] Department of Medicinal Chemistry, Virginia Commonwealth University, Richmond, VA 23284, USA
[c] Interdepartmental Program in Neuroscience, University of Utah, Salt Lake City, UT 84112, USA
[d] Department of Medicinal Chemistry, University of Utah, Salt Lake City, UT 84112, USA

ARTICLE INFO

Article history:
Received 10 February 2012
Revised 24 March 2012
Accepted 3 April 2012
Available online 16 April 2012

Keywords:
Angiogenesis
Matrigel
Small molecules
Inhibitors
Polysulfonated molecules

ABSTRACT

Tumor-associated angiogenesis is a complex process that involves the interplay among several molecular players such as cell-surface heparan sulfate proteoglycans, vascular endothelial growth factors and their cognate receptors. PI-88, a highly sulfonated oligosaccharide, has been shown to have potent anti-angiogenic activity and is currently in clinical trials. However, one of the major drawbacks of large oligosaccharides such as PI-88 is that their synthesis often requires numerous complex synthetic steps. In this study, several novel polysulfonated small molecule carbohydrate mimetics, which can easily be synthesized in fewer steps, are identified as promising inhibitors of angiogenesis in an in vitro tube formation assay.

The inhibition of tumor-associated angiogenesis has been one of the primary methods of controlling cancers for several decades.[1–3] Heparan sulfate proteoglycans (HSPGs), composed of sulfonated glycosaminoglycan (GAG) chains attached to a protein core, are key players in stimulating tumor-associated angiogenesis.[2,4] HSPGs facilitate cell signalling by acting as co-receptors for a variety of pro- and anti-angiogenic factors such as FGF, VEGF, and endostatin.[5–8] Infact, cell surface HS is essential for endothelial tube formation in vitro.[9]

Several studies have utilized HS-/Heparin-based drugs to control angiogenesis.[10] Recently, ReGeneraTing Agents (RGTAs) were found to enhance angiogenesis by increasing the affinity of VEGF-165 for its cognate receptor.[11] In contrast, low molecular weight heparin was found to have anti-angiogenic properties in rat corneas.[12] PI-88, a highly sulfonated oligosaccharide (phosphomannopentose sulfate) which entered clinical trials, has potent anti-angiogenic properties.[13] Additionally, JG3 (oligomannurate sulfate), a recently discovered marine-derived oligosaccharide, inhibits heparanase-associated angiogenesis.[14] In vivo testing of PG545, an HS mimetic, also showed promise in a recent preclinical study in a murine tumor model.[15] These and other heparin-based inhibitors demonstrate the power of sulfonated saccharides in anti-cancer treatments. However, nearly all HS mimetics discovered thus far as angiogenesis inhibitors are high molecular weight oligo- or poly- saccharide derivatives.

High molecular weight HS/heparin derivatives are notoriously difficult to prepare in a homogenous form. Additionally, distinct HS sequences possessing different sulfation patterns and/or chain lengths may have agonistic or antagonistic effects.[16,17] Finding medically relevant HS/heparin derivatives requires exhaustive library screening, a task made difficult by the problems of synthesis. Thus, we reasoned that small molecules that (1) mimic HS; (2) are much smaller than oligosaccharides; (3) are homogenous; (4) are easily prepared; and (5) function as angiogenesis inhibitors, would be more clinically effective than current HS/Heparin-based oligosaccharide drugs. Previously we found novel small molecule fluoro-xylosides that potently reduced tumor-associated angiogenesis by inhibiting HS biosynthesis in vitro.[18] However, these molecules required cellular entry to be effective. Small molecule angiogenesis inhibitors that can assert their action outside cells are far more desirable than carbohydrate-based oligo- and polysaccharides because of their potentially favorable pharmacokinetic properties.

To test this hypothesis, we designed a library of 18 sulfonated non-carbohydrate small molecules that can be expected to mimic heparin/HS due to their highly charged nature. Using a microwave sulfonation protocol that we previously developed and rigorously

* Corresponding author. Address: 30 S 2000 E, Skaggs Hall Rm. 307, University of Utah, Salt Lake City, UT 84112, USA. Tel.: +1 801 587 9474; fax: +1 801 585 9119.
E-mail address: KUBY@pharm.utah.edu (B. Kuberan).
† These authors contributed equally to this work.

0960-894X/$ - see front matter © 2012 Elsevier Ltd. All rights reserved.
http://dx.doi.org/10.1016/j.bmcl.2012.04.014

characterized, we synthesized molecules belonging to the flavone, flavan, chalcone, stillbene, styrene, and isoquinoline scaffolds, representing significant diversity at the three-dimensional level (Fig. 1).[19–21] Furthermore, the synthesized molecules contain 1–5 sulfate groups and are under 500 Da in size; therefore, they have similar charge density, sulfate functionality, and size as HS/heparin di-/tri-saccharides and should mimic HS/heparin functions.

These molecules were screened in an in vitro assay of tumor-associated angiogenesis which utilizes reduced growth factor basement membrane extract (RGF-BME) derived from the Englebreth-Holm-Swarm (EHS) mouse sarcoma. When bovine lung microvascular endothelial cells (BLMVEC) are cultured on RGF-BME, they spontaneously form tube-like structures. The development of these 'tubes' in vitro mimics an important step in the formation of blood vessels in vivo. An extensive tube-like network with significant branching and tube length indicates normal angiogenesis. On the other hand, disjointed groups of cells forming short tubes that are not interconnected exemplify the inhibition of angiogenesis. Several previous studies have utilized this matrigel tube formation assay.[18,22]

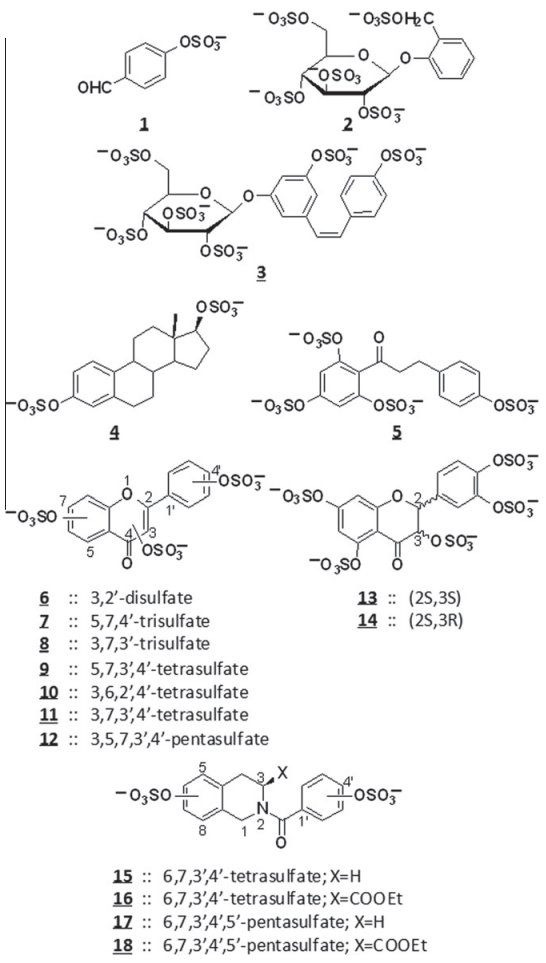

Figure 1. Chemical structures of the library of sulfonated small molecules.

We initially screened the library at a number of different concentrations and found that several molecules completely abolished tube formation. Control wells contained either no compound (positive control) or sulforaphane (negative control). Sulforaphane, found in broccoli and other cruciferous vegetables, is a potent anticancer agent provided by the assay manufacturer.[23] Screening of the 18 molecules (Fig. 1) led to the identification of **4**, **5**, **6**, **7** and **9** as potent inhibitors of angiogenesis at 100 μM (Fig. 2). While untreated wells and inactive mimetics showed significant branching and interconnectivity, endothelial cells treated with these sulfonated molecules were dispersed and formed small cell clumps without much network formation.

Based on our findings, it is possible to glimpse into structure–activity relationships that play a role in vascular tube formation; although, this process is considerably complex and involves a large number of probable mechanisms. The active molecules, **4**, **5**, **6**, **7** and **9**, carry two, three, or four sulfate groups per scaffold (Fig. 1). However, the inhibitory activity was not proportional to number of sulfate groups as several tetra- and penta- sulfonated molecules (e.g., **10**–**18**) were found to be inactive. A comparison of structures of the molecules that exhibit inhibitory activity shows that the minimal 'pharmacophore' appears to be two sulfate groups at an optimal distance of 5–10 Å as found in scaffolds **4**, **5**, and **7**. This suggests that structural selectivity is involved in the process. Additionally, due to the highly charged nature of these molecules, they probably inhibit tube formation via a chelation or competition mechanism outcompeting cell-surface heparan sulfates for pro-angiogenic factors such as FGF. We have previously shown that disruption of cell surface HS by heparitinases and by GAG biosynthesis inhibitors halts tube-formation.[9,18] The current study presents an alternative approach which utilizes sulfonated small molecules to inhibit tube formation by competing with the functions of cell surface HS.

This work presents the first small, synthetic, non-saccharide, highly sulfonated heparin/HS mimetics that possess anti-angiogenic function. The compounds in the current study are likely to be clinically superior to current carbohydrate-based high molecular weight drugs which have shown significant anti-cancer potential in clinical trails.[13] Molecules **4**, **5**, **6**, **7**, and **9** have lower molecular weights, can potentially modulate a variety of signalling pathways, are easy to synthesize, and probably exert their activity outside cells without the need for cell penetration. Due to these properties, it is expected that the current molecules will have more favorable pharmacokinetic properties and clinical application. Additional scaffolds will be developed to identify more potent angiogenesis inhibitors and to ascertain the mechanism of action of these molecules. In vivo testing of these compounds will lead to the identification of potential drug candidates for further studies.

Experimental information

Tube formation assay: A premixed solution of 1×10^5 BLMVEC, heparin/HS mimetic inhibitors, and MCDB-131 media were added to matrigel in a 96 well plate, in duplicate. After incubation for 16 h at 37 °C, cells were imaged with an Olympus IX81.

Synthesis: All tested compounds were synthesized in one step from their phenolic and/or alcoholic precursors using microwave-assisted synthesis, as described previously.[19] Briefly, the precursor and trimethylamine sulfur trioxide complex at a molar ratio of 1:6 per –OH group were mixed in acetonitrile and exposed to microwaves (50 W) at 90 °C for 30 min. The purity of the sulfonated compounds was assayed using reverse polarity capillary electrophoresis, as previously described[20] and found to be >95%. (see Supplementary material for details).

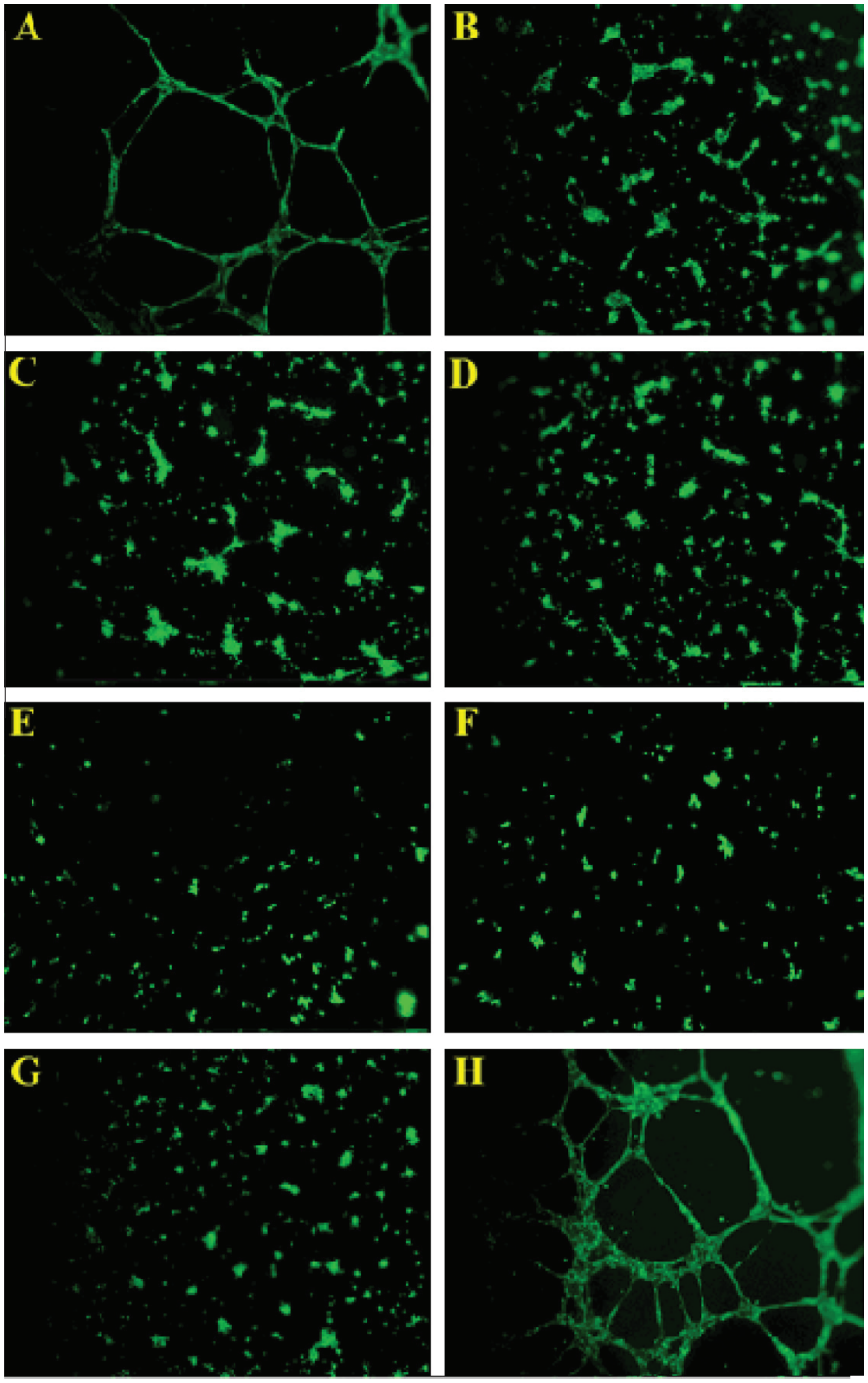

Figure 2. An in vitro tube formation assay was utilized to identify angiogenesis inhibitors. Wells were treated at a concentration of 100 μM. Representative panels in this figure are: (A) Positive untreated control, (B) sulforaphane negative control, (C) **9**, (D) **4**, (E) **5**, (F) **6**, (G) **7**, and (H) **12**.

Acknowledgements

This work was supported by the NIH Grant PO1-HL107152 to B.K/U.R.D and by NIH Grants HL099420 and HL090586, AHA Grant EIA 0640053N, and Grant 6-46064 from the A. D. Williams Foundation to U.R.D.

Supplementary data

Supplementary data associated with this article can be found, in the online version, at http://dx.doi.org/10.1016/j.bmcl.2012.04.014.

References and notes

1. Folkman, J. *N. Eng. J. Med.* **1971**, *285*, 1182.
2. Iozzo, R. V.; Sanderson, R. D. *J. Cell Mol. Med.* **2011**, *15*, 1013.
3. Tanaka, K.; Konno, Y.; Kuraishi, Y.; Kimura, I.; Suzuki, T.; Kiniwa, M. *Bioorg. Med. Chem. Lett.* **2002**, *12*, 623.
4. Raman, K.; Kuberan, B. *Curr. Chem. Biol.* **2010**, *4*, 20.
5. Nakato, H.; Kimata, K. *Biochim. Biophys. Acta* **2002**, *1573*, 312.
6. Folkman, J.; Shing, Y. *Adv. Exp. Med. Biol.* **1992**, *313*, 355.
7. Sasaki, T.; Larsson, H.; Kreuger, J.; Salmivirta, M.; Claesson-Welsh, L.; Lindahl, U.; Hohenester, E.; Timpl, R. *EMBO J.* **1999**, *18*, 6240.
8. Sasisekharan, R.; Ernst, S.; Venkataraman, G. *Angiogenesis* **1997**, *1*, 45.
9. Raman, K.; Kuberan, B. *Biochem. Biophys. Res. Commun.* **2010**, *398*, 191.
10. McKenzie, E. A. *Br. J. Pharmacol.* **2007**, *151*, 1.
11. Rouet, V.; Meddahi-Pelle, A.; Miao, H. Q.; Vlodavsky, I.; Caruelle, J. P.; Barritault, D. *J. Biomed. Mater. Res.* **2006**, *78*, 792.
12. Lepri, A.; Benelli, U.; Bernardini, N.; Bianchi, F.; Lupetti, M.; Danesi, R.; Del Tacca, M.; Nardi, M. *J. Ocul. Pharmacol.* **1994**, *10*, 273.
13. Chow, L. Q.; Gustafson, D. L.; O'Bryant, C. L.; Gore, L.; Basche, M.; Holden, S. N.; Morrow, M. C.; Grolnic, S.; Creese, B. R.; Roberts, K. L.; Davis, K.; Addison, R.; Eckhardt, S. G. *Cancer Chemother. Pharmacol.* **2008**, *63*, 65.
14. Zhao, H.; Liu, H.; Chen, Y.; Xin, X.; Li, J.; Hou, Y.; Zhang, Z.; Zhang, X.; Xie, C.; Geng, M.; Ding, J. *Cancer Res.* **2006**, *66*, 8779.
15. Dredge, K.; Hammond, E.; Handley, P.; Gonda, T. J.; Smith, M. T.; Vincent, C.; Brandt, R.; Ferro, V.; Bytheway, I. *Br. J. Cancer* **2011**, *104*, 635.
16. Liu, D.; Shriver, Z.; Venkataraman, G.; El Shabrawi, Y.; Sasisekharan, R. *Proc. Natl. Acad. Sci. U.S.A.* **2002**, *99*, 568.
17. Azizkhan, R. G.; Azizkhan, J. C.; Zetter, B. R.; Folkman, J. *J. Exp. Med.* **1980**, *152*, 931.
18. Raman, K.; Ninomiya, M.; Nguyen, T. K.; Tsuzuki, Y.; Koketsu, M.; Kuberan, B. *Biochem. Biophys. Res. Commun.* **2010**, *404*, 86.
19. Raghuraman, A.; Riaz, M.; Hindle, M.; Desai, U. R. *Tetrahedron Lett.* **2007**, *48*, 6754.
20. Gunnarsson, G. T.; Riaz, M.; Adams, J.; Desai, U. R. *Bioorg. Med. Chem.* **2005**, *13*, 1783.
21. Liang, A.; Thakkar, J. N.; Desai, U. R. *J. Pharm. Sci.* **2010**, *99*, 1207.
22. Garonna, E.; Botham, K. M.; Birdsey, G. M.; Randi, A. M.; Gonzalez-Perez, R. R.; Wheeler-Jones, C. P. *PLoS One* **2011**, *6*, e18823.
23. Asakage, M.; Tsuno, N. H.; Kitayama, J.; Tsuchiya, T.; Yoneyama, S.; Yamada, J.; Okaji, Y.; Kaisaki, S.; Osada, T.; Takahashi, K.; Nagawa, H. *Angiogenesis* **2006**, *9*, 83.

Supplementary materials and methods

Discovery of novel sulfonated small molecule s that inhibit vascular tube formation

Karthik Raman [a,#], Rajesh Karuturi [b,#], Vimal P. Swarup [a], Umesh R. Desai [b], Balagurunathan Kuberan [a,c,d,*]

Materials

Bovine lung microvasc ular endothelial cells (BLMVEC) of low passage were kindly provided by Dr. Randall Dull of the University of Utah. MCDB -131 complete media was purchased from Vec Technologies (Rensselaer, NY). Reduced growth factor basement membrane matrix (RGF -BME), ca lcein, and sulforaphane were purchased from Trevigen Inc. (Gaithersburg, MD). Tryp LE Express was purchased from Invitrogen Inc. (Carlsbad, CA). All other reagents were purchased from Aldrich Chemical (Mi lwaukee, WI) and used without further purificati on. Polyphenolic precursors used in the synthesis of sulfonated molecules were either synthesized in the laboratory as described earlier [1] or purchased from Indofine (Somerville, NJ) and Sigma (St. Louis, MO).

In vitro m atrigel tube formation assay

BLMV EC were cultured in MCDB -131 media in a humidified 37 ∫C incubator. Cells were split 24 hrs prior to conducting tube formation assays in order to keep them in the log phase of growth. RGF -BME was thawed overnight at 4 ∫C in a frost free refrigerator. Fi fty µl of RGF -BME was then plated out in wells of a chilled 96 well plate using chilled pipette tips. The RGF -BME was allowed to solidify to form the matrigel matrix in the humidified incubator at 37 ∫C. Concurrently, BLMVEC were suspended by incubation with Tryp LE Express and counted using a hemacytometer. After the matrigel had formed, a premixed solution of 1 x 10^5 cells, heparan sulfate mimetic inhibitors, and MCDB -131 media were then added to wells in the 96 well plates in duplicate. The plates we re then incubated in the humidified incubator for 16 hrs prior to Calcein staining and imaging. Cells were first observed under a light microscope to observe their morphology. Subsequently, media was removed from each well containing cells by gentle dabbi ng with a paper towel. The wells were then washed twice with chilled PBS and 100 µl of 2 µM Calcein AM was added to each well. After incubating cells for 30 minutes in the incubator, the cells were washed twice with chilled PBS. They were immediately im aged with an Olympus IX81 microscope attached to a color CCD Filter and a GFP emission filter using 485 nm excitation/520 nm emission.

Synthesis of sulfonated m olecules

P rocedure for microwave -assisted sulfonation : To a stirred solution of the polyphenol o r polyalcohol in MeCN (1 ñ 5 mL) at RT, Et_3N (10 eqv per ñOH group) and $Me_3N{:}SO_3$ complex (6 eqv per ñOH) were added. The reaction vessel was sealed and micro -waved (CEM Discover synthesizer, Cary, NC) for 30 min at 90 ^{0}C. Several reaction tubes were pooled for isolation of the product. The MeCN layer was decanted and pooled, while the residue was washed with MeCN (5 mL) and centrifuged. The combined MeCN layers were concentrated in vacuo. Water (5 mL) was added to the residue and stirred for 10 min. The wat er layer was concentrated to approximately 2 mL, loaded onto a Sephadex G10 column (160 cm) and chromatographed using water as eluent. Fractions were combined based on capillary electrophoresis profiles, concentrated and re -loaded onto a SP Sephadex C25 co lumn for sodium exchange. Appropriate fractions were pooled, concentrated in vacuo, and lyophilized to obtain a white powder.

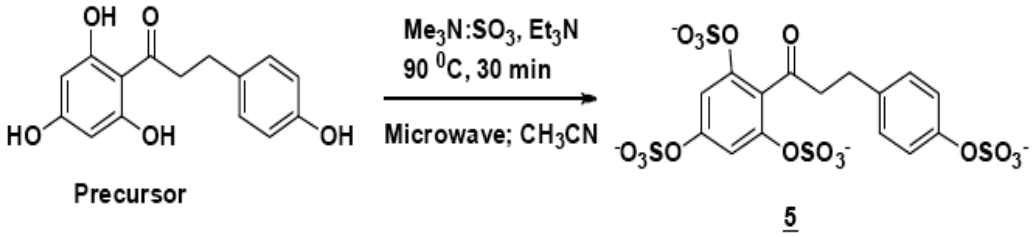

Scheme 1. A general reaction scheme for synthesizing sulfonated small molecular scaffolds.

Spectral characteristics of the sulfonated compounds not reported earlier are as follows:

5: ^{1}H NMR (DMSO, 400 MHz): 7.09 (m, 6 H), 3.06 (t, 2 H, J = 2.04Hz), 2.81 (t, 2 H, J =2.04Hz). ^{13}C NMR (DMSO, 100 MHz): 153.5, 151.3, 149.6, 136.13, 128.38, 120.38, 109.33, 39.74, 35.23. ESI -MS (-ve) m/z Calcd for $C_{15}H_{10}Na_4O_{17}S_4$: 681.84; found, 659.02 (M -Na)$^{+}$.

6: ^{1}H NMR (DMSO, 400 MHz): 8.18 (m, 1 H), 7.85 (m, 1 H), 7.6 (m, 6 H). ^{13}C NMR (DMSO, 100 MHz): 178.22, 157.34, 154.92, 151.63, 136.1, 133.7, 131.22, 130.71, 125.08, 124.74, 123.88, 122.35, 121.77, 120.01, 118.46. ESI ñMS (+ve) m/z Calcd for $C_{15}H_8Na_2O_{10}S_2$: 458.33; found, 481.08 (M+Na)$^{+}$.

8: ^{1}H NMR (DMSO, 400 MHz): 7.97(m, 2 H), 7.83 (m, 1 H), 7.55 (m, 1 H), 7.41 (m, 2 H), 7.24 (m, 1 H). ^{13}C NMR (DMSO, 100 MHz): 172.84, 158.09, 155.24, 153.19, 135.17, 131.82, 128.49, 125.99, 123.92, 122.53, 120.38, 118.46, 106.79. ESI -MS (-ve) m/z Calcd for $C_{15}H_7Na_3O_{14}S_3$: 576.33; found, 530.14 (M -2Na)$^{+}$.

10: ^{1}H NMR (DMSO, 400MHz): 7.91 (m, 1 H), 7.61 (d, 1 H, J =3.2 Hz), 7.55 (m, 2 H), 7.35 (d, 1 H, J =2.1 Hz), 7.05 (m, 1 H). ^{13}C NMR (DMSO, 100 MHz): 175.4, 155.5, 151.04, 135.6, 131.12, 127.18, 119.1, 117.08, 114.47, 113.51. ESI -MS (-ve) m/z Calcd for $C_{15}H_6Na_4O_{18}S_4$: 693.80; found, 670.99 (M -Na)$^{+}$.

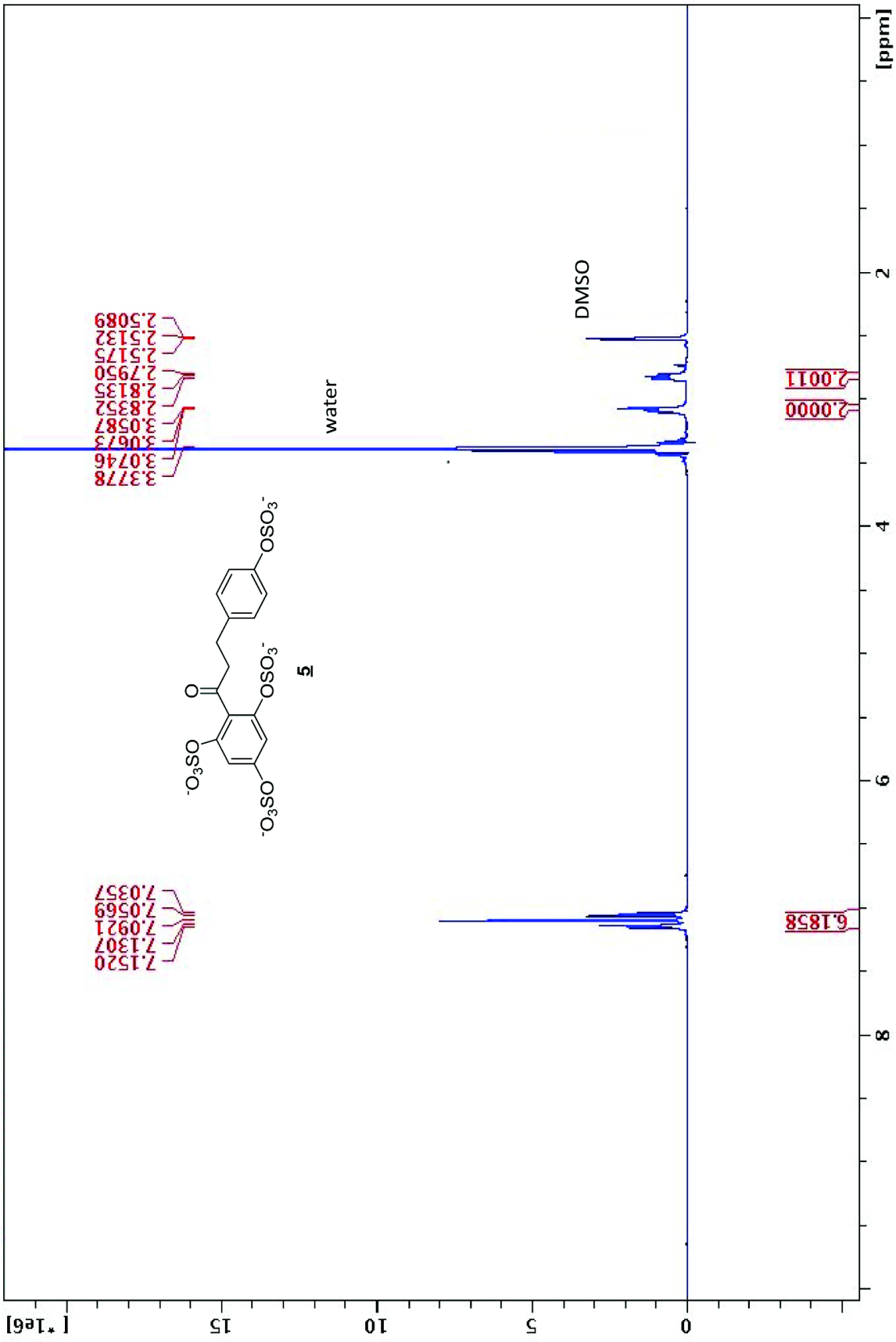
[*1e6]
15
10
5
0
[ppm]
2
4
6
8
DMSO
water
2.0011
2.0000
6.1858
7.1520
7.1307
7.0921
7.0569
7.0357
3.3778
3.0746
3.0673
3.0587
2.8352
2.8135
2.7950
2.5175
2.5132
2.5089
OSO3-
OSO3-
-O3SO
-O3SO
O
5

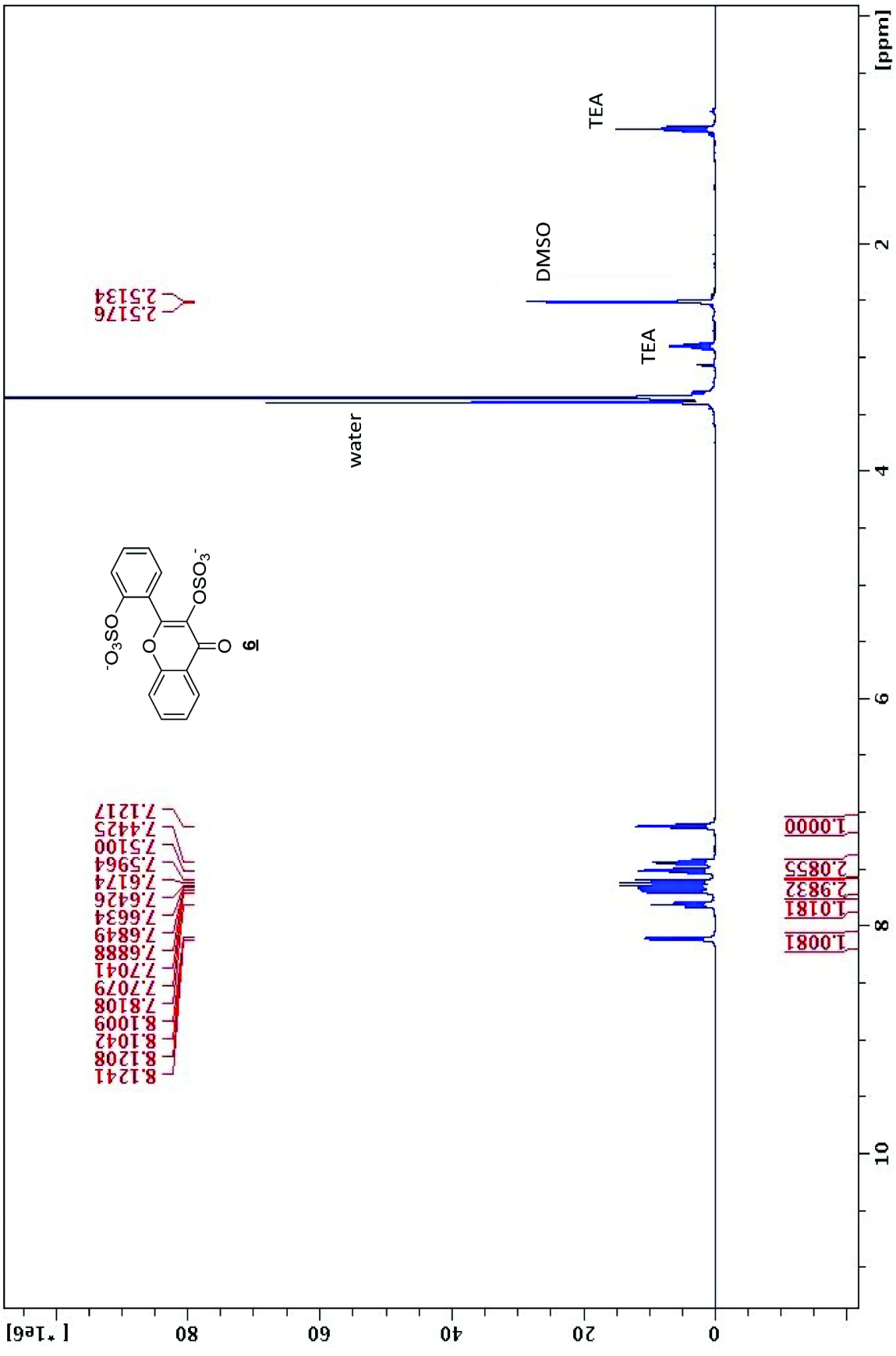
[*1e6]
0
20
40
60
80
[ppm]
10
8
6
4
2
water
TEA
DMSO
TEA
2.5176
2.5134
8.1241
8.1208
8.1042
8.1009
7.8108
7.7079
7.7041
7.6888
7.6849
7.6634
7.6426
7.6174
7.5964
7.5100
7.4425
7.1217
1.0000
2.0855
2.9832
1.0181
1.0081
9

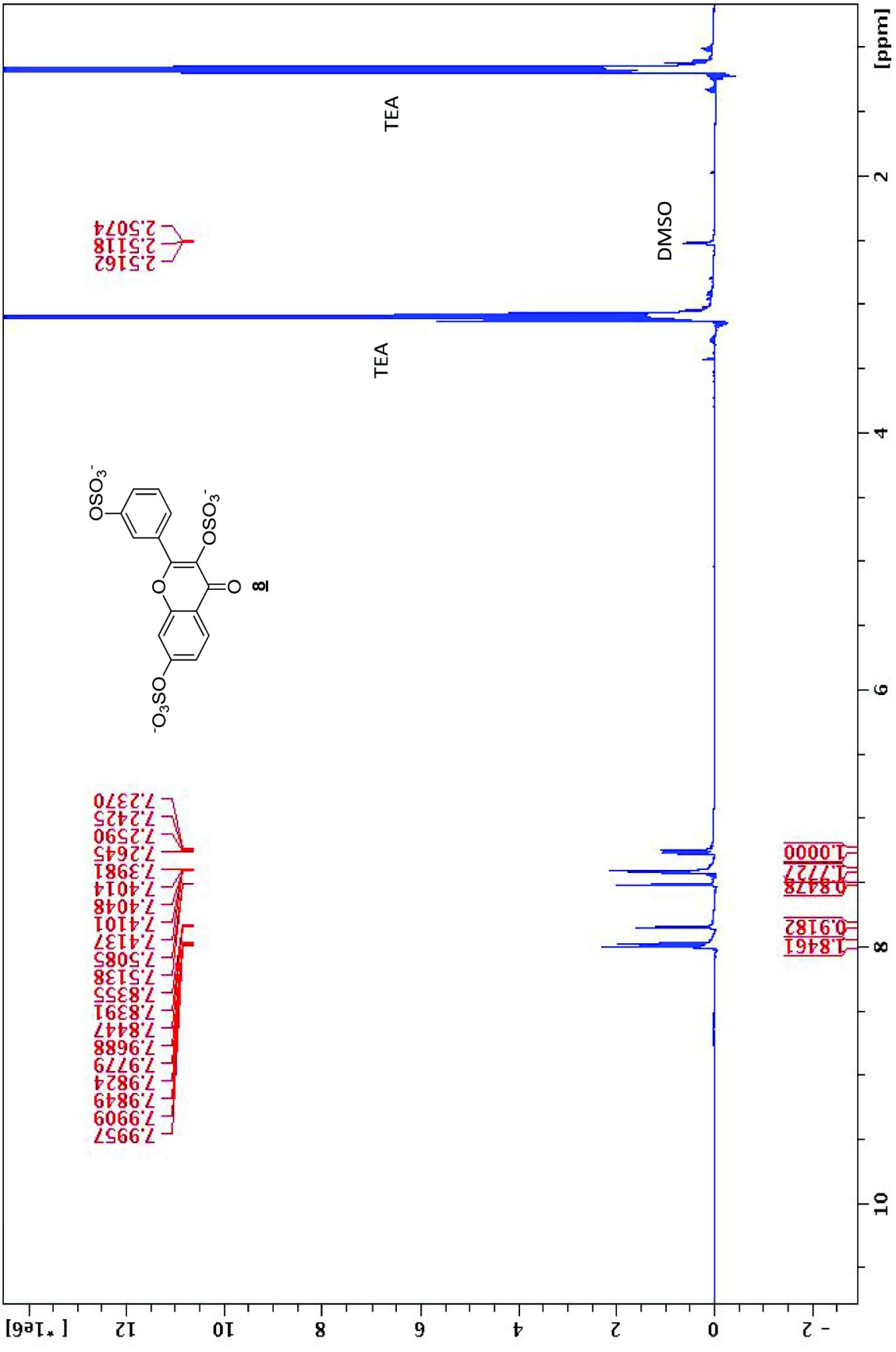
TEA
DMSO
TEA
2.5162
2.5118
2.5074
7.9957
7.9909
7.9849
7.9824
7.9779
7.9688
7.8447
7.8391
7.8355
7.5138
7.5085
7.4137
7.4101
7.4048
7.4014
7.3981
7.2645
7.2590
7.2425
7.2370
1.8461
0.9182
0.8478
1.7727
1.0000
[*1e6]
[ppm]

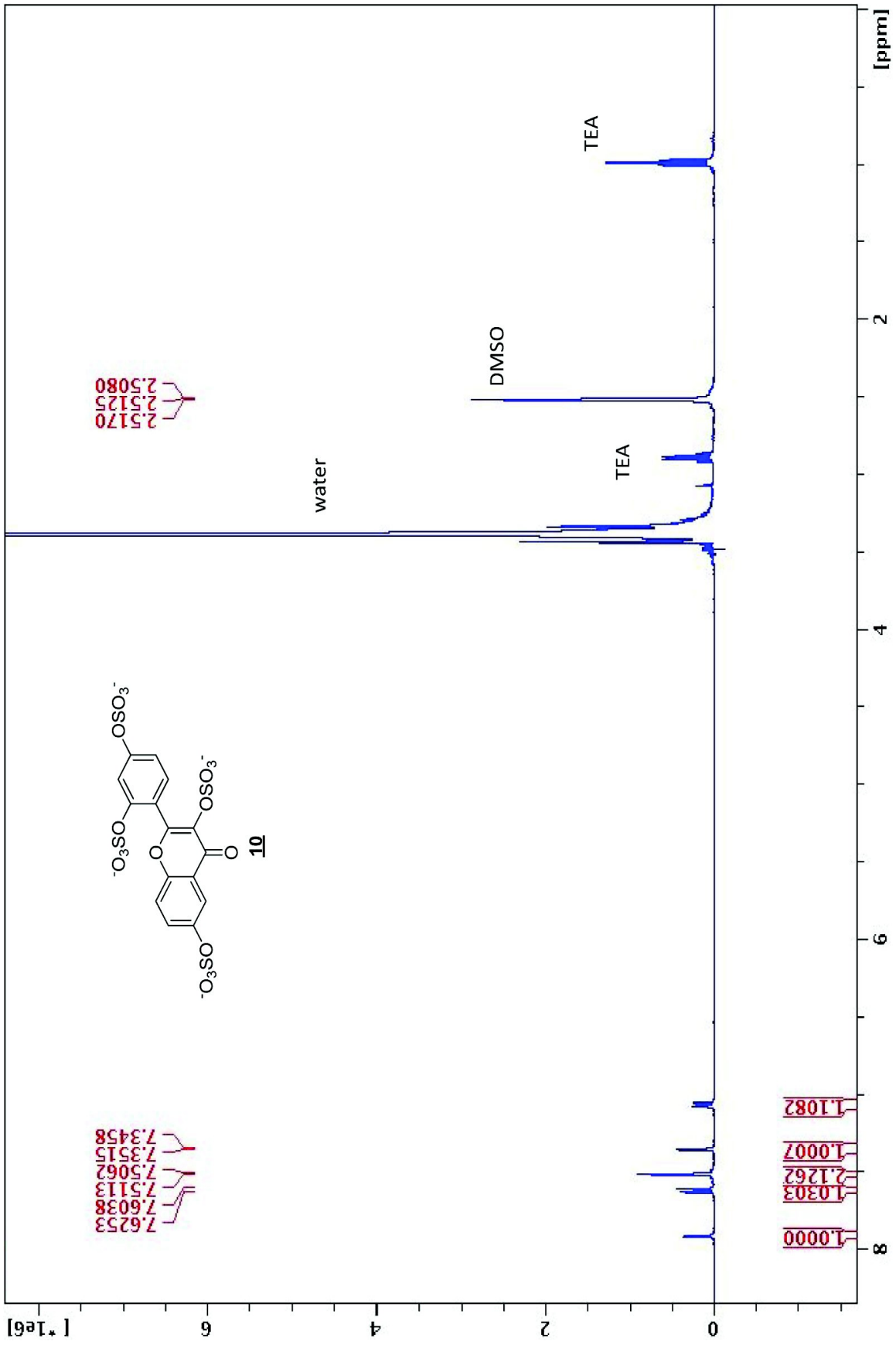
7.6253
7.6038
7.5113
7.5062
7.3515
7.3458
2.5170
2.5125
2.5080
1.0000
1.0303
2.1262
1.0007
1.1082
water
DMSO
TEA
TEA
10
[*1e6]
[ppm]

References

[1] Verghese , J.; Liang , A.; Sidhu , P. P.; Hindle , M.; Zhou , Q.; Desai , U. R. Bioorg Med Chem Lett 2009, 19, 4126.

2.5.1 Additional Analysis of Data

Additional analysis of data from the persulfonated mimetics experiments are presented in Figure 2.4.

2.6 Chemogenesis of an Anti-Angiogenic Glycosaminoglycan

Manuscript reprinted with permission from: Raman, K., Arungundram, S., and Kuberan, B. (2014) Chemogenesis of an antiangiogenic glycosaminoglycan, ACS *Med. Chem. Lett.*.

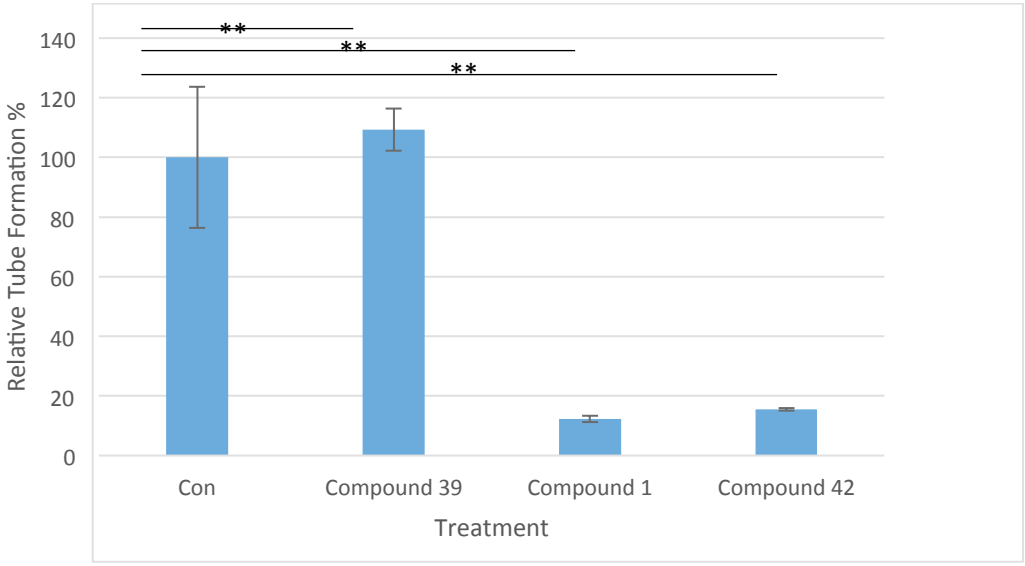

Figure 2.4. Relative tube formation when BLMVEC are treated with persulfonated HS mimetics. ** indicates P<0.05 as determined by a one-tailed paired t-test. Relative tube formation indicates the relative total mesh area covered by tubes. It is evident that mimetic *39* is not as efficacious as *1* or *42* at inhibiting tube formation. Due to their highly charged nature, sulfated mimetics are likely to exert their activity outside of cells by competing with cell-surface heparan sulfates for binding to growth factors such as FGFs and VEGFs. Error bars indicate standard deviations.

ACS Medicinal Chemistry Letters

Letter

pubs.acs.org/acsmedchemlett

Chemogenesis of an Antiangiogenic Glycosaminoglycan

Karthik Raman,[†] Sailaja Arungundram,[‡] and Balagurunathan Kuberan*[,†,‡,§]

[†]Department of Bioengineering, University of Utah, Salt Lake City, Utah 84112, United States

[‡]Department of Medicinal Chemistry, University of Utah, Salt Lake City, Utah 84112, United States

[§]Interdepartmental Program in Neuroscience, University of Utah, Salt Lake City, Utah 84112, United States

Supporting Information

ABSTRACT: In this letter we report a facile chemical conversion of heparin, a potent anticoagulant with minimal antiangiogenic activity, into an effective antiangiogenic glycosaminoglycan through optimized chemical approaches. This work highlights the potential for industrial scale production of a therapeutic anticancer glycosaminoglycan.

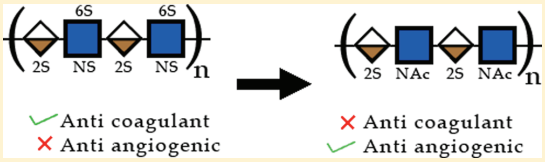

KEYWORDS: *Acharan sulfate, angiogenesis, heparan sulfate, synthesis, heparin*

Glycosaminoglycans (GAGs) such as heparan sulfate (HS) and chondroitin sulfate (CS) are linear polyanionic molecules typically linked to proteins. Because of their molecular diversity, they are involved in a variety of pathophysiological processes including cell signaling and development, growth and morphogenesis, angiogenesis, inflammation, and tumor progression.[1−3]

Acharan sulfate is a sulfonated GAG from the giant African snail *Achatina fulica*.[4] It has a unique structure that is unlike heparin or heparan sulfate. In naturally occurring glycosaminoglycans, sulfate groups may be located on the 2-*N*, 3-*O*, and 6-*O* positions of glucosamine residues, as well as the 2-*O* position of uronic acid residues. Heparin is primarily composed of trisulfated disaccharides of 2*N*-sulfamido-6-*O*-sulfo-α-D-glucopyranoside (1 → 4)-2-*O*-sulfo-α-L-idopyranosyluronate, whereas heparan sulfate is primarily composed of monosulfated disaccharides of 2*N*-sulfamido-α-D-glucopyranoside(1 → 4)-β-D-glucopyranosyluronate. Conversely, the primary structure of acharan sulfate is composed of 2*N*-acetamido-α-D-glucopyranoside (1 → 4)-2-*O*-sulfo-α-L-idopyranosyluronate. This sequence is rarely produced in human tissue as epimerization of glucuronic acid to iduronic acid requires the presence of neighboring *N*-sulfo groups.[5]

On the basis of its unique structure, acharan sulfate is a potentially valuable molecular medicine for treating cancers. Previously, several studies have discussed heparin's inherent anticancer properties.[6] However, unfractionated heparin is a potent anticoagulant and cannot be used for cancer therapy due to bleeding complications. The presence of 3-*O*, 6-*O*, and *N*-sulfo groups on heparin allow it to bind to antithrombin through a unique pentasaccharide sequence.[6] Unlike heparin, acharan sulfate is nonanticoagulant and mitigates fibroblast growth factor (FGF) signaling without binding to FGF directly.[7] Acharan sulfate lacks all three critical sulfate groups required for binding antithrombin and acting as an anticoagulant. Additionally, acharan sulfate effectively prevents vascular endothelial growth factor-induced (VEGF) angiogenesis in models of inflammation.[8] Furthermore, acharan sulfate shows no toxicity in vitro when tested at concentrations as high as 5 mg mL^{-1}.[7]

Current methods for procuring acharan sulfate require tedious isolation from snail tissue. Additionally, there is a possibility of contamination with other sulfated polysaccharides when isolating acharan sulfate directly from tissue. To overcome these challenges, there is a need for a chemical or chemoenzymatic process to synthesize acharan sulfate.

In this letter, we report a facile preparation of a GAG similar to acharan sulfate from heparin, a widely available polysaccharide that can be obtained in large quantities (Scheme 1). This GAG is synthesized from the pyridinium salt of heparin in three steps including: complete 6-*O* desulfation, *N*-desulfation, and *N*-acetylation. As reported previously, there is a concomitant removal of 3-*O*-sulfates when heparin is subjected to 6-*O*- or *N*-desulfation.[9,10] The presence of repeating disaccharides of *N*-acetyl-D-glucosamine (GlcNAc) and 2-*O*-sulfo-iduronic acid in the synthesized polymer was confirmed by nuclear magnetic resonance (NMR) and strong anion exchange high performance liquid chromatography (SAX-HPLC) analysis (Figure S1 and Table S1, Supporting Information). The molecular weight of the resultant polymer was analyzed on size exclusion chromatography (SEC)-HPLC (Figure S2, Supporting Information). As expected, desulfation of the low molecular weight heparin precursor leads to a removal of sulfate residues and a reduction in the ability to attract water molecules. Additionally, since heparin was utilized as the precursor, the final product has a very high iduronic acid content as confirmed by NMR analysis (Figure S5, Supporting Information).

Received: December 4, 2013
Accepted: April 4, 2014

   dx.doi.org/10.1021/ml400498d | *ACS Med. Chem. Lett.* XXXX, XXX, XXX−XXX

Scheme 1. Synthesis of an Acharan Sulfate-Like GAG from Heparin

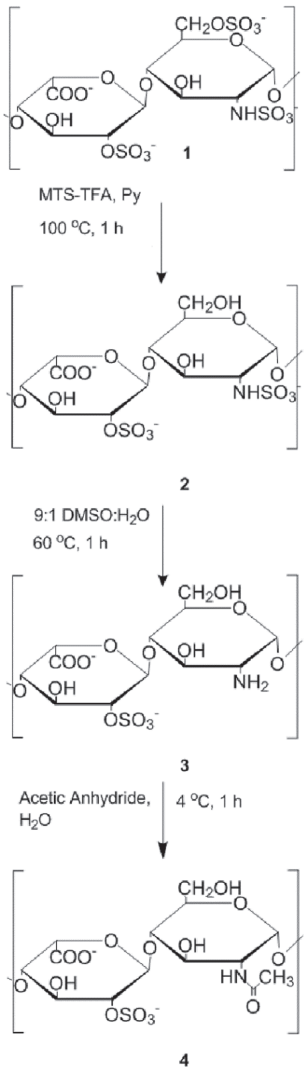

Complete 6-*O*-desulfation results in the generation of a C6-hydroxyl group on the GlcNAc residues, in agreement with resonances for H6 a,b (^{1}H NMR, 3.90 ppm; ^{13}C NMR, 59.84 ppm). In comparison, the H6 a,b proton signals resonate at ~4.3 ppm in the heparin starting material. Upon complete de-*N*-sulfation and *N*-acetylation, a new signal appears at 2.09 ppm ^{1}H and 22.07 ppm ^{13}C, in agreement with the *N*-acetyl CH_3 group. The H2 proton signal of the newly formed GlcNAc residue is shifted downfield to 4.03 ppm (53.76 ppm ^{13}C) from the 3.3 ppm signal observed for that of $GlcNHSO_4$.

The proton signal corresponding to the sulfonated O<u>H</u>−C_2 appears at 4.29 ppm confirming the presence of 2-*O*-sulfated hydroxyl group on the IdoA residues. The structural assignment of the synthetic acharan sulfate-like molecule (Table S1, Supporting Information) is in agreement with the published data.[4,11] However, the mimetic differs from natural acharan sulfate due to the lower abundance of 2-*O*-sulfate groups present on the polymer backbone. Natural acharan sulfate has more than 90 percent 2-*O* sulfated disaccharide residues, whereas heparin, the precursor for the current synthesis, also includes several disaccharides that do not contain 2-*O* sulfates.[12]

To confirm the antiangiogenic activity of the newly synthesized GAG, a robust in vitro tube formation assay was utilized (Figure 1). In this assay, vascular endothelial cells were grown on matrigel where they form tube-like structures. The efficacy of antiangiogenic compounds can be determined by examining their effects on tube branching, number, and length. It is evident that the synthesized acharan sulfate-like GAG was effective at 1 and 2 mg/mL concentrations. Observing the

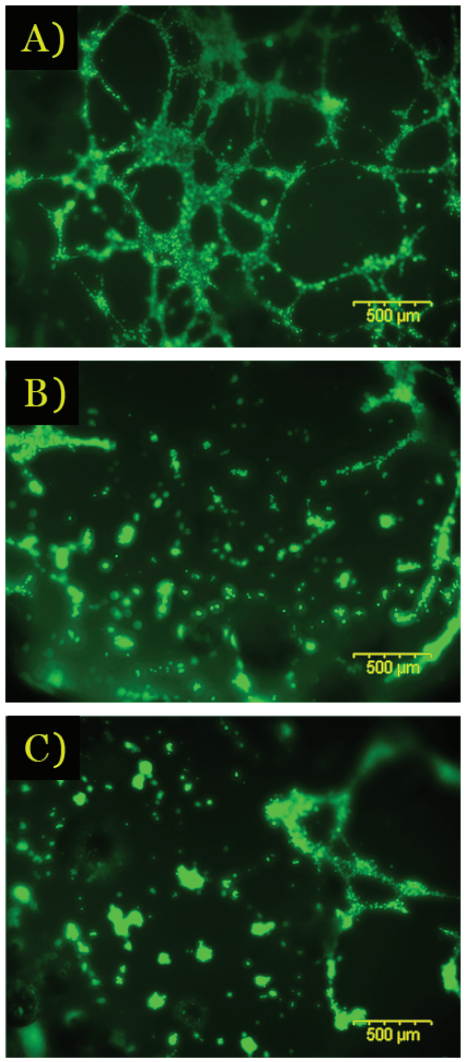

Figure 1. Inhibition of BLMVEC tube formation upon treatment with the acharan sulfate-like polysaccharide. Representative panels are (A) control tube formation, (B) 1 mg/mL mimetic, and (C) 2 mg/mL mimetic. Experiments were performed three times in duplicate wells.

dx.doi.org/10.1021/ml400498d | *ACS Med. Chem. Lett.* XXXX, XXX, XXX−XXX

branching, number, and length of tubes shows that, upon treatment, endothelial cells formed very few tubes and that the majority of cells form clusters that are not connected to a branched network. In contrast, heparin had a negligible effect on tube formation at 1 and 2 mg/mL concentrations (Figure S3, Supporting Information). Additionally, the mimetic was less effective at 0.5 mg/mL (Figure S4, Supporting Information). It is likely that increasing the 2-*O* sulfate content of the mimetic will likely enhance its antiangiogenic potential.

For decades, it has been known that preventing tumor-associated angiogenesis is an effective method for controlling cancer growth.[13] While several angiogenesis inhibitors such as Avastin have been developed previously, these therapies typically target singular molecular functions.[14] Proteoglycans, present on cell membranes and in the extracellular matrix, are integral components in tumor progression and angiogenesis. In contrast to typical antiangiogenic therapeutics, proteoglycan-based therapeutics have the potential to affect several signaling pathways involved in tumor-associated angiogenesis, invasion, and metastasis.[15] However, although several GAG-based therapeutic agents such as PI-88 have been discovered, very few of them have been utilized to treat patients.[16,17] One of the primary reasons for the lack of clinical application of GAG-based therapeutics is their tedious synthesis, frequently involving several low-yield steps and difficult purification techniques.[18] Additionally, naturally derived therapeutic GAGs such as acharan sulfate cannot be obtained in sufficient quantities to be utilized in the clinic.

In this letter, we provide a novel and simple method for synthesizing an antiangiogenic acharan sulfate-like GAG from heparin, a readily available and widely used clinical anticoagulant. The newly synthesized polymer is biologically active at low concentrations, effectively inhibits tube formation in vitro, and can be produced in large quantities. Because of its similarity to acharan sulfate, the mimetic is also likely to be non-anticoagulant. Further optimization and preclinical evaluation of this molecule is currently underway to determine its in vivo efficacy. Further studies are necessary to determine the exact molecular mechanism of action of the synthetic acharan sulfate mimetic.

■ ASSOCIATED CONTENT

Ⓢ Supporting Information

Experimental details, SAX-HPLC analysis, effect of heparin on tube formation, effect of other acharan sulfate concentrations, and NMR data. This material is available free of charge via the Internet at http://pubs.acs.org.

■ AUTHOR INFORMATION

Corresponding Author

*(B.K.) Fax: (+1) 801-581-9119. E-mail: kuby@pharm.utah.edu.

Funding

This work was supported by NIH grants PO1-HL107152 and GM075168 to B.K and by the NIH fellowship F31CA168198 to K.R.

Notes

The authors declare no competing financial interest.

■ REFERENCES

(1) Nakato, H.; Kimata, K. Heparan sulfate fine structure and specificity of proteoglycan functions. *Biochim. Biophys. Acta* **2002**, *1573* (3), 312−8.

(2) Sasisekharan, R.; Shriver, Z.; Venkataraman, G.; Narayanasami, U. Roles of heparan-sulphate glycosaminoglycans in cancer. *Nat. Rev. Cancer* **2002**, *2* (7), 521−8.

(3) Cummings, R. D. The repertoire of glycan determinants in the human glycome. *Mol. BioSyst.* **2009**, *5* (10), 1087−104.

(4) Kim, Y. S.; Jo, Y. Y.; Chang, I. M.; Toida, T.; Park, Y.; Linhardt, R. J. A new glycosaminoglycan from the giant African snail *Achatina fulica*. *J. Biol. Chem.* **1996**, *271* (20), 11750−5.

(5) Jacobsson, I.; Lindahl, U.; Jensen, J. W.; Roden, L.; Prihar, H.; Feingold, D. S. Biosynthesis of heparin. Substrate specificity of heparosan *N*-sulfate D-glucuronosyl 5-epimerase. *J. Biol. Chem.* **1984**, *259* (2), 1056−63.

(6) Atha, D. H.; Lormeau, J. C.; Petitou, M.; Rosenberg, R. D.; Choay, J. Contribution of 3-O- and 6-O-sulfated glucosamine residues in the heparin-induced conformational change in antithrombin III. *Biochemistry* **1987**, *26* (20), 6454−61.

(7) Wang, H.; Toida, T.; Kim, Y. S.; Capila, I.; Hileman, R. E.; Bernfield, M.; Linhardt, R. J. Glycosaminoglycans can influence fibroblast growth factor-2 mitogenicity without significant growth factor binding. *Biochem. Biophys. Res. Commun.* **1997**, *235* (2), 369−73.

(8) Ghosh, A. K.; Hirasawa, N.; Lee, Y. S.; Kim, Y. S.; Shin, K. H.; Ryu, N.; Ohuchi, K. Inhibition by acharan sulphate of angiogenesis in experimental inflammation models. *Br. J. Pharmacol.* **2002**, *137* (4), 441−8.

(9) Ishihara, M.; Takano, R.; Kanda, T.; Hayashi, K.; Hara, S.; Kikuchi, H.; Yoshida, K. Importance of 6-O-sulfate groups of glucosamine residues in heparin for activation of FGF-1 and FGF-2. *J. Biochem.* **1995**, *118* (6), 1255−60.

(10) Nagasawa, K.; Inoue, Y.; Kamata, T. Solvolytic desulfation of glycosaminoglycuronan sulfates with dimethyl sulfoxide containing water or methanol. *Carbohydr. Res.* **1977**, *58* (1), 47−55.

(11) Yates, E. A.; Santini, F.; Guerrini, M.; Naggi, A.; Torri, G.; Casu, B. 1H and 13C NMR spectral assignments of the major sequences of twelve systematically modified heparin derivatives. *Carbohydr. Res.* **1996**, *294*, 15−27.

(12) Kim, Y. S.; Ahn, M. Y.; Wu, S. J.; Kim, D. H.; Toida, T.; Teesch, L. M.; Park, Y.; Yu, G.; Lin, J.; Linhardt, R. J. Determination of the structure of oligosaccharides prepared from acharan sulfate. *Glycobiology* **1998**, *8* (9), 869−77.

(13) Folkman, J. Tumor angiogenesis: therapeutic implications. *N. Engl. J. Med.* **1971**, *285* (21), 1182−6.

(14) Rosen, L. S. Clinical experience with angiogenesis signaling inhibitors: focus on vascular endothelial growth factor (VEGF) blockers. *Cancer Control* **2002**, *9* (2 Suppl), 36−44.

(15) Rosen, S. D.; Lemjabbar-Alaoui, H. Sulf-2: an extracellular modulator of cell signaling and a cancer target candidate. *Expert Opin. Ther. Targets* **2010**, *14* (9), 935−49.

(16) Khachigian, L. M.; Parish, C. R. Phosphomannopentaose sulfate (PI-88): heparan sulfate mimetic with clinical potential in multiple vascular pathologies. *Cardiovasc. Drug Rev.* **2004**, *22* (1), 1−6.

(17) Basche, M.; Gustafson, D. L.; Holden, S. N.; O'Bryant, C. L.; Gore, L.; Witta, S.; Schultz, M. K.; Morrow, M.; Levin, A.; Creese, B. R.; Kangas, M.; Roberts, K.; Nguyen, T.; Davis, K.; Addison, R. S.; Moore, J. C.; Eckhardt, S. G. A phase I biological and pharmacologic study of the heparanase inhibitor PI-88 in patients with advanced solid tumors. *Clin. Cancer Res.* **2006**, *12* (18), 5471−80.

(18) Lin, F.; Lian, G.; Zhou, Y. Synthesis of Fondaparinux: modular synthesis investigation for heparin synthesis. *Carbohydr. Res.* **2013**, *371*, 32−9.

SUPPLEMENTARY MATERIALS

Materials and Methods

Materials

Hog Mucosal Heparin was acquired from Ming Han Chemicals (Oakland, CA). Heparitinase I, II, and III were expressed and purified from *fiavobacterium heparinum* as previously described. [1] DEAE-Sepharose gel was purchased from Amersham Biosciences. The analytical grade strong anion exchange (SAX) column was obtained from Dionex. Disaccharide standards for SAX were obtained from Iduron Inc (Manchester, UK). The G2000 SWxl analytical grade size exclusion column (SEC) was obtained from Tosoh Biosciences. Bovine lung microvascular endothelial cells (BLMVEC) and MCDB-131 endothelial media were acquired from Vec Technologies (Rensselaer, NY). Tryp LE Express trypsin was acquired from Invitrogen. All other reagents and solvents were from Sigma Aldrich.

Synthesis of Acharan Sulfate Mimetic

The synthesis of acharan sulfate-like glycosaminoglycan (Scheme 1) involves 6-*O*- and *N*-desulfation followed by *N*-acetylation. 100 mg of heparin, **1**, was first 6-*O* desulfated as previously described to yield **2**. [2] Briefly, the pyridinium salt of heparin was prepared by passing 100 mg of heparin in water over amberlite H+ cation exchange resin, collecting the eluant on ice, and adding pyridine to the eluant till a pH greater than 9. This solution was then concentrated in a rotary evaporator. The resulting material was then dissolved in 10 ml of pyridine. Next, 2 ml of *N*-methyltrimethylsilyl-trifluoroacetamide (MTS-TFA) was added to the reaction and it was stirred at 110 °C for 60 min. This mixture was concentrated on a rotary evaporator at 40 °C for 30 minutes. Subsequently it was quenched with 5 ml of water and precipitated by addition of 30 ml of ethanol saturated with sodium acetate. To complete the precipitation, the turbid mixture was refrigerated at -20 °C overnight. Subsequently, the precipitate was dissolved in water and dialyzed for 3 days against water. The retentate was then lyophilized.

The resulting 6-*O* desulfated heparin was *N*-desulfated by a previously described procedure. [3] 60 mg of 6-*O* desulfated heparin was converted into the pyridinium salt and dissolved in 10 ml of 9:1 DMSO:H_2O. This mixture was heated at 60 C for 60 minutes. This substrate was subsequently dialyzed and lyophilized as before to yield **3**.

Finally, the 6-*O* and *N*-desulfated polymer **3** was *N*-acetylated according to the method developed by Levvy et al.[4] Polymer **3** was dissolved in ice-cold 10 % methanol containing 0.05 M $NaCO_3$. To this mixture 1 ml of ice-cold acetic anhydride was added for 1 h at 10-minute intervals and the reaction pH was maintained in the range of 7-7.5 with 10% methanol saturated with Na_2CO_3 on ice. At the end, the reaction was precipitated with 6 volumes of ethanol and the precipitate was dialyzed and lyophilized to yield the final acharan sulfate mimetic, **4.**

NMR Sample Preparation

Approximately 7 mg of the acharan sulfate-like glycosaminoglycan was repeatedly (3x) dissolved in 1 ml portions of D_2O (Sigma-Aldrich, 99.9%) and then evaporated to replace exchangeable ^1H with ^2H and to remove residual H_2O. The final dried material was dissolved in 200 µL D_2O. Acetone was added (5%) for internal chemical shift referencing.

NMR Spectroscopy

One- and two-dimensional (1D, 2D) spectra were recorded on an Inova 600 spectrometer at 25 °C and proton chemical shifts were referenced to the acetone methyl signal at 2.22 ppm and 33 ppm ^{13}C. 1D proton, 2D [^1H, ^1H] TOCSY (100 ms mixing time), and 2D [^{13}C,^1H] HMQC experiments were recorded, processed using Agilent Software VnmrJ version 3.2 revision A, and resonances assigned using standard approaches.

Disaccharide Analysis of Acharan Sulfate Mimetic

The acharan sulfate mimetic was digested with a mixture of heparitinase I, II, and III overnight. Subsequently, samples were boiled for 1 minute and centrifuged to remove denatured proteins. Disaccharides were then analyzed using SAX-HPLC as previously described. [5] SAX analysis was performed by loading disaccharides onto a SAX column and eluting with a linear gradient of 0 to 1 M NaCl in 70 mM phosphate buffer (pH 3.0) for 60 min at a 1 ml/min flow rate. They were detected using an inline UV detector by measuring absorbance at 232 nm.

Size Exclusion Chromatography (SEC)

The acharan sulfate mimetic and heparin were first conjugated to fluoresceinamine through an EDC-NHS chemical procedure as described previously.[6] After purification from free fluoresceinamine, 20 µg of the resultant polymers were dissolved in 250 µl of water and analyzed by size exclusion chromatography.[6] Size exclusion chromatography was executed using a constant flow rate of 0.5 ml/min of size exclusion buffer (100 mM NaH_2PO_4, 150 mM NaCl, pH 6.8) over the course of 75 minutes. Detection occurred using an inline fluorescence detector with excitation/emission wavelengths of 485 nm/535 nm respectively.

Tube Formation Assay

Twenty four hours prior to tube formation assays, BLMVEC were split to maintain growth in the log phase. Reduced growth factor basement membrane extract (RGF-BME, Trevigen) was thawed overnight at 4 °C. Fifty µl of RGF-BME was then plated out in wells of a chilled 96 well plate using chilled pipette tips and incubated for 1 h at 37 °C. Concurrently, BLMVEC were suspended by incubation with Tryp LE Express. After setting the RGF-BME, 1 x 10^5 cells were then added to each well along with MCDB-131 complete media and substrates of interest. The plates were then incubated at 37 °C for 16 hours prior to Calcein staining and imaging.

Calcein Staining

Media was gently removed and each well was washed twice with PBS. Subsequently, 100 µl of 2 µM Calcein AM was added to each well. Cells were incubated for 30 min and then washed once again with PBS. Images were acquired with an Olympus IX81 microscope attached to a color CCD filter and a GFP emission filter using 485 nm excitation/520 nm emission.

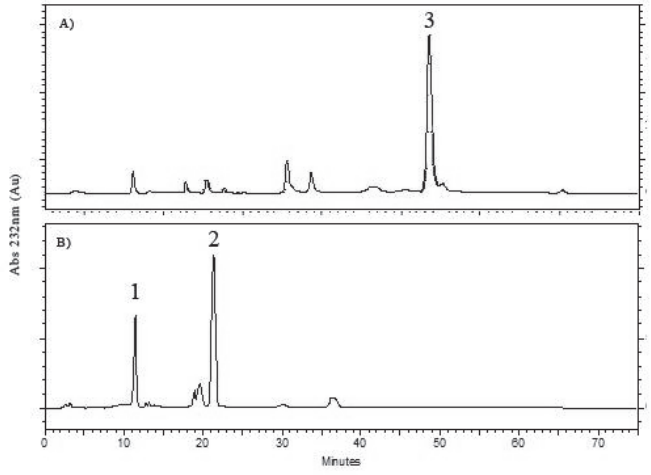

Figure S1. SAX-HPLC (Strong anion exchange-high pressure liquid chromatography) profiles of Heparin precursor (A) and synthetic acharan sulfate mimetic (B). Major peaks are: 1) ΔUA-GlcNAc (2*N*-acetamido- α-D-glucopyranoside (1→4)- α-$\Delta^{4,5}$-pyranosyluronate) and 2) ΔUA2S-GlcNAc (2*N*-acetamido- α-D-glucopyranoside (1→4)- 2-*O*-sulfo- α-

$\Delta^{4,5}$-pyranosyluronate) and 3) ΔUA2S-GlcNS6S (2*N*-sulfamino-6-*O*-sulfo-α-D-glucopyranoside (1→4)- 2-*O*-sulfo- α-$\Delta^{4,5}$-pyranosyluronate).

Table S1. NMR spectral assignment for synthetic acharan sulfate mimetic.

Proton/Carbon (H/C)	GlcNAc	IdoA
H-1/C-1	5.14/93.82	5.23/99.37
H-2/C-2	4.03/53.76	4.29/63.68
H-3/C-3	3.58/69.99	4.37/73.52
H-4/C-4	3.81/76.61	4.05/70.72
H-5/C-5	3.91/71.2 or 69.88	4.93/67.31
H-6a,-6b/C-6	3.90, 3.90/59.84	
NAc	2.09/22.07	

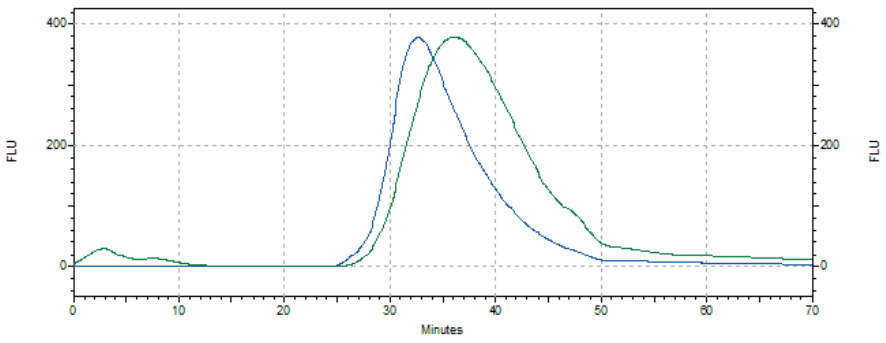

Figure S2. SEC-HPLC profiles of synthetic acharan sulfate mimetic (green) and heparin (blue). After chemical desulfation, the acharan sulfate mimetic has a lower molecular weight than the starting heparin.

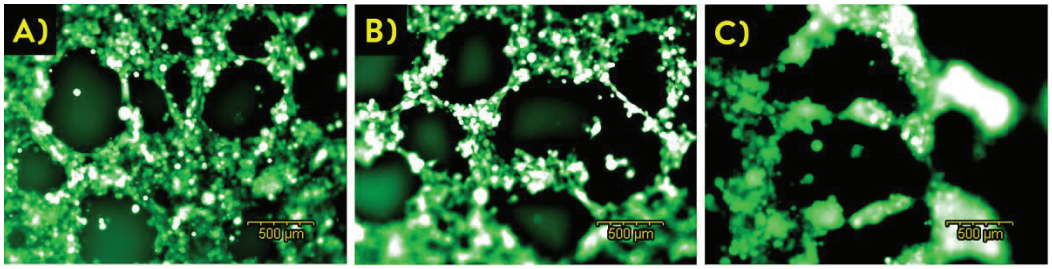

Figure S3. Tube formation in the presence of heparin. Representative panels are A) Untreated cells, B) 1 mg/ml Heparin, and C) 2 mg/ml Heparin.

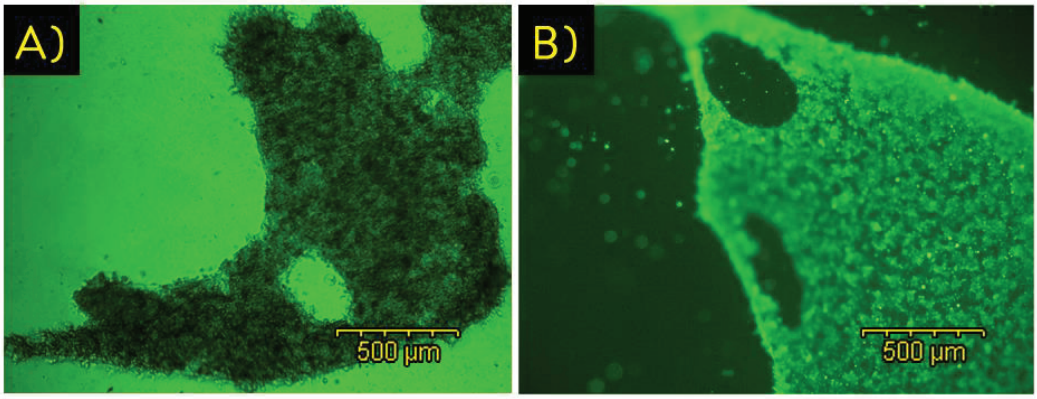

Figure S4. Tube formation in the presence of 0.5 mg/ml of acharan sulfate mimetic. At this concentration the inhibition of tube formation is less apparent. However, cells are still unable to form extensive tube networks and only some tubes are visible at this concentration. Representative panels are A) Brightfield of treated cells, B) Calcein-stained tubes under fluorescence.

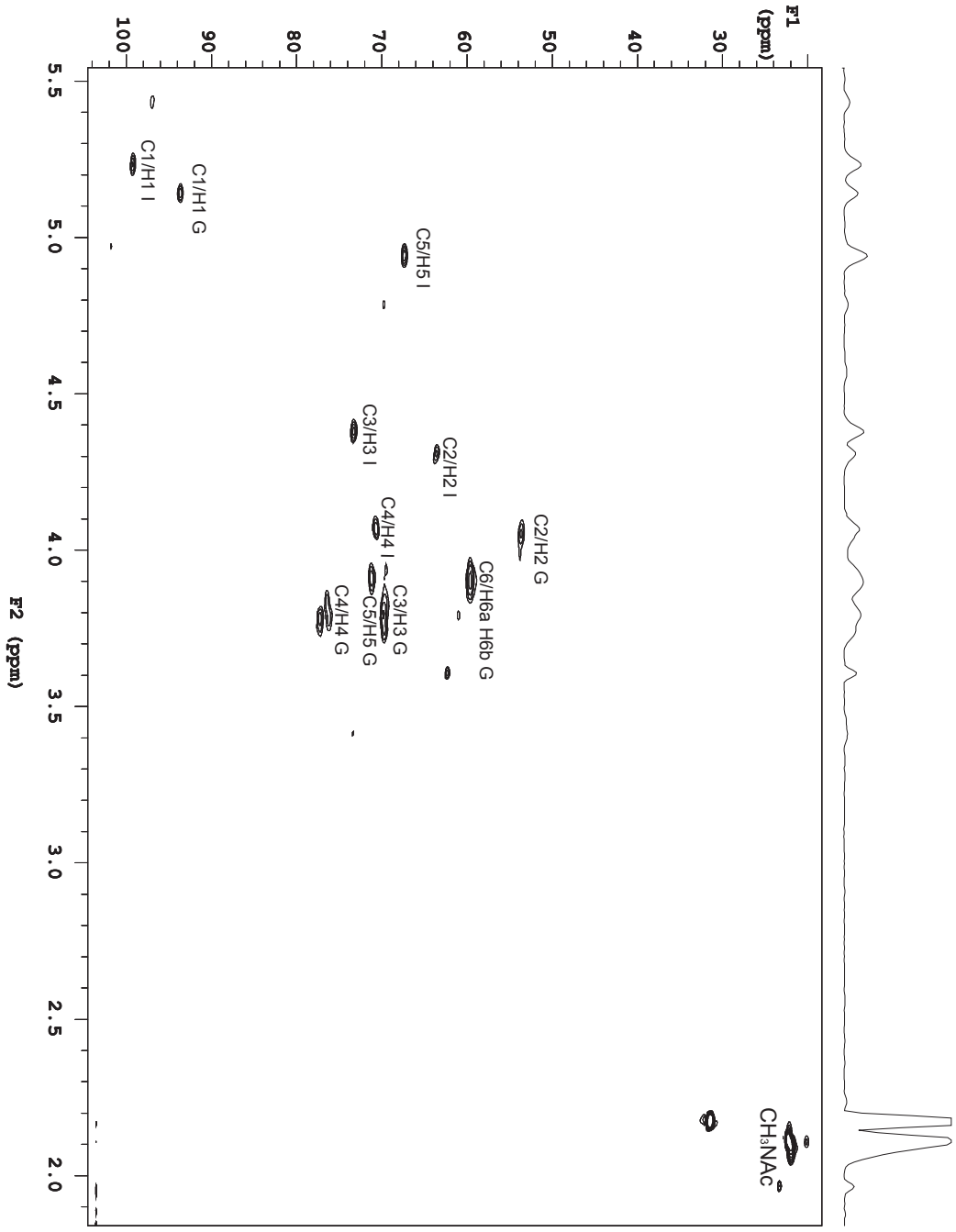

Figure S5. 2-D NMR of acharan sulfate mimetic. Here, I represents iduronic acid-2S and G represents glucosamine.

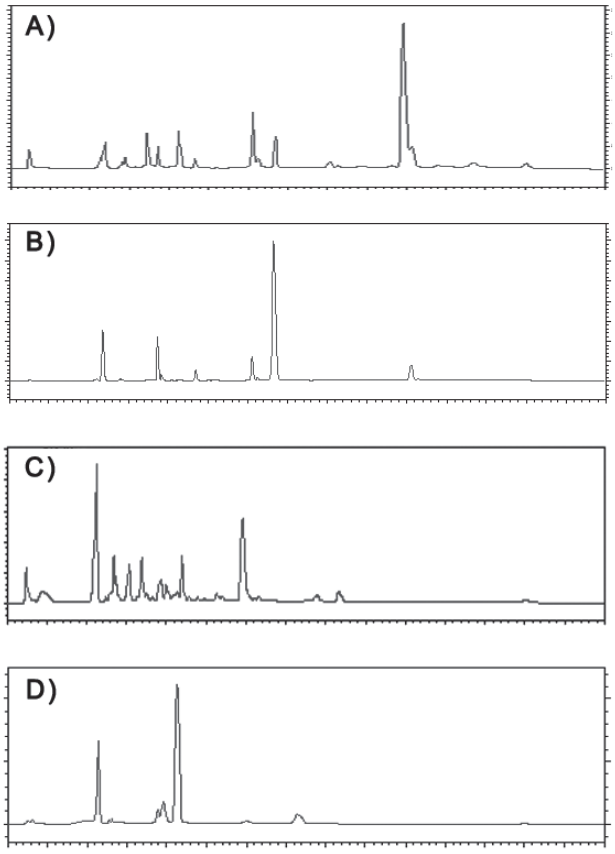

Figure S6. Disaccharide profiles of intermediates in the production of synthetic acharan sulfate mimetic analyzed via SAX-HPLC. Representative profiles are: A) Heparin precursor, B) 6-*O*-desulfated heparin, C) Partially N-desulfated and 6-O desulfated Heparin, and D) Acharan Sulfate mimetic. Completely 6-O-desulfated and N-desulfated heparin is not cleaved by a mixture of heparitinase I, II, and III efficiently.

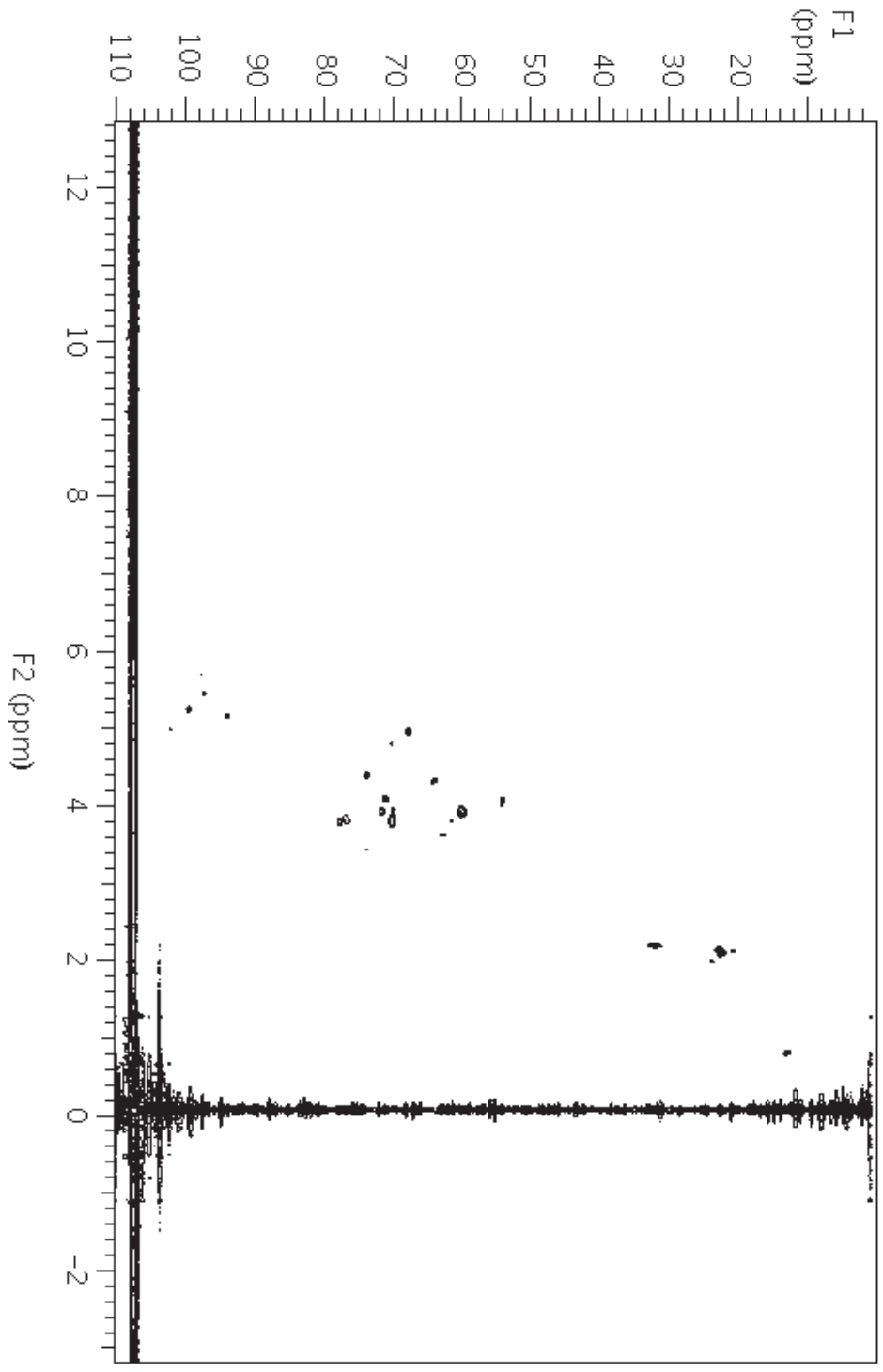

Figure S7. Full 2-D HMQC NMR spectra of acharan sulfate mimetic.

REFERENCES

1. Babu, P.; Kuberan, B., Fluorescent-tagged heparan sulfate precursor oligosaccharides to probe the enzymatic action of heparitinase I. *Anal. Biochem.* **2010,** 396, (1), 124-32.

2. Ishihara, M.; Takano, R.; Kanda, T.; Hayashi, K.; Hara, S.; Kikuchi, H.; Yoshida, K., Importance of 6-O-sulfate groups of glucosamine residues in heparin for activation of FGF-1 and FGF-2. *J. Biochem.* **1995,** 118, (6), 1255-60.

3. Nagasawa, K.; Inoue, Y.; Kamata, T., Solvolytic desulfation of glycosaminoglycuronan sulfates with dimethyl sulfoxide containing water or methanol. *Carbohydr. Res.* **1977,** 58, (1), 47-55.

4. Levvy, G. A.; McAllan, A., The N-acetylation and estimation of hexosamines. *Biochem. J.* **1959,** 73, 127-32.

5. Raman, K.; Nguyen, T. K.; Kuberan, B., Is N-sulfation just a gateway modification during heparan sulfate biosynthesis? *FEBS. Lett.* **2011,** 585, (21), 3420-3.

6. Raman, K.; Mencio, C.; Desai, U. R.; Kuberan, B., Sulfation patterns determine cellular internalization of heparin-like polysaccharides. *Mol. Pharm.* **2013,** 10, (4), 1442-9.

2.6.1 Additional Analysis of Data

Additional analysis of data from acharan sulfate experiments is presented in Figure 2.5.

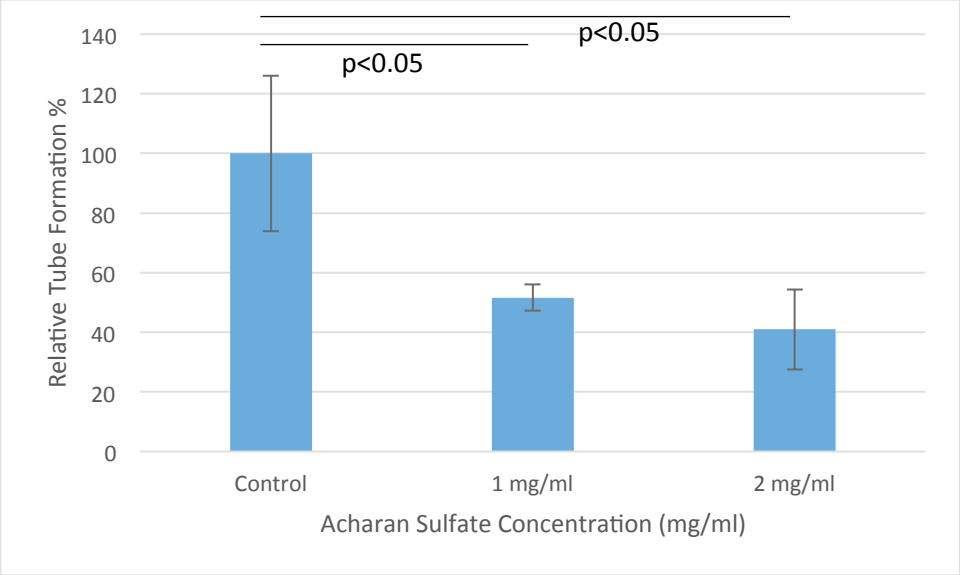

Figure 2.5. Relative tube formation when BLMVEC are treated with Acharan Sulfate-like glycosaminoglycan. Relative tube formation indicates the relative total mesh area covered by tubes. *P* values are determined using a 1-tailed paired t-test vs. control tube formation. Error bars indicate standard deviations.

2.6.2 References

1. Kuberan, B.; Ethirajan, M.; Victor, X. V.; Tran, V.; Nguyen, K.; Do, A., "Click" xylosides initiate glycosaminoglycan biosynthesis in a mammalian cell line. *Chembiochem* **2008,** 9, (2), 198-200.

2. Nguyen, T. K.; Tran, V. M.; Sorna, V.; Eriksson, I.; Kojima, A.; Koketsu, M.; Loganathan, D.; Kjellen, L.; Dorsky, R. I.; Chien, C. B.; Kuberan, B., Dimerized glycosaminoglycan chains increase FGF signaling during zebrafish development. *ACS Chem Biol* **2013**, 8, (5), 939-48.

CHAPTER 3

DEVELOPMENT AND *IN VITRO* EVALUATION OF A MODIFIED HEPARIN-DOXORUBICIN CONJUGATE AS AN ANTICANCER THERAPEUTIC

3.1 Introduction

As an adjuvant therapy to xylosides and other GAG mimetics which alter tumor angiogenesis and invasion, a drug delivery vehicle that can deliver toxic cargo and alter tumor growth is necessary. It is likely that attacking cancer growth using chemotherapeutics, in addition to attacking invasion and angiogenesis using xylosides, will yield a more potent and effective treatment strategy than the state of the art. However, a majority of DDV developed are simple carriers that target toxic cargo to tumors and are then excreted. By utilizing a GAG-based DDV, it is possible to develop a dual-action vehicle where both the drug cargo as well as the carrier may be therapeutic. Additionally, PG-based DDV are naturally biodegradable and biocompatible. Previously, several heparin-based DDV have been developed and conjugated to a variety of small molecule cargo such as paclitaxel. While such conjugates showed efficacy *in vitro* and *in vivo*, these studies were not translated into the clinic due to heparin's inherent anticoagulant activity.

Therefore, in order to develop a proteoglycan based carrier that is not anticoagulant, a series of chemically modified heparins were synthesized and

systematically tested for their ability to internalize into cells and localize to the nucleus in multiple cancer cells. The rate of internalization, saturation point, cellular localization, and internalization mechanisms of these were investigated. It was found that heparosan and *N*-sulfo heparosan are the most promising GAGs for use as drug delivery vehicles due to their ability to internalize into cells the greatest extent relative to heparin. Heparosan was even found to localize to the nucleus of U87 Mg glioma cells. Sulfation pattern significantly affects the ability of modified heparins to internalize into cells. However the mechanism of nuclear entry of GAGs remains a mystery.

Next, heparosan and *N*-sulfo heparosan were conjugated to doxorubicin and tested for their relative ability to reduce cell viability of various cancer cells compared to a heparin-doxorubicin conjugate. Against doxorubicin-sensitive cells, heparosan and *N*-sulfo heparosan were more efficacious than heparin at delivering doxorubicin. Against doxorubicin-resistant cells, heparosan was not effective whereas *N*-sulfoheparosan was more effective than heparin. All doxorubicin-conjugates were able to enter the nuclei of U87Mg and HT-29 cells. Additionally, it was not necessary to attach doxorubicin to the polymers using a labile linker. Therefore, not only are GAG-based polymeric DDV excellent at overcoming drug resistance in cells, but they are also much more stable than traditional DOX-polymer conjugates which require labile linkers to function. Furthermore, with a natural ability to target cellular nuclei, GAG-based DDV represent a significant advancement over other state-of-the-art polymeric doxorubicin delivery vehicles. However, it is noteworthy that GAGs serve several biological roles and may affect multiple cellular processes when utilized as DDV. Rigorous clinical and animal testing is necessary to determine the significance of these side-effects.

3.2 Sulfation Patterns Determine Cellular Internalization of Heparin-like Polysaccharides

Reprinted with permission from: Raman, K., Mencio, C., Desai, U. R., and Kuberan, B. (2013) Sulfation patterns determine cellular internalization of heparin-like polysaccharides, *Mol. Pharm., 10*, 1142-1449. Copyright 2013 American Chemical Society.

molecular pharmaceutics

Brief Article

pubs.acs.org/molecularpharmaceutics

Sulfation Patterns Determine Cellular Internalization of Heparin-Like Polysaccharides

Karthik Raman,[†] Caitlin Mencio,[‡] Umesh R. Desai,[§] and Balagurunathan Kuberan*[,†,‡,∥]

[†]Department of Bioengineering, University of Utah, Salt Lake City, Utah 84112, United States

[‡]Interdepartmental Program in Neuroscience, University of Utah, Salt Lake City, Utah 84112, United States

[§]Department of Medicinal Chemistry, Virginia Commonwealth University, Richmond, Virginia 23284, United States

[∥]Department of Medicinal Chemistry, University of Utah, Salt Lake City, Utah 84112, United States

Supporting Information

ABSTRACT: Heparin is a highly sulfated polysaccharide that serves biologically relevant roles as an anticoagulant and anticancer agent. While it is well-known that modification of heparin's sulfation pattern can drastically influence its ability to bind growth factors and other extracellular molecules, very little is known about the cellular uptake of heparin and the role sulfation patterns serve in affecting its internalization. In this study, we chemically synthesized several fluorescently labeled heparins consisting of a variety of sulfation patterns. These polysaccharides were thoroughly characterized using anion exchange chromatography and size exclusion chromatography. Subsequently, we utilized flow cytometry and confocal imaging to show that sulfation patterns differentially affect the amount of heparin uptake in multiple cell types. This study provides the first comprehensive analysis of the effect of sulfation pattern on the cellular internalization of heparin or heparan sulfate like polysaccharides. The results of this study expand current knowledge regarding heparin internalization and provide insights into developing more effective heparin-based drug conjugates for applications in intracellular drug delivery.

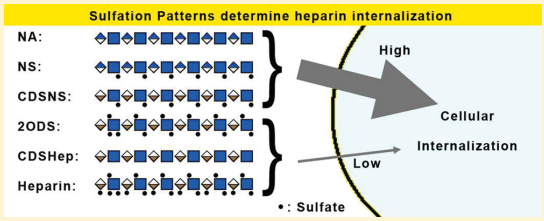

KEYWORDS: *heparin, cellular uptake, internalization, nucleus localization, heparan sulfate, heparosan*

INTRODUCTION

Heparin is a complex, biocompatible, biodegradable, and water-soluble glycosaminoglycan that is commonly found within mast cell granules. While its biological role is unclear, heparin is utilized clinically for its anticoagulant properties. As an agonist of antithrombin, heparin is an effective treatment against deep-vein thrombosis and pulmonary emboli.[1] Recent studies have also shown that heparin has potent anticancer properties including an ability to hinder cancer invasion, metastasis, and tumor-derived angiogenesis.[2−4]

It is well-known that altering heparin's sulfation pattern can affect its biochemical properties. N-Desulfation of heparin, removal of 2-*O* sulfate groups from iduronic acid residues, and removal of 6-*O* sulfate groups from glucosamine residues within heparin can inhibit heparin−FGF interactions.[5−7] Additionally, *N*-sulfate and 3-*O* sulfate groups are critical to heparin's anticoagulant activity.[8,9]

Several recent publications have utilized covalently conjugated heparin-based drug delivery vehicles (DDV) to deliver anticancer molecules such as paclitaxel and litocholate.[10,11] Conjugation to heparin provides additional therapeutic value because both the DDV and the drug prevent cancer progression. However, it is still unclear how altering heparin's sulfation patterns can affect its cellular internalization, localization, and efficacy as a DDV. Previously, researchers have identified heparin scavenger receptors; however, these receptors have not yet been isolated and their substrate specificities remain unknown.[12−14]

In this article, we chemically modify heparin and heparosan, a heparin precursor isolated from *E. coli* K5, to show that modification of heparin's sulfation pattern leads to increased cellular uptake, providing hints to define the ligand specificities of heparin receptors in cells. These exciting results provide new insight into heparin/heparan sulfate biology and the design of more effective heparin-conjugates for drug delivery.

MATERIALS AND METHODS

Materials. HT-29 colon cancer cells and BXPC-3 pancreatic cancer cells were provided by Dr. Scott Kuwada (University of Hawaii). U87-Mg glioma cells were obtained from Dr. Randy Jensen (University of Utah). Hog mucosal heparin was obtained from Ming Han Chemicals (Oakland, CA). K1 CHO cells were obtained from the ATCC. DEAE-Sepharose gel was purchased from Amersham Biosciences. The analytical grade strong anion exchange column, size exclusion column,

Received: November 26, 2012
Revised: January 28, 2013
Accepted: February 11, 2013
Published: February 11, 2013

dx.doi.org/10.1021/mp300679a | *Mol. Pharmaceutics* 2013, 10, 1442−1449

and weak anion exchange column were obtained from Dionex and Tosoh Biosciences. Disaccharide standards for strong anion exchange were obtained from Iduron Inc. (Manchester, U.K.). Heparitinase I, II, and III from *Flavobacterium heparinum* were expressed as previously described.[15] Cell culture reagents were from Invitrogen Inc. Internalization inhibitors chlorpromazine (CPZ), filipin (FIL), dynasore (DYN), 5-(*N*-ethyl-*N*-isopropyl) amiloride (EIPA), and all other reagents and solvents were from Sigma-Aldrich.

Synthesis of Modified Heparins (M. Heps). Briefly, heparosan (NA), *N*-sulfo heparosan (NS), completely desulfated heparin (CDSHep), completely desulfated N-resulfated heparin (CDSNS), and 2-*O* desulfated heparin (2ODS) were synthesized as described in the literature.[16−19] After extensive dialysis, each substrate was digested with a cocktail of heparitinase I, II, and III and subjected to disaccharide analysis by strong anion exchange chromatography.[20] More specifically, the substrates were prepared as described in the following sections.

Heparosan (NA). Heparosan capsular polysaccharide was first isolated and purified from *E.Coli* K5 as previously described in the literature.[16] The resulting polysaccharide was then further purified by dialysis against running water through a 3000 MWCO membrane for 3 days. After complete lyophilization, the product was weighed and characterized through anion exchange chromatography as described in the Supporting Information.

N-Sulfated Heparosan (NS). As described in the literature, N-sulfated heparosan was prepared by N-deacetylation of heparosan followed by N-sulfation.[17] N-deacetylation was carried out by treating 1 g of heparosan with 2.5 M NaOH in water at 55 °C overnight. Next, N-deacetylated heparosan was neutralized to pH 7.0 and treated with 2.5 g each of $NaCO_3$ and triethylamine−sulfur trioxide complex and stirred for 24 h at 48 °C. The pH of this reaction was maintained below pH 10 by the addition of HCl. Subsequently, an additional 2.5 g each of $NaCO_3$ and triethylamine−sulftur trioxide complex was added, and the reaction was stirred for an additional 24 h. The resulting polysaccharide was dialyzed, lyophilized, and chemically characterized in a similar manner to NA.

Completely Desulfated Heparin (CDSHep). CDSHep was prepared by utilizing published protocols.[18] The pyridinium salt of heparin was first synthesized by passing a solution of 1 g of heparin in water through a column packed with Amberlite cation exchange resin. The resulting eluant was collected on ice, adjusted to pH 9 with pyridine, stirred for 30 min, and then concentrated in a rotary evaporator. One-hundred milligrams of the pyridinium salt of heparin was then completely desulfated by stirring overnight at 100 °C in a 10 mL mixture of 9:1 DMSO/methanol. The resulting polysaccharide was dialyzed, lyophilized, and characterized as stated before.

Completely Desulfated N-Resulfated Heparin (CDSNS). To synthesize CDSNS, CDSHep was subjected to N-sulfation as previously described for NS preparation.

2-O Desulfated Heparin (2ODS). According to a previously published protocol, 10 mg of heparin was mixed with 1 mg of $NaBH_4$ in 10 mL of 0.4 N NaOH.[19] This mixture was then frozen in a −80 refrigerator and lyophilized to dryness. The resulting crusty yellow solid was subsequently redissolved in water and neutralized to pH 7 with acetic acid. This polymer was then dialyzed for 3 days, lyophilized, and characterized as stated before.

Fluoresceinamine Conjugation to M. Heps. First, a stock of 100 mg of fluoresceinamine (FA) was dissolved in a 1 mL mixture of 3:2:1 DMSO/acetonitrile/acetone. Additionally, a stock containing 22 mg of 1-ethyl-3-(3-dimethylaminopropyl)carbodiimide (EDC) in 1 mL of water was created. Next, 100 mg of each M. Hep substrate was dissolved in 1 mL of water. Three-hundred microliters of the FA stock was added to the M. Hep along with 300 μL of the EDC stock. This mixture was stirred overnight at room temperature and subsequently dialyzed and lyophilized. Utilizing FA modified heparins, the molecular weight of FA−M. Heps was analyzed by size exclusion high-performance liquid chromatography (HPLC) as described previously.[20] The charge density of each substrate was analyzed by weak anion-exchange HPLC as described previously.[20]

Cell Treatment with FA−M. Heps. Approximately 50 000 cells were trypsinized and added into wells of a 96 well plate with DMEM containing 10% FBS and 1% penicillin/streptomycin (P/S). After approximately 16 h, cells were adherent, and the media was replaced with HAMS F-12 containing 10% FBS and 1% P/S. To these wells, 200 μg of each FA−M. Hep was added, and cells were incubated for 6 h in a humidified cell culture incubator.

Fluorescence-Assisted Cell Sorting. After treatment with FA−M. Heps, cells were resuspended in trypsin without phenol red. Trypsin was neutralized with HAMS F-12 media containing 10% FBS, and cell suspensions were analyzed on a FACScan instrument (Becton Dickenson Immunocytometry Systems, Mountain View, CA) with computer-aid from CellQuant software. A minimum of 5000 gated events were captured for each sample and used for comparison purposes.

Confocal Imaging. For confocal imaging, approximately 50 000 cells were grown on glass coverslips within 35 mm cell culture dishes with 1 mL of media. Subsequently, 200 μg of FA−M. Hep conjugates were added, and cells were allowed to internalize M. Heps for 16 h in a humidified incubator. Subsequently, the media was removed, and cells were washed twice with PBS. Five-hundred microliters of 4% paraformaldehyde solution was then added to the cells, and cells were maintained for 10 min at room temperature. Next, cells were washed twice with PBS and stained with DAPI and Rhodamine Phalloidin for 10 min each. After incubation with cellular stains, cells were mounted onto microscope slides and imaged with an FV1000-XY Confocal Olympus IX81 microscope with a 60× oil immersion lens.

RESULTS

The central goal of this study is to determine whether modulation of heparin's sulfation pattern affects its cellular internalization. To achieve this goal, a library of fluorescein-amine-conjugated M. Heps was synthesized (Figure 1) and extensively characterized via analysis of sulfation pattern, charge density, and size (Table S1 and Figure S1, Supporting Information). A variety of cells were incubated with each M. Hep, and FACS was utilized to analyze the total amount of conjugate that was internalized after 6 h (Figure 2). Next, the cellular localization of each conjugate was assessed using confocal microscopy in two different cell lines, HT-29 colon cancer cells and U87-Mg glioma cells (Figures 3 and 4). The rate and mechanism of uptake of each conjugate was also assessed using FACS (Figures 5 and 6).

Sulfation Pattern Affects the Internalization of M. Heps into Multiple Cell Types. To determine the effects of

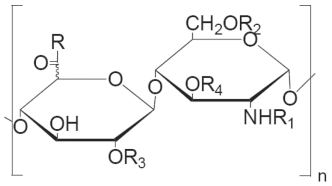

R: OH or Fluorescein

NA*:	R_1 : Ac	R_2,R_3,R_4 : H	
NS*:	R_1 : OSO_3^-	R_2,R_3,R_4 : H	
CDSNS:	R_1 : OSO_3^-	R_2,R_3,R_4 : H	
2ODS:	R_1 : OSO_3^-	R_2 : OSO_3^-	R_3,R_4 : H
CDSHep:	R_1,R_2,R_3,R_4 : H		
Heparin:	R_1,R_2,R_3,R_4 : OSO_3^-		

* Non-epimerized substrates containing only glucuronic acid

Figure 1. Structures of modified heparins prepared in this study.

sulfation pattern on internalization, experiments were conducted to test the relative internalization of several M. Heps in the following cell lines (Figure 2): bovine lung microvascular endothelial cells (BLMVEC), chinese hamster ovary K1 cells (CHO K1), BXPC-3 human pancreatic cancer cells, HT-29 human colorectal cancer cells, and U87-Mg human glioma cells.

All cells were incubated with fluoresceinamine-conjugated M. Heps for 6 h and subsequently subjected to analysis by FACS (Figure 2). Relative to heparin, M. Hep substrates showed drastically altered internalization into different cell types. NA, NS, and CDSNS fluoresceinamine conjugates were internalized into all cell types significantly more than heparin. However, a partially positively charged polymer, CDSHep, was not internalized to the same extent as NA, NS, or CDSNS in all the cell lines tested. Furthermore, NS, not NA, was internalized to the greatest extent in all cell types tested; thus, these results indicate that uptake may be receptor-mediated and that the receptor recognizes and internalizes NS more than other M. Heps tested.

M. Heps Are Found Throughout Cellular Bodies. To examine the effect of sulfation patterns on cellular localization, U87-Mg and HT-29 cells were incubated with FA–M. Hep conjugates overnight, and localization was analyzed by confocal microscopy (Figures 3 and 4). Rhodamine Phalloidin was utilized as a red dye to identify cellular actin, and DAPI was utilized to label the cellular nuclei. Z-Slices were chosen so as to minimize colocalization of the actin stain with the nuclear stain.

Confocal images indicate that NS, CDSNS, 2ODS, CDSHep, and heparin all colocalize with cellular actin in U87-MG cells and are found throughout cell bodies. Interestingly, NA colocalizes with DAPI, showing that this substrate may enter the nuclei of U87-MG cells. However, in HT-29 cells, all the M. Heps are found in cell bodies, thus indicating that nuclear localization may be both sulfation pattern-dependent and cell-specific.

Sulfation Patterns Affect the Rate of Internalization of M. Heps into Cells. In addition to the extent of internalization, the effects of sulfation pattern on the rate of substrate internalization into HT-29 cells was analyzed by incubating

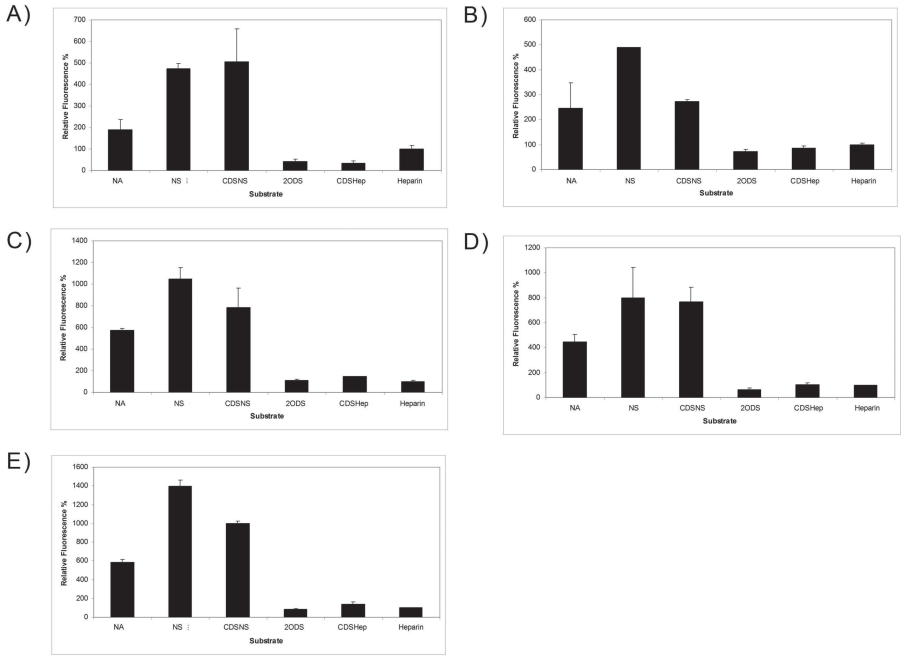

Figure 2. Sulfation patterns determine the total amount of cellular uptake of M. Heps at 6 h. The different panels indicate M. Hep uptake in (A) BLMVEC, (B) K1 CHO, (C) BXPC-3, (D) HT-29, and (E) U87-Mg cells. Values are normalized against heparin and show that M. Heps such as NA, NS, and CDSNS show enhanced cell uptake relative to heparin. Internalization of M. Heps was determined by fluorescence assisted cell sorting analysis as described in the experimental section. Cellular auto fluorescence at the settings used was minimal.

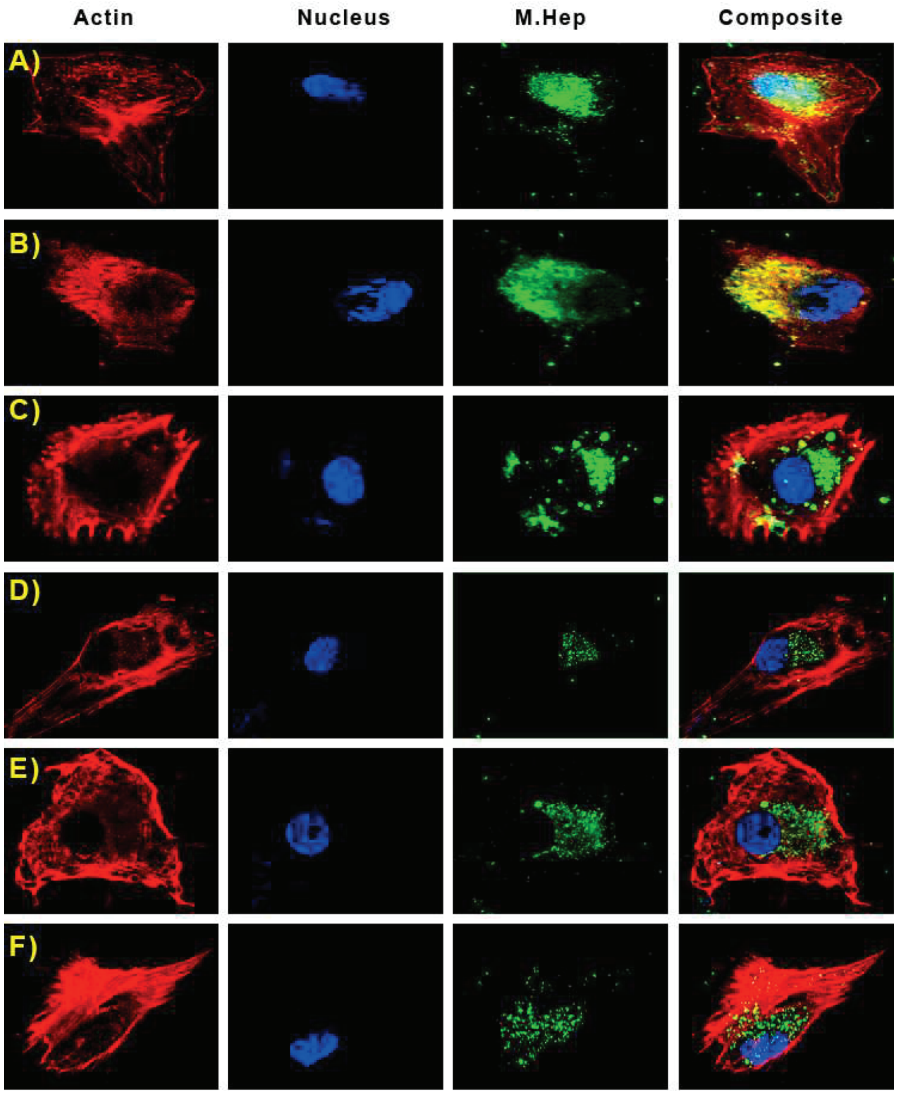

Figure 3. Sulfation patterns determine the cellular localization of M. Heps in U87-Mg cells. Panels in this image are fluorescence from Rhodamine Phalloidin (actin), DAPI (nucleus), fluoresceinamine (M. Heps), and an overlay of all fluorophores. Representative substrates are (A) NA, (B) NS, (C) CDSNS, (D) 2ODS, (E) CDSHep, and (F) Heparin. It is evident that NA polymers colocalize with DAPI in the nucleus of U87-Mg cells.

equal amounts of each substrate with cells for various time points (Figure 5). Compared to the amount of each substrate internalized after 30 h, NA and CDSHep saturated the fastest. NS, CDSNS, and 2ODS saturated at an intermediate rate, while heparin saturated at a slower rate. Cellular recognition of GAG sulfation patterns probably determines the rate of saturation.

In contrast, sulfation patterns do not determine the concentration dependence of internalization (Figure 6). Only CDSHep showed a significant departure from heparin by saturating at lower concentrations than all other polymers tested. This is most likely due to its amine functionality, as NA and other substrates did not show similar concentration dependence.

DISCUSSION

In recent years, heparin-based conjugates have shown promise in preclinical studies as drug delivery vehicles. One of the reasons for their efficacy is because heparin−drug conjugates are able to attack cancer cells using multiple pathways; both the drug and the DDV are able to mitigate tumor progression.[21−24] However, the role of sulfation patterns in the cellular uptake of heparin is largely unknown. In this article, chemically modified heparosan from *E. coli* K5 and chemically modified heparin are utilized to show that sulfation patterns determine heparin cellular uptake into several cell types. This knowledge inspires new designs of chemically modified heparin−drug conjugates that are favorable for drug delivery but lack heparin's inherent

dx.doi.org/10.1021/mp300679a | *Mol. Pharmaceutics* 2013, 10, 1442−1449

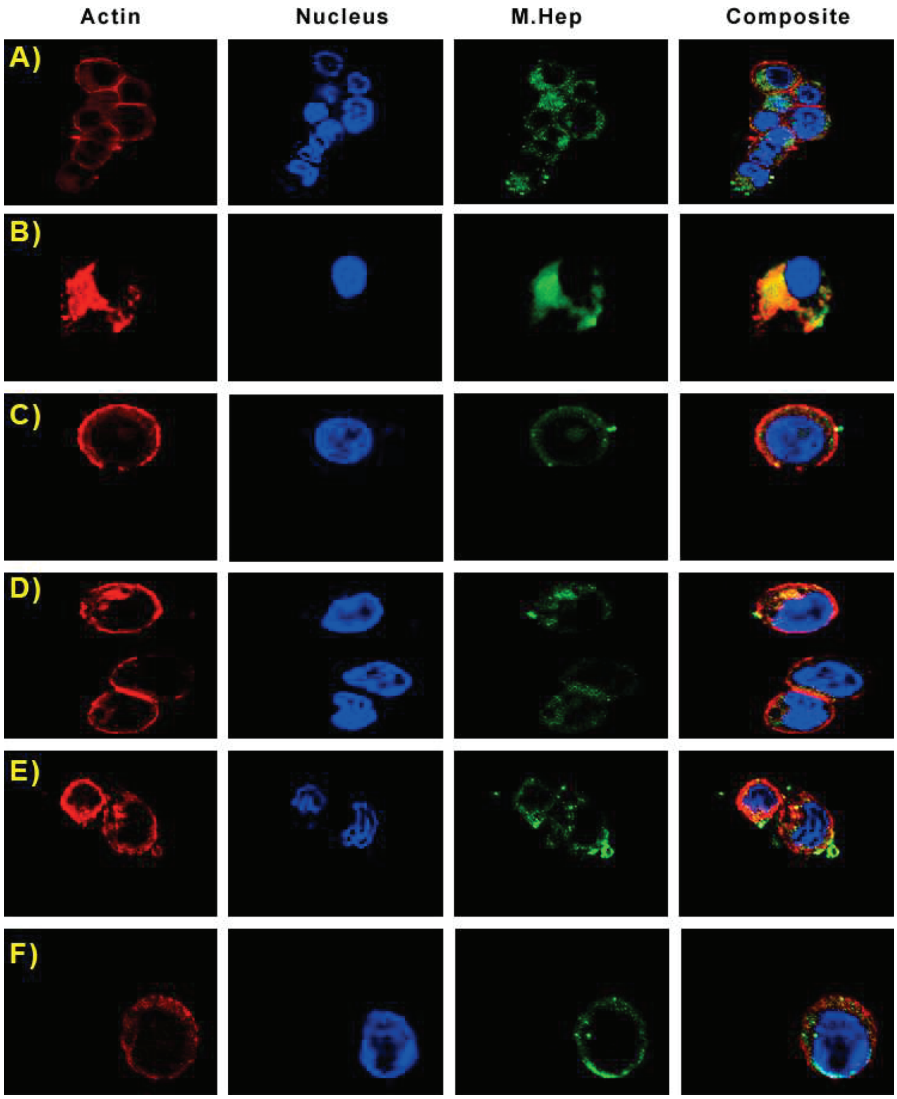

Figure 4. Sulfation patterns determine the cellular localization of M. Heps; however, no nuclear localization is visible for any substrate in HT-29 cells. Panels in this image are fluorescence from Rhodamine Phalloidin (actin), DAPI (nucleus), fluoresceinamine (M. Heps), and an overlay of all fluorophores. Representative substrates are (A) NA, (B) NS, (C) CDSNS, (D) 2ODS, (E) CDSHep, and (F) Heparin.

drawbacks such as bleeding complications and heparin-induced thrombocytopenia. Additionally, the results of this study further provide hints to illuminate the ligand specificities of elusive heparin scavenger receptors.

Previous studies have found that modification of sulfation pattern can alter the biological properties of heparin. Controlling the amount of 2-*O*, 3-*O*, and 6-*O* sulfation can drastically affect heparin's ability to bind ligands.[5,8,9,25] To test our hypothesis that sulfation patterns affect cellular internalization and the effectiveness of heparin as a DDV, we designed a library of heparins to represent a diverse group of polymers with different sulfation patterns and densities (Figure 1). CDSHep was the only substrate determined to have free amine groups, and hence, it had the least negative charge density. Unaltered heparin had the highest negative charge, while other substrates had intermediate charge density. We also specifically designed molecules derived from heparosan that were non-epimerized and those derived from heparin that contained high iduronic acid content. Analysis by size exclusion chromatography revealed that only minor differences in size and polydispersity exist among the different substrates (Table S1 and Figure S1, Supporting Information).

After structural characterization, a variety of cell types were treated with M. Heps and analyzed via FACS to determine the uptake of each M. Hep (Figure 2). The experiment was designed to include both tumorigenic and nontumorigenic cell types. As hypothesized, modifying the sulfation patterns of heparin and heparosan significantly altered cellular internal-

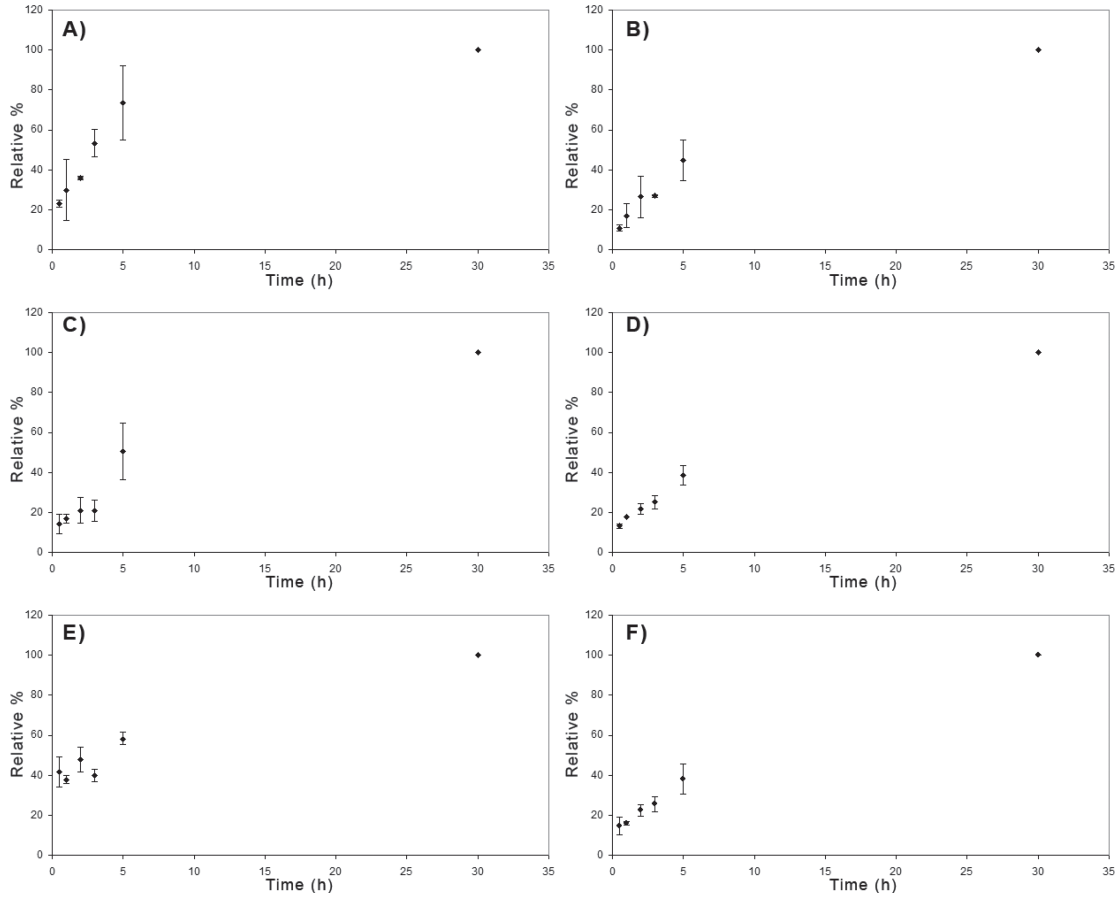

Figure 5. Sulfation patterns determine rate of entry of M. Heps into HT-29 colon cancer cells. Values are normalized to the 30 h time points for each substrate. Representative panels indicate the time-dependent internalization of (A) NA, (B) NS, (C) CDSNS, (D) 2ODS, (E) CDSHep, and (F) Heparin.

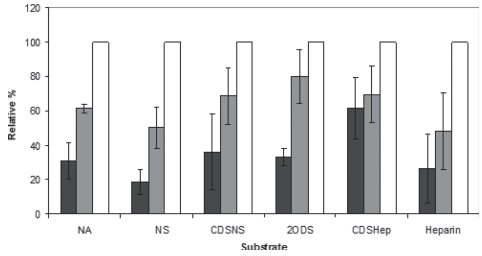

Figure 6. Sulfation pattern has little effect on the concentration dependence of internalization. Representative bars indicate the relative fluorescence measured by FACS when 20 μg (black), 100 μg (gray), or 200 μg (white) of M. Heps were incubated with cells for 24 h. Values are normalized to the total substrate internalized after 24 h when 200 μg of the respective substrate are added.

ization. One would expect that CDSHep, the most positively charged polymer, would be internalized by cells to the greatest extent. However, NA, NS, and CDSNS accumulated inside the cell to a much larger extent than CDSHep, 2ODS, and heparin in all cell types tested. This indicates that sulfation pattern, not charge density, determines cellular internalization of M. Heps. These results also give a glimpse into the substrate specificities of elusive heparin uptake receptors.[12−14] While researchers have not yet isolated these receptors, it is clear that sulfation pattern greatly affects cellular uptake of heparin and that these receptors prefer *N*-sulfo heparosan to any of the other M. Heps tested. Further evidence that heparin uptake may be receptor driven is determined by the concentration dependence of the internalization of M. Heps (Figure 6). If internalization was a purely diffusion-driven process, then the concentration dependence of internalization would be linear with concentration. However, it is evident that incubating cells with five times and ten times more substrate does not lead to a linear dose-dependent increase in internalization.

Next, the cellular localization of M. Heps was sought after to determine the effects of sulfation pattern on subcellular targeting. Previously, it was found that glycosaminoglycans (GAGs) and proteoglycans (PGs) such as syndecan-1 and glypican-1 can enter the nucleus.[26−30] Additionally, antiproliferative GAGs primed by xylosides can enter cellular nuclei and modulate histone 3 acetylation and cellular growth.[31] Heparin-poly-β-amino ester complexes have also been found to

dx.doi.org/10.1021/mp300679a | *Mol. Pharmaceutics* 2013, 10, 1442−1449

modulate nuclear transcription factors.[32] However, researchers have not yet identified if sulfation patterns affect the nuclear entry of these PGs and GAGs. Therefore, we examined the cellular localization of M. Heps tagged with fluoresceinamine by utilizing confocal microscopy (Figures 3 and 4). The majority of M. Heps were found throughout cell bodies and excluded from the nucleus in both HT-29 and U87-Mg cells. However, in U87-Mg, NA was found to colocalize with DAPI. On the basis of these results, it may be possible to deduce that sulfation patterns can affect the nuclear entry of GAGs. It is unlikely that charge density was responsible for nuclear entry, as CDSHep did not enter the nuclei. Additionally, none of the epimerized substrates were visible in the nucleus suggesting that chain flexibility may affect nuclear entry as well. However, additional biochemical proof will be necessary to further understand the differential localization of heparin and heparin-like polymers.

In conclusion, this research presents the first comprehensive evidence that sulfation pattern, not charge density, determines heparin/heparan sulfate cellular uptake into several cell types. While the M. Heps are found throughout cells, nuclear localization of these GAGs may be both sulfation pattern and cell-type dependent. The results of this study have broad implications in cell biology, heparan sulfate biochemistry, and drug delivery vehicle design. However, several new questions now surface: Why do NS and NA polymers enter cells to a greater extent than heparin? Do NA or NA/NS domains of heparan sulfate promote cellular uptake and nuclear localization of syndecans and glypicans? Additionally, would developing NA-, NS-, or CDSNS-based DDV yield better tumor-targeting capability than heparin-based DDV? In-depth analysis of nuclear localization and in vivo drug targeting is necessary to answer these intriguing questions.

■ ASSOCIATED CONTENT

Ⓢ Supporting Information

Charge and size of M. Heps. Effect of treatment with multiple uptake inhibitors. This material is available free of charge via the Internet at http://pubs.acs.org.

■ AUTHOR INFORMATION

Corresponding Author

*Tel: (+1) 801-587-9474. Fax: (+1) 801-585-9119. E-mail: kuby@pharm.utah.edu.

Author Contributions

The manuscript was written through contributions of all authors. All authors have given approval to the final version of the manuscript.

Notes

The authors declare no competing financial interest.

■ ACKNOWLEDGMENTS

This work was supported by NIH grants P01HL107152 and R01GM075168 to B.K., and by the NIH fellowship F31CA168198 to K.R.

■ ABBREVIATIONS

M. Hep, modified heparin; FGF, fibroblast growth factor; DDV, drug delivery vehicle; CPZ, chlorpromazine; FIL, filipin; DYN, dynasore; EIPA, 5-(*N*-ethyl-*N*-isopropyl) amiloride; FA, fluoresceinamine; NA, heparosan; NS, *N*-sulfo heparosan; CDSHep, completely desulfated heparin; CDSNS, completely desulfated N-resulfated heparin; 2ODS, 2-*O* desulfated heparin; HS, heparan sulfate

■ REFERENCES

(1) Hull, R.; Delmore, T.; Genton, E.; Hirsh, J.; Gent, M.; Sackett, D.; McLoughlin, D.; Armstrong, P. Warfarin sodium versus low-dose heparin in the long-term treatment of venous thrombosis. *N. Engl. J. Med.* **1979**, *301* (16), 855−858.

(2) Borsig, L. Antimetastatic activities of modified heparins: selectin inhibition by heparin attenuates metastasis. *Semin. Thromb. Hemostasis* **2007**, *33* (5), 540−546.

(3) Vlodavsky, I.; Mohsen, M.; Lider, O.; Svahn, C. M.; Ekre, H. P.; Vigoda, M.; Ishai-Michaeli, R.; Peretz, T. Inhibition of tumor metastasis by heparanase inhibiting species of heparin. *Invasion Metastasis* **1994**, *14* (1−6), 290−302.

(4) Folkman, J.; Langer, R.; Linhardt, R. J.; Haudenschild, C.; Taylor, S. Angiogenesis inhibition and tumor regression caused by heparin or a heparin fragment in the presence of cortisone. *Science* **1983**, *221* (4612), 719−725.

(5) Guimond, S.; Maccarana, M.; Olwin, B. B.; Lindahl, U.; Rapraeger, A. C. Activating and inhibitory heparin sequences for FGF-2 (basic FGF). Distinct requirements for FGF-1, FGF-2, and FGF-4. *J. Biol. Chem.* **1993**, *268* (32), 23906−23914.

(6) Lundin, L.; Larsson, H.; Kreuger, J.; Kanda, S.; Lindahl, U.; Salmivirta, M.; Claesson-Welsh, L. Selectively desulfated heparin inhibits fibroblast growth factor-induced mitogenicity and angiogenesis. *J. Biol. Chem.* **2000**, *275* (32), 24653−24660.

(7) Sugaya, N.; Habuchi, H.; Nagai, N.; Ashikari-Hada, S.; Kimata, K. 6-O-sulfation of heparan sulfate differentially regulates various fibroblast growth factor-dependent signalings in culture. *J. Biol. Chem.* **2008**, *283* (16), 10366−10376.

(8) Atha, D. H.; Lormeau, J. C.; Petitou, M.; Rosenberg, R. D.; Choay, J. Contribution of 3-*O*- and 6-*O*-sulfated glucosamine residues in the heparin-induced conformational change in antithrombin III. *Biochemistry* **1987**, *26* (20), 6454−6461.

(9) Danishefsky, I.; Ahrens, M.; Klein, S. Effect of heparin modification on its activity in enhancing the inhibition of thrombin by antithrombin III. *Biochim. Biophys. Acta* **1977**, *498* (1), 215−222.

(10) Wang, Y.; Wang, Y.; Xiang, J.; Yao, K. Target-specific cellular uptake of taxol-loaded heparin-PEG-folate nanoparticles. *Biomacromolecules* **2010**, *11* (12), 3531−3538.

(11) Yu, M. K.; Lee, D. Y.; Kim, Y. S.; Park, K.; Park, S. A.; Son, D. H.; Lee, G. Y.; Nam, J. H.; Kim, S. Y.; Kim, I. S.; Park, R. W.; Byun, Y. Antiangiogenic and apoptotic properties of a novel amphiphilic folate-heparin-lithocholate derivative having cellular internality for cancer therapy. *Pharm. Res.* **2007**, *24* (4), 705−714.

(12) Falcone, D. J. Heparin stimulation of plasminogen activator secretion by macrophage-like cell line RAW264.7: role of the scavenger receptor. *J. Cell Physiol.* **1989**, *140* (2), 219−226.

(13) Watanabe, J.; Haba, M.; Urano, K.; Yuasa, H. Uptake mechanism of fractioned [(3)*H*]heparin in isolated rat kupffer cells: involvement of scavenger receptors. *Biol. Pharm. Bull.* **1996**, *19* (4), 581−586.

(14) Watanabe, J.; Muranishi, H.; Haba, M.; Yuasa, H. Uptake of fluorescein isothiocyanate (FITC)-fractionated heparin by rat parenchymal hepatocytes in primary culture. *Biol. Pharm. Bull.* **1993**, *16* (9), 939−941.

(15) Babu, P.; Kuberan, B. Fluorescent-tagged heparan sulfate precursor oligosaccharides to probe the enzymatic action of heparitinase I. *Anal. Biochem.* **2009**, *396* (1), 124−132.

(16) Kuberan, B.; Lech, M.; Zhang, L.; Wu, Z. L.; Beeler, D. L.; Rosenberg, R. D. Analysis of heparan sulfate oligosaccharides with ion pair-reverse phase capillary high performance liquid chromatography-microelectrospray ionization time-of-flight mass spectrometry. *J. Am. Chem. Soc.* **2002**, *124* (29), 8707−8718.

(17) Lloyd, A. G.; Embery, G.; Fowler, L. J. Studies on heparin degradation. I. Preparation of (35 S) sulphamate derivatives for studies on heparin degrading enzymes of mammalian origin. *Biochem. Pharmacol.* **1971**, *20* (3), 637−648.

(18) Nagasawa, K.; Inoue, Y.; Kamata, T. Solvolytic desulfation of glycosaminoglycuronan sulfates with dimethyl sulfoxide containing water or methanol. *Carbohydr. Res.* **1977**, *58* (1), 47−55.
(19) Ishihara, M.; Kariya, Y.; Kikuchi, H.; Minamisawa, T.; Yoshida, K. Importance of 2-*O*-sulfate groups of uronate residues in heparin for activation of FGF-1 and FGF-2. *J. Biochem.* **1997**, *121* (2), 345−349.
(20) Victor, X. V.; Nguyen, T. K.; Ethirajan, M.; Tran, V. M.; Nguyen, K. V.; Kuberan, B. Investigating the elusive mechanism of glycosaminoglycan biosynthesis. *J. Biol. Chem.* **2009**, *284* (38), 25842−25853.
(21) Vannucchi, S.; Pasquali, F.; Chiarugi, V. P.; Ruggiero, M. Heparin inhibits A431 cell growth independently of serum and EGF mitogenic signalling. *FEBS Lett.* **1991**, *281* (1−2), 141−144.
(22) Norrby, K. Heparin and angiogenesis: a low-molecular-weight fraction inhibits and a high-molecular-weight fraction stimulates angiogenesis systemically. *Haemostasis* **1993**, *23* (Suppl1), 141−149.
(23) Folkman, J.; Weisz, P. B.; Joullie, M. M.; Li, W. W.; Ewing, W. R. Control of angiogenesis with synthetic heparin substitutes. *Science* **1989**, *243* (4897), 1490−1493.
(24) Engelberg, H. Actions of heparin that may affect the malignant process. *Cancer* **1999**, *85* (2), 257−272.
(25) Krauel, K.; Hackbarth, C.; Furll, B.; Greinacher, A. Heparin-induced thrombocytopenia: in vitro studies on the interaction of dabigatran, rivaroxaban, and low-sulfated heparin, with platelet factor 4 and anti-PF4/heparin antibodies. *Blood* **2012**, *119* (5), 1248−1255.
(26) Ishihara, M.; Fedarko, N. S.; Conrad, H. E. Transport of heparan sulfate into the nuclei of hepatocytes. *J. Biol. Chem.* **1986**, *261* (29), 13575−13580.
(27) Richardson, T. P.; Trinkaus-Randall, V.; Nugent, M. A. Regulation of heparan sulfate proteoglycan nuclear localization by fibronectin. *J. Cell Sci.* **2001**, *114* (Pt 9), 1613−1623.
(28) Hsia, E.; Richardson, T. P.; Nugent, M. A. Nuclear localization of basic fibroblast growth factor is mediated by heparan sulfate proteoglycans through protein kinase C signaling. *J. Cell. Biochem.* **2003**, *88* (6), 1214−1225.
(29) Chen, L.; Sanderson, R. D. Heparanase regulates levels of syndecan-1 in the nucleus. *PLoS One* **2009**, *4* (3), e4947.
(30) Liang, Y.; Haring, M.; Roughley, P. J.; Margolis, R. K.; Margolis, R. U. Glypican and biglycan in the nuclei of neurons and glioma cells: presence of functional nuclear localization signals and dynamic changes in glypican during the cell cycle. *J. Cell Biol.* **1997**, *139* (4), 851−864.
(31) Nilsson, U.; Johnsson, R.; Fransson, L. A.; Ellervik, U.; Mani, K. Attenuation of tumor growth by formation of antiproliferative glycosaminoglycans correlates with low acetylation of histone H3. *Cancer Res.* **2010**, *70* (9), 3771−3779.
(32) Berry, D.; Lynn, D. M.; Sasisekharan, R.; Langer, R. Poly(beta-amino ester)s promote cellular uptake of heparin and cancer cell death. *Chem. Biol.* **2004**, *11* (4), 487−498.

Supplementary Information

Analysis of substrate sulfation density was carried out utilizing weak anion exchange chromatography (Table S1). Substrates that elute earlier have less charge (fewer sulfate groups) than those that bind more strongly and elute later. Thus, with regard to sulfation density, heparin migrated the slowest on the weak anion exchange column – indicating that it was the most highly sulfated GAG. On the other hand, complete desulfation of heparin using solvolysis drastically lowered its retention time. In order of sulfation density (as determined by the peak retention time at max height), the substrate order is: CDSHep, NA, NS, CDSNS, 2ODS, and heparin (Hep).

Substrate	Retention Time (min)
NA	20.08
NS	26.83
CDSNS	32.61
2ODS	51.003
CDSHep	14.5
Heparin	51.32

Table S1. M. Hep retention times as determined by weak anion exchange chromatography.

To analyze the sulfation patterns of the M. Heps, all substrates were digested with heparitinase I, II, and III to yield disaccharide units. These disaccharides were assessed using strong anion exchange chromatography and compared to known disaccharide standards. Heparin predominantly contains ΔIdoA2S-GlcNS6S disaccharides as reported previously.[1, 2] Other abundant disaccharide fragments include ΔUA-GlcNS6S and ΔUA-GlcNS. As expected, 2-O desulfation under alkaline conditions completely converted ΔUA2S-GlcNS6S disaccharides to ΔUA-GlcNS6S disaccharides (2ODS).

Similarly, complete desulfation yielded a polymer containing only ΔUA-GlcNH$_2$ residues (CDSHep). N-resulfation of this substrate yielded a polymer containing ΔUA-GlcNS residues (CDSNS). NS is structurally similar to CDSNS, except that it lacks iduronic acid residues (epimerization). Additionally, CDSHep includes N-amine groups instead of N-Acyl groups and is more positively charged than NA.

To further characterize the molecules, size exclusion chromatography was utilized to probe the molecular weight and polydispersity of the various substrates (Fig. S1). Molecular weight analysis revealed that the NA and NS that we produced are slightly larger polymers than Heparin and CDSHep. Alkaline treatment of HS chains (2ODS) and complete desulfation/N-resulfation (CDSNS) yielded smaller polymers than native heparin. Only minor differences in polydispersity were observed among the library of substrates (inferred from the peak width at half height of size exclusion traces).

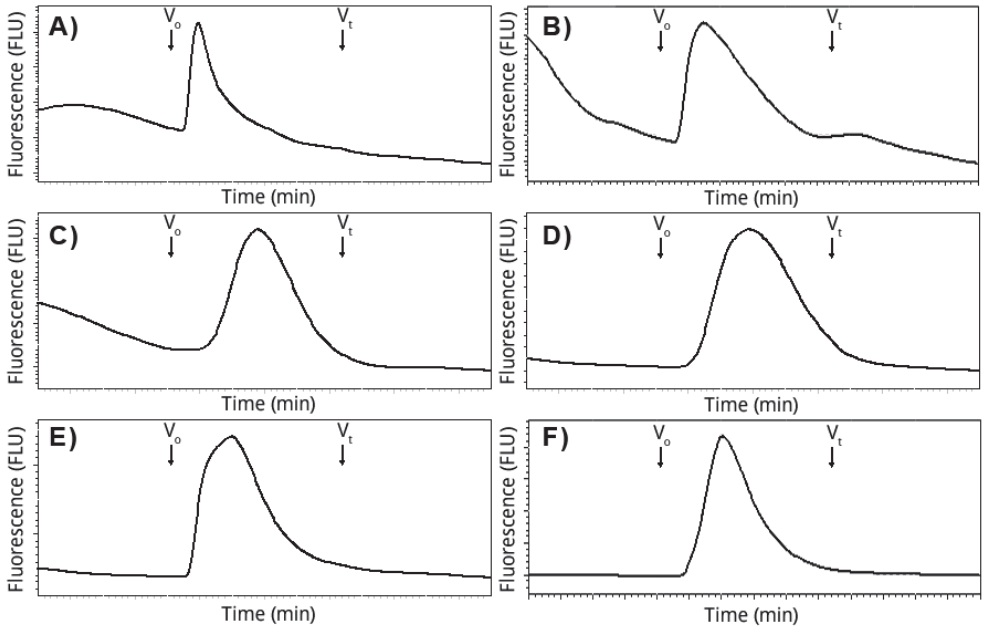

Figure S1. Size exclusion chromatography traces of the M. Heps. Substrates that elute earlier are larger in size. Representative traces are: **A)** NA, **B)** NS, **C)** CDSNS, **D)** 2ODS, **E)** CDSHep, **F)** Heparin.

After internalization experiments, we pursued the mechanism of internalization of NS and Heparin into BLMVEC to determine why NS entered cells to a far greater extent than any other substrate (Fig. S2). Previous research has suggested that heparin may enter through receptor mediated internalization using scavenger receptors, but researchers have not determined the internalization mechanisms of NS.[3-5] A series of inhibitors were utilized to determine the mechanism of internalization of NS into BLMVEC. While neither Filipin nor Chlorpromazine had an effect on the uptake of NS, sucrose-, EIPA-, and dynasore- treatment all significantly reduced BLMVEC uptake of NS. It is likely that NS utilizes multiple pathways to enter cells including receptor-mediated endocytosis, dynamin-mediated internalization, and macropinocytosis.

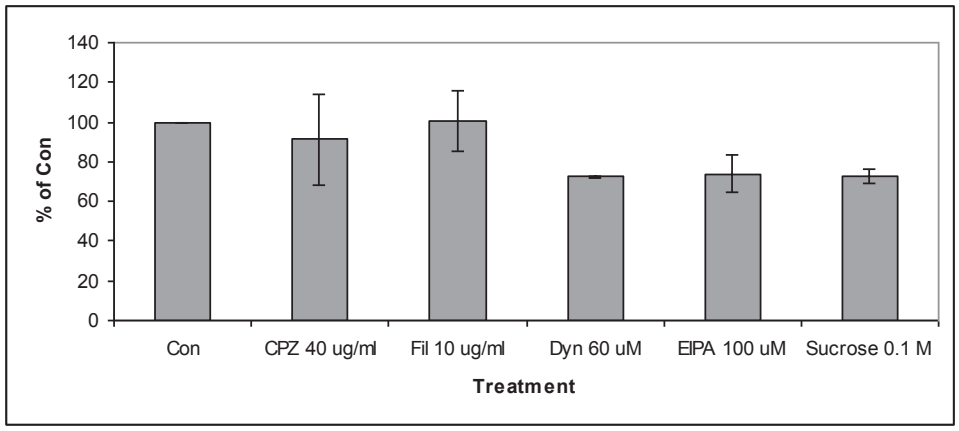

Figure S2. NS enters BLMVEC through dynamin, macropinocytosis, and receptor mediated endocytosis. BLMVEC were treated with inhbitors including chlorpromazine (CPZ, a clatherin-mediated endocytosis inhibitor), Filipin (Fil, a caveolin-mediated endocytosis inhibitor), dynasore (Dyn, a dynamin-mediated internalization inhibitor), 5-(N-Ethyl-N-isopropyl) amiloride (EIPA, a macropinocytosis inhibitor), and sucrose (a broad-spectrum receptor-mediated internalization inhibitor). Initially a range of concentrations of each inhibitor were tested. This data represents the maximal inhibition of NS internalization without significant cell death.

To further analyze the mechanism of internalization, a combinatorial treatment with multiple inhibitors was utilized to test if NS uptake could be reduced further (Fig. S3). It was found that combinatorial treatments with multiple inhibitors further reduced uptake of NS and heparin. However, higher dosages of the inhibitors led to significant reduction in cell viability. This reduction in cell viability was expected because Heparan sulfates, analogues of heparin and NS, are rapidly turned over in cells and play integral roles in cell growth and differentiation.[6] Inhibiting multiple pathways that determine NS and

heparin internalization may also interfere with heparan sulfate recycling and thus enhance cell death.

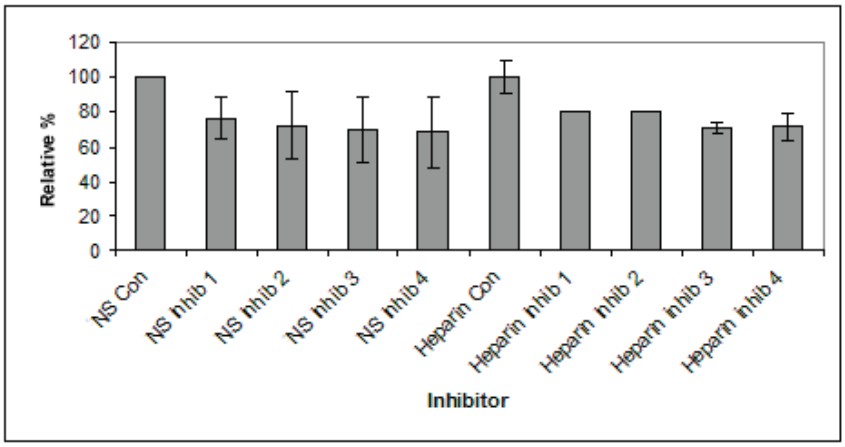

Figure S3. Treatment of NS and heparin with a multiple concentrations of a mixture of inhibitors reveals that NS and heparin enter cells by utilizing dynamin, receptor mediated endocytosis, and macropinocytosis. The concentrations of inhibitors tested included: 0.02 M sucrose with 8 uM dynasore and 20 uM EIPA (inhib 1), 0.04 M sucrose with 16 uM dynasore and 40 uM EIPA (inhib 2), 0.06 M sucrose with 24 uM dynasore and 60 uM EIPA (inhib 3), and 0.08 M sucrose with 32 uM dynasore and 80 uM EIPA (inhib 4).

REFERENCES

1. Jacobsson, I.; Hook, M; Pettersson, I.; Lindahl, U.; Larm, O.; Wiren, E.; von Figura, K., Identification of N-sulphated disaccharide units in heparin-like polysaccharides. *Biochem J* **1979,** 179, (1), 77-87
2. Lindahl, U. and O. Axelsson, Identification of iduronic acid as the major sulfated uronic acid of heparin. *J Biol Chem* **1971,** 246, (1), 74-82.
3. Nakamura, T.; Yuasa, H.; Inoue, K.; Hayashi, Y.; Watanabe, J., Uptake of FH by two types of scavenger-like receptors in rat liver parenchymal cells in primary culture, *Biol Pharm Bull* **2002,** 25, (3), 356-60.
4. Urano, K.; Haba, M.; Yuasa, H.; Watanabe, J., Kinetic characterization of binding and internationalization of fractionated [3h]heparin in rat liver parenchymal cells in primary culture, *Biol Pharm Bull* **1997,** 20, (6), 680-3.

5. Haba, M.; Urano, K.; Yuasa, H.; Watanabe, J., Molecular weight dependency in the uptake of fractionated [3H]heparin in isolated rat Kupffer cells, *Biol Pharm Bull* **1996,** 19, (6), 864-8.
6. Takeuchi, Y.; Sakaguchi, K.; Yanagishita, M.; Aurbach, GD.; Hascall, VC., Extracellular calcium regulates distribution and transport of heparan sulfate proteoglycans in a rat parathyroid cell line, *J Biol Chem* **1990,** 265, 23, 13661-8.

3.2.1 Additional Analysis

Internalization of variably sulfated polymers is shown in Figure 3.6. It is noteworthy that cell association was distinguished from cell internalization by washing cells thoroughly with PBS prior to fixation. Additionally, for FACS studies, the use of trypsin to degrade cell surface proteins and untether cells from the surface also decreases association of polymers with cell surface.

3.3 A Potent Heparin-Based Doxorubicin Conjugate Overcomes Drug Resistant Cancer Cells

3.3.1 Introduction

Proteoglycans, composed of a protein core decorated with several glycosaminoglycan side chains, are critical components of the extracellular matrix and play a variety of roles during cancer progression.[1-3] Heparin, the most highly sulfated natural glycosaminoglycan, is primarily used as a clinical anticoagulant but also has potent anticancer activity, including an ability to inhibit tumor invasion, metastasis, and angiogenesis.[4, 5] Furthermore, Heparin contains several carboxyl and amine functional groups that are amenable for conjugating drugs or other molecular cargo. Due to these favorable properties, several researchers have designed heparin-based drug conjugates for use as drug delivery vehicles for cancer.

Nanoparticles composed of heparin-drug conjugates are particularly effective *in vivo* against tumors. Recently it was found that heparin-all-trans-retinoic acid nanoparticles (LHR) loaded with paclitaxel effectively reduced the size of breast cancer xenografts in mice and showed favorable pharmacokinetic and pharmacodynamic

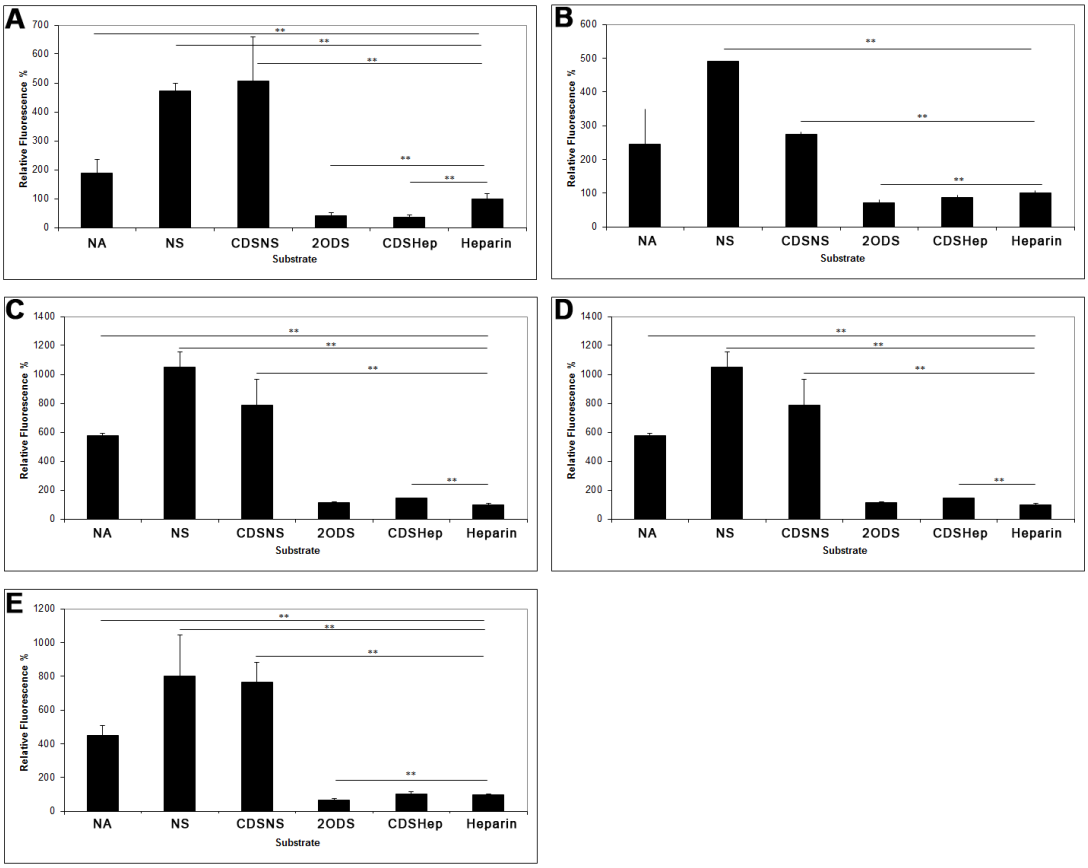

Figure 3.6. Internalization of variably sulfated polymers into different cell types. Cells utilized were: A) BLMVEC, B) K1 CHO, C) BXPC-3, D) HT-29, and E) U87 Mg. Relative fluorescence denotes the amount of fluorescence (and therefore substrate) detected within cells by FACS. ** indicates $P<0.05$ as determined by a 1-tailed paired t-test. Error bars indicate standard deviations.

properties.[6] Heparin-folic acid-paclitaxel nanoparticles loaded with additional paclitaxel (HFT-T) were also found to effectively treat folic acid-positive neck cancers in tumor bearing mice.[7] Direct conjugates of heparin and drugs such as paclitaxel and litocholate have also been developed.[8, 9]

It is well known that changing the sulfation patterns of heparin or heparan sulfate can have dramatic effects on their ability to bind to the FGF-1, FGF-2 and FGF-4.[10, 11] Additionally, a particular pentasaccharide sequence consisting of a 3-*O* sulfate group, an *N*-sulfate group, and a 6-*O* sulfate group is responsible for heparin's potent anticoagulant activity.[12] However, researchers are yet to determine the effects of sulfation pattern on heparin's potency as a drug delivery vehicle.

Recently, we have shown that sulfation patterns determine the uptake of heparin and heparin-like polysaccharides into various cell types including HT-29 colon cancer cells, K1 CHO cells, bovine lung microvascular endothelial cells, and U87 Mg brain cancer cells.[13] This work also demonstrated that heparosan (NA) and *N*-*s*ulfo heparosan (NS) can be internalized into cells through a receptor-mediated mechanism at a higher rate and to a greater extent than heparin. In some cell lines, NA was found to colocalize specifically within the nucleus, similar to a recent discovery that hyaluronic acid-drug conjugates can enter cellular nuclei.[14] Therefore, we hypothesized that generating drug conjugates of these heparin-like polysaccharides would yield superior anticancer effects to heparin-based conjugates.

To test this hypothesis, we developed doxorubicin conjugates of NA, NS, and heparin and tested their efficacy against drug-resistant and drug-sensitive cell lines. We also analyzed the cellular localization of these polymers and investigated the likely

mechanism of action of their enhanced anticancer activity. Taken together, this study provides new insights into the design of a glycosaminoglycan-based drug delivery vehicle and suggests that conjugates of heparin-like polysaccharides and chemotherapeutics have great potential in overcoming drug-resistant tumors.

3.3.2 Materials and Methods

HT-29 human colon cancer cells were provided by Dr. Scott Kuwada (University of Hawaii). Hog mucosal heparin was obtained from Ming Han Chemicals (Oakland, CA). DEAE-Sepharose gel was purchased from Amersham Biosciences. The analytical grade strong anion exchange column and size exclusion column were obtained from Dionex, and Tosoh Biosciences, respectively. Disaccharide standards for strong anion exchange were obtained from Iduron Inc (Manchester, UK). Heparitinase I, II and III from *flavobacterium heparinum* were expressed as previously described.[15] Cell culture reagents were from Invitrogen Inc. The cell titer blue cell viability assay kit was from Promega Inc. The Caspase-3 activity assay kit was obtained from Roche Applied Science Inc. All other reagents and solvents including doxorubicin hydrochloride were from Sigma-Aldrich.

To synthesize the DOX conjugates of NA, NS, and heparin, an EDC/Sulfo-NHS conjugation procedure was utilized. First, 10 mg of polysaccharide was incubated in 2 mls of pH 8.5 HEPES buffer. Next, 3 equivalents of N-Ethyl-N′-(3-dimethylaminopropyl)carbodiimide hydrochloride were added to the reaction along with 2 equivalents of N-Hydroxysulfosuccinimide sodium salt and stirred for 2 hours at room temperature. Then, 1.2 equivalents of doxorubicin hydrochloride were added to the reaction and stirred overnight at room temperature. Subsequently, the conjugates were

loaded onto a DEAE Sepharose column (0.5 ml) preequilibriated with 10 column volumes of wash buffer (20 mM NaOAc buffer (pH 6.0), 0.1 M NaCl, 0.01% Triton X-100). The column was then washed with 30 column volumes of wash buffer. Bound conjugates were then eluted with 6 column volumes of elution buffer (20 mM NaOAc,1 M NaCl, pH 6.0). Finally, polymer conjugates were dialyzed through a 1000 MWCO filter membrane and lyophilized to dryness.

Polysaccharide conjugates were analyzed by strong anion exchange chromatography to confirm polysaccharide purity as previously described.[16] Size exclusion chromatography was utilized to analyze conjugate molecular weight and to assess the amount of free drug as previously described.[16] Dynamic light scattering (Malvern Inc.) was utilized to analyze conjugate hydrodynamic radius.

Polymer-drug conjugate concentration in stock solutions was analyzed using a carbazole assay for uronic acid content, as previously described.[17] Briefly, various standards of heparosan polymer were prepared and 50 µl of each standard concentration was loaded into wells of a 96 well plate in triplicate. Polymer-conjugates were also loaded into wells of the 96 well plate in duplicate. Next, 200 µl of sodium tetraborate solution (25 mM sodium tetraborate in concentrated H_2SO_4) was added to each well containing sample and heated in boiling water for 10 minutes. Next, plates were cooled and 50 µl of carbazole solution (0.125% carbazole in ethanol) was added to each well. Plates were heated in boiling water once again for 10 minutes, cooled, and the absorbance of solutions was read at 520 nm. Drug loading on the polymers was analyzed through fluorescent spectroscopy by comparing known quantities of the polymer-conjugate solution to a standard curve of DOX. Plates were read using fluorescence

excitation/emission at 470 nm/600 nm.

Cell viability upon drug or conjugate treatment was assessed using a Cell Titer Blue viability assay kit according to the manufacturer's protocol. Briefly, 25,000 cells were added into wells of a 96 well plate in 200 µl of HAMS F-12 media. After cells attached, the media was replaced with fresh HAMS F-12 media and appropriate amounts of each drug or drug conjugate were added into each well. Cells were grown for 3 days in a humidified incubator and subsequently the media was replaced with 125 µl of fresh HAMS F-12 media in addition to 50 µl of cell titer blue reagent. After 3 hours of incubation in a cell culture incubator, 25 µl of 3% SDS was added into each well to stop cellular metabolic activity and plates were read in a fluorescent spectrometer with excitation/emission 560 nm/590 nm.

Caspase-3 activity upon treatment with DOX conjugates was analyzed using a caspase-3 activity assay according to the manufacturer's protocol. First, a monolayer of HT-29 cells was grown in 96 well plates. On the next day, media from the wells was replaced with 100 µl of HAMS F-12 and 10 µM of DOX or equivalent DOX concentrations were added and left overnight in a cell culture incubator. Subsequently, after 16 hours, nonsterile 96 well plates were coated with Anti-Caspase 3 antibody in coating buffer for 1 hour at 37° C. Then cells were lysed in 100 µl of lysis buffer (DTT solution) for 1 minute on ice within the cell culture plate. The lysate was added onto the anticaspase plate and left at 37 for 1 hour. After washing, the caspase substrate was added and incubated for 3 hours at 37° C. Subsequently, upon conversion of the caspase substrate to a fluorescent substrate, the plate fluorescence was measured at excitation/emission of 400 nm/505 nm.

For confocal imaging, approximately 50,000 cells were grown on glass coverslips within 35 mm cell culture dishes with 1 ml media. Subsequently, drug conjugates with 1 μM of equivalent drug concentration were added into each well, respectively, and cells were allowed to internalize the conjugates for 16 hours in a humidified incubator. Next, the media was removed and cells were washed twice with PBS. Cells were then fixed with 500 μl of 4% paraformaldehyde solution for 10 minutes at room temperature. Next, cells were washed twice with PBS and stained with DAPI for 10 minutes. After incubation with the nuclear stain, cells were mounted onto microscope slides and imaged with an FV1000-XY Confocal Olympus IX81 microscope using a 60X oil immersion lens.

3.3.3 Results

The central goal of this study is to determine whether the sulfation patterns of heparin and heparin-like polysaccharides affect their ability to deliver anticancer drugs to drug resistant tumors. To accomplish this goal, NA-DOX, NS-DOX, and HEP-DOX conjugates were chemically synthesized and characterized (Figure 3.7). Subsequently, the *in vitro* anticancer activities were tested with both DOX-sensitive HT-29 colon cancer cells and DOX-resistant A2780 AD ovarian carcinoma cells using a cell viability assay (Figure 3.8). Confocal microscopy was utilized to evaluate the cellular localization of the conjugates in multiple cell types including HT-29 cells, U87 Mg human glioma cells, and A2780 AD cells (Figure 3.9). Additionally, to assess the mechanistic details of how DOX and DOX-conjugates affected cell viability, the effects of the free drug and the conjugates on caspase-3 activity were examined (Figure 3.10)

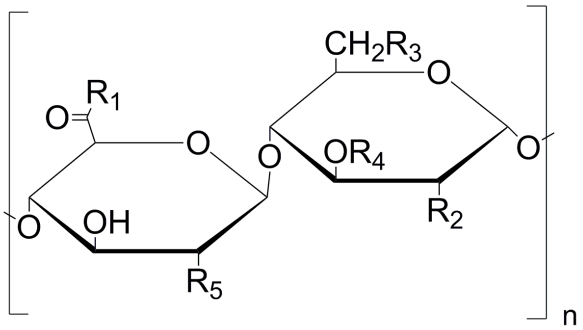

R_1: OH or -DOX

NA: R_2 : 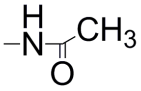 $R_3 = R_4 = R_5 = OH$

NS: R_2 : $-NHSO_3^-$ $R_3 = R_4 = R_5 = OH$

HEP: R_2 : $-NHSO_3^-$ R_4:H/SO_3^- $R_3 = R_5 = SO_3^-$

Figure 3.7. Structure of DOX conjugates tested for their anticancer activity.

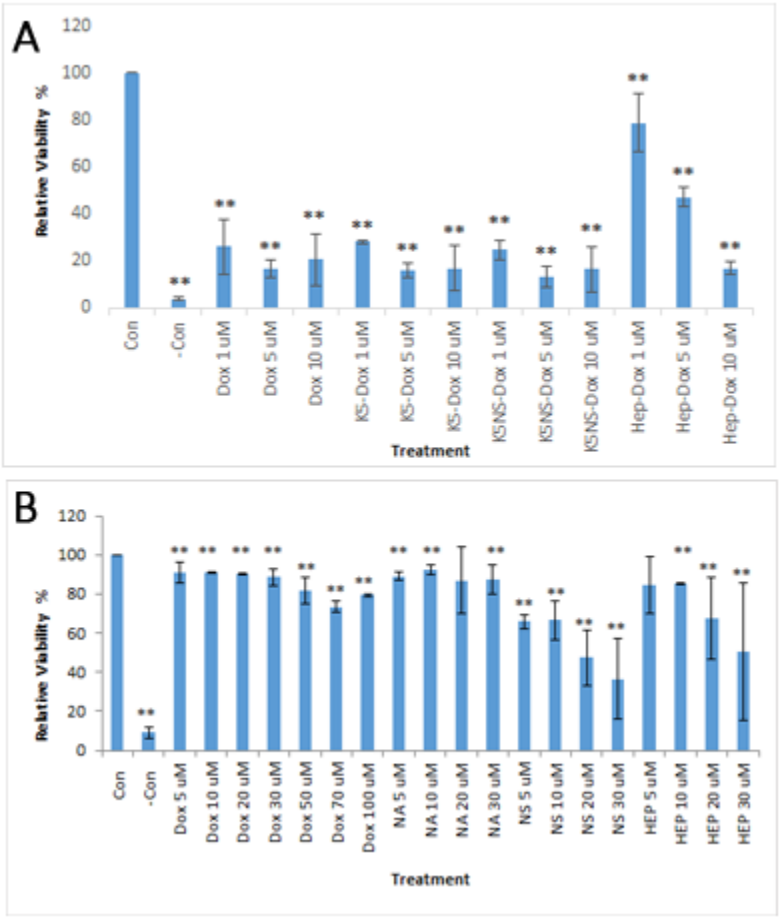

Figure 3.8. Evaluation of DOX conjugate anticancer efficacy against. A) DOX-sensitive HT-29 human colon cells, n = 3. **B)** DOX-resistant A2780 AD human ovarian carcinoma cells, n = 4. Percentages are calculated relative to control, untreated cells. ** indicates $P<0.05$ as determined by a 1 tailed paired t-test vs. control cells. Error bars indicate standard deviation.

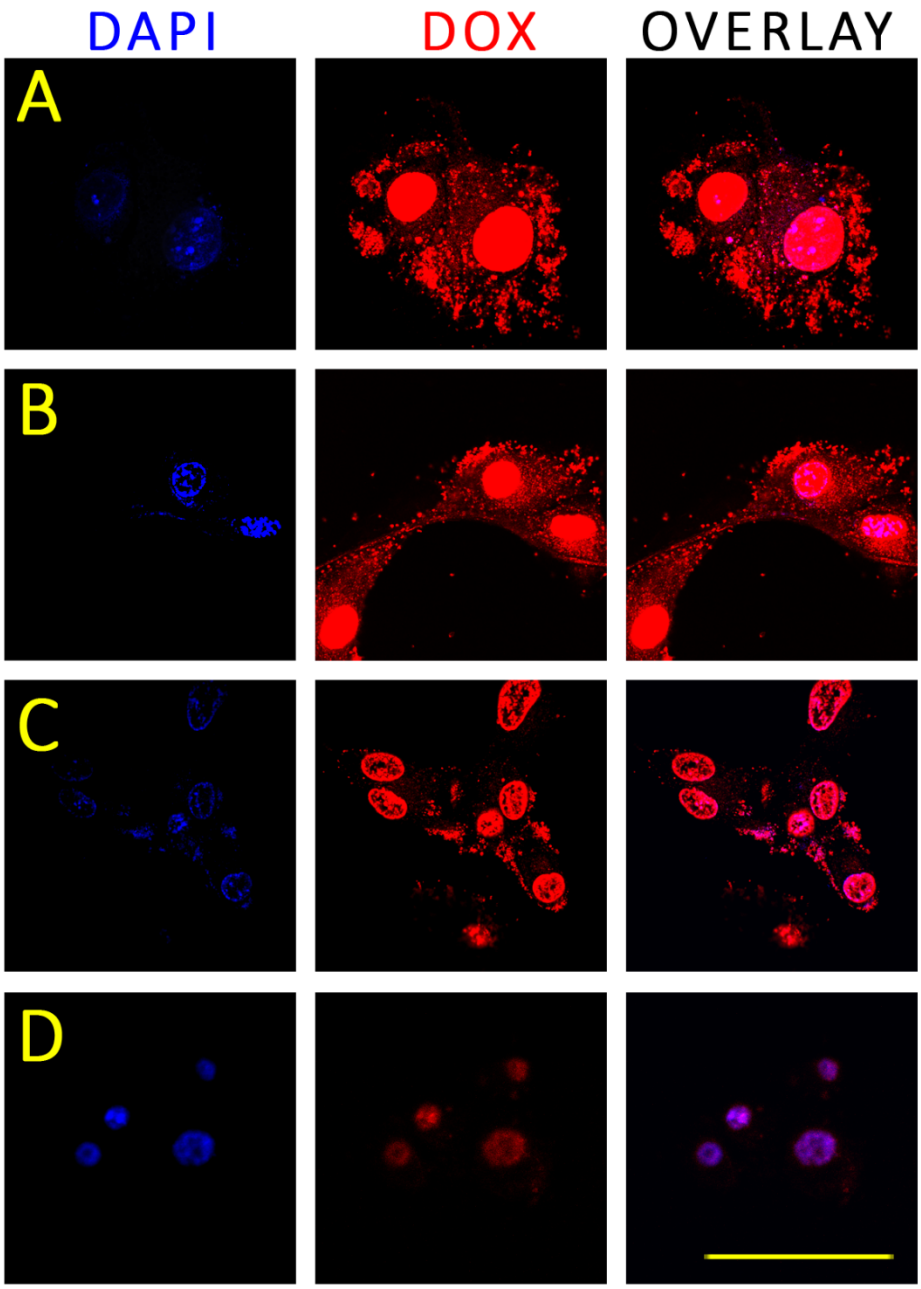

Figure 3.9. Localization of free DOX and DOX-conjugates in U87 Mg human glioma cells. Representative panes are **A)** DOX treated cells, **B)** NA-DOX treated cells, **C)** NS-DOX treated cells, and **D)** HEP-DOX treated cells. Scale Bar: 50 μm.

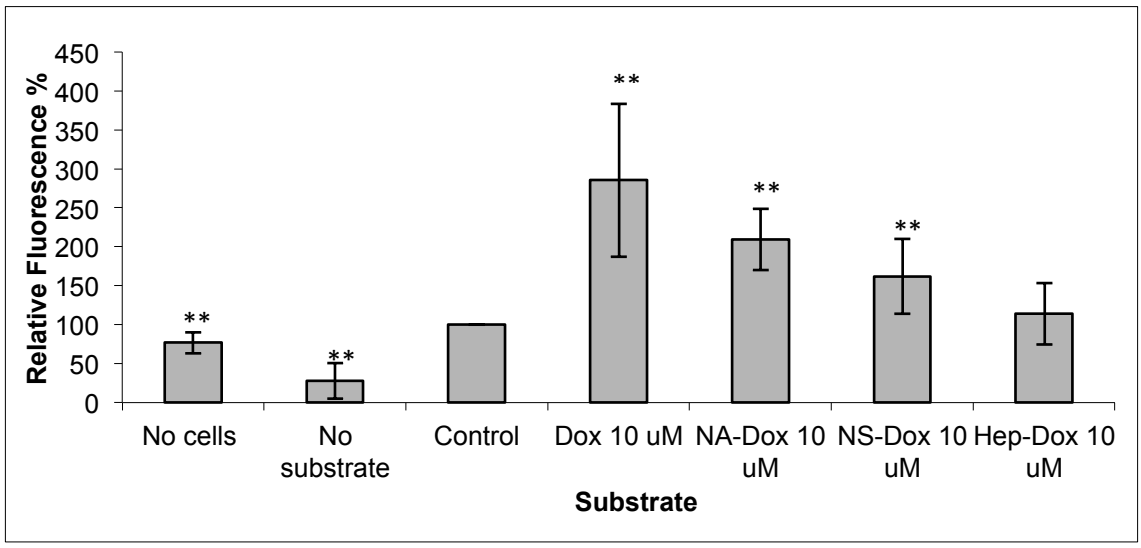

Figure 3.10. Caspase-3 activation upon treatment with DOX or DOX conjugates determined using FIENA. Fluorescence in the FIENA indicates caspase activity upon treatment. Relative percentages are based on control, untreated cells. ** indicates $P<0.05$ as determined by a paired 1-tailed t-test relative to control. Error bars indicate standard deviation.

To evaluate the *in vitro* anticancer activity of DOX conjugates of NA and NS vs. heparin-DOX, a cell viability assay was utilized (Figure 3.8). HT-29 colon cancer cells were incubated with each conjugate and with the free drug for 3 days in duplicate wells. It was found that, compared to heparin-DOX, both NA-DOX and NS-DOX conjugates had significantly more antitumor activity. Interestingly, in triplicate experiments, it was found that the anticancer activity of both the heparosan conjugates was comparable to the free drug. When DOX-resistant A2780 cells were treated with each conjugate, it was observed that free DOX and NA-DOX were not effective against these cells even at high concentrations. HEP-DOX was partially effective against the DOX-resistant cells, while NS-DOX was the most effective anticancer agent and overcame cellular drug resistance.

Next, to evaluate the cellular localization of the doxorubicin conjugates, confocal microscopy was utilized to assess the differences in cellular internalization of DOX alone and DOX conjugates in three different cell lines (Figure 3.9, and see supplement). Images were taken with identical exposure settings so that differences in signal intensity could also be observed. After incubation with appropriate substrates for 1 day, it was found that the free drug and all the conjugates were found throughout cells in vesicles. Free DOX and DOX conjugates were also found in the nucleus in HT-29 and U87 Mg cells. Heparin-DOX clearly had lower signal intensity compared to DOX alone or NA-DOX conjugates. Additionally, when incubated with A2780 AD cells, all the polymers were internalized to a lesser extent compared to DOX-sensitive cells.

To discern the molecular mechanism of drug action, HT-29 cells were incubated with 10 μM DOX or conjugates containing 10 μM equivalent DOX concentrations and evaluated using a commercially available fluorescent immunosorbent enzyme assay

(FIENA). It was found that upon treatment, the free drug elicited a three-fold increase in Caspase-3-driven apoptosis activity. Similarly, both the NA-DOX and the NS-DOX conjugates increased caspase-3 apoptosis activity dramatically while HEP-DOX did not affect caspase-3 apoptosis activity significantly after 1 day.

3.3.4 Discussion

For over a decade it has been known that targeted drug delivery to cancers using polymeric carriers overcomes drug resistance, improves therapeutic efficacy, and minimizes drug side effects. More recently, there has been increasing interest in developing novel polymeric scaffolds that are biocompatible, biodegradable, and highly hydrophilic. Heparin, a highly sulfated, natural, anticoagulant glycosaminoglycan, meets these criteria and also intrinsically serves as an excellent anticancer polymer because of its ability to inhibit tumor associated angiogenesis, metastasis, and invasion.[1, 4, 5] Due to its unique properties, and the ease with which it can be modified, several heparin-based drug delivery vehicles have been developed.[6-9] However, researchers have not yet investigated the putative correlation between heparin's sulfation pattern and its efficacy as a drug delivery vehicle. From our previous studies, we have discovered that modification of heparin's sulfation pattern can dramatically affect its internalization into a variety of cell types as well as its nuclear localization.[13] In particular, NA and NS are internalized almost 10- fold more than heparin. In this article, we developed doxorubicin conjugates of NA and NS in order to quantify drug delivery efficacy as a function of sulfation pattern.

Doxorubicin conjugates were synthesized using EDC-NHS chemistry (Figure 3.7) and the purified product was analyzed by size exclusion chromatography (see

supplement). Disaccharide analysis using strong anion exchange chromatography confirmed that NA contained only ΔUA-GlcNAc disaccharides while NS contained ΔUA-GlcNS disaccharides and HEP contained a mixture of disaccharides with the majority being ΔUA2S-GlcNS6S, as previously described in literature (see supplement).[16, 18, 19] Dynamic light scattering experiments revealed that extremely dilute solutions of the conjugates contained particles that were ~3 nm in size while more concentrated solutions consisted of polydisperse particles that were ~200 nm in size (see supplement). It can be argued that these particle sizes are incorrect because they are too large for such small polymers. However, aggregation of heparin in solution into tightly bound self-assembled particles has been described previously.[20, 21] Self-aggregation makes it difficult to determine the hydrodynamic radius of each individual polymer. Additionally, aggregates may trap free drug and confound the relationship between molecular weight and particle size. It is still unknown how heparin-like GAGs form molecular aggregates. As micromolar concentrations of heparin and the other polymers were utilized in viability assays, it can be assumed that all the conjugates were being utilized in the self-assembled state.

To test the efficacy of the doxorubicin conjugates, a cell viability assay was performed (Figure 3.8). Against DOX-sensitive HT-29 cells, it was found that DOX, NA-DOX and NS-DOX were all more effective than HEP-DOX. However, against DOX-resistant A2780 cells, the order of effectiveness followed the pattern: DOX < NA-DOX < HEP-DOX < NS-DOX. However, to determine a more precise IC50 of these conjugates, experiments utilizing a set of serial dilutions may be necessary.

Light scattering experiments confirmed that all the conjugates are small (<5 nm);

therefore, it is likely that particle size was not a determinant in the effectiveness of the polymers. With regard to charge density, NA-DOX has the lowest charge density while HEP-DOX has the highest charge density (as determined by the number of sulfate groups per chain). However, as NS-DOX was the most effective polymer against both DOX-sensitive and DOX-resistant cells, charge density did not determine the effectiveness of the polymers. Therefore, it can be concluded that the sulfation pattern of NS uniquely affected its effectiveness as a drug delivery vehicle, and this suggests that NS-DOX is recognized by cells differently compared to NA-DOX and HEP-DOX. While the mechanism of NS-DOX uptake was not specifically tested, previous studies with NA-Fluorescein and NS-Fluorescein polymers indicate that uptake occurs through several mechanisms including macropinotytosis, dynamin-mediated endocytosis, and receptor-mediated endocytosis.

Next, the cellular localization of all the conjugates was visualized using confocal microscopy to further understand why NS-DOX was the most effective vehicle (Figure 3.9 and see supplement). It was found that like free DOX, all the conjugates co-localized with DAPI, a nuclear stain. However, subtle differences were observed among the different treatments. In DOX-sensitive cells, HEP-DOX had the lowest fluorescent intensity in the nucleus (and it was the least effective treatment against DOX-sensitive cells). DOX and NA-DOX brightly stained the nucleus as well as other components of the cell body. NS-DOX was the only conjugate to brightly label the nucleus specifically. In DOX-resistant cells, no noticeable differences were observed between any of the treatment samples (see supplement). Previous studies corroborate our results that heparin-based vehicles can localize to the nucleus. Proteoglycans such as Glypican-1 and

Syndecan-1, consisting of protein cores and several heparin-like glycosaminoglycan side chains, enter cellular nuclei and modulate transcription.[22-24] Heparan sulfate, a sulfated glycosaminoglycan present on cell surfaces and in the extra cellular matrix, has also been found within the nuclei of hepatocytes.[25] Heparin-Poly(beta-amino ester) conjugates were also found to enter cellular nuclei and modulate cell death.[26]

Additionally, the mechanism of action of the conjugates was investigated to understand the differential cytotoxicity of the DOX-conjugates (Figure 3.10). Caspase-3 activation is commonly linked to the induction of cellular apoptosis through a variety of pathways that degrade DNA and prevent DNA repair as is the case with DOX.[27] Using a fluorescent immunosorbent enzyme caspase-3 activity assay, it was determined that NA-DOX and NS-DOX conjugates were significantly more effective than HEP-DOX at enhancing Caspase-3 activity. After 16 hours of treatment, HEP-DOX only slightly increased cellular apoptotic activity while free DOX, NA-DOX, and NS-DOX drastically increased caspase-3 activity in DOX-sensitive cells. It is interesting to note that these polymers were all effective even though the doxorubicin-polymer linkage was synthesized via a nonlabile amide bond. Recently, conjugates of doxorubicin and hyaluronic acid, a similar glycosaminoglycan, have been shown to affect cancer cells without the need for a labile linker.[14] It is thus likely that heparin-based DOX conjugates may function through similar mechanisms as hyaluronic acid-DOX conjugates.

This study presents the first biochemical evidence that glycosaminoglycan sulfation patterns determine their efficacy as drug delivery vehicles. Heparin-like polysaccharides discussed in this article demonstrate differential internalization, cytotoxicity, cellular localization, and ability to overcome drug resistance. Additionally, since a labile linker is

not necessary for drug efficacy, these conjugates are easier to produce and more scalable than traditional hydrazone conjugates of DOX. Therefore, heparin-based drug delivery vehicles offer a promising approach to treat drug-resistant cancers. Future efforts will focus on assessing the therapeutic utility of these polymer-DOX conjugates *in vivo* against a variety of drug-resistant and drug-sensitive cancers.

3.3.5 References

1. Morimoto-Tomita, M.; Uchimura, K.; Bistrup, A.; Lum, D. H.; Egeblad, M.; Boudreau, N.; Werb, Z.; Rosen, S. D., Sulf-2, a proangiogenic heparan sulfate endosulfatase, is upregulated in breast cancer. *Neoplasia* **2005,** 7, (11), 1001-10.

2. Borsig, L.; Wong, R.; Hynes, R. O.; Varki, N. M.; Varki, A., Synergistic effects of L- and P-selectin in facilitating tumor metastasis can involve nonmucin ligands and implicate leukocytes as enhancers of metastasis. *Proc Natl Acad Sci U S A* **2002,** 99, (4), 2193-8.

3. Ruoslahti, E., The Walter Herbert Lecture. Control of cell motility and tumour invasion by extracellular matrix interactions. *Br J Cancer* **1992,** 66, (2), 239-42.

4. Vlodavsky, I.; Abboud-Jarrous, G.; Elkin, M.; Naggi, A.; Casu, B.; Sasisekharan, R.; Ilan, N., The impact of heparanese and heparin on cancer metastasis and angiogenesis. *Pathophysiol Haemost Thromb* **2006,** 35, (1-2), 116-27.

5. Sasisekharan, R.; Shriver, Z.; Venkataraman, G.; Narayanasami, U., Roles of heparan-sulphate glycosaminoglycans in cancer. *Nat Rev Cancer* **2002,** 2, (7), 521-8.

6. Hou, L.; Yao, J.; Zhou, J.; Zhang, Q., Pharmacokinetics of a paclitaxel-loaded low molecular weight heparin-all-trans-retinoid acid conjugate ternary nanoparticulate drug delivery system. *Biomaterials* **2012***,* 33, (21), 5431-40.

7. Wang, X.; Li, J.; Wang, Y.; Cho, K. J.; Kim, G.; Gjyrezi, A.; Koenig, L.; Giannakakou, P.; Shin, H. J.; Tighiouart, M.; Nie, S.; Chen, Z. G.; Shin, D. M., HFT-T, a targeting nanoparticle, enhances specific delivery of paclitaxel to folate receptor-positive tumors. *ACS Nano* **2009,** 3, (10), 3165-74.

8. Wang, Y.; Xin, D.; Liu, K.; Zhu, M.; Xiang, J., Heparin-paclitaxel conjugates as drug delivery system: synthesis, self-assembly property, drug release, and antitumor activity. *Bioconjug Chem* **2009,** 20, (12), 2214-21.

9. Yu, M. K.; Lee, D. Y.; Kim, Y. S.; Park, K.; Park, S. A.; Son, D. H.; Lee, G. Y.; Nam, J. H.; Kim, S. Y.; Kim, I. S.; Park, R. W.; Byun, Y., Antiangiogenic and apoptotic properties of a novel amphiphilic folate-heparin-lithocholate derivative having cellular internality for cancer therapy. *Pharm Res* **2007,** 24, (4), 705-14.

10. Guimond, S.; Maccarana, M.; Olwin, B. B.; Lindahl, U.; Rapraeger, A. C., Activating and inhibitory heparin sequences for FGF-2 (basic FGF). Distinct requirements for FGF-1, FGF-2, and FGF-4. *J Biol Chem* **1993,** 268, (32), 23906-14.

11. Lundin, L.; Larsson, H.; Kreuger, J.; Kanda, S.; Lindahl, U.; Salmivirta, M.; Claesson-Welsh, L., Selectively desulfated heparin inhibits fibroblast growth factor-induced mitogenicity and angiogenesis. *J Biol Chem* **2000,** 275, (32), 24653-60.

12. Rosenberg, R. D., Actions and interactions of antithrombin and heparin. *N Engl J Med* **1975,** 292, (3), 146-51.

13. Raman, K.; Mencio, C.; Kuberan, B., Sulfation patterns determine cellular internalization of heparin-like polysaccharides. *Molecular Pharmaceutics* **2013,** 10, (4), 1442-9.

14. Oommen, O. P.; Garousi, J.; Sloff, M.; Varghese, O. P., Tailored doxorubicin-hyaluronan conjugate as a potent anticancer glyco-drug: An alternative to prodrug approach. *Macromol Biosci* **2014**, 14, (3), 327-33.

15. Babu, P.; Kuberan, B., Fluorescent-tagged heparan sulfate precursor oligosaccharides to probe the enzymatic action of heparitinase I. *Anal Biochem* **2010**, 396, (1), 124-32.

16. Victor, X. V.; Nguyen, T. K.; Ethirajan, M.; Tran, V. M.; Nguyen, K. V.; Kuberan, B., Investigating the elusive mechanism of glycosaminoglycan biosynthesis. *J Biol Chem* **2009,** 284, (38), 25842-53.

17. Bitter, T.; Muir, H. M., A modified uronic acid carbazole reaction. *Anal Biochem* **1962,** 4, 330-4.

18. Jacobsson, I.; Hook, M.; Pettersson, I.; Lindahl, U.; Larm, O.; Wiren, E.; von Figura, K., Identification of N-sulphated disaccharide units in heparin-like polysaccharides. *Biochem J* **1979,** 179, (1), 77-87.

19. Lindahl, U.; Axelsson, O., Identification of iduronic acid as the major sulfated uronic acid of heparin. *J Biol Chem* **1971,** 246, (1), 74-82.

20. Spinelli, F. J.; Kiick, K. L.; Furst, E. M., The role of heparin self-association in the gelation of heparin-functionalized polymers. *Biomaterials* **2008,** 29, (10),

1299-306.

21. Gaigalas, A. K.; Hubbard, J. B.; LeSage, R.; Atha, D. H., Physical characterization of heparin by light scattering. *J Pharm Sci* **1995,** 84, (3), 355-9.
22. Chen, L.; Sanderson, R. D., Heparanase regulates levels of syndecan-1 in the nucleus. *PLoS One* **2009,** 4, (3), e4947.

23. Liang, Y.; Haring, M.; Roughley, P. J.; Margolis, R. K.; Margolis, R. U., Glypican and biglycan in the nuclei of neurons and glioma cells: presence of functional nuclear localization signals and dynamic changes in glypican during the cell cycle. *J Cell Biol* **1997,** 139, (4), 851-64.

24. Richardson, T. P.; Trinkaus-Randall, V.; Nugent, M. A., Regulation of heparan sulfate proteoglycan nuclear localization by fibronectin. *J Cell Sci* **2001,** 114, (Pt 9), 1613-23.

25. Ishihara, M.; Fedarko, N. S.; Conrad, H. E., Transport of heparan sulfate into the nuclei of hepatocytes. *J Biol Chem* **1986,** 261, (29), 13575-80.

26. Berry, D.; Lynn, D. M.; Sasisekharan, R.; Langer, R., Poly(beta-amino ester)s promote cellular uptake of heparin and cancer cell death. *Chem Biol* **2004,** 11, (4), 487-98.

27. Cohen, G. M., Caspases: the executioners of apoptosis. *Biochem J* **1997,** 326 (Pt 1), 1-16.

3.3.6 Supplementary Information

Polysaccharide conjugates were analyzed by utilizing size exclusion chromatography and measuring absorbance at 480 nm. Results revealed that no free drug was present in the conjugates. All the conjugates were also of similar sizes. NA-DOX and NS-DOX were found to be slightly larger than HEP-DOX (Figure 3.S1). However, it is unlikely that these minor size differences affect biological activity as it has previously been determined that large differences in molecular weight are required for changes in pharmacokinetic and pharmacodynamic properties of biodegradable polymers.[1]

Samples were also analyzed by utilizing strong anion exchange chromatography to determine the disaccharide composition of each polymer (Figure 3.S2). Polysaccharides were first digested with heparitinase I, II, and III and then analyzed on a linear 1 M NaCl gradient from 0-100% over 50 minutes, as previously described.[2] Elution time is dependent on the charge density of disaccharides. Heparin, as expected, had the highest charge density while NS has a median charge density, and NA had the lowest density.

A Malvern Zetasizer dynamic light scattering instrument was utilized to analyze the hydrodynamic radius of the DOX conjugates of heparin and heparin-like polysaccharides. As reported in literature, heparin self assembles when utilized in concentrated samples (Table 3.S1, Figure 3.S3) whereas dilute samples reveal a much lower hydrodynamic radius (Table 3.S2).[3, 4] Samples show a large polydispersity due to the inherent heterogeneity in heparin.

Drug loading on the polysaccharides was analyzed by utilizing a fluorescence spectrophotometer to determine DOX concentration in solutions with known amounts of

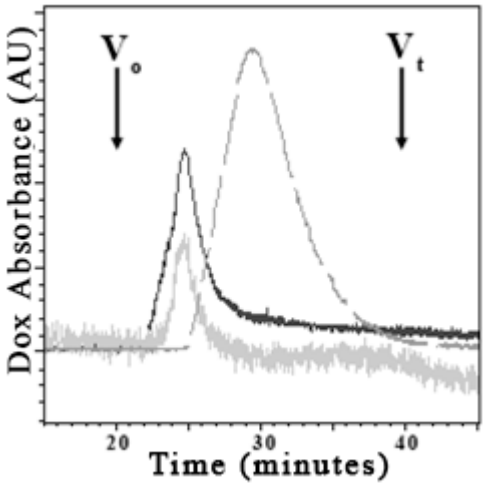

Figure 3.S1. Size exclusion chromatographs of DOX conjugates determined by measuring absorbance at 480 nm. Representative traces are: NA( ), NS ( ), and HEP( ).

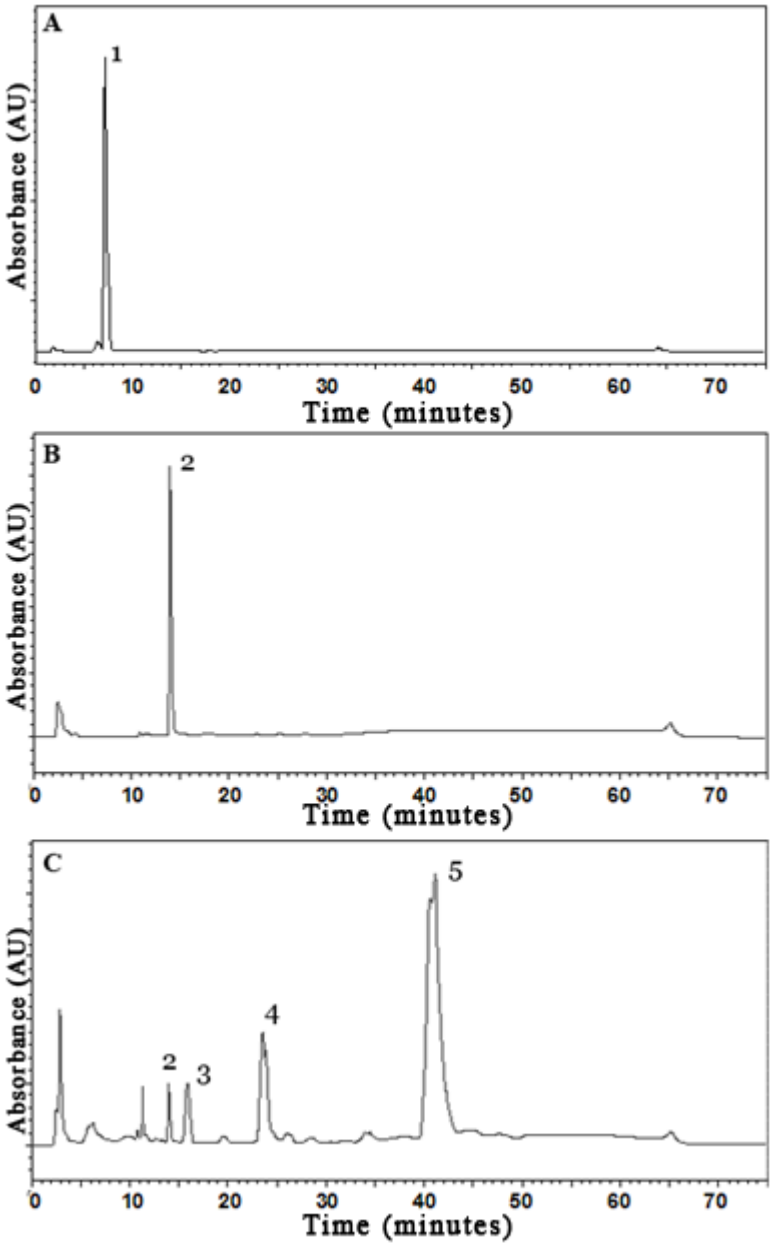

Figure 3.S2. Disaccharide composition of polysaccharides determined by measuring absorbance at 232 nm. Representative panels are: **A)** NA **B)** NS and **C)** HEP. NA contains only ΔUA-GlcNAc disaccharides (**1**), while NS contains ΔUA-GlcNS disaccharides (**2**). Heparin contains a complex sulfation pattern with the majority of disaccharides being ΔUA2S-GlcNS6S (**5**). Additional disaccharides include ΔUA-GlcNS (**2**), ΔUA-GlcNAc6S (**3**), and ΔUA-GlcNS6S (**4**).

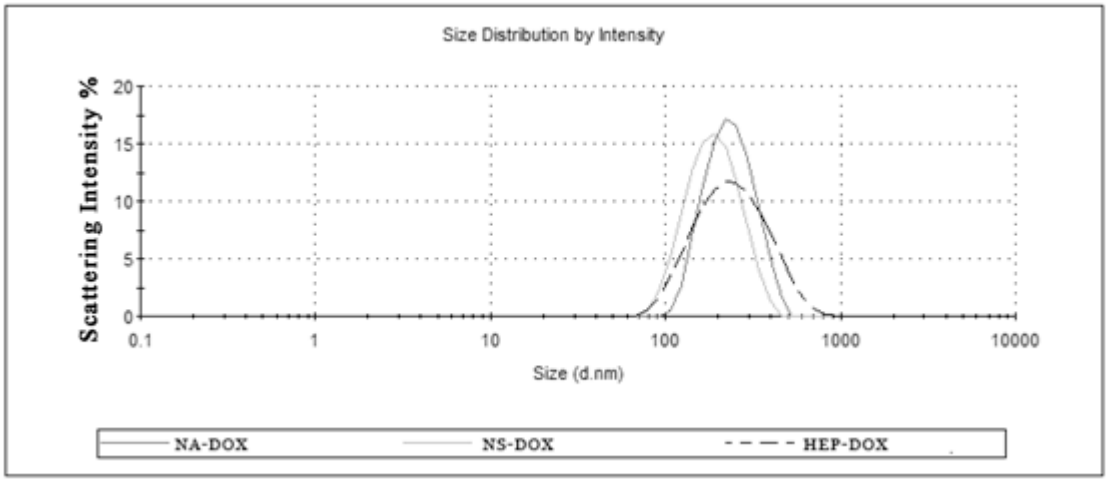

Figure 3.S3. DLS results with 5 µM samples of NA-DOX, NS-DOX, and HEP-DOX. Scattering intensity correlates with the size of the particles in the samples. Higher scattering intensity indicates larger molecular weight.

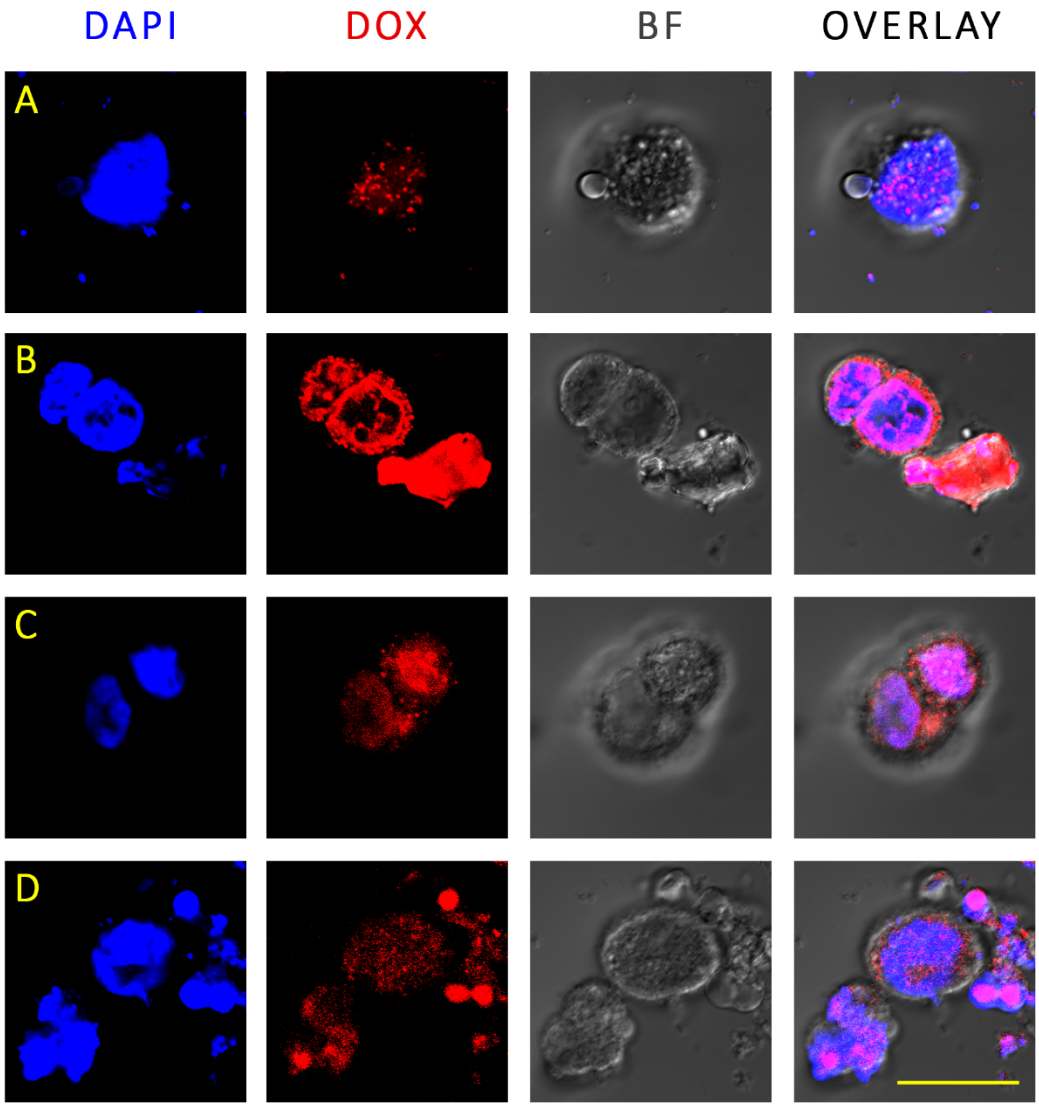

Figure 3.S4. Localization of free DOX and DOX-conjugates in HT-29 colon cancer cells. Representative panels are **A)** DOX treated cells, **B)** NA-DOX treated cells, **C)** NS-DOX treated cells, and **D)** HEP-DOX treated cells. BF represents bright field images of cells. Scale Bars: 25 μm

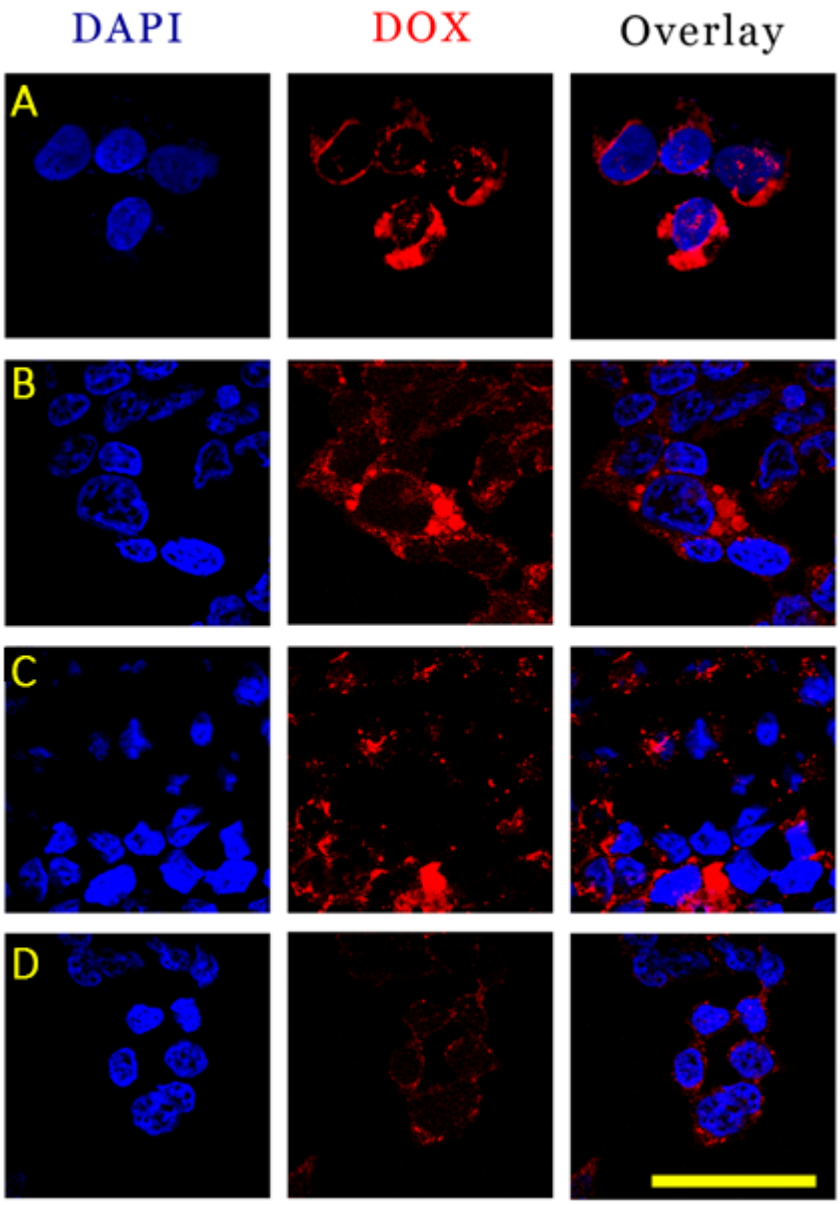

Figure 3.S5. Localization of free DOX and DOX-conjugates in A2780AD DOX-resistant ovarian carcinoma cells. Representative panels are **A)** DOX treated cells, **B)** NA-DOX treated cells, **C)** NS-DOX treated cells, and **D)** HEP-DOX treated cells. Scale Bar: 50 μm.

Table 3.S1. DLS results with 5 μM samples of NA-DOX, NS-DOX, and HEP-DOX.

Sample Name	Size (d.nm)
NA-DOX	212.6
NS-DOX	168.9
HEP-DOX	202.6

Table 3.S2. DLS results with 100 nM samples of NA-DOX, NS-DOX, and HEP-DOX.

Sample Name	Z-Average (d.nm)
NA-DOX	1.112
NS-DOX	3.337
HEP-DOX	4.24

conjugates as described in the methods section. The weight percent of DOX (Table 3.S3) was calculated using the formula:

$$\frac{g\ of\ DOX}{g\ of\ DOX + g\ of\ Polymer} = weight\ \%$$

Based on the weight percentages identified, approximately 1 molecule of DOX is attached per polymer chain. An alternative means of measuring DOX concentration may be to use acid hydrolysis of DOX and detect the aglycon.[5]

To determine the cellular localization of DOX-conjugates, confocal microscopy was utilized (as described in the methods section). In addition to determining the cellular localization of polymers in U87 Mg glioma cells, HT-29 colon cancer cells and A2780 AD DOX-resistant ovarian carcinoma cells were also analyzed.

Table 3.S3. Drug loading on DOX conjugates.

Substrate	DOX wt%	# of DOX per polymer chain
NA-DOX	1.54	~1
NS-DOX	1.63	~1
HEP-DOX	0.67	~1

3.3.7 Supplementary References

1. Etrych, T.; Kovar, L.; Strohalm, J.; Chytil, P.; Rihova, B.; Ulbrich, K., Biodegradable star HPMA polymer-drug conjugates: Biodegradability, distribution and antitumor efficacy. *J Control Release* **2011***,* 154, (3), 241-8.

2. Victor, X. V.; Nguyen, T. K.; Ethirajan, M.; Tran, V. M.; Nguyen, K. V.; Kuberan, B., Investigating the elusive mechanism of glycosaminoglycan biosynthesis. *J Biol Chem* **2009,** 284, (38), 25842-53.

3. Spinelli, F. J.; Kiick, K. L.; Furst, E. M., The role of heparin self-association in the gelation of heparin-functionalized polymers. *Biomaterials* **2008,** 29, (10), 1299-306.

4. Gaigalas, A. K.; Hubbard, J. B.; LeSage, R.; Atha, D. H., Physical characterization of heparin by light scattering. *J Pharm Sci* **1995,** 84, (3), 355-9.

5. Etrych, T.; Mrkvan, T.; Chytil, P.; Koňák, Č.; Říhová, B.; Ulbrich, K., N-(2-hydroxypropyl) methacrylamide-based polymer conjugates with pH-controlled activation of doxorubicin. I. New synthesis, physicochemical characterization and preliminary biological evaluation. *J App Pol Sci* **2008**, 109, (5), 3050-61.

CHAPTER 4

IN VITRO AND *IN VIVO* EVALUATION OF A COMBINATION THERAPY USING CLICK-XYLOSIDE AND HEPAROSAN-DOX CONJUGATE

4.1 Introduction

Proteoglycans (PG) are composed of core proteins attached to multiple glycosaminoglycan (GAG) side chains. Located on the cell surface and within the extracellular matrix, PGs are critical components of multiple pathophysiological functions because of their ability to bind growth factors, chemokines, and lectins.[1-3] PG side chains include heparan sulfate, chondroitin sulfate, dermatan sulfate, and keratan sulfate. It is well known that the sulfation patterns of GAGs are necessary for their function in a variety of pathophysiological processes.[4, 5] As an example, heparin is a GAG that binds antithrombin and elicits anticoagulant activity in the body; however, its activity requires the presence of a pentasaccharide sequence composed of *N*-sulfated glucosamine, 6-*O* sulfated glucosamine, and 3-*O* sulfated glucosamine residues in close proximity.[6, 7]

Previously we have demonstrated that sulfation patterns determine the cellular internalization and nuclear localization of multiple heparan sulfate GAGs in a variety of cancer cells.[8] Relative to heparin, *N*-acetyl heparosan (NA) and *N*-sulfo heparosan (NS) internalize to a significantly greater extent. Based on these results, we have also

developed doxorubicin conjugates of NA, NS, and heparin as shown in the previous chapter. *In vitro* data suggest that both NA and NS are more effective at delivering doxorubicin to the nucleus of cancer cells than heparin. Doxorubicin activity is preserved even when the drug is attached covalently via an amide linkage. It is likely that NA and NS doxorubicin conjugates will be more chemically stabile during long term storage compared to traditional doxorubicin conjugates such as those that utilize hydrazo-linkages to attach DOX to the vehicle.[9, 10]

Previously, we have also demonstrated that xylosides, small molecules consisting of a xylose residue attached to an aglycone, have the ability to inhibit tumor progression. When cells are treated with xylosides, these small molecules enter cellular golgi and prime GAG chains.[11-13] Without cellular anchors, the primed GAGs are released into the surrounding ECM and are able to compete with endogenous PGs. In our studies we have found that click-xylosides can reduce tumor invasion and 4-fluoro-xylosides mitigate tumor-associated angiogenesis. Researchers have also found that 2(6-hydroxynaphthyl)-beta-D-xylopyranoside significantly reduces tumor growth *in vivo*.[14] Additionally, it has been reported that β-D-xyloside inhibits the invasive capability of HeLa cells in culture medium containing SDF-1/CXCL12.[15] Xylosides may effectively reduce tumor invasion and angiogenesis when used as part of a combinatorial therapy regime with a chemotherapeutic agent.

To deliver chemotherapeutics, several GAG-based drug vehicles have been developed previously.[16-18] However, the majority of these vehicles have been unable to cross the blood brain barrier (BBB) to deliver their drug cargo to gliomas. In order to develop a universal GAG-based drug delivery vehicle, it is necessary to increase the

ability of the vehicle to partition across the blood brain barrier and release its cargo. Methods for increasing BBB penetration include increasing the hydrophobicity of the carrier, enhancing BBB permeability transiently, modification of carriers with brain targeting macromolecules or peptides, and inhibition of brain efflux pumps.[19-21] Enhancement of temporary BBB transcytosis is typically achieved by utilizing hypertonic mannitol infusions or bradykinin to contract brain capillary endothelial cells and increase intercellular space.[22, 23] Additionally, a variety of macromolecules may also increase BBB penetration including holo-transferrin, aprotinin, and angiopep, which utilize receptor-mediated endocytosis to enter the brain parenchyma.[24, 25] To reduce brain efflux of drugs, PG-1 and BCRP inhibitors such as elacridar have been successfully utilized in previous studies.[26, 27]

In this study, we develop heparosan-doxorubicin-aprotinin (HDA) conjugates and test their effectiveness at reducing tumor growth *in vitro* and *in vivo* in flanks and in the brain. HDA conjugates are analyzed for their ability to enter cellular nuclei and to reduce cellular viability. In conjunction with HDA conjugates, click-xyloside is utilized to reduce tumor invasion, and the combination therapy with HDA and xyloside is tested for its efficacy *in vivo* against intracranial and flank tumors. *In vivo* the biodistribution of HDA conjugates is also assessed and an infusion of both bradykinin and elacridar is evaluated for its ability to enhance the efficacy of the combination therapy in the brain. This study demonstrates that both xylosides and HDA conjugates are effective anticancer therapeutics and warrant further study in clinical research.

4.2 Materials and Methods

Heparosan from E. Coli K5 and Heparitinase I, II and III from *flavobacterium heparinum* were expressed and purified as previously described.[28] Bovine lung aprotinin for synthesis of conjugate was acquired from Sigma Aldrich. HT-29 colon cancer cells were a kind gift from Dr. Scott Kuwada (University of Hawaii). The analytical grade strong anion exchange column and size exclusion column were acquired from Dionex and Tosoh Biosciences, respectively. HPMA standards for size exclusion chromatography were acquired from Dr. Jindrich Kopecek (University of Utah). Disaccharide standards for strong anion exchange were obtained from Iduron Inc (Manchester, UK). The transwell invasion assay kit and matrigel for animal experiments were acquired from BD Biosciences. The cell titer blue viability assay kit was acquired from Fisher Scientific. Doxorubicin was acquired from Aksci Inc. All other materials were acquired from Sigma Aldrich.

Ten mg of Heparosan was dissolved in 600 µl of water and stirred at 150 rpm at room temperature. Next, 1.5 equivalents of 1-Ethyl-3-[3-dimethylaminopropyl]carbodiimide hydrochloride (EDC) per disaccharide and 1.5 equivalents of N-Hydroxysulfosuccinimide sodium salt (Sulfo-NHS) per disaccharide were added after dissolving in a total of 400 µl of EDC coupling buffer (10 mM HEPES buffer, pH 8.5). The mixture was then stirred for 2 hours prior to addition of 1 equivalent of doxorubicin-hydrochloride per disaccharide dissolved in 300 µl of 200 proof ethanol. This reaction was capped and stirred overnight at room temperature. After 20 hours, the mixture was centrifuged at 4000 rpm for 10 minutes. It was then filtered through a 3000 MWCO amicon centrifugal filter to remove excess doxorubicin, EDC, and sulfo-NHS.

Subsequently, the polymer-doxorubicin conjugate was diluted to 1 ml with EDC coupling buffer. An additional 1.5 equivalents each of EDC and Sulfo-NHS was added and stirred for an additional 2 hours prior to addition of 1 equivalent of aprotinin per disaccharide. This mixture was stirred overnight once again and on the following day it was concentrated through a 10,000 MWCO centrifugal filter to remove any unreacted heparosan-doxorubicin conjugate and excess aprotinin. Next, the conjugate was loaded onto a DEAE Sepharose column (0.5 ml) preequilibriated with 10 column volumes of wash buffer (20 mM NaOAc buffer (pH 6.0), 0.1 M NaCl, 0.01% Triton X-100). The column was then washed with 30 column volumes of wash buffer. Bound GAGs were then eluted with 6 column volumes of elution buffer (20 mM NaOAc,1 M NaCl, pH 6.0). Finally, the concentrated mixture was filtered through 100,000 and 30,000 MWCO centrifugal filters to remove aggregates.

Subsequently, the HDA conjugates were analyzed by size-exclusion chromatography using a G3000 SWxL column operated at a constant flow rate of 0.5 ml/minute of size exclusion buffer (100 mM KH_2PO_4, 150 mM NaCl, pH 6.0). Conjugates were also analyzed using dynamic light scattering (Malvern Zetasizer) at a 10 μM concentration of doxorubicin and via transmission electron microscopy at a 1 mg/ml concentration of heparosan. To analyze the sulfation pattern of heparosan, strong anion exchange chromatography was utilized. Fifty μg samples of heparosan were digested with a cocktail of heparitinase I, II, and III and eluted at a rate of 1 ml/minute with an increasing gradient of NaCl from 0.1 M to 1 M over the course of 75 minutes. Disaccharides were detected using an inline UV detector at 232 nm absorption.

A carbazole assay for uronic acid content was utilized to determine heparosan

concentration in solution as previously described.[29] Briefly, multiple standards of heparosan polymer were prepared and 50 µl of each standard was loaded into wells of a 96 well plate in triplicate. HDA was also loaded into wells of the 96 well plate. Subsequently, 200 µl of sodium tetraborate solution (25 mM sodium tetraborate in concentrated H_2SO_4) was added to each well containing sample. After mixing, the sample was heated in boiling water for 10 minute. Next, plates were cooled for 10 minutes and 50 µl of carbazole solution (0.125% carbazole in 200 proof ethanol) was added to each well. Plates were heated again in boiling water for 10 minutes, cooled, and the absorbance of solutions was read at 520 nm.

Drug loading on the HDA conjugates was analyzed through fluorescent spectroscopy by comparing known quantities of the polymer-conjugate solution to a standard curve of DOX. Plates were read using fluorescence excitation/emission at 470 nm/600 nm.

Cell viability upon drug or conjugate treatment was assessed using a Cell Titer Blue viability assay. Twenty five thousand cells were added into the wells of a 96 well plate in 200 µl of HAMS F-12 media. Cells were left to attach for 4 hours. Next, the media was replaced with fresh HAMS F-12 media and appropriate amounts of each drug or drug conjugate were added into each well in 200 µl of total volume per well. Cells were treated for 3 days in a humidified incubator and subsequently the media was replaced with 125 µl of fresh HAMS F-12 media. Fifty µl of cell titer blue reagent was added into the well and after a 3 hour incubation, 25 µl of 3% SDS was added into each well to stop cellular metabolic activity. Plates were then read in a fluorescent spectrometer with excitation/emission 560 nm/590 nm.

Approximately 50,000 cells were grown on glass coverslips within 35 mm cell culture. One μM of equivalent drug concentration were added into each well and cells were incubated in a humidified incubator for 16 hours. The media was removed and cells were washed twice with PBS. Subsequently, cells were fixed with 500 μl of 4% paraformaldehyde solution for 10 minutes at room temperature. Next, cells were washed twice with PBS and stained with a DAPI solution for 10 minutes. After incubation with the nuclear stain, cells were washed again and mounted onto microscope slides and imaged with an FV1000-XY Confocal Olympus IX81 microscope using a 60X oil immersion lens.

F98 Rat Glioma cells were added to the top well of a 6 well Boyden chamber at a density of $1x10^5$ cells/well in. Next, HAMS/ F-12 media with penicillin/streptomycin was added to the top well and media with 10% fetal bovine serum was added to the bottom well. Xylosides or other solutions were added to both the top and bottom well in appropriate quantities and mixed together well with media. Invasion chambers were maintained in a humidified incubator at 37℃ for 3 days while cells migrated. After this time period, supernatant from the top well was aspirated and the top half containing matrigel was removed using a cotton swab. The top well was then washed twice with PBS. Subsequently the PET membranes were cut from the well using a razor and placed in trypsin to remove cells that had invaded through and deposited on the bottom side of the PET membrane. Invaded cells were then counted using a hemacytometer.

F98 cells (1×10^6 cells) were suspended in 100 μl of matrigel and injected into the flanks of athymic CD-1 nu/nu male nude mice of 12 weeks of age. The flank xenografts were allowed to grow for 2 weeks prior to treatment.

CD-1 nu/nu athymic nude mice were anesthetized under isoflurane. An incision was made above the scalp, the cerebral membrane was scraped away, and a needle-guide system was used to inject approximately 50,000 F98 cells (in 3 μl of matrigel) 1 mm axial and 1 mm sagittal to the bregma. The injection was carried out over the course of 1 minute. Subsequently, dental cement was used to close the injection hole and biocompatible glue was used to seal the scalp.

I.P. injections were carried out without anesthesia in the peritoneal cavity near the rear right leg. I.V. infusions were carried out by inserting a 28 guage needle into the lateral tail vein. Mice were anesthetized under isoflurane anesthesia and injections were performed using an injection pump and a 40 μl catheter attached to the needle. Infusions were given over 10 minutes into the tail vein. Doxorubicin was injected at a 1 mg/kg dose given as one bolus in i.p. injections and as an infusion in i.v. injections at a rate of 0.2 mg/kg/minute over 10 minutes. Bradykinin was injected at a rate of 20 μg/kg/minute for i.v. injections. Elacridar was injected at a rate of 0.25 mg/kg/minute for i.v. injections. Dosing of HDA conjugates and Doxorubicin were equivalent in i.v. add i.p. injections. For i.p. injections xyloside was dosed at 30 mg/kg. For i.v. injections, xyloside was injected at a rate of 3 mg/kg/minute for 10 minutes. All mice were injected once with multiple therapeutics being injected as a cocktail.

Mice were injected with Doxorubicin (2 mg/kg) and HDA conjugates (2 mg/kg equivalent dox), each dissolved in PBS i.p. on Day 1. After 24 hours, mice were sacrificed using carbon dioxide and cervical dislocation and organs were harvested and chilled at -20℃. Analysis was performed by first washing tissues with PBS solution three times through vigorous vortexing and subsequently by homogenizing tissue in nuclear

lysis buffer (10 mM Hepes, 1 mM $MgSO_4$, 1 mM $CaCl_2$, pH 7.4) using a microtip sonicator. One hundred µl of the homogenate was then dissolved in 900 µl of extraction buffer (0.01% TritonX-100, 0.015% acidified isopropanol v/v [81 mM HCl in isopropanol]) and extracted overnight at -20℃. The next day, samples were centrifuged at 12,000 rpm for 10 minutes and doxorubicin fluorescence was quantified using a plate reader with excitation/emission wavelengths of 470 nm/600 nm.

4.3 Results

The goals of this part of the dissertation research are to demonstrate that HDA conjugates and xylosides are both effective antitumor agents *in vitro* and *in vivo*. Additionally, this research seeks to determine if either molecule is effective at bypassing the blood brain barrier to treat intracranial gliomas. Furthermore, the combination therapy consisting of both xylosides and the HDA conjugate is evaluated to determine its relative efficacy compared to either treatment individually in both flank and intercranial tumors. In order to reach these goals, HDA conjugates are synthesized through EDC coupling chemistry and characterized using strong anion exchange chromatograpy, size exclusion chromatography, dynamic light scattering, and transmission electron microscopy. Next, HDA conjugates and xylosides are tested *in vitro* for their efficacy singularly and in combination against a variety of cancer cells. Both molecules are also tested for their ability to reduce glioma invasion *in vitro* and the cellular localization of HDA conjugates is tracked. The *in vivo* biodistribution of HDA conjugates are also analyzed prior to treatment of flank and intercranial tumors.

HDA conjugates were synthesized using EDC chemistry by first attaching doxorubicin to heparosan, removing unreacted substrates, and subsequently attaching

aprotinin to the heparosan-dox conjugates (Figure 4.1 and see supplement). The full HDA conjugates are approximately 20 kDa – 30 kDa in size when compared to HPMA standards of sizes 40 kDa and 80 kDa (Figure 4.2a). The starting heparosan polymer is approximately 8-10 kDa in size and aprotinin is approximately 6500 Da in size. Less than 1 % of free drug remains in the solution when comparing the AUC of the HDA conjugate vs. the small peak that elutes at 45 minutes corresponding to small molecules such as fluoresceinamine. The amount of polymer in a unit of solution is determined using the carbazole assay for uronic acid content (see supplement). The doxorubicin loading on the polymer can be determined using a fluorescence-based standard curve. Each polymer chain is found to carry approximately 6-10 doxorubicin molecules (see supplement). To corroborate the high loading of DOX on these polymers, an alternative method might include acid hydrolysis of the conjugate and subsequent detection of the DOX aglycon. Additionally, a BCA assay for protein content is performed to determine that 1-2 aprotinin molecules are attached per chain of polymer (see supplement).

The HDA conjugates form aggregates in solution and these aggregates are visible under TEM imaging to be approximately 50 nm or more in length (Figure 4.2b). Previously, several other research groups have noted that heparin, a similar glycosaminoglycan, forms aggregates in solution.[30, 31] High DOX loading on these polymers may also be one cause for aggregation. DLS measurements also show that the nonaggregate particles are approximately 6.8 nm in size (Figure 4.2c). Additionally, after digesting heparosan with heparitinase I, II, and III, a characteristic ΔUA-GlcNAc disaccharide is found to elute at approximately 10 min, indicating that the polymer substrate used to synthesize the HDA polymer conjugate is natural and biodegradable

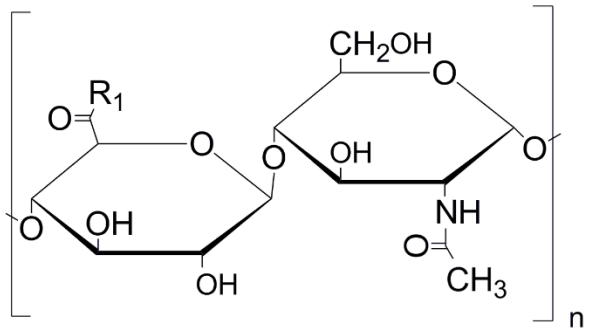

R_1: OH, -DOX or -APROTININ

Figure 4.1. Structure of Heparosan-Doxorubicin-Aprotinin conjugate.

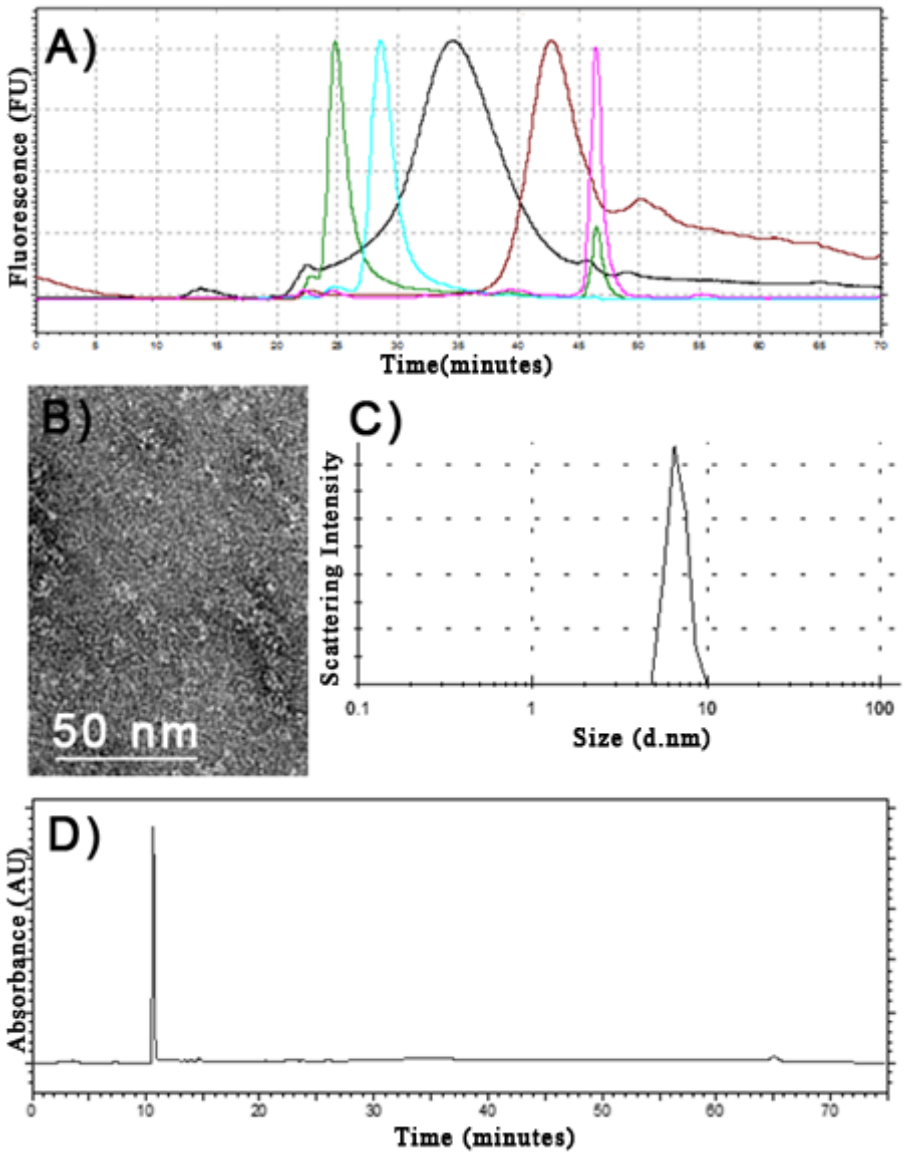

Figure 4.2. Characterization of Heparosan-Dox-Aprotinin conjugate. A) Size exclusion profile of Heparosan starting material and final conjugate. Representative traces are HPMA 80,000 Da (———), HPMA 40,000 Da (———), Heparosan-Dox-Aprotinin conjugate (———), Heparosan starting material (———), and Fluorescein amine (———). B) TEM image of conjugate. C) DLS profile of conjugate with a size of 6.83 nm ± 0.84 nm. D) Disaccharide profile of heparosan starting material corresponding to a ΔUA-GlcNAc disaccharide.

(Figure 4.2d).

After synthesis and characterization, HDA conjugates were tested for their therapeutic efficacy *in vitro* (Figure 4.3). Cell lines tested included F98 rat glioma cells, CH157 human meningioma cells, and HT-29 human colon cancer cells. The indicated concentrations of HDA were based on equivalent doxorubicin concentration so that cell treatments could be normalized and compared to control untreated cell proliferation. Xylosides were also tested for their effects on cell viability and were utilized at 100 μM concentrations because previous studies indicated that at this concentration *in vitro* cell invasion was severely thwarted. Based on these results it is apparent that HDA conjugates are as effective as doxorubicin at the concentrations tested. Additionally, xylosides have no effect on cell viability *in vitro* in combination with HDA or as singular therapies. Furthermore, aprotinin-dox conjuates are not as effective as heparosan-dox-aprotinin conjugates, demonstrating that heparosan increases the therapeutic efficacy of the drug conjugate.

To determine the cellular localization of HDA conjugates, CH157 cells were treated transiently with the conjugates for 1 day, fixed, and then imaged using a confocal microscope (Figure 4.4). Meningioma cells were utilized because they are large and easy to visualize. At equivalent settings, it is apparent that both doxorubicin and HDA conjugates can enter cellular nuclei. Typical polymer conjugates of doxorubicin utilize labile schiff bases to release the drug within the cell so that it may exert its anticancer activity in the nucleus.[9, 10] However, HDA conjugates utilize covalent linkages between the drug and the polymer and are still able to target cellular nuclei to deliver the drug. Xyloside was also tested *in vitro* for its ability to restrict tumor invasion (Figure 4.5). In

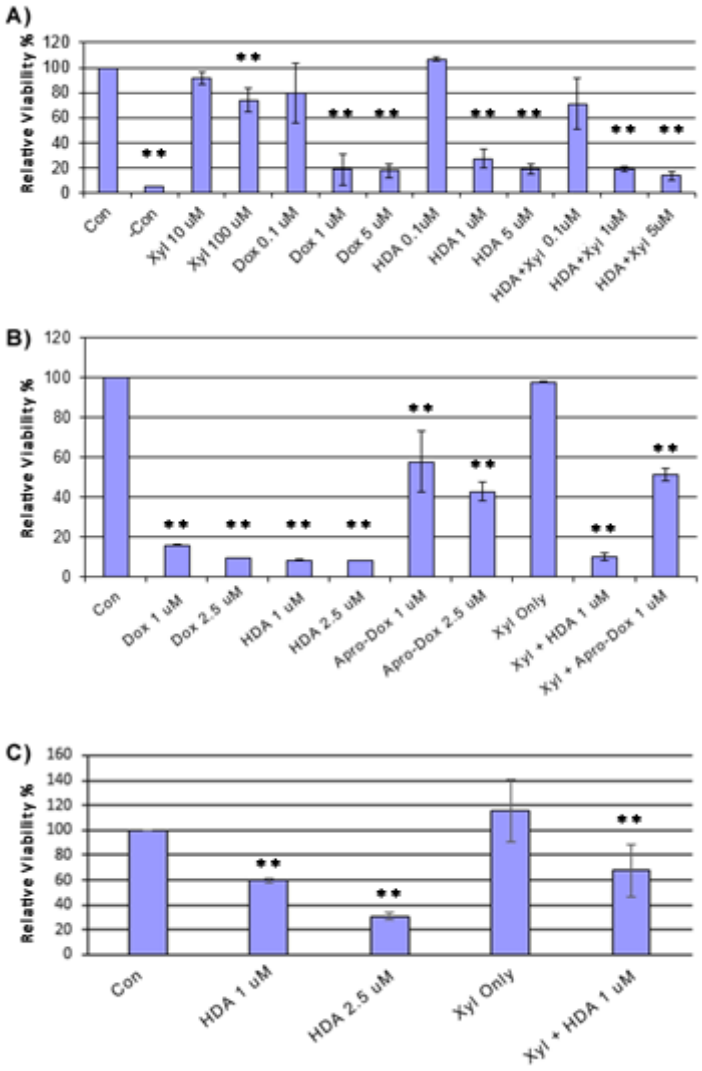

Figure 4.3. Viability assays of HDA conjugates and Xylosides with multiple cell lines. A) F98 glioma viability with Xyloside alone, Dox alone, HDA conjugate alone, and combination therapy with HDA + Xyloside. B) CH157 meningioma cell viability showing efficacy of Dox alone, HDA alone, Xyloside alone, combination therapy, and Aprotinin-Dox as a control to demonstrate improved efficacy with heparosan polymer vs. without heparosan polymer. C) HT-29 colon cancer cell viability with HDA alone, Xyloside alone, and with HDA + Xyloside. In combination therapy xylosides were utilized at 100 μM concentration. Concentration values in μM are equivalent doxorubicin concentrations, except in xyloside-only treatments. ** indicates $P<0.05$ as determined by a one-tailed paired t-test relative to control untreated samples. Error bars denote standard deviation.

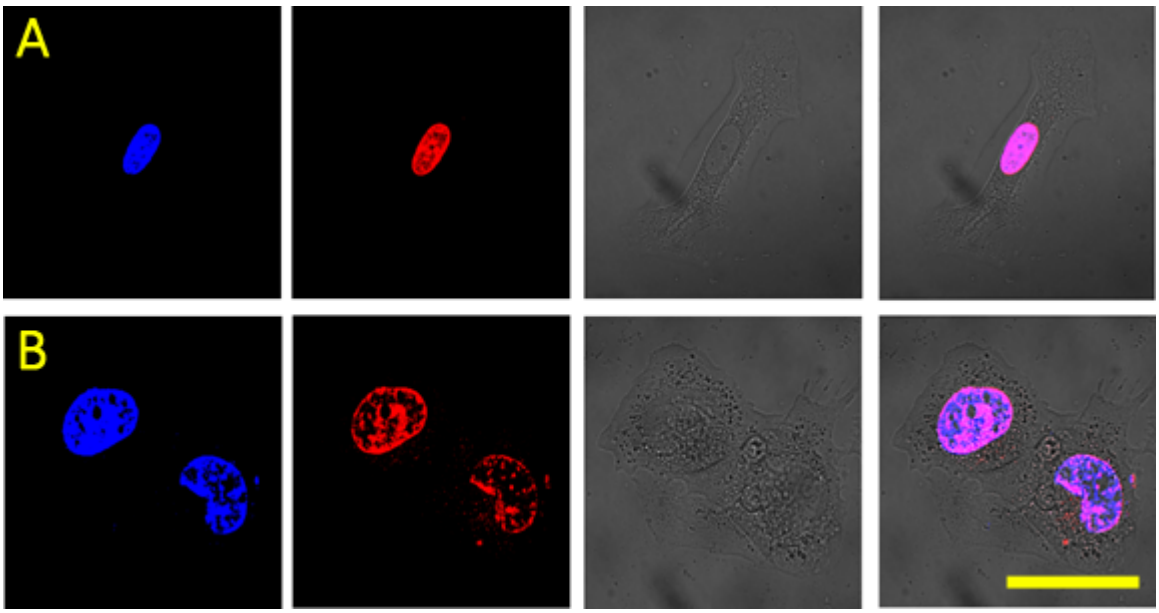

Figure 4.4. Localization of doxorubicin and HDA conjugate in CH157 meningioma cells. Representative panels are DOX (A) and HDA (B). Scale Bar: 50 μm

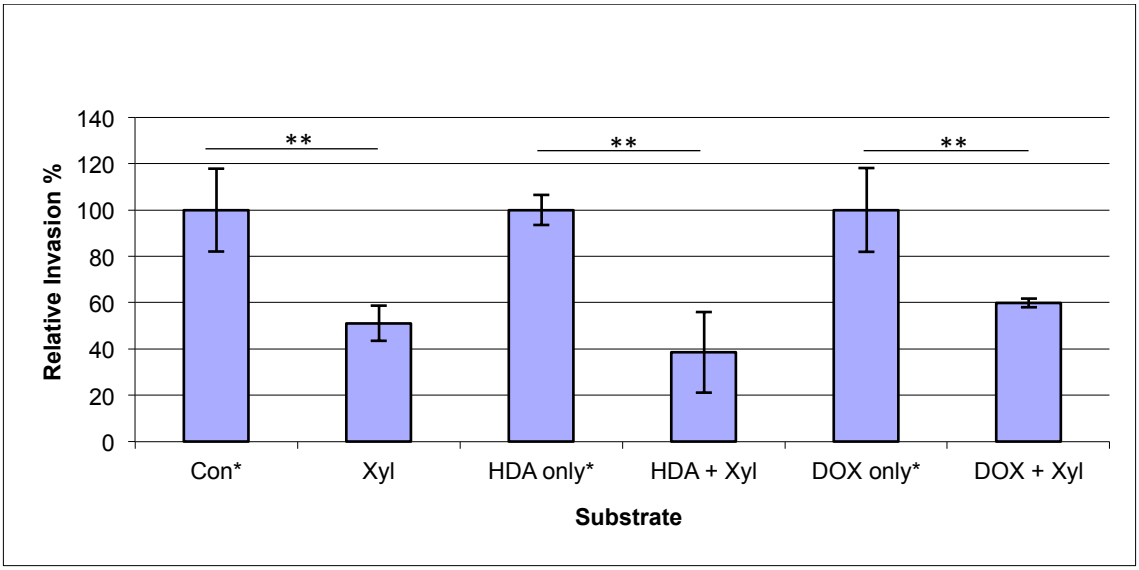

Figure 4.5. Relative inhibition of F98 glioma invasion. For each set of results, the invasion with xylosides is normalized to invasion without xyloside. ** indicates $P<0.05$ as determined by a one-tailed paired t-test vs. control cells that were not treated with xyloside in each pair of experiments. Error bars represent the standard deviation.

the invasion assay performed, a two-well Boyden chamber assay is utilized to determine the efficacy of antiinvasive therapeutics. Here, the top well consists of a floor made out of PET membrane with 8 μm pores layered with matrigel on top. Cells are added on top of the matrigel layer and a chemotactic gradient causes cells to invade through the matrigel layer and deposit on the bottom of the PET membrane over the course of 3 days. Cells found below the PET membrane are then counted and recorded. Based on the results, it was found that xyloside effectively reduced the invasion of F98 cells in this *in vitro* invasion assay. With xyloside treatment, F98 invasion through the matrigel was reduced approximately 50 percent. Additionally, the effectiveness of the xyloside was not hindered in combination with doxorubicin or with HDA conjugate. As expected, HDA and DOX treatment significantly reduced cell viability. Therefore, values displayed in Figure 4.5 are paired and normalized to treatments without xyloside.

The biodistribution of HDA conjugates and doxorubicin was determined by injecting CD-1 nu/nu male mice with conjugates and harvesting organs after a period of 24 hours (Figure 4.6). After homogenizing tissue in nuclear lysis buffer (doxorubicin localizes to nuclei), acidified isopropanol was used to extract the doxorubicin from the homogenized tissue. Data were normalized to PBS treated mice that had no doxorubicin in order to account for tissue auto-fluorescence. It is apparent that the conjugate entered the brain significantly more than doxorubicin, which is known not to enter the brain in therapeutic quantities. Additionally, the HDA conjugate localizes to the tumor more effectively than doxorubicin. Furthermore, relative to doxorubicin, the conjugate does not localize to the heart tissue as effectively. As doxorubicin is a known cardiotoxic agent, it is likely that the HDA conjugate will be more tolerable by patients.

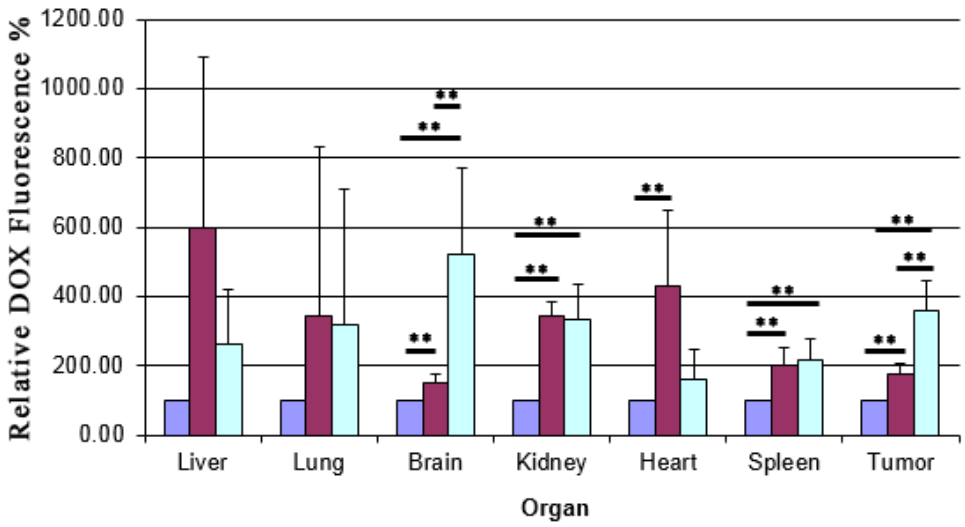

Figure 4.6. Relative biodistribution of DOX and HDA conjugate in mice 24 hours after an injection of 2 mg/kg i.p. Relative DOX fluorescence indicates tissue levels of the drug. Representative peaks are PBS injected mice ( ), 2 mg/kg i.p. doxorubicin injected mice ( ), and 2 mg/kg equivalent dose of HDA conjugate injected mice ( ). ** indicates $P<0.05$ as determined by a one-tailed paired t-test comparing each set of organs vs. PBS treated samples in the set. Error bars represent standard deviations.

To test the efficacy of HDA conjugates *in vivo*, a flank model of F98 rat gliomas was utilized (Figure 4.7). F98 tumor xenografts were grown in the flanks of CD-1 nu/nu male mice until tumors were palpable and subsequently mice were treated with doxorubicin or HDA i.p. once per week. Mice received xyloside five times per week, as indicated, respectively. When mice were noticeably showing signs of pain or sickness, they were sacrificed according to established IACUC protocols. Once all PBS treated mice were sacrificed, the experiment was ended and the data were analyzed. Future studies will follow mice for a longer period of time. Data from these experiments indicate that the HDA conjugate was as effective as DOX at reducing flank tumor growth. Additionally, it was found that xyloside was as effective as DOX at reducing flank tumor growth. Combination treatment with both xylosides and HDA conjugates did not show significant improvement compared to individual treatments according to growth data. Combination therapy may even be deleterious to the individual efficacies of each treatment (HDA or xyloside). However, in terms of survival, it was found that only one mouse went into remission with no noticeable sign of tumors in the flank or brain. This mouse was being treated using the combination therapy and warrants further investigation. These data also indicate that mice with late stage tumors can be effectively treated with DOX, HDA conjugates, and xyloside. After determining that HDA conjugates and xylosides were effective at treating tumor xenografts in the flank, the treatment strategy was tested in an orthotopic intercranial F98 glioma model (Figure 4.8). Cells utilized in this model are extremely invasive and stably transfected with luciferace for ease of imaging. I.P. injections of luciferin are quickly metabolized by luciferase and cells are tracked in an *in vivo* imaging system. To set up the model, F98 cells were

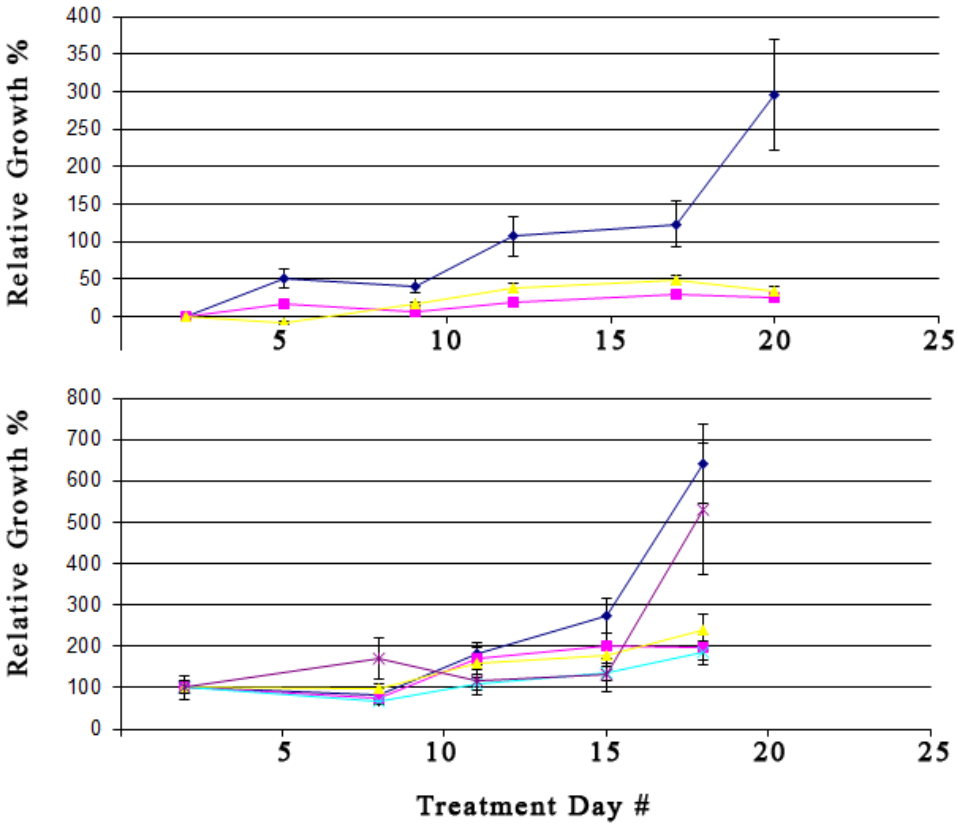

Figure 4.7. Treatment efficacy of HDA conjugate and combination therapy against F98 cells in mouse flanks. (n=5) DOX and HDA conjugates were injected i.p. at 1 mg/kg dose or dose equivalent of DOX once per week. Xyloside was injected at 30 mg/kg five times per week. Treatment days refer to the numerical number of days after treatment was started because tumors were established. Average tumor volume prior to treatment start was 184 ± 78 mm^3. Representative panels are: A) Treatment initiated after 2 weeks, Control mice ( ), DOX treatment group ( ), and HDA treatment group ( ). B) Treatment initiate after 3 weeks. Traces for Control mice ( ), Xyloside-treated mice ( ), Doxorubicin treated mice ( ), HDA treated mice ( ), and HDA + Xyloside treated mice ( ). Error bars indicate standard deviations.

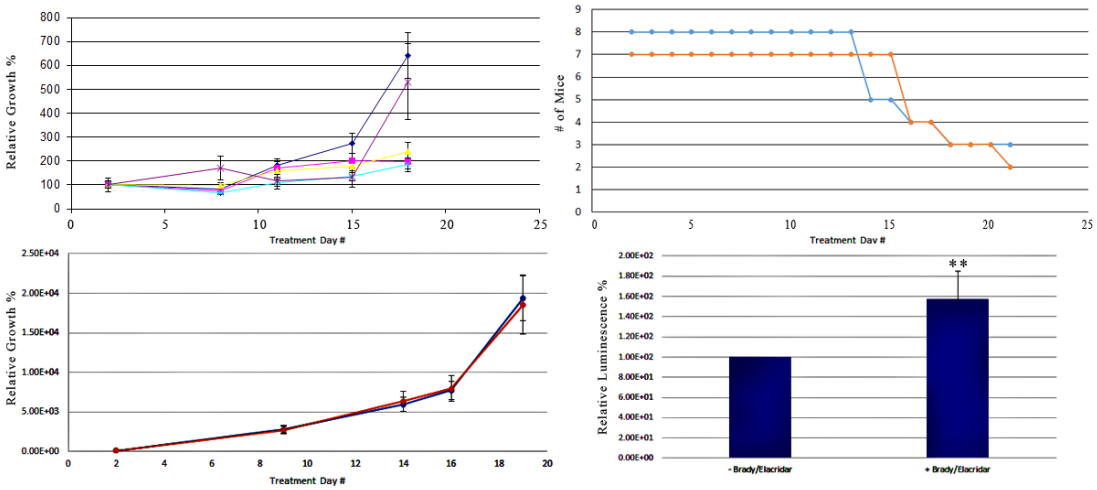

Figure 4.8. Efficacy of conjugate and combination therapy against orthotopic intracranial F98 glioma. Representative panels are described. A) Intercranial tumor growth after i.p. injection of PBS ( ), Xyloside ( ), 1 mg/kg Doxorubicin ( ), 1 mg/kg equivalent HDA conjugate ( ), and 1 mg/kg equiv. dose HDA with 30 mg/kg xyloside ( ). Treatments initiated 1 week after implantation of tumors in the brain. B) Intercranial tumor growth after i.v. infusion of PBS ( ) and 0.2 mg/kg/min equiv. dose of HDA and 3 mg/kg/min xyloside in combination with 20 μg/kg/min bradykinin and 0.25 mg/kg/min elacridar ( ). Treatments initiated 2 days after tumor implantation in the brain. C) Survival curve after i.v. infusion of PBS ( ) and combination therapy with bradaykinin and elacridar ( ). D) Internal control demonstrating increased D-luciferin permeability upon i.v. infusion of bradykinin and elacridar. ** indicates $P<0.05$ as determined by a one-tailed paired t-test. Error bars indicate standard deviations.

injected slowly within the brain near the bregma. The skull was resealed with dental cement and tumors were allowed to establish prior to treatment. Initially, orthotopic tumors were treated with doxorubicin (once per week), HDA conjugates (once per week), xylosides (five times per week), and combination therapy via i.p. injections. However, as these treatments were unable to reduce tumor growth (Figure 4.8a), a follow-up experiment was conducted where the following experimental modifications were devised: a) treatments were initiated 2 days after tumor implantation, b) bradykinin was infused i.v. with the injection to increase BBB penetration and c) elacridar was infused with the injection to reduce drug efflux through BCRP and PG-1, and d) all combination therapy treatments and PBS for control mice were given 3 times per week. Through this experiment it was found that bradykinin and elacridar increased luciferin signal in the brain, thus indicating that BBB penetration was increased (Figure 4.8d). However, even with these improvements, it was found that a combination therapy with HDA conjugates and xylosides was unable to reduce brain tumor growth and coincidentally mouse survival was unaffected (Figure 4.8c).

4.4 Discussion

In recent years, a plethora of novel drug delivery systems designed to target tumors have been developed. However, the majority of these vehicles are designed to merely deliver their therapeutic cargo and then to be excreted. Very few DDV have been designed where both the drug as well as the carrier may be therapeutic. Glycosaminoglycans provide a novel scaffold on which to design DDV because they have several inherent advantages: GAGs are biologically active and can be tailored to mitigate tumor progression, they are biocompatible and biodegradable, and they have

several functional groups which can be modified with targeting moieties and therapeutic cargo. GAGs such as heparin, acharan sulfate, and PI-88 have demonstrated significant antitumor efficacy by mitigating tumor growth, invasion, metastasis, inflammation, and angiogenesis in animal models.[32-34] Thus, we tested the efficacy of several different GAGs as potential drug delivery vehicles by analyzing their internalization properties and cellular localization. Heparosan, an unsulfated GAG, showed promise in our studies due to its rapid internalization and nuclear localization in U87Mg glioma cells. Heparosan-DOX conjugates were able to target cellular nuclei and induce apoptosis without the need for a labile hydrazone linker between the drug and the polymer indicating that the conjugate would be more attractive because of its shelf stability. Additionally, through conjugation of aprotinin with heparosan-DOX, HDA conjugates were expected to traverse the BBB and to reduce tumor-associated inflammation due to aprotinin's intrinsic biology whereby Aprotinin utilized LRP-1 to permeate the brain via receptor-mediated endocytosis.[25]

In addition to novel drug delivery vehicles, there has been a growing demand for nontoxic anticancer therapeutics. Chemotherapeutics are notorious for their devastating side effects whereby patients undergoing therapy typically have nausea, hair loss, weight loss, and several other symptoms that reduce their quality of life. Xylosides, small molecules that increase GAG biosynthesis in cells and GAG secretion, provide a novel methodology for treating cancers without toxic side effects. By utilizing GAGs generated by xylosides, it is possible to fight tumor growth without the introduction of unnatural and toxic organic molecules. Xylosides have successfully been utilized at molar concentrations without any effect on cell viability *in vitro*.[35, 36]

In this study, the efficacy of a combination therapy composed of HDA conjugates and click-xyloside against flank and cranial tumors was assessed. First, HDA conjugates were characterized via size exclusion chromatography, transmission electron microscopy (TEM), dynamic light scattering (DLS), and strong anion exchange chromatography (Figure 4.2). The HDA conjugates are approximately 20 kDa – 30 kDa in size with less than 1 percent free drug. In solution the conjugates are approximately 6.8 nm in size when analyzed by DLS and larger when analyzed by TEM. It is expected that heparosan also aggregates in solution like heparin.[30, 31]

Next, the *in vitro* efficacy and localization of HDA conjugates and combination therapy were assessed (Figure 4.3 and 4.4). It was determined that HDA conjugates are as effective as doxorubicin in reducing F98 cell viability and growth. Xyloside had minor effects on cell viability and a combination therapy with HDA conjugates and xyloside showed similar efficacy as the equivalent HDA conjugate. Aprotinin conjugates of doxorubicin were not as effective as HDA conjugates at reducing cell viability. It is likely that heparosan improves the overall drug delivery efficacy by improving cellular uptake as shown previously.[8] F98 glioma cells, HT-29 colon cancer cells, and CH157 meningioma cells all showed similar results. Confocal microscopy also confirmed that HDA conjugates localized to cellular nuclei. It is noteworthy that HDA conjugates could deliver the drug and affect cell viability without utilizing a cleavable linker between the doxorubicin and the polymer. Previously, several studies have demonstrated that GAGs are able to localize to cellular nuclei.[37-39] Additionally, Hyaluronic acid-DOX conjugates have been found to reduce tumor viability without the use of a labile linker. Perhaps HDA conjugates also utilize similar mechanistic pathways, as these similar GAGs, to

affect cell viability. Additionally we have shown that heparosan is able to enter the nucleus of U87 Mg cells.[8] However, the mechanisms of uptake of GAGs into cellular nuclei and drug action without a labile linker remain unclear. Therefore, it is likely that the polymer conjugate remains intact and shuttles doxorubicin to the nucleus of cells where the drug is active. Surprisingly, the attached polymer does not significantly affect the efficacy of the drug. Subsequently, when the invasive capability of F98 cells was assessed, it was found that xyloside dramatically lowered the invasive capability of cells *in vitro*. The addition of HDA conjugates and doxorubicin had little effect on the efficacy of xylosides.

The *in vivo* evaluation of HDA conjugates was carried out by determining the biodistribution of the conjugate, testing the efficacy of therapy in mouse flanks, and subsequently testing in mouse brains. Biodistribution data were assessed 24 hrs after a single dose of 2 mg/kg DOX or HDA conjugate (Figure 4.6). Organs in animals were harvested and tissue was lysed to release doxorubicin in cell nuclei. The released doxorubicin was extracted into acidified isopropanol and sample fluorescence was analyzed. It was found that compared to doxorubicin, HDA conjugates localized significantly more to the brain and the tumor. Additionally, conjugates were found in the liver and heart to a lesser extent than doxorubicin. It is likely that aggregation and the enhanced permeability and retention effect were responsible for the localization of HDA conjugates in tumor tissue.[40] Furthermore, aprotinin is known to target inflammatory sites and may have aided tumor targeting.[41, 42] As doxorubicin is a known cardiotoxic chemotherapeutic, the reduction in localization to the heart may indicate that the HDA conjugate will be more tolerable to patients.[43, 44] These results also indicate that HDA

conjugates may be effective in targeting and treating intracranial gliomas.

Treatment of F98 xenografts grown in mouse flanks was evaluated after growing tumors for 2 weeks (Figure 4.7A) or 3 weeks (Figure 4.7B). HDA conjugates were as effective as DOX at reducing F98 growth in the flank. Compared to mice treated with PBS, both DOX and HDA conjugates significantly slowed growth of the tumors and improved the quality of life. These results indicate that HDA conjugates are effective at reducing tumor growth both *in vivo* and *in vitro*. Additionally, it was found that xyloside effectively reduced tumor growth in the flanks at a dose of 30 mg/kg. As this xyloside has been found to be nontoxic at high concentrations *in vitro*, these results indicate that click-xylosides may be promising anticancer therapeutics. Previously, it has been found that various *O*-xylosides inhibit the growth of tumors in mice.[14] However, these xylosides were unstable O-xylosides which could undergo hydrolysis or be cleaved by glycosidases to release toxic organic moieties (free naphthol and benzyl groups). Furthermore, these xylosides only primed low molecular weight GAGs. Therefore, their mechanism of action against tumors and chemical toxicity *in vivo* was difficult to discern. In contrast, click-xyloside, utilized in this study, is hydrolytically stable and able to prime large molecular weight GAGs.

The efficacy of HDA conjugates and xyloside against orthotopic gliomas was evaluated after growing intracranial tumors for 1 week and subsequently initiating treatment with i.p. injections (Figure 4.8A). Results demonstrate that there was no significant effect of treatment on glioma growth in any of the treatment groups. To further improve the efficacy with which treatments cross the BBB, treatments were given i.v. with bradykinin and elacridar as infusions over 10 min (Figure 4.8B). Bradykinin is

known to cause contractions of brain capillary cells and to chemically open the BBB.[22, 23] Additionally, elacridar prevents the efflux of drugs through PG-1 and BCRP efflux pumps in the BBB.[26, 27] However, chemical opening of the BBB and reduction of drug efflux did not show any synergistic effect with combination therapy on brain tumor growth or mouse survival (Figure 4.8B and Figure 4.8C). Confirmation of BBB chemical opening was observed by testing luciferin signal in the brain with and without bradykinin and elacridar (Figure 4.8D). Luciferin uptake into brain tumor cells was enhanced 60 percent after bradykinin and elacridar infusion in the tail vein. Since DOX, HDA, and xyloside all effectively treated flank tumors, it is likely that these therapeutics cannot cross the BBB without modification and therefore are unable to treat orthotopic gliomas. It is noteworthy that the use of HDA conjugates with XYL as a combination therapy against orthotopic brain tumors yielded poorer results than control untreated mice. The mechanism behind the antagonistic relationship between these treatments is still unclear. In conclusion, HDA conjugates and xyloside show promise as potential therapeutics to target and treat cancers. HDA conjugates are likely to be less toxic than DOX, can be modified with a variety of imaging and targeting moieties, and have the unique ability to interfere with tumor nuclei without the need for cleavable drug linkers. Additionally, xylosides are nontoxic modulators of tumor growth and have tremendous potential for *in vivo* use as anticancer therapeutics. However, further modification is necessary to improve their flux across the BBB. Efforts are currently underway to directly infuse these therapeutics into the brain and determine their efficacy.

4.5 References

1. Hacker, U.; Nybakken, K.; Perrimon, N., Heparan sulphate proteoglycans: the sweet side of development. *Nat Rev Mol Cell Biol* **2005,** 6, (7), 530-41.

2. Iozzo, R. V.; Sanderson, R. D., Proteoglycans in cancer biology, tumour microenvironment and angiogenesis. *J Cell Mol Med* **2011***,* 15, (5), 1013-31.

3. Poole, A. R., Proteoglycans in health and disease: structures and functions. *Biochem J* **1986,** 236, (1), 1-14.

4. Feyzi, E.; Trybala, E.; Bergstrom, T.; Lindahl, U.; Spillmann, D., Structural requirement of heparan sulfate for interaction with herpes simplex virus type 1 virions and isolated glycoprotein C. *J Biol Chem* **1997,** 272, (40), 24850-7.

5. Maccarana, M.; Casu, B.; Lindahl, U., Minimal sequence in heparin/heparan sulfate required for binding of basic fibroblast growth factor. *J Biol Chem* **1994,** 269, (5), 3903.

6. Xia, G.; Chen, J.; Tiwari, V.; Ju, W.; Li, J. P.; Malmstrom, A.; Shukla, D.; Liu, J., Heparan sulfate 3-O-sulfotransferase isoform 5 generates both an antithrombin-binding site and an entry receptor for herpes simplex virus, type 1. *J Biol Chem* **2002,** 277, (40), 37912-9.

7. Zhang, L.; Lawrence, R.; Schwartz, J. J.; Bai, X.; Wei, G.; Esko, J. D.; Rosenberg, R. D., The effect of precursor structures on the action of glucosaminyl 3-O-sulfotransferase-1 and the biosynthesis of anticoagulant heparan sulfate. *J Biol Chem* **2001,** 276, (31), 28806-13.

8. Raman, K.; Mencio, C.; Desai, U. R.; Kuberan, B., Sulfation patterns determine cellular internalization of heparin-like polysaccharides. *Mol Pharm* **2013***,* 10, (4), 1442-9.

9. Yu, Y.; Chen, C. K.; Law, W. C.; Weinheimer, E.; Sengupta, S.; Prasad, P. N.; Cheng, C., Polylactide-graft-doxorubicin nanoparticles with precisely controlled drug loading for pH-triggered drug delivery. *Biomacromolecules* **2014***,* 15, (2), 524-32.

10. Wang, Y.; Ma, S.; Xie, Z.; Zhang, H., A synergistic combination therapy with paclitaxel and doxorubicin loaded micellar nanoparticles. *Colloids Surf B Biointerfaces* **2013**, 116C, 41-48.

11. Nguyen, T. K.; Tran, V. M.; Sorna, V.; Eriksson, I.; Kojima, A.; Koketsu, M.; Loganathan, D.; Kjellen, L.; Dorsky, R. I.; Chien, C. B.; Kuberan, B., Dimerized glycosaminoglycan chains increase FGF signaling during zebrafish development. *ACS Chem Biol* **2013***,* 8, (5), 939-48.

12. Lugemwa, F. N.; Esko, J. D., Estradiol beta-D-xyloside, an efficient primer for heparan sulfate biosynthesis. *J Biol Chem* **1991,** 266, (11), 6674-7.

13. Fritz, T. A.; Lugemwa, F. N.; Sarkar, A. K.; Esko, J. D., Biosynthesis of heparan sulfate on beta-D-xylosides depends on aglycone structure. *J Biol Chem* **1994,** 269, (1), 300-7.

14. Mani, K.; Belting, M.; Ellervik, U.; Falk, N.; Svensson, G.; Sandgren, S.; Cheng, F.; Fransson, L. A., Tumor attenuation by 2(6-hydroxynaphthyl)-beta-D-xylopyranoside requires priming of heparan sulfate and nuclear targeting of the products. *Glycobiology* **2004,** 14, (5), 387-97.

15. Brule, S.; Friand, V.; Sutton, A.; Baleux, F.; Gattegno, L.; Charnaux, N., Glycosaminoglycans and syndecan-4 are involved in SDF-1/CXCL12-mediated invasion of human epitheloid carcinoma HeLa cells. *Biochim Biophys Acta* **2009,** 1790, (12), 1643-50.

16. Thomas, M. B.; Radhakrishnan, K.; Gnanadhas, D. P.; Chakravortty, D.; Raichur, A. M., Intracellular delivery of doxorubicin encapsulated in novel pH-responsive chitosan/heparin nanocapsules. *Int J Nanomedicine* **2013***,* 8, 267-73.

17. Deng, X.; Cao, M.; Zhang, J.; Hu, K.; Yin, Z.; Zhou, Z.; Xiao, X.; Yang, Y.; Sheng, W.; Wu, Y.; Zeng, Y., Hyaluronic acid-chitosan nanoparticles for co-delivery of MiR-34a and doxorubicin in therapy against triple negative breast cancer. *Biomaterials* **2014**, 35, (14), 4333-44.

18. Qiu, L.; Li, Z.; Qiao, M.; Long, M.; Wang, M.; Zhang, X.; Tian, C.; Chen, D., Self-assembled pH-responsive hyaluronic acid-g-poly(l-histidine) copolymer micelles for targeted intracellular delivery of doxorubicin. *Acta Biomater* **2014**, 10, (5), 2024-35.

19. Kozlovskaya, L.; Stepensky, D., Quantitative analysis of the brain-targeted delivery of drugs and model compounds using nano-delivery systems. *J Control Release* **2013**, 171, (1), 17-23.

20. Pardridge, W. M., Drug and gene delivery to the brain: the vascular route. *Neuron* **2002,** 36, (4), 555-8.

21. Blumling Iii, J. P.; Silva, G. A., Targeting the brain: advances in drug delivery. *Curr Pharm Biotechnol* **2012***,* 13, (12), 2417-26.

22. Pappius, H. M.; Savaki, H. E.; Fieschi, C.; Rapoport, S. I.; Sokoloff, L., Osmotic opening of the blood-brain barrier and local cerebral glucose utilization. *Ann Neurol* **1979,** 5, (3), 211-9.

23. Emerich, D. F.; Dean, R. L.; Osborn, C.; Bartus, R. T., The development of the bradykinin agonist labradimil as a means to increase the permeability of the blood-brain barrier: from concept to clinical evaluation. *Clin Pharmacokinet* **2001,** 40, (2), 105-23.

24. Skarlatos, S.; Yoshikawa, T.; Pardridge, W. M., Transport of [125I]transferrin through the rat blood-brain barrier. *Brain Res* **1995,** 683, (2), 164-71.

25. Xin, H.; Sha, X.; Jiang, X.; Chen, L.; Law, K.; Gu, J.; Chen, Y.; Wang, X.; Fang, X., The brain targeting mechanism of Angiopep-conjugated poly(ethylene glycol)-co-poly(epsilon-caprolactone) nanoparticles. *Biomaterials* **2012***,* 33, (5), 1673-81.

26. Barraud de Lagerie, S.; Comets, E.; Gautrand, C.; Fernandez, C.; Auchere, D.; Singlas, E.; Mentre, F.; Gimenez, F., Cerebral uptake of mefloquine enantiomers with and without the P-gp inhibitor elacridar (GF1210918) in mice. *Br J Pharmacol* **2004,** 141, (7), 1214-22.

27. Kemper, E. M.; Verheij, M.; Boogerd, W.; Beijnen, J. H.; van Tellingen, O., Improved penetration of docetaxel into the brain by co-administration of inhibitors of P-glycoprotein. *Eur J Cancer* **2004,** 40, (8), 1269-74.

28. Kuberan, B.; Lech, M.; Zhang, L.; Wu, Z. L.; Beeler, D. L.; Rosenberg, R. D., Analysis of heparan sulfate oligosaccharides with ion pair-reverse phase capillary high performance liquid chromatography-microelectrospray ionization time-of-flight mass spectrometry. *J Am Chem Soc* **2002,** 124, (29), 8707-18.

29. Bowness, J. M., Application of the carbazole reaction to the estimation of glucuronic acid and flucose in some acidic polysaccharides and in urine. *Biochem J* **1957,** 67, (2), 295-300.

30. Gaigalas, A. K.; Hubbard, J. B.; LeSage, R.; Atha, D. H., Physical characterization of heparin by light scattering. *J Pharm Sci* **1995,** 84, (3), 355-9.

31. Spinelli, F. J.; Kiick, K. L.; Furst, E. M., The role of heparin self-association in the gelation of heparin-functionalized polymers. *Biomaterials* **2008,** 29, (10), 1299-306.

32. Chow, L. Q.; Gustafson, D. L.; O'Bryant, C. L.; Gore, L.; Basche, M.; Holden, S. N.; Morrow, M. C.; Grolnic, S.; Creese, B. R.; Roberts, K. L.; Davis, K.; Addison, R.; Eckhardt, S. G., A phase I pharmacological and biological study of PI-88 and docetaxel in patients with advanced malignancies. *Cancer Chemother Pharmacol* **2008,** 63, (1), 65-74.

33. Lee, Y. S.; Yang, H. O.; Shin, K. H.; Choi, H. S.; Jung, S. H.; Kim, Y. M.; Oh, D. K.; Linhardt, R. J.; Kim, Y. S., Suppression of tumor growth by a new glycosaminoglycan isolated from the African giant snail Achatina fulica. *Eur J*

Pharmacol **2003,** 465, (1-2), 191-8.

34. Lever, R.; Page, C. P., Non-anticoagulant effects of heparin: an overview. *Handb Exp Pharmacol* **2012**, (207), 281-305.

35. Kuberan, B.; Ethirajan, M.; Victor, X. V.; Tran, V.; Nguyen, K.; Do, A., "Click" xylosides initiate glycosaminoglycan biosynthesis in a mammalian cell line. *Chembiochem* **2008,** 9, (2), 198-200.

36. Victor, X. V.; Nguyen, T. K.; Ethirajan, M.; Tran, V. M.; Nguyen, K. V.; Kuberan, B., Investigating the elusive mechanism of glycosaminoglycan biosynthesis. *J Biol Chem* **2009,** 284, (38), 25842-53.

37. Chen, L.; Sanderson, R. D., Heparanase regulates levels of syndecan-1 in the nucleus. *PLoS One* **2009,** 4, (3), e4947.

38. Liang, Y.; Haring, M.; Roughley, P. J.; Margolis, R. K.; Margolis, R. U., Glypican and biglycan in the nuclei of neurons and glioma cells: presence of functional nuclear localization signals and dynamic changes in glypican during the cell cycle. *J Cell Biol* **1997,** 139, (4), 851-64.

39. Richardson, T. P.; Trinkaus-Randall, V.; Nugent, M. A., Regulation of heparan sulfate proteoglycan nuclear localization by fibronectin. *J Cell Sci* **2001,** 114, (Pt 9), 1613-23.

40. Kobayashi, H.; Watanabe, R.; Choyke, P. L., Improving conventional enhanced permeability and retention (EPR) effects; what is the appropriate target? *Theranostics* **2013***,* 4, (1), 81-9.

41. Saxena, P.; Thompson, P.; d'Udekem, Y.; Konstantinov, I. E., Kallikrein-kinin system: a surgical perspective in post-aprotinin era. *J Surg Res* **2011***,* 167, (1), 70-7.

42. Siebeck, M.; Fink, E.; Weipert, J.; Jochum, M.; Fritz, H.; Spannagl, M.; Kroworsch, P.; Shimamoto, K.; Schweiberer, L., Inhibition of plasma kallikrein with aprotinin in porcine endotoxin shock. *J Trauma* **1993,** 34, (2), 193-8.

43. Lefrak, E. A.; Pitha, J.; Rosenheim, S.; Gottlieb, J. A., A clinicopathologic analysis of adriamycin cardiotoxicity. *Cancer* **1973,** 32, (2), 302-14.

44. Merrill, J.; Greco, F. A.; Zimbler, H.; Brereton, H. D.; Lamberg, J. D.; Pomeroy,

T. C., Adriamycin and radiation: synergistic cardiotoxicity. *Ann Intern Med* **1975,** 82, (1), 122-3.

4.6 Supplementary Information

Table 4.S1. Summary of Characterization Data

Molecular Weight	
Starting Materials	
Heparosan	10,000 Da approx.
Aprotinin	6511 Da
Doxorubicin	579.98 Da
Final Conjugate	
Conjugate MW	20,000-30,000 Da appox.
DOX molecules per chain	6-10 molecules per chain
Aprotinin molecules per chain	1-2 molecules per chain
Free Drug %	< 1% by AUC
Hydrodynamic Size	
Conjugate Size by DLS	6.83 nm ± 0.84 nm
Aprotinin Size by DLS	1.65 nm.[1]
11,000 Da Heparin Size by DLS	3.2 nm.[2]

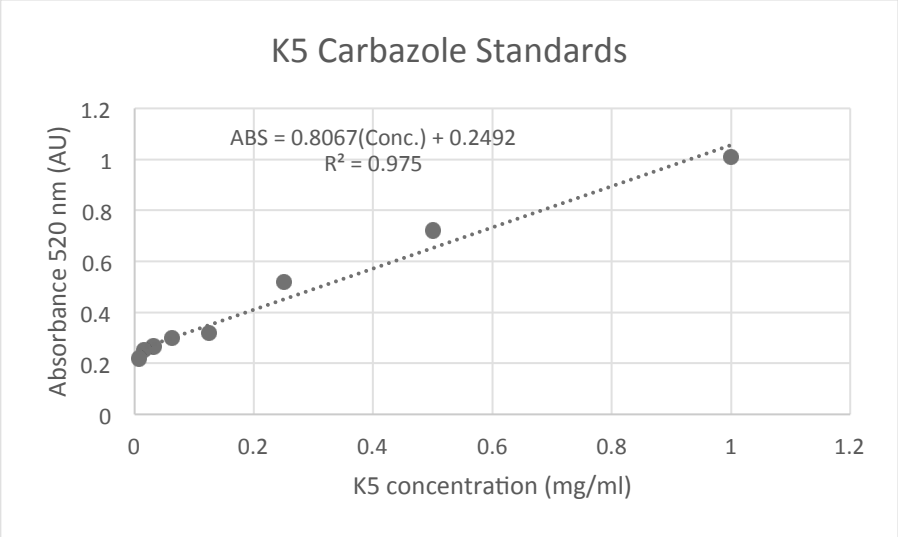

Figure 4.S1. Uronic acid calibration curve and trendline based on 520 nm absorbance of carbazole.

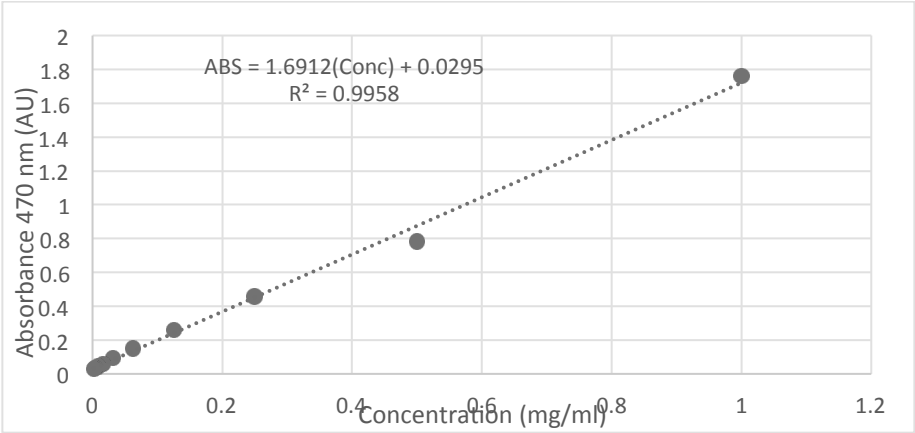

Figure 4.S2. Doxorubicin concentration calibration curve and trendline based on 470 nm absorbance of doxorubicin.

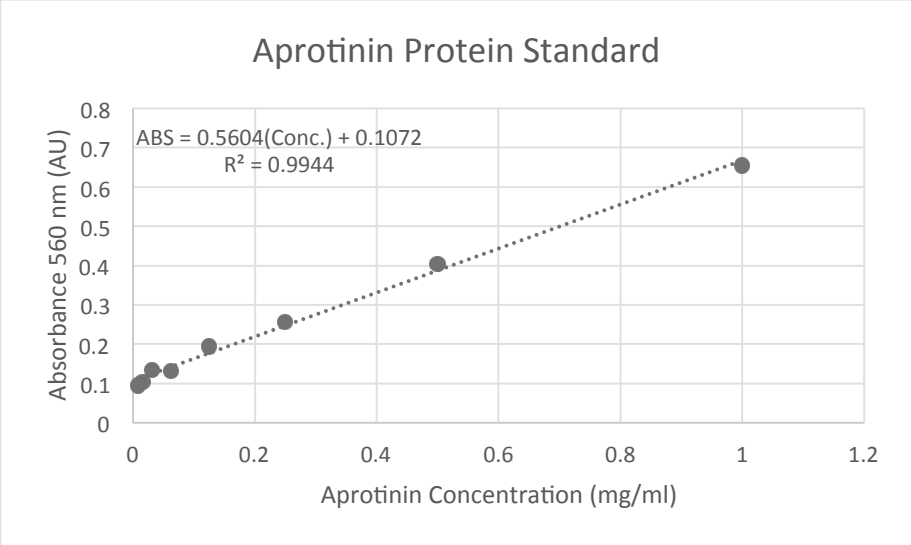

Figure 4.S3. Aprotinin concentration calibration curve and trendline based on 560 nm absorbance of a BCA reagent.

CHAPTER 5

CONCLUSIONS

5.1 Conclusions

Cancer remains a challenging disease to treat. Glioblastomas, in particular, are a devastating form of cancer that are difficult to treat because of the sensitivity of brain tissue and the difficulty of circumventing the blood brain barrier. The current treatment regime consists of temozolomide and radiation and increases two-year survival of patients to 27 percent.[1] In this dissertation, we develop novel glycosaminoglycan based therapeutics and drug delivery vehicles for targeting and treating glioblastomas and other cancers. Chapter 2 describes the development of several xylosides and glycosaminoglycan mimetics that can hinder tumor angiogenesis and invasion. Chapter 3 describes the development and evaluation of novel glycosaminoglycan-based drug delivery vehicles which are biocompatible, biodegradable, target tumor nuclei, and overcome drug resistance. Chapter 4 describes the *in vivo* efficacy of HDA, in combination with xyloside therapy, against aggressive flank and intercranial tumors. These studies demonstrate that glycosaminoglycan-based therapeutics and vehicles are extremely effective against tumors outside the brain. However, further optimization is necessary to deliver them systemically and treat brain tumors.

Among the different novel therapeutics developed and tested in this dissertation, click-xylosides, in particular, show promise. Click-xylosides are hydrolytically stable,

small sugars, which are nontoxic and induce glycosaminoglycan synthesis after enter cell Golgi. The newly released glycosaminoglycans then compete with cell surface glycosaminoglycans and alter cell signaling and biology. Interestingly, we have found that they not only reduce cell invasion *in vitro* but also dramatically affect tumor growth *in vivo* in mouse flanks. No anticancer activity was detected against intracranial gliomas. However, as these molecules induce no cell toxicity *in vitro*, it may be possible to utilize them at much higher dosages *in vivo* and further reduce tumor growth without any concomitant toxicity. It may even be possible to directly infuse these small-molecules into the brain. Previously, researchers have found that *O*-xylosides can inhibit tumor growth, but these molecules were toxic to cells due to the unstable hydrolytically-cleavable linkages between the sugar and the aglycone.[2] Click-xylosides evaluated in this dissertation are a significant advancement over this previous technology and ongoing studies are evaluating the antitumor potential of Click-xylosides as part of a directly infused therapy into the brain.

Fluoro-xylosides, sulfated small-molecule GAG mimetics, and sulfated polymeric GAG mimetics also provide alternate strategies to reduce tumor growth. As demonstrated in Chapter 2, fluoro-xylosides dramatically reduce glycosaminoglycan synthesis and also affect tumor-associated angiogenesis. However, systemic introduction of these molecules is likely a major challenge due to myriad of roles that GAGs play in physiology. Targeted xyloside therapy may provide one solution to the effective use of fluoro-xylosides *in vivo*.[3] Alternatively, GAG mimetics may be utilized to affect tumor angiogenesis. Both small-molecule and polymeric mimetics are promising because of their inherent scalability. Using simple microwave sulfation protocols it is possible to generate

production-scale quantities of small molecule GAG mimetics. Additionally, the polymeric mimetic discussed in Chapter 2 can be quickly synthesized from heparin, a globally-available clinical anticoagulant. Future studies will determine the *in vivo* efficacy of these molecules.

The studies performed as part of this dissertation also demonstrate the efficacy and clinical relevance of a novel GAG-based drug delivery vehicle. After thorough analysis of the effect of sulfation pattern on GAG uptake into cells, Heparosan and *N*-sulfo heparosan were both found to have several advantages as drug delivery vehicles. It was found that both polymers were significantly more effective at delivering doxorubicin into cells compared to heparin. Additionally, DOX conjugates of both polymers were able to target cellular nuclei and deliver DOX without the need for labile drug-polymer linkers. A DOX conjugate of *N*-sulfoheparosan was also found to overcome doxorubicin resistance in cells at low concentrations. Furthermore, both polymers are simple to produce, biodegradable, and biocompatible.

Further evaluation of the DOX conjugates from Chapter 3 *in vivo* was carried out by conjugating aprotinin to heparosan-DOX. With aprotinin, it was expected that the conjugates would circulate systemically and localize to all organs including the brain. *In vivo* efficacy experiments with an aprotinin conjugate of heparosan-DOX (HDA) indicated that the conjugate dramatically reduces tumor growth in mouse flanks. However, the conjugates did not demonstrate any antiglioma efficacy. Further modification and evaluation is necessary to enhance the brain penetration of HDA conjugates. While co-infusions of bradykinin/elacridar were attempted as a method to improve brain bioavailability, even this methodology was ineffective at increasing the

antiglioma efficacy. Perhaps conjugation of Angiopep to heparosan-DOX may yield promising results similar to recent conjugates of angiopep and paclitaxel.[4]

In addition to individual treatments with xyloside and HDA conjugates, combination therapy with both HDA conjugates and click-xyloside was also evaluated. It was found that combination therapy was equally effective at reducing tumor growth in mouse flanks and in mouse brains. No significant advantage was identified between individual treatment with HDA conjugates and combination therapy consisting of HDA conjugates along with click-xyloside. Varying the dosage of either treatment may affect the *in vivo* efficacy of the combination therapy. It may be possible that alternative dosages of either xyloside or conjugate have a synergistic effect *in vivo* whereby the combination of both therapies is more effective than either therapy alone.[5] Nonetheless, click-xylosides and HDA conjugates remain promising targets for further development due to their efficacy as singular treatments.

5.2 References

1. Omuro, A.; DeAngelis, L. M., Glioblastoma and other malignant gliomas: a clinical review. *Jama* **2013***,* 310, (17), 1842-50.

2. Mani, K.; Belting, M.; Ellervik, U.; Falk, N.; Svensson, G.; Sandgren, S.; Cheng, F.; Fransson, L. A., Tumor attenuation by 2(6-hydroxynaphthyl)-beta-D-xylopyranoside requires priming of heparan sulfate and nuclear targeting of the products. *Glycobiology* **2004,** 14, (5), 387-97.

3. Tran, V. M.; Victor, X. V.; Yockman, J. W.; Kuberan, B., RGD-xyloside conjugates prime glycosaminoglycans. *Glycoconj* **2010***, J* 27, (6), 625-33.

4. Drappatz, J.; Brenner, A.; Wong, E. T.; Eichler, A.; Schiff, D.; Groves, M. D.; Mikkelsen, T.; Rosenfeld, S.; Sarantopoulos, J.; Meyers, C. A.; Fielding, R. M.; Elian, K.; Wang, X.; Lawrence, B.; Shing, M.; Kelsey, S.; Castaigne, J. P.; Wen, P. Y., Phase I study of GRN1005 in recurrent malignant glioma. *Clin Cancer Res* **2013***,* 19, (6), 1567-76.

5. Victor, X. V.; Nguyen, T. K.; Ethirajan, M.; Tran, V. M.; Nguyen, K. V.; Kuberan, B., Investigating the elusive mechanism of glycosaminoglycan biosynthesis. *J Biol Chem* **2009,** 284, (38), 25842-53.

APPENDIX

HEPARAN SULFATE BIOSYNTHESIS

A1.1 Introduction

In addition to studies on a combined drug delivery strategy to target and treat cancers, studies were performed on heparan sulfate biosynthesis and biology. The current state of understanding of the biosynthesis of heparan sulfates involves a series of steps that starts with the assembly of a linkage tetrasaccharide where xylose is first attached to the serine residue of a core protein. Subsequently three more sugar residues are added onto this chain (galactose, galactose, and glucuronic acid). After the assembly of this region, the chain is elongated and *N*-sulfated by N-Deacetylase-N-sulfotransferase (NDST) enzymes. Next, C5-epimerase (C5-EPI) converts some glucuronic acid residues to iduronic acid residues. Subsequently the chain is concurrently modified by 2-*O*-Sulfotransferase, 3-*O*-Sulfotransferase, and 6-*O*-Sulfotransferase. It is necessary for NDST to act on the chain before C5-EPI due to the substrate specificity of the C5-EPI. Additionally, C5-EPI does not modify the polymer after *O*-Sulfotransferases act on the chain. Therefore, conventionally it is known that NDST is a gateway modification and that NDST can only act on a nascent chain. The results of our studies show that NDST is

not just a gateway modification during heparan sulfate biosynthesis. Using chemoenzymatially synthesized heparan sulfate polymers we show that NDST may act even after *O*-sulfotransferases modify a growing chain unlike C5-EPI.

A1.2 Is N-Sulfation Just a Gateway Modification During Heparan Sulfate Biosynthesis?

Manuscript reproduced with permission from: Raman, K., Nguyen, T. K., and Kuberan, B. (2011) Is *N*-Sulfation just a gateway modification during heparan sulfate biosynthesis? *FEBS Lett., 585*, 3420-3423.

FEBS Letters 585 (2011) 3420–3423

FEBS Letters

journal homepage: www.FEBSLetters.org

Is *N*-sulfation just a gateway modification during heparan sulfate biosynthesis?

Karthik Raman [a], Thao Kim Nu Nguyen [a], Balagurunathan Kuberan [a,b,c,*]

[a] Department of Bioengineering, University of Utah, Salt Lake City, UT 84112, USA
[b] Department of Medicinal Chemistry, University of Utah, Salt Lake City, UT 84112, USA
[c] Interdepartmental Program in Neuroscience, University of Utah, Salt Lake City, UT 84112, USA

ARTICLE INFO

Article history:
Received 9 August 2011
Revised 14 September 2011
Accepted 26 September 2011
Available online 2 October 2011

Edited by Felix Wieland

Keywords:
Heparan sulfate
N-Deacetylase–*N*-sulfotransferase
Biosynthesis
GAGOSOME
Proteoglycan
Assembly mechanism

ABSTRACT

Several biologically important growth factor–heparan sulfate (HS) interactions are regulated by HS sulfation patterns. However, the biogenesis of these combinatorial sulfation patterns is largely unknown. *N*-Deacetylase/*N*-sulfotrasferase (NDST) converts *N*-acetyl-D-glucosamine residues to *N*-sulfo-D-glucosamine residues. This enzyme is suggested to be a gateway enzyme because *N*-sulfation dictates the final HS sulfation pattern. It is known that *O*-sulfation blocks C5-epimerase, which acts immediately after NDST action. However, it is still unknown whether *O*-sulfation inhibits NDST action in a similar manner. In this article we radically change conventional assumptions regarding HS biosynthesis by providing in vitro evidence that *N*-sulfation is not necessarily just a gateway modification during HS biosynthesis.

1. Introduction

Heparan sulfate proteoglycans (HSPGs) are composed of core proteins attached to sulfated glycosaminoglycan (GAG) side chains. They play important roles as co-receptors for several molecules including fibroblast growth factors (FGF), hepatocyte growth factor (HGF), glial cell derived neurotrophic factor (GDNF), and vascular endothelial growth factors (VEGF) [1]. By acting as co-receptors, they are involved in a variety of pathological and physiological processes such as tumor progression and embryonic development [2–4]. The role of HS as a co-receptor depends greatly on its sulfation pattern. For example, HS–FGF2 interactions require the presence of *N*-sulfated glucosamine units, 2-*O* sulfated iduronic acid units, and 6-*O* sulfated glucosamine units [5,6].

To generate the diverse sulfation patterns present in HS chains, the biosynthesis of HS involves a complex interplay between several enzymes that are predicted to be co-localized within GAGOSOMEs [7–12]. HS biosynthesis begins with the formation of a linkage region composed of one xylose residue, two galactose residues and one glucuronic acid residue. Next, the HS chain is extended by Ext-1 and Ext-2. As the polymerization takes place, *N*-deacetylase/*N*-sulfotrasferase enzyme isoforms (NDST) convert *N*-acetyl-D-glucosamine residues in the nascent chain into *N*-sulfo-D-glucosamine residues. There are four known NDST isoforms that have different deacetylation/sulfation abilities and are expressed variably in different tissues [13–17]. The *N*-sulfate groups added by these enzymes determine the domain structure of HS because subsequent modifications by C5-epimerase, 2-*O* sulfotransferase, 3-*O* sulfotransferase, and 6-*O* sulfotransferase are dictated by the location of *N*-sulfate groups [18]. The order of modifications will have enormous implications in generating diverse structures of biological significance [19].

It is well known that C5-epimerase, which converts glucuronic acid residues to iduronic acid residues after NDST modification, is inhibited by *O*-sulfation [20]. However, it is unknown whether NDST, which confers the first modification of HS chains, is influenced similarly by the presence of nearby *O*-sulfate groups. Earlier studies have shown that NDST can act on a variety of substrates [21–28]. However, these studies have not elucidated the site of action of NDST within the larger heparanome (which contains non-sulfated (NA), heavily sulfated (NS) and mixed (NA/NS) domains). Earlier studies estimated the levels of radioactive [^{35}S]-sulfate incorporation into a variety of substrates in the presence of NDST without analyzing the corresponding disaccharides. Therefore, it is unknown whether *O*-sulfation inhibits NDST activity, i.e. NDST could just be modifying *N*-acetyl glucosamine (GlcNAc) residues in the non-sulfated NA domains within the heparanome.

This study utilizes NDST-2, a robust enzyme isoform which shows equal *N*-deacetylase and *N*-sulfotransferase activity, to determine the site of action of NDST on HS for the first time and to probe whether *O*-sulfation affects *N*-deactylation/*N*-sulfation.

* Corresponding author at: University of Utah, 30 S 2000 E, Skaggs Hall Room 307, Salt Lake City, UT 84112, USA. Fax: +1 801 585 9119.
E-mail address: kuby.balagurunathan@utah.edu (B. Kuberan).

0014-5793/$36.00
doi:10.1016/j.febslet.2011.09.030

These in vitro results are obtained from studying the action of NDST-2 on a mature HS chain and on a synthetic enzymatically-generated substrate.

2. Materials and methods

2.1. Materials

Heparan sulfate from bovine kidney was procured from Seikagaku. DEAE-Sepharose gel was purchased from Amersham Biosciences. [^{35}S]Na_2SO_4 and Ultima-FloAP scintillation fluid were purchased from Perkin Elmer Life and Analytical Sciences. [^{32}S]PAPS and HS disaccharide standards were purchased from Iduron and Sigma–Aldrich. SF-900 II SFM media was purchased from Invitrogen. [^{35}S]PAPS was prepared as reported earlier [19]. Heparitinases I, II, and III from *flavobacterium heparinum* were cloned and expressed as previously described. All other reagents and solvents were from Sigma–Aldrich.

2.2. Purification of NDST-2

Fifteen millilitres of NDST-2 viral stock was added to 2×10^9 Sf9 cells in 1 l of SF900 II SFM media. Infected cells were shaken at a rate of 150 rpm in a humidified incubator maintained at 28 °C for 4 days. After 4 days, the cell suspension was centrifuged at 1000×*g* for 30 min to pellet cells. To the supernatant, PIPES solution was added to a final concentration of 10 mM and the pH of the solution was adjusted to 7.0. Next, a solution containing phenylmethylsulfonyl fluoride in 10 ml isopropanol was added to a final concentration of 1 mM. The supernatant was then chilled on ice for 1 h prior to centrifugation at 4000×*g* for 1 h. The supernatant was then diluted 1:2 with ddH_2O and filtered through a 0.45 μm pore-size PES membrane under vacuum. This solution was then loaded onto a 100-ml column of ToyoPearl AF heparin 650 M. The column was washed with 600 ml of PCG-50 (10 mM PIPES, pH 7.0, 2% glycerol, 0.6% CHAPS, 50 mM NaCl) and eluted with a 450-ml linear gradient of 50–1000 mM NaCl in PCG. Aliquots of selected fractions were then analyzed to check NDST-activity as described later in the methods section utilizing a heparan sulfate substrate instead of K5NS. Positive fractions were then pooled and concentrated using an Amicon YM-10 membrane.

2.3. Preparation of partially N-sulfated 6-O-sulfated K5 heparosan

All reactions were performed in a buffer consisting of 25 mM MES (pH 7.0), 0.02% Triton X-100, 2.5 mM $MgCl_2$, 2.5 mM $MnCl_2$, 1.25 mM $CaCl_2$ and 0.75 mg/ml BSA. Four hundred and eighty micrograms of K5 heparosan was combined with 200 μg of [^{32}S]PAPS and 40 μl of NDST-2 in a 600 μl reaction volume. The product was analyzed after digestion with Heparitinases I, II, and III, using strong anion exchange HPLC (SAX-HPLC) with an inline UV detector measuring absorbance at 232 nm. Ten micrograms of partially *N*-sulfated K5 heparosan was incubated with 10 μl of 6-OST-3 and 3 μl of [^{35}S]PAPS (0.5×10^7 CPM) in a 50 μl reaction. An aliquot of the radioactive sample was then desalted through a 3000 MWCO filter, digested with Heparitinases I, II, and III, and analyzed using SAX-HPLC with an inline radiometry detector. Radioactive disaccharides were eluted with a linear gradient of 0–1 M NaCl in 70 mM phosphate buffer (pH 3.0) for 60 min and co-injected HS disaccharide standards were used to confirm their identity.

2.4. Enzymatic reactions of NDST-2

Heparan sulfate or K5NAc/NS6S were treated with NDST-2 by incubating 10 μg of substrate with 10 μl of NDST-2, 10 μl of MES, and 3 μl of [^{35}S]PAPS (0.5×10^7 CPM) in a 50 μl reaction overnight. The next day, an additional 10 μg of [^{32}S]PAPS was added along with 10 μl of NDST-2 to saturate all possible modification sites. The modified products were then desalted, digested, and analyzed.

3. Results and discussion

To demonstrate that *N*-sulfation is not just a gateway modification and to elucidate the site of action of NDST enzymes on a mature HS chain, bovine kidney HS was incubated with NDST-2 in the presence of [^{35}S]PAPS. The resulting polymer chain was treated with Heparitinases I, II, and III, and the resulting radio-labeled disaccharides were co-injected with disaccharide standards and analyzed by strong anion exchange chromatography (Fig. 1a). A chromatogram of the HS from bovine kidney is included in the Supplementary materials (Fig. S1).

After NDST-2 treatment of HS, the disaccharides generated by heparitinase treatment are: ΔUA-GlcN[^{35}S] and ΔUA-GlcN[^{35}S]6S

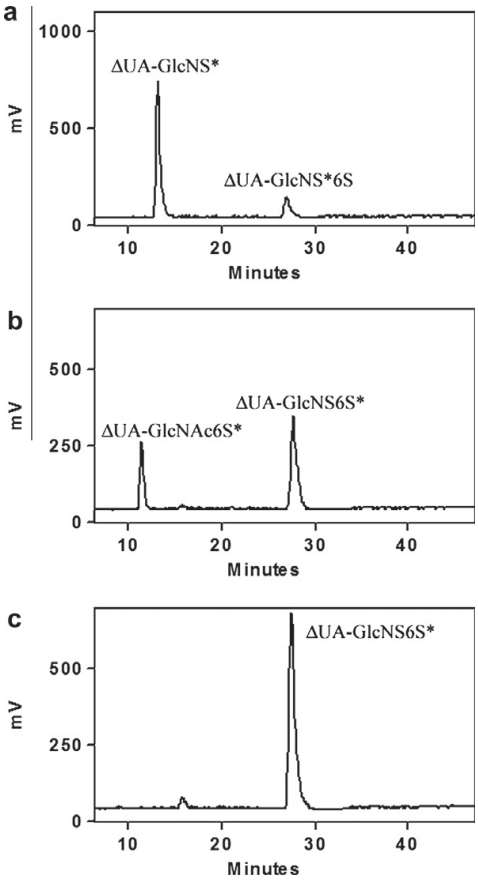

Fig. 1. Radiometric traces of disaccharides formed by digesting polysaccharides with Heparitinases I, II, and III. (a) Disaccharides formed when HS is treated with NDST-2 and digested with Heparitinases I, II, and III. (b) Disaccharides of partially *N*-sulfated, 6-*O* sulfated heparosan, a synthetic substrate designed to test the activity of NDST-2 without neighboring group effects from other *O*-sulfates. The ratio of GlcNS6S/GlcNAc6S peaks is ~0.6. (c) Disaccharides of NDST-2 treated partially *N*-sulfated, 6-*O* sulfated heparosan. After NDST-2 addition, the GlcNS6S/GlcNAc6S ratio increases. Thus 6-*O* sulfation does not inhibit NDST-2 action. The peaks in the chromatograms were determined by comparison to co-injected standards.

Thus, only ΔUA-GlcNAc and ΔUA-GlcNAc6S residues on mature HS chains can be *N*-sulfated. Surprisingly, the HS chains did not have any additional modification sites. One would expect that small amounts of (GlcA/IdoA)2S-GlcNAc sequences would also be sulfated by NDST, however the expected disaccharide product, ΔUA2S-GlcN[^{35}S], was not found after digestion of the polysaccharides with Heparitinases I, II, and III. This observation points to the possibility that other *O*-sulfates may inhibit NDST action. However, such a claim is difficult to test because of the rare nature of *N*-acetylated 2-*O* sulfated disaccharide units and the difficulties involved in synthesizing such substrates using chemoenzymatic methods.

While NDST was found to act on 6-*O* sulfated residues in HS, it is difficult to analyze the true sites of modification because nearby sulfate groups can influence the action of the enzyme on the polymer chain. To further confirm the hypothesis that NDST modifies GlcNAc6S sites on HS, and to negate any such neighboring group effects, a synthetic substrate consisting of this residue was synthesized by 6-*O*-sulfation of 50% *N*-sulfated heparosan with 6-OST-3 in the presence of [^{35}S]PAPS (Fig. 2, polysaccharide 1). Treating this polysaccharide with NDST-2 in the presence of [^{32}S]PAPS then allowed us to observe the conversion of GlcNAc6[^{35}S] residues to GlcNS6[^{35}S] residues (Fig. 1b and c). It is noteworthy that all GlcNAc6[^{35}S] residues were converted to GlcNS6[^{35}S] residues – confirming that 6-*O*-sulfation does not inhibit NDST enzymatic action.

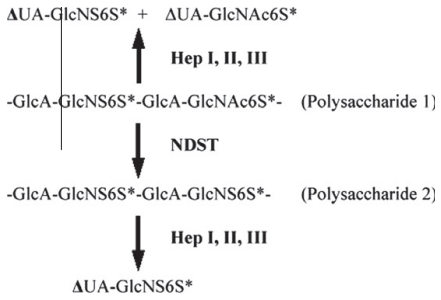

Fig. 2. Modification of polysaccharide 1 by NDST. (*) Indicates that this sulfate group is [^{35}S] and the radiolabeled product, after digestion with Heparitinases I, II, and III, are resolved and visualized on the radiochromatogram shown in Fig. 1.

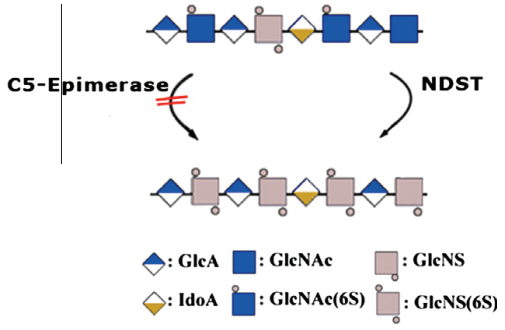

Fig. 3. The comparative effect of *O*-sulfation on the action of NDST and C5-epimerase. After the formation of the linkage region and subsequent polymerization, NDST enzymes add on the first sulfate residues onto a nascent chain. C5-Epimerase and several *O*-sulfotransferases then further modify the HS chain. C5-Epimerase cannot act on this mature chain due to *O*-sulfates which block its activity. However, NDST can still act on this substrate and thus *N*-sulfation is much more than just a gateway modification during heparan sulfate biosynthesis.

Based on these results, it is evident that the conventional view of NDST, as a gateway enzyme, provides incomplete information. This study provides in vitro evidence showing that NDST acts on the mature HS chain and modifies it after it has been 6-*O*-sulfated – thus NDST-mediated modification is not necessarily just a gateway modification during HS biosynthesis (see Fig. 3). Extending the findings reported here to probe the action of NDST in vivo is beyond the scope of the current work. Nevertheless, one can conclusively state that current and previously reported in vitro experiments have undoubtedly helped demonstrate that *O*-sulfation differentially affects the action of two early biosynthetic enzymes, NDST and C5-epimerase [9,20]. One can envision that in vivo evidence delineating the exact sequence of HS biosynthetic events and the exact action of biosynthetic enzymes may require complex cellular experiments involving isotope enriched molecules and sophisticated instruments [29]. In conclusion, the results of this study redefine the role of NDST during HS biosynthesis and provide new insights into the actions of GAGOSOMES.

Acknowledgements

This work was supported by National Institutes of Health grants (R01GM075168, R01NS057144, P01HL107152), Human Frontier Science Program, and American Heart Association National Scientist Development Award to B.K. T.N. acknowledges a graduate fellowship support from the Vietnam Education Foundation.

Appendix A. Supplementary data

Supplementary data associated with this article can be found, in the online version, at doi:10.1016/j.febslet.2011.09.030.

References

[1] Zhang, L. (2010) Glycosaminoglycan (GAG) biosynthesis and GAG-binding proteins. Prog. Mol. Biol. Transl. Sci. 93, 1–17.
[2] Raman, K. and Kuberan, B. (2010) Chemical tumor biology of heparan sulfate proteoglycans. Curr. Chem. Biol. 4, 20–31.
[3] Bulow, H.E. and Hobert, O. (2004) Differential sulfations and epimerization define heparan sulfate specificity in nervous system development. Neuron 41, 723–736.
[4] Cortes, M., Baria, A.T. and Schwartz, N.B. (2009) Sulfation of chondroitin sulfate proteoglycans is necessary for proper Indian hedgehog signaling in the developing growth plate. Development 136, 1697–1706.
[5] Guimond, S., Maccarana, M., Olwin, B.B., Lindahl, U. and Rapraeger, A.C. (1993) Activating and inhibitory heparin sequences for FGF-2 (basic FGF). Distinct requirements for FGF-1, FGF-2, and FGF-4. J. Biol. Chem. 268, 23906–23914.
[6] Sugaya, N., Habuchi, H., Nagai, N., Ashikari-Hada, S. and Kimata, K. (2008) 6-*O*-Sulfation of heparan sulfate differentially regulates various fibroblast growth factor-dependent signalings in culture. J. Biol. Chem. 283, 10366–10376.
[7] Esko, J.D. and Selleck, S.B. (2002) Order out of chaos: assembly of ligand binding sites in heparan sulfate. Annu. Rev. Biochem. 71, 435–471.
[8] Victor, X.V., Nguyen, T.K., Ethirajan, M., Tran, V.M., Nguyen, K.V. and Kuberan, B. (2009) Investigating the elusive mechanism of glycosaminoglycan biosynthesis. J. Biol. Chem. 284, 25842–25853.
[9] Lindahl, U., Kusche, M., Lidholt, K. and Oscarsson, L.G. (1989) Biosynthesis of heparin and heparan sulfate. Ann. N.Y. Acad. Sci. 556, 36–50.
[10] Presto, J., Thuveson, M., Carlsson, P., Busse, M., Wilen, M., Eriksson, I., Kusche-Gullberg, M. and Kjellen, L. (2008) Heparan sulfate biosynthesis enzymes EXT1 and EXT2 affect NDST1 expression and heparan sulfate sulfation. Proc. Natl. Acad. Sci. USA 105, 4751–4756.
[11] Prydz, K., Dick, G. and Tveit, H. (2008) How many ways through the Golgi maze? Traffic 9, 299–304.
[12] Ponighaus, C., Ambrosius, M., Casanova, J.C., Prante, C., Kuhn, J., Esko, J.D., Kleesiek, K. and Gotting, C. (2007) Human xylosyltransferase II is involved in the biosynthesis of the uniform tetrasaccharide linkage region in chondroitin sulfate and heparan sulfate proteoglycans. J. Biol. Chem. 282, 5201–5206.
[13] Pettersson, I., Kusche, M., Unger, E., Wlad, H., Nylund, L., Lindahl, U. and Kjellen, L. (1991) Biosynthesis of heparin. Purification of a 110-kDa mouse mastocytoma protein required for both glucosaminyl *N*-deacetylation and *N*-sulfation. J. Biol. Chem. 266, 8044–8049.
[14] Kusche-Gullberg, M., Eriksson, I., Pikas, D.S. and Kjellen, L. (1998) Identification and expression in mouse of two heparan sulfate glucosaminyl *N*-deacetylase/*N*-sulfotransferase genes. J. Biol. Chem. 273, 11902–11907.

[15] Aikawa, J. and Esko, J.D. (1999) Molecular cloning and expression of a third member of the heparan sulfate/heparin GlcNAc *N*-deacetylase/*N*-sulfotransferase family. J. Biol. Chem. 274, 2690–2695.
[16] Humphries, D.E., Lanciotti, J. and Karlinsky, J.B. (1998) cDNA cloning, genomic organization and chromosomal localization of human heparan glucosaminyl *N*-deacetylase/*N*-sulphotransferase-2. Biochem. J. 332 (Pt 2), 303–307.
[17] Aikawa, J., Grobe, K., Tsujimoto, M. and Esko, J.D. (2001) Multiple isozymes of heparan sulfate/heparin GlcNAc *N*-deacetylase/GlcN *N*-sulfotransferase. Structure and activity of the fourth member, NDST4. J. Biol. Chem. 276, 5876–5882.
[18] Sheng, J., Liu, R., Xu, Y. and Liu, J. (2011) The dominating role of *N*-deacetylase/*N*-sulfotransferase 1 in forming domain structures in heparan sulfate. J. Biol. Chem. 286, 19768–19776.
[19] Nu Nguyen, T.K., Raman, K., Tran, V.M. and Kuberan, B. (2011) Investigating the mechanism of the assembly of FGF1-binding heparan sulfate motifs. FEBS Lett. 585, 2698–2702.
[20] Jacobsson, I., Lindahl, U., Jensen, J.W., Roden, L., Prihar, H. and Feingold, D.S. (1984) Biosynthesis of heparin. Substrate specificity of heparosan *N*-sulfate D-glucuronosyl 5-epimerase. J. Biol. Chem. 259, 1056–1063.
[21] Jansson, L., Hook, M., Wasteson, A. and Lindahl, U. (1975) Biosynthesis of heparin. Solubilization and partial characterization of *N*- and *O*-sulphotransferases. Biochem. J. 149, 49–55.
[22] Riesenfeld, J., Hook, M. and Lindahl, U. (1980) Biosynthesis of heparin. Assay and properties of the microsomal *N*-acetyl-D-glucosaminyl *N*-deacetylase. J. Biol. Chem. 255, 922–928.
[23] Brandan, E. and Hirschberg, C.B. (1988) Purification of rat liver *N*-heparan-sulfate sulfotransferase. J. Biol. Chem. 263, 2417–2422.
[24] Hashimoto, Y., Orellana, A., Gil, G. and Hirschberg, C.B. (1992) Molecular cloning and expression of rat liver *N*-heparan sulfate sulfotransferase. J. Biol. Chem. 267, 15744–15750.
[25] Wei, Z., Swiedler, S.J., Ishihara, M., Orellana, A. and Hirschberg, C.B. (1993) A single protein catalyzes both *N*-deacetylation and *N*-sulfation during the biosynthesis of heparan sulfate. Proc. Natl. Acad. Sci. USA 90, 3885–3888.
[26] Eriksson, I., Sandback, D., Ek, B., Lindahl, U. and Kjellen, L. (1994) cDNA cloning and sequencing of mouse mastocytoma glucosaminyl *N*-deacetylase/*N*-sulfotransferase, an enzyme involved in the biosynthesis of heparin. J. Biol. Chem. 269, 10438–10443.
[27] Mandon, E., Kempner, E.S., Ishihara, M. and Hirschberg, C.B. (1994) A monomeric protein in the Golgi membrane catalyzes both *N*-deacetylation and *N*-sulfation of heparan sulfate. J. Biol. Chem. 269, 11729–11733.
[28] Orellana, A., Hirschberg, C.B., Wei, Z., Swiedler, S.J. and Ishihara, M. (1994) Molecular cloning and expression of a glycosaminoglycan *N*-acetylglucosaminyl *N*-deacetylase/*N*-sulfotransferase from a heparin-producing cell line. J. Biol. Chem. 269, 2270–2276.
[29] Tran, V.M., Nguyen, T.K., Raman, K. and Kuberan, B. (2011) Anal. Bioanal. Chem. 399, 559–570.

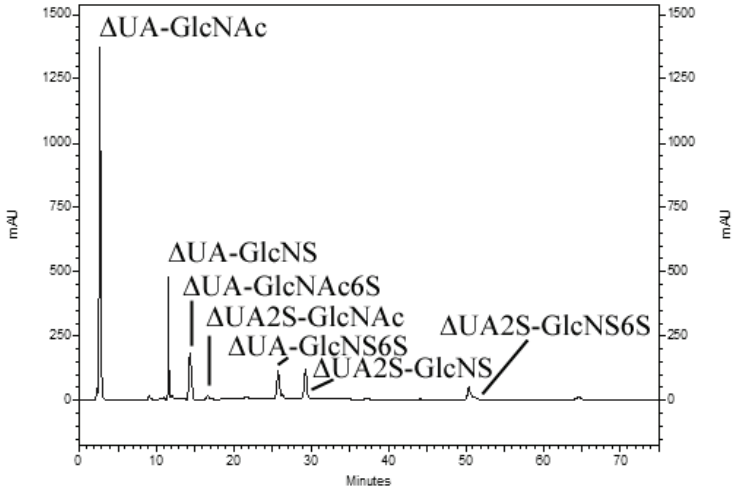

Figure S1. Heparan Sulfate from bovine kidney.

Table 4.S1. Summary of Characterization Data